DEVELOPMENT OF NOVEL DRUG-LIKE MOLECULES FOR TARGETED THERAPY

Dissertation

zur Erlangung des Grades

des Doktors der Naturwissenschaften

der Naturwissenschaftlich-Technischen Fakultät

der Universität des Saarlandes

von

Master of Science (Molecular Science)

Lorenz Albrecht Siebenbürger

Saarbrücken

2019

Tag des Kolloquiums: 28. Februar 2020

Dekan: Prof. Dr. Guido Kickelbick

Berichterstatter: Prof. Dr. Rolf W. Hartmann

Prof. Dr. Uli Kazmaier

Akad. Mitglied: Dr. Stefan Boettcher

Vorsitz: Prof. Dr. Claus-Michael Lehr

Die vorliegende Arbeit wurde von November 2013 bis November 2019 unter Anleitung von Herrn Univ.- Prof. Dr. Rolf W. Hartmann in der PharmBioTec GmbH, in der Fachrichtung Pharmazeutische und Medizinische Chemie der Naturwissenschaftlich-Technischen Fakultät der Universität des Saarlandes, sowie am Helmholtz Institut für Pharmazeutische Forschung Saarland (HIPS) in der Abteilung Drug Design and Optimization (DDOP) angefertigt.

Zusammenfassung

Die Implementierung neuer Techniken wie hoch-aufgelöste Massenspektrometrie, Next-Generation Sequencing oder Computersimulationen haben unser Verständnis von Krankheiten verändert. Neue Therapieformen entwickeln sich hin zu spezialisierten zielgerichteten Therapien. Diese neuen Medikamente erhöhen die Wirksamkeit in kleineren Patientengruppen, mit verringerten Nebenwirkungen im Vergleich zu Breitband-Arzneistoffen. Die Onkologie war jeher ein Vorreiter in diesem Feld, aber das Konzept kann auch auf andere pharmakologische Bereiche angewendet werden, wie z.B. die Endokrinologie.

Der erste Teil dieser Arbeit behandelt die Entwicklung neuer anti-angiogener Wirkstoffe für die zielgerichtete Krebstherapie. Neue Matrix Metalloprotease Inhibitoren wurden entwickelt, welche einen strukturell weniger konservierten Teil dieser Enzymklasse adressieren. Dabei wurde hohe Aktivität und Selektivität dieser Inhibitoren in verschiedenen Krebszelllinien erreicht.

Teil Zwei handelt von der Entwicklung von 17β-HSD2 Inhibitoren zur zielgerichteten endokrinen Therapie von Knochenbrüchen und Osteoporose. Zunächst wurde die Aktivität, Selektivität und metabolische Stabilität einer Inhibitorklasse optimiert, welche eine deutlich gesteigerte Stabilität der Frakturen in einem *in vivo* Proof-of-Principle Modell in der Maus zeigte. Des Weiteren wurde die Klasse vereinfacht und für Osteoporose optimiert, was zu verbesserten Eigenschaften nach oraler Gabe in einer Pharmakokinetik Studie in der Maus führte.

Summary

Implementation of novel techniques such as high-resolution mass-spectrometry, next generation sequencing or computer simulations have altered our understanding of diseases. Therapy forms emerge that turn away from the *one-fits-all* paradigm towards highly specialized targeted therapies. These novel medications increase efficacy in smaller groups of patients, and reduce side effects observed with outdated broad-spectrum drugs. Oncology research has been a pioneer in this field, but the concept can also be applied to other pharmacological areas such as endocrinology.

The first part of this thesis deals with the development of novel anti-angiogenic drugs for targeted-cancer therapy. Novel matrix metalloprotease inhibitors were synthesized, targeting a structurally less conserved part of enzyme class. High activity and selectivity could be achieved in different cancer cell lines, depending on the molecular structure of the inhibitors.

Part two deals with the development of 17β-HSD2 inhibitors for targeted-endocrine therapy of decreased bone fracture healing and osteoporosis. First, a class of inhibitors was optimized in activity, selectivity and metabolic stability to be successfully tested in an *in vivo* proof-of-principle mouse fracture model, leading to highly increased stability of the fractures. In a second step, this class was simplified and further optimized for osteoporosis therapy, showing increased properties after oral administration in a mouse pharmacokinetic study.

Publications included in this thesis

Chapter I: Siebenbürger, L.; de Vries, I.; Hernandez-Olmos, V.; Schnur, S.; Posel, R.; Hartmann R.W.; Börger, C.; Towards allosteric MMP inhibition: SAR studies of arylamides lead to selective MMP inhibitors for anti-angiogenic cancer therapy and beyond. ***to be submitted after patent filing***

Chapter II (Publication I): Abdelsamie, A. S.; Herath, S.; Biskupek, Y.; Börger, C.; Siebenbürger, L.; Salah, M.; Scheuer, C.; Marchais-Oberwinkler, S.; Frotscher, M.; Pohlemann, T.; Menger, M. D.; Hartmann, R. W.; Laschke, M. W.; van Koppen, C. J; (2019) Targeted Endocrine Therapy: Design, Synthesis, and Proof-of-Principle of 17β-Hydroxysteroid Dehydrogenase Type 2 Inhibitors in Bone Fracture Healing. *J. Med. Chem. 62* (3), 1362–1372. DOI: 10.1021/acs.jmedchem.8b01493.

Chapter III (Publication II): Siebenbuerger, L.; Hernandez-Olmos, V.; Abdelsamie, A. S.; Frotscher, M.; van Koppen, C. J; Marchais-Oberwinkler, S.; Scheuer, C.; Laschke, M. W.; Menger, M. D.; Boerger, C.; Hartmann R. W.; (2018) Highly Potent 17β-HSD2 Inhibitors with a Promising Pharmacokinetic Profile for Targeted Osteoporosis Therapy. *J. Med. Chem. 61* (23), 10724-10738. DOI:10.1021/acs.jmedchem.8b01373

Publications of the author not included in this thesis

Abdelsamie, A.S. van Koppen, C.J. Bey, E.; Salah, M.; Börger, C.; Siebenbürger, L.; Laschke, M. W.; Menger, M. D.; Frotscher, M. (2017) Treatment of Estrogen-Dependent Diseases: Design, Synthesis and Profiling of a Selective 17β-HSD1 Inhibitor with Sub-Nanomolar IC50 for a Proof-of-Principle Study. *Eur. J. Med. Chem. 127*, 944–957. DOI: 10.1016/j.ejmech.2016.11.004.

Emmerich, J.; van Koppen, C. J.; Burkhart, J. L.; Hu, Q.; Siebenbürger, L.; Boerger, C.; Scheuer, C.; Laschke, M. W.; Menger, M. D.; Hartmann, R. W. (2017) Lead Optimization Generates CYP11B1 Inhibitors of Pyridylmethyl Isoxazole Type with Improved Pharmacological Profile for the Treatment of Cushing's Disease. *J. Med. Chem. 60* (12), 5086–5098. DOI: 10.1021/acs.jmedchem.7b00437.

Abdelsamie, A. S.; Salah, M.; Siebenbürger, L.; Hamed, M. M.; Börger, C.; van Koppen, C. J.; Frotscher, M.; Hartmann, R. W. (2019) Development of Potential Preclinical Candidates with Promising in Vitro ADME Profile for the Inhibition of Type 1 and Type 2 17β-Hydroxysteroid Dehydrogenases: Design, Synthesis, and Biological Evaluation. *Eur. J. Med. Chem. 178*, 93–107. DOI: 10.1016/j.ejmech.2019.05.084.

Abdelsamie, A. S.; Salah, M.; Siebenbürger, L.; Merabet, A.; Scheuer, C.; Frotscher, M.; Müller, S. T.; Zierau, O.; Vollmer, G.; Menger, M. D.; Laschke, M. W.; van Koppen, C. J.; Marchais-Oberwinkler, S.; Hartmann, R. W. (2019) Design, Synthesis, and Biological Characterization of Orally Active 17β-Hydroxysteroid Dehydrogenase Type 2 Inhibitors Targeting the Prevention of Osteoporosis. *J. Med. Chem.* DOI: 10.1021/acs.jmedchem.9b00932.

Contribution report

Publication I: The author developed the HPLC-MS methods for the bioanalysis of the studied compounds. He executed the sample preparations, measurements and performed the data analysis. He was involved in writing the manuscript.

Publication II: The author designed and synthesized the majority of the studied compounds. He performed the purification and characterization, performed the enzymatic activity assays, *in vitro* metabolic stability assays and solubility determination. He developed the HPLC-MS methods for the studied compounds and performed all the bioanalysis and data analysis and conceived and wrote the manuscript.

Abbreviations

A-dione	androstenedione
ADME	absorption-distribution-metabolism-excretion
ATP	adenosine triphosphate
AUC	area-under-the-curve
BMP	bone morphogenetic protein
BPH	benign prostatic hyperplasia
c-FLIP	cellular FLICE (FADD-like IL-1β-converting enzyme)-inhibitory protein
CoA	coenzyme A
CTLA	cytotoxic T-lymphocyte-associated protein
CYP	cytochrome P450 enzyme
Da	dalton
DISC	death-inducing signaling complex
DNA	deoxyribonucleic acid
E1	estrone
E2	estradiol
ECM	extracellular matrix
ER	estrogen receptor
FDA	food and drug administration
GnRH	gonadotropin releasing hormone
HPLC	high-performance liquid chromatography
HSD	hydroxysteroid dehydrogenase
Ig	immunoglobulin
IL	interleukin
LD	lethal dose
MMP	matrix metalloprotease
MMS	musculoskeletal syndrome

MS	mass spectrometry
MT-MMP	membrane-type matrix metalloprotease
NADH	nicotinamide adenine dinucleotide
NADPH	nicotinamide adenine dinucleotide phosphate
PAPS	phosphoadenosine-phosphosulfate
PD-1	programmed cell death protein 1
PEX	hemopexin
PoP	proof-of-principle
PTH	parathyroid hormone
PK	pharmacokinetic
RANKL	receptor activator of nuclear factor kappa-B ligand
SAR	structure-activity relationship
SERM	selective estrogen receptor modulator
SPR	surface plasmon resonance
T	testosterone
TIMP	tissue inhibitor of metalloproteinase
TRAIL	tumor necrosis factor-related apoptosis-inducing ligand
UDPGA	uridine diphosphate glucuronic acid
VEGF	vascular endothelial growth factor

Table of contents

Zusammenfassung IV

Summary V

Publications included in this thesis VI

Publications of the author not included in this thesis VI

Contribution report VIII

Abbreviations IX

Table of contents XI

1. INTRODUCTION 1

1.1. Targeted therapies in oncology 1

1.1.1. Signal transduction inhibitors 2
1.1.2. Gene expression modulators 3
1.1.3. Apoptosis inducers 4
1.1.4. Immunotherapeutics 5
1.1.5. Angiogenesis inhibitors 5
1.1.5.1. Matrix metalloproteinases in tumor angiogenesis and cancer cell invasion 7
1.1.6. Hormone therapeutics 10

1.2. Targeted therapies in endocrinology 12

1.2.1. Osteoporosis and impaired bone fracture healing 14
1.2.2. Role of 17β-HSDs in steroid metabolism 16

1.3. Outline 18

1.4. Literature-described inhibitors 19

1.4.1. MT-MMP1 inhibitors 19
1.4.2. 17β-HSD2 inhibitors 20

2. AIMS OF THE THESIS 22

3. RESULTS 24

3.1. Chapter I: Towards allosteric MMP inhibition: SAR studies of arylamides lead to selective MMP inhibitors for anti-angiogenic cancer therapy and beyond 24

3.2. Chapter II: Targeted Endocrine Therapy: Design, Synthesis, and Proof-of-Principle of 17β-Hydroxysteroid Dehydrogenase Type 2 Inhibitors in Bone Fracture Healing 57

3.3. Chapter III: Highly Potent 17β-HSD2 Inhibitors with a Promising Pharmacokinetic Profile for Targeted Osteoporosis Therapy 69

4. FINAL DISCUSSION 85

4.1. PEX binders as a promising approach for the development of next-generation MMP inhibitors 85

4.2. Development and *Proof-of-Principle* evaluation of 17β-HSD2 inhibitors for bone fracture healing 90

4.3. Development of highly active 17β-HSD2 inhibitors for targeted osteoporosis therapy 94

5. REFERENCES 98

6. SUPPORTING INFORMATION 116

6.1 Supporting Information for Publication I (Chapter II) 117

6.1 Supporting Information for Publication II (Chapter III) 190

The references listed in chapter 5 belong to chapter 1 and 4. Each subchapter in chapter 3 has its own references, which are listed individually inside the chapter.

1. Introduction

1.1. Targeted therapies in oncology

Over the past decades, the implementation of new analysis methods such as next generation-genome sequencing, proteomics, metabolomics as well as computer-based data analysis, has altered the view of biomedical research on the pathogenesis and treatment mechanisms of several diseases. The unraveling of complex biochemical pathways in pathological conditions has led to a deeper understanding of the diseases and, hence, to a plethora of novel pharmacological targets and therapeutic strategies. These strategies are turning away from the "one-fits-all" paradigm towards a more highly specialized, selective approach to treat smaller groups of patients, according to the personalized medicine approach.[1] In this field, oncology research has played a pioneering role, as the unique heterogeneity of cancer, and the high cytotoxicity and severe side effects linked with classical chemotherapeutics, hinder their success rate.[2] The determination of cancer phenotypes and the understanding of the underlying biology is enabling a shift from drugs which non-specifically target rapidly dividing cells rather than tumor cells alone, to agents that address the targets with high selectivity and efficacy. The aim of this targeted therapy approach in oncology is either to deliver drugs selectively to the target cancer tissue (targeted drug-delivery approach) or to selectively address genes or proteins which are specific to cancer cells or the environment surrounding them that promote cancer growth. These drugs aim to address targets that are specific to the cancer cells, e.g. blocking cancer cell proliferation, promoting cell cycle regulation or inducing apoptosis.[3] Targeted drug-delivery is an active field of research[4], but it will not be further discussed here. According to the NIH, targeted therapy agents can be divided into six main categories (figure 1):

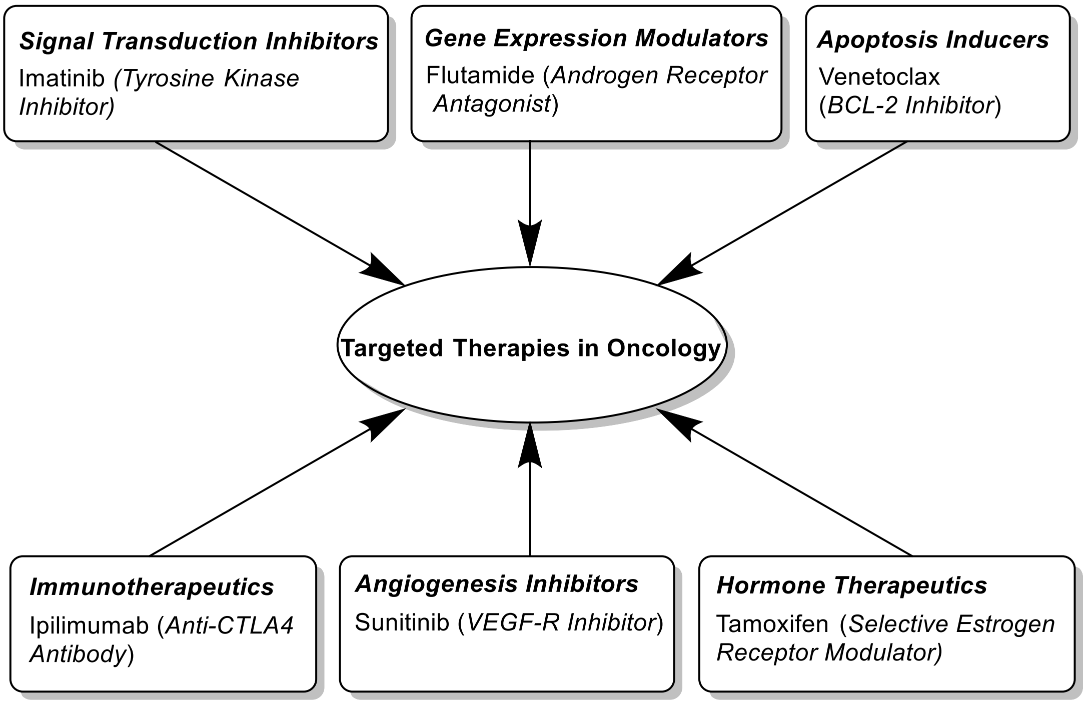
Signal Transduction Inhibitors
Imatinib (Tyrosine Kinase Inhibitor)
Gene Expression Modulators
Flutamide (Androgen Receptor Antagonist)
Apoptosis Inducers
Venetoclax (BCL-2 Inhibitor)
Targeted Therapies in Oncology
Immunotherapeutics
Ipilimumab (Anti-CTLA4 Antibody)
Angiogenesis Inhibitors
Sunitinib (VEGF-R Inhibitor)
Hormone Therapeutics
Tamoxifen (Selective Estrogen Receptor Modulator)

Figure 1: Classification of targeted therapy drugs in oncology, examples, and their respective mechanism of action, see proceeding chapters 1.1.1 -1.1.6 for references.

1.1.1. Signal transduction inhibitors

Signal transduction inhibition for cancer therapy exploits the fact that cancer cells compromise an unstable genome. For example, polyploidy or mutations of pro-oncogenes or loss-of-function mutations lead to the transition of normal cells into cancer cells. This change in the genome is active as long as the cancer cell is alive and, hence, these cells differ in their signaling and metabolic networks significantly from healthy ones. In different cancer types, specific signaling pathways are highly up regulated and thus prone to inhibition with anti-cancer agents targeting a single signaling protein. Signaling pathways have to be seen as biochemical networks, and healthy cells are able to sustain the stress given by the drug making use of redundant pathways which take over the function of those which have been inhibited.[5] Kinases, enzymes that transfer a phosphate group to a residue of another protein to transmit a signal, are the targets most addressed with this approach. So far, hundreds of kinases have been associated to cancer initiation, survival and proliferation and they are among the most studied targets for cancer therapy.[6]

1.1.2. Gene expression modulators

Therapeutic modulation of gene expression consists in interfering with the transcription of mRNA from DNA of cancer cells with various types of inhibitors. Altered signaling cascades in cancer cells often lead to aberrant expression of a certain gene, which is highly essential for the cancer cells to survive.[7] Hence, interference at the transcriptional level of such oncogenes is generally considered a promising approach to target cancer. The transcription process is regulated at three different levels[8]: at the first level, binding of transcription factors to specific promoter/enhancer regions of the gene enables the recruiting of the transcriptional machinery. This interaction is often altered in cancer and can be addressed by inhibiting correct binding of the transcription factors to DNA by competing with them for DNA binding or by binding to the transcription factor itself.[9] The second level consists of protein–protein interactions of transcription factors to other proteins, frequently other transcription factors or transcription regulators, which either stabilize their complex with DNA or the transcription factors by posttranslational modifications. Inhibitors could be utilized to interrupt these interactions. The third level consists of epigenetic control of genes by modification of either the DNA strand, to restrict access of transcription factors to certain promoters or cis-regulatory regions, or by modification of histones, to dictate the packaging of the DNA strand and hence, availability for transcription in general. Observations have been made that epigenetic modifications are often altered in cancer[10] which indicates that oncogene expression can be inhibited by epigenetic gene control in a positive manner. Despite the tremendous scientific effort and vast amount of targets and drug-like compounds developed so far following this approach[11], the only approved drugs exploiting this mechanism are molecules which interfere with steroid receptors, such as the androgen or estrogen receptor. This topic will be in depth discussed later (chapter 1.6).

1.1.3. Apoptosis inducers

Apoptosis represents the programmed death of cells necessary to maintain a healthy survival/death balance of metazoan cells and acts as a safeguard for genomic integrity.[12] Apoptosis can be generally accomplished through two different pathways, intrinsic and extrinsic. The intrinsic pathway, is triggered when cytochrome c is released from mitochondrial into the cytosol, which, via a cascade of proteases, called caspases, starting with caspase-9, leads to the breakdown of the nucleus and, hence, apoptosis. Permeability of the outer mitochondrial membrane is mainly regulated by proteins of the BCL-2 family[13], which are upregulated in almost 50% of all analyzed cancer types.[14] This dysregulation renders cancer cells resistant to traditional radio- and chemo-therapy.[15] Selective BCL-2 inhibitors, such as Venetoclax, are already used in clinic to treat severe forms of chronic lymphocytic leukemia[16], with more types of cancers currently undergoing clinical trials. The second, or extrinsic, pathway induces apoptosis via *stimuli* to receptors on the cell surface. So called death ligands like tumor necrosis factor or Fas ligand bind to tumor necrosis factor death receptor members, leading to the death-inducing signaling complex (DISC) via initiator caspases-8 and -10, which bind to adaptor molecules at the cytosolic portion of the receptors. The initiator caspases get activated and activate other caspases like -3, -6 and -7 which lead to rapid degradation of the cytosolic components and finally to apoptosis.[17] Death ligands that trigger apoptosis via the extrinsic pathway are expressed at the surface of cell types of the immune system, such as lymphocytes, macrophages or dendritic cells, which are used for cellular housekeeping by the immune system. However, cancer cells are able to withstand the attack by the immune system through either downregulation or loss of function expression of the death receptors, or by expression of soluble forms, which act as decoy receptors for the ligands displayed by the immune cells.[18] Furthermore, endogenous inhibitors of initiator caspases like c-FLIP are highly upregulated in various cancer types and lead to termination of the apoptosis signal given by death receptors.[19] Despite promising *in vitro* results, targeted therapy using recombinant death receptor ligands such as dulanermin, a tumor necrosis factor-related apoptosis-inducing ligand (TRAIL), has led to disappointing results in clinical trials[20], probably because of the short half-life of the drug.[21]

1.1.4. Immunotherapeutics

Immunotherapy for cancer makes use of the body’s own immune system to tackle cancer. As briefly described in the previous paragraph, immune cells are able to induce cell apoptosis by activating the death receptors on their surface and they can recognize malignant cells with their major histocompatibility complex molecules because of tumor-associated antigens displayed on the cancer cell surface.[22] However, surface display of such antigens is lost in some cancers, which makes it almost impossible for the immune system to recognize these malignant cells.[23] Successful recognition by T cells is further modulated via activation of CD28-type receptors with B7-type ligands on the surface of the cells. Some of the ligands are called immune checkpoints and inhibit T lymphocyte activation in physiological conditions such as inflammation, to protect the body from excessive tissue damage.[24] Cancer cells express these checkpoint molecules to induce an inhibitory effect on the immune system, so called T cell exhaustion. Tumors are able to manipulate the immune system in such a way, that they are surrounded by “deactivated” immune cells by creating an immunosuppressive, protumorogenic, and prometastatic microenvironment.[25] The development of antibodies targeting these checkpoint molecules or receptors to inhibit the suppressive immune signals given by cancer cells has led to a tremendous success in targeted cancer immunotherapy. Currently, a set of checkpoint inhibitors are already approved for cancer therapy and there are hundreds of clinical trials being performed at the moment targeting the Programmed cell death protein 1 (PD-1) or cytotoxic T-lymphocyte-associated protein 4 (CTLA4) pathway.[26]

1.1.5. Angiogenesis inhibitors

Like organs, tumors are dependent on the supply of oxygen and nutrients by their host body,[27] but they further manipulate the surrounding tissue to generate an environment in which they are able to grow. Physiological angiogenesis, the formation and sprouting of blood vessels, is tightly regulated by a balance between proangiogenic signal molecules and endogenous angiogenesis inhibitors. Upon hypoxia, cancer cells secrete pro-angiogenic factors that cause new blood vessels to grow towards the stimuli given by the tumor. This process is termed “angiogenic switch” and involves a complex interplay between cancer cells and the surrounding tissue.[28] First, the endothelial collagen layer, the so called basement membrane of capillaries is degraded by proteases of endothelial cells, which migrate into the extracellular matrix (ECM) by further degradation. These tip cells follow a gradient of chemokines, mostly vascular endothelial growth factor (VEGF), that are secreted by the cancer cells and sprout into the ECM after pericyte detachment and dilation of the blood vessel triggered by VEGF itself.[29] Following these cells, are other endothelial cells which are less invasive, but establish a lumen to support the tip cells.[30] A new basement membrane is formed and pericytes are attaching to stabilize the newly formed blood vessel.[31] The structure and composition of vasculature formed by tumor cells differs significantly from physiological vasculature, due to the abnormal cellular growth induced by highly increased proangiogenic factors such as VEGF by the tumor cells, leading to leaky capillaries and less-organized growth of the vasculature. Besides wound healing,[32] the physiological process of angiogenesis remains quiet in adults and development of angiogenesis inhibitors can be seen as an attractive approach for targeted therapy.[33] Besides thalidomide or its derivatives, which target endothelial cells by a not yet fully understood mechanism[34], several antiangiogenic agents have been approved by the FDA for cancer treatment.[35] Currently, different kinds of VEGF pathway-targeting anti-angiogenic agents are used alone, or in combination with other therapy forms. Antibodies have been developed to target either VEGF as a ligand or its receptor, VEGF-R, and subtypes, which inhibit downstream signaling of the cytokine. Furthermore, fusion proteins have been developed which trap soluble VEGF and other cytokines.[36] Small molecule inhibitors have been approved as VEGF-R inhibitors, the receptor which processes the binding of VEGF downstream in the cytosol via a tyrosine-kinase mechanism. These inhibitors bind to the kinase activation loop by either occupying the ATP binding site in the open conformation or by targeting the loop in its closed conformation via an allosteric binding site.[37] Despite high effects on patient survival rates for some cancer types, like metastatic renal cell carcinoma, anti-angiogenic cancer therapy targeting the VEGF pathway is not effective in all kinds of cancer.[35] Differences in vascular biology, meaning different upregulated pro-angiogenic pathways may be the reason for initial, or acquired resistance of cancer types to current anti-angiogenic therapy.[33]

1.1.5.1. Matrix metalloproteinases in tumor angiogenesis and cancer cell invasion

The degradation of the basement membrane and the ECM is mainly accomplished by matrix metalloproteinases (MMPs). This class of zinc-containing proteases consists of 23 members in the human body. They are grouped in five major categories, depending on their substrate preferences and/or structure (figure 2.)

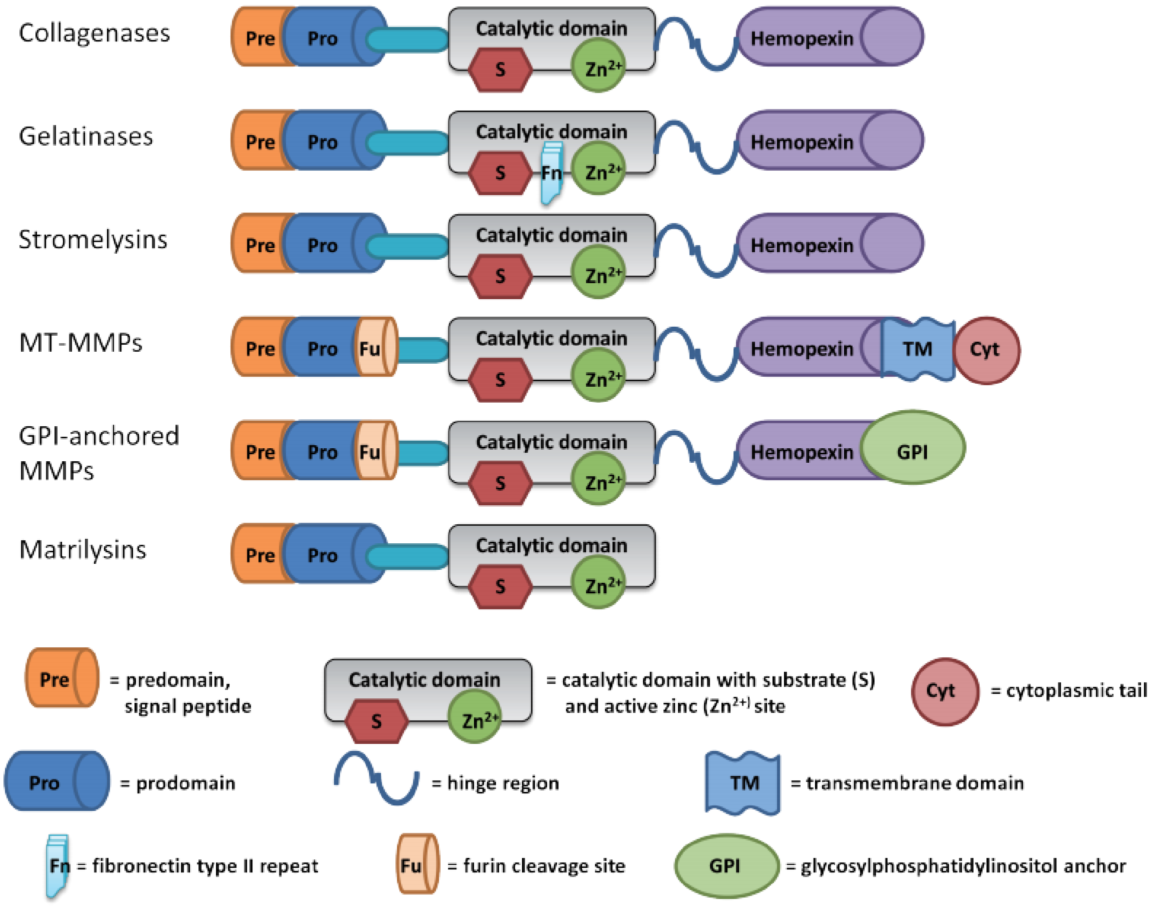
Collagenases
Gelatinases
Stromelysins
MT-MMPs
GPI-anchored MMPs
Matrilysins
Pre
Pro
Fu
Catalytic domain
S
Fn
Zn2+
Hemopexin
TM
Cyt
GPI
Pre = predomain, signal peptide
Catalytic domain = catalytic domain with substrate (S) and active zinc (Zn2+) site
Cyt = cytoplasmic tail
Pro = prodomain
= hinge region
TM = transmembrane domain
Fn = fibronectin type II repeat
Fu = furin cleavage site
GPI = glycosylphosphatidylinositol anchor

Figure 2: Classification of MMPs according to their substrate specificity and structural features, image taken from Langers, A.M.J., 2012, Doctoral thesis, Leiden University.

The most simple form are the matrilysins (MMP7&26), which consist of a signal peptide, a pro-domain and the catalytic domain with the zinc ion incorporated.[38] They are capable of degrading a wide spectrum of non-fibrillar components of the ECM such as gelatin or fibronectin. Collagenases (MMP1, 8 & 13) are able to cleave triple-helical substrates such as collagen I, II and III by possessing an additional collagen binding site, the hemopexin (PEX) domain. All types of MMPs, except matrilysins, possess this additional domain, which is connected to the catalytic domain via a hinge region. It allows the enzymes a plethora of protein-protein interactions, functioning either as an additional substrate binding site, or serving as an additional site for regulation of the enzyme activity. The hemopexin domain forms an additional binding site for endogenous inhibitors or activators, allowing downstream regulation.[39] Stromelysins (MMP3, 10 &11) have a similar structure to collagenases but show a broader substrate specificity like matrilysins. Gelatinases (MMP2 &9) have a modified catalytic domain with fibronectin type 2 inserts, serving as an additional collagen binding site and have a substrate preference for gelatin and type IV collagen.[40] Membrane-type MMPs (MT-MMPs) are a special form of MMPs and are connected to the cell membrane via a transmembrane domain (MT-MMP1, 2 & 3) or GPI-anchor (MT-MMP4 & 6). MT-MMP1 is the most studied one of this type. Because of overlapping activities, most MMP knockout mice do not show defects in angiogenesis, but MT-MMP1 deficient mice show severe defects in angiogenesis as well as skeletal defects.[41] In fact, MT-MMP1 can be seen as a key player in cell motility in the process of angiogenesis and cancer cell migration.[42] MT-MMP1 activity and function is regulated in a complex interplay between endogenous inhibitors, cellular receptors and the ECM.[43] The interactions of the enzyme with other proteins are mainly accomplished via the PEX domain, which serves as a hub for protein-protein interactions (figure 3). Most importantly, MT-MMP1 accomplishes direct degradation of the ECM components (fibrillar and non-fibrillar); furthermore, it is able to activate gelatinase proMMP-2 via binding to the PEX domain, and collagenase proMMP-13, two MMPs which are able to cleave collagen type IV, the major component of the basement membrane. Moreover, MT-MMP1 is able to cleave laminin-5, another major component of the basement membrane, stimulating cell motility.[44] MT-MMP1 sheds different receptors of the ECM on the cellular surface such as CD44 and syndecan-1, which is essential for cell motility.[45] Localization of MT-MMP1 occurs predominantly at the leading edge of the migrating cells, so called invadopodia. This process is accomplished by interaction of the PEX domain with CD44H, a hyaluronic acid receptor on the cell surface that connects the ECM to the actin cytoskeleton of the cell.[46] MT-MMP1 is also directly involved in VEGF signaling by interacting with the VGFR-R2 receptor and the kinase src in the cellular membrane via the catalytic, cytoplasmic and PEX domain.[47] MT-MMP1 also sheds complement component receptor 1q, C1qR on the surface of proliferating cells, which, in a soluble form, impairs the immune response to cancer cells mediated by the complement system.[48] MMPs are secreted inactivated as a zymogen with their active site blocked by a cysteine switch motif, which is cleaved *in vivo* by other proteases.[49] Some MMPs (e.g. MT-MMPs) have a furin-cleaving site and are expressed in their active form undergoing translocation in the Golgi apparatus.[38] MMP activity is tightly regulated via their endogenous inhibitors, tissue inhibitors of metalloproteinase (TIMPs), a group of four different peptides with specific affinities for the different groups of MMPs. TIMPs bind directly to the active site, or, as mentioned above, via the hemopexin domain to MMPs.[50] In human adults, MMP expression levels are generally low and are only upregulated under circumstances where ECM remodeling is present, such as wound healing, inflammation, tissue remodeling, metastasis formation and angiogenesis.[51] Nearly all types of cancer overexpress MMPs, and high expression levels of certain MMPs can be correlated with tumor invasiveness and poor prognosis.[52] Cancer cells themselves express MMPs, or induce nearby cells to produce MMPs via secretion of growth factors or cytokines via the “angiogenic switch” process.[53] The above mentioned findings highlight the role of MMPs, especially MT-MMP1 in cellular invasion processes. In contrast to conventional anti-angiogenic agents that target VEGF signaling or similar pathways, inhibition of MT-MMP1 would directly inhibit the cellular process of endothelial and cancer cell migration, and would therefore be an attractive approach for anti-angiogenic and targeted cancer cell therapy.

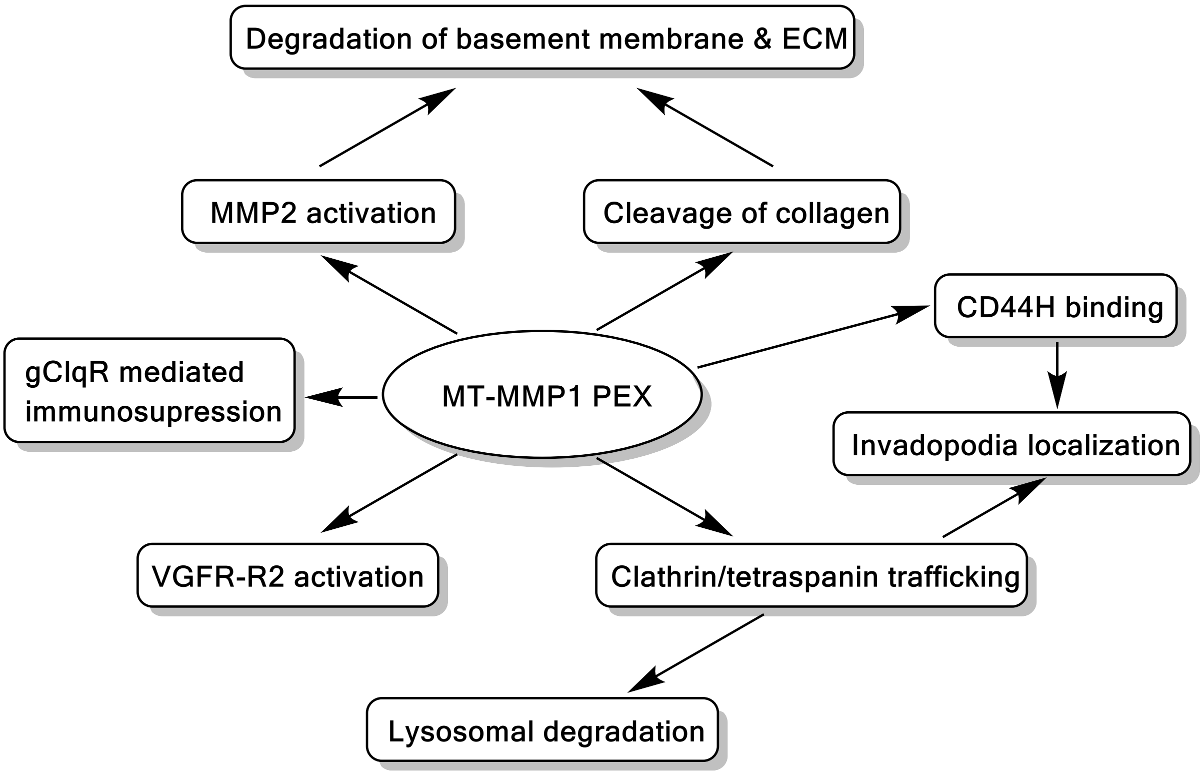
Degradation of basement membrane & ECM
MMP2 activation
Cleavage of collagen
CD44H binding
gClqR mediated immunosupression
MT-MMP1 PEX
Invadopodia localization
VGFR-R2 activation
Clathrin/tetraspanin trafficking
Lysosomal degradation

Figure 3: Protein-Protein interaction partners of MT-MMP1 via its PEX domain and resulting biological processes, see preceding paragraph for references.

1.1.6. Hormone therapeutics

As already briefly mentioned above, steroid receptors act as transcription factors in gene expression and steroid hormones are highly potent regulators of cell proliferation. Synthesis of these hormones follows a multistep biosynthesis scheme in different organs of the human body. A detailed pathway of steroid hormone production is depicted in figure 4. Dysregulation of this steroid production and response in the target tissue can hence lead to uncontrolled cell proliferation and, eventually, cancer under various conditions. Tumors which possess abnormalities to hormone response are referred as hormone-dependent malignancies and include cancer types like breast, endometrial, and prostate adenocarcinomas or uterine sarcomas.[54] Therapeutic agents can either block hormone synthesis or interfere with their target receptors by blocking or activating it. Besides peptidic agents like Somatostatin analogues[55] or gonadotropin-releasing hormone receptor agonists and antagonists[56], hormone therapeutics for cancer interfere with steroid receptors or metabolism. Corticosteroids represent an effective class of drugs for the treatment of lymphoid cancer types due to their antineoplastic effect on this kind of tissue[57], but are accompanied by severe side effects like adrenal insufficiency, immunosuppression or osteoporosis, especially in elderly people.[58] Progestins are applied to treat hormone-sensitive cancer types because of their inhibitory effect on the hypothalamic-pituitary-gonadal axis, resulting in decreased production of estrogens. Furthermore, they have strong antineoplastic effect on progesterone- and estrogen-receptor-positive endometrial and breast cancer.[59] Side effects like thromboembolism or osteoporosis need to be monitored carefully in treated patients.[54]

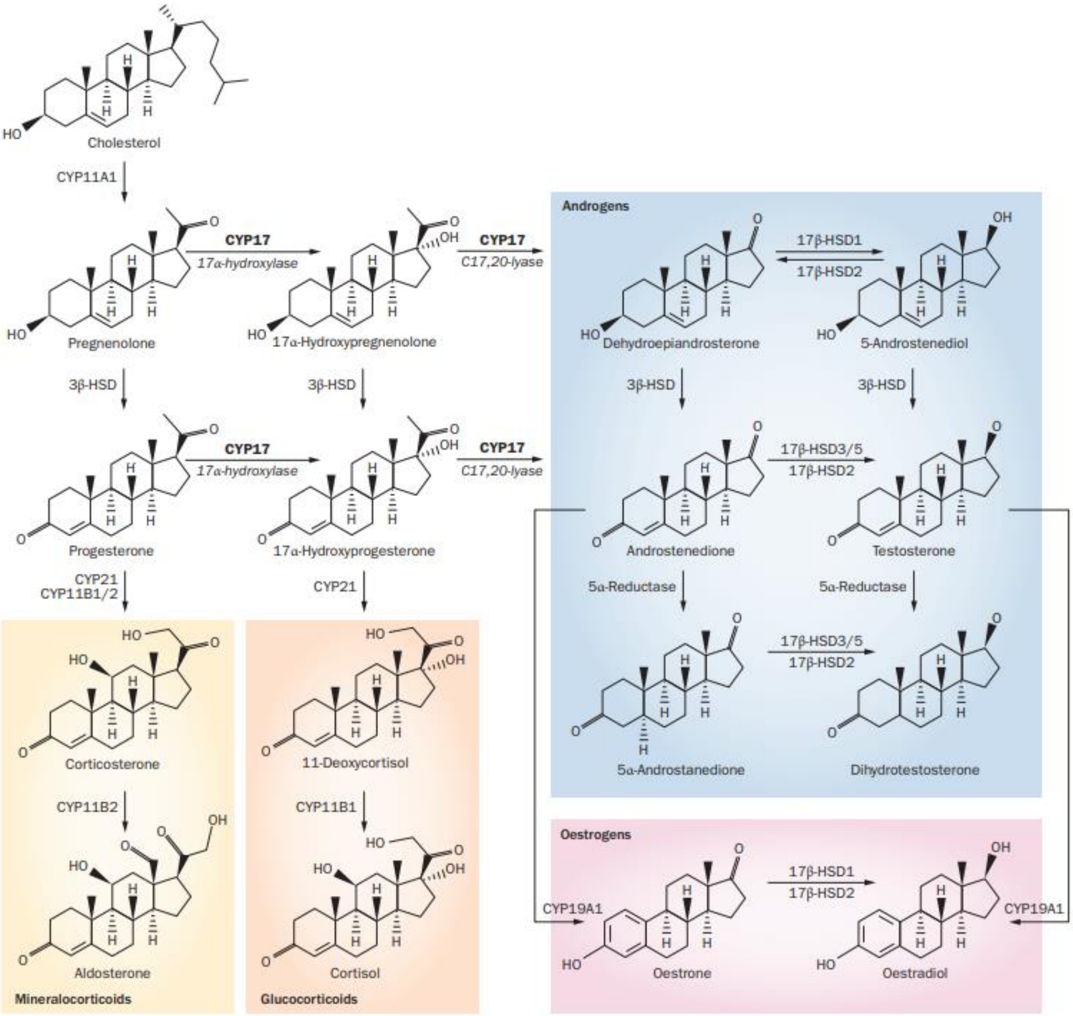
Cholesterol
CYP11A1
CYP17
17α-hydroxylase
CYP17
C17,20-lyase
Androgens
Pregnenolone
17α-Hydroxypregnenolone
Dehydroepiandrosterone
17β-HSD1
17β-HSD2
5-Androstenediol
3β-HSD
3β-HSD
3β-HSD
3β-HSD
CYP17
17α-hydroxylase
CYP17
C17,20-lyase
Progesterone
17α-Hydroxyprogesterone
Androstenedione
17β-HSD3/5
17β-HSD2
Testosterone
CYP21
CYP11B1/2
CYP21
5α-Reductase
5α-Reductase
Corticosterone
11-Deoxycortisol
5α-Androstanedione
17β-HSD3/5
17β-HSD2
Dihydrotestosterone
CYP11B2
CYP11B1
Oestrogens
CYP19A1
17β-HSD1
17β-HSD2
CYP19A1
Aldosterone
Cortisol
Oestrone
Oestradiol
Mineralocorticoids
Glucocorticoids

Figure 4: Biosynthetic pathway of steroid hormones & involved enzymes, taken from Yin et al.[62]

Besides castration induced by gonadotropin-releasing hormone receptor agonists and antagonists or surgery, androgen production can be inhibited more selectively by the application of CYP17 inhibitors in different prostate cancer types. Inhibition of CYP17 leads to deprivation of androgens and estrogens, even in cancer types that are able to produce these hormones themselves in an intra- or paracrine manner, thus being resistant to conventional hormone deprivation therapies.[60] Abiraterone is the most prominent agent targeting CYP17. Being a metabolite of the pro-drug abiraterone acetate, abiraterone and its metabolite, Δ^4-abiraterone, are potent inhibitors of various pathways of *de novo* androgen synthesis in tumors, as well as antagonists of the androgen receptor, making the drug effective in different kinds of prostate cancer.[61,62] This promiscuity of the drug leads, on one hand, to effective shutdown of multiple pathways to androgens, but, on the other hand, leads to side effects like fluid retention or hypokalemia, due to secondary mineralocorticoid excess caused by the dual inhibition of the 17-hydroxylase function of CYP17 and CYP11B1.[63] Furthermore, inhibition of various hepatic CYP enzymes results in hepatotoxicity and altered plasma levels of co-administered drugs.[62] Aromatase or CYP19 inhibitors are a class of drugs that inhibit estrogen synthesis from androgens, leading to estrogen deprivation, and are mainly administered to postmenopausal estrogen receptor-positive breast cancer patients. Hormone therapy can act on the biosynthesis of the corresponding hormones, as described above, or directly interact with the target steroid receptors. Selective estrogen receptor modulators (SERMs) are a class of drugs binding to the estrogen receptor (ER), modulating its activity as a transcription factor, depending on the target tissue. The activity of the drug to act either as an agonist or antagonist on the ER in the target tissue depends, aside for different affinities to the receptor subtypes, on the conformational changes induced in the receptor structure upon binding, modulating the interaction of the receptor complex with different coactivators or corepressors, which are heterogeneously expressed in ER positive tissues.[64] Tamoxifene for example, which, besides aromatase inhibitors, is first-line treatment for ER-positive breast cancer, shows antagonistic behavior in breast tissue, while being an agonist in the bone, cardiovascular system and endometrium, therefore preventing side effects associated with total depletion of estrogens, e.g. osteoporosis, but inducing endometrial abnormalities or increasing endometrial cancer risk, which need to be monitored carefully.[65]

1.2. Targeted therapies in endocrinology

The concept of targeted therapy is not strictly bound to cancer therapy alone, but can be transferred to other types of diseases, as well. In diseases of endocrine origin, treatment often alters systemic hormone levels, affecting both dysregulated and healthy tissues targeted by the hormone in question, which leads to side effects in healthy tissue and a disturbance of the hypothalamus-pituitary gland - organ axes of the hormones (Figure 5). Deeper understanding of hormone biosynthesis and action on a local tissue level enables the concept of “endocrine-targeted therapies”, which aim at altering hormone concentrations locally in the target tissue, rather than in the whole body, hence reducing systemic side effects. Benign prostatic hyperplasia (BPH) is a noncancerous enlargement of the prostate occurring mostly in elderly men. The increased pressure on the urethra by the enlarged prostate leads to lower urinary tract symptoms like problems in urinating, total loss of bladder control, urinary tract infections or chronic kidney problems.[66] The exact causes of BPH are unknown, but age-related changes in metabolism, hormone levels and inflammatory mechanisms have been proposed.[66] Although serum levels of androgens are not clearly elevated in patients with BPH[67], androgens do play a permissive role in the pathogenesis of BPH.[68]

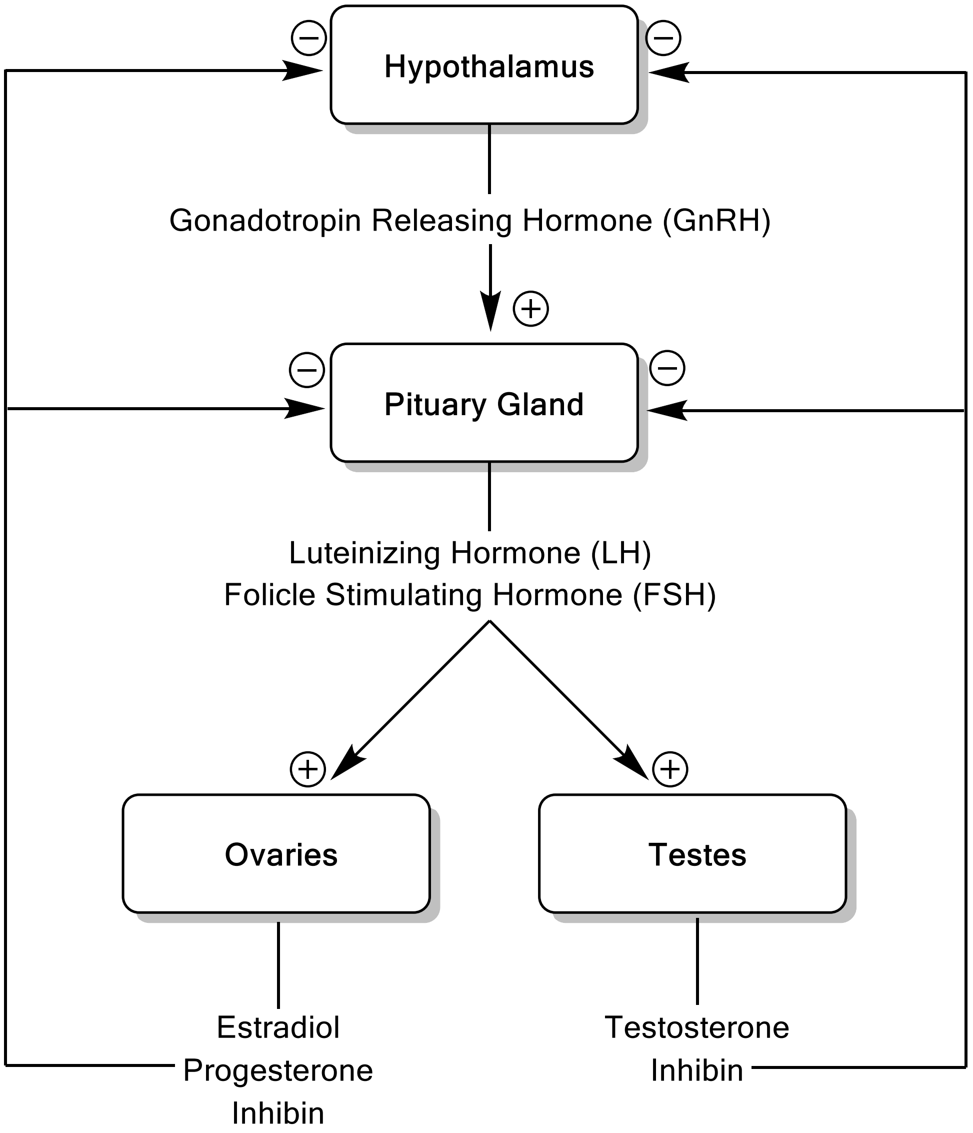
Hypothalamus
Gonadotropin Releasing Hormone (GnRH)
Pituary Gland
Luteinizing Hormone (LH)
Folicle Stimulating Hormone (FSH)
Ovaries
Testes
Estradiol
Progesterone
Inhibin
Testosterone
Inhibin
⊖
⊕

Figure 5: Hypothalamus - pituary - gonad axis; + stands for stimulation, - for inhibition

Inside prostate cells, circulating testosterone is metabolized to dihydrotestosterone, an androgen with much higher affinity to the androgen receptor, by the enzyme 5α-reductase.[69] Inhibition of this enzyme is therefore an attractive approach for targeted therapy to selectively decrease androgen levels inside the prostate, avoiding side effects like osteoporosis or erectile dysfunction that are accompanied by systemic androgen deprivation therapy with Gonadotropin-releasing hormone (GnRH) medications.[70] Another promising approach for targeted endocrine therapy is inhibition of 11β-Hydroxysteroid Dehydrogenase Type 1 to selectively decrease cortisol levels in target tissue to treat glucocorticoid associated diseases like metabolic syndrome, atherosclerosis or type 2 diabetes mellitus[71,72], and highly active drug-candidate molecules have been developed.[73]

1.2.1. Osteoporosis and impaired bone fracture healing

Osteoporosis is a common disease and characterized by increased fragility and decreased density and structure of the bone, caused by an aberrated bone remodeling process.[74] Two different cell types maintain healthy bone. The first ones are osteoblasts, which form new bone mass; secondly, osteoclasts, which break down old bone mass. An imbalance in number and activity of these cells causes decreased bone formation and increased bone resorption, leading to osteoporosis.[75] The disease affects mostly elderly women after menopause, as the highly diminished activity of the ovaries strongly affects systemic estrogen levels, but elderly men can also suffer from the disease.[76] Besides low estrogen levels, calcium and vitamin D deficiencies also contribute to the development of osteoporosis.[77] Estrogens directly act on the bone remodeling process via binding to the ER in osteoblasts and osteoclasts, directly altering cellular proliferation or differentiation of these cell lines, but also via the release of various cytokines such as receptor activator of nuclear factor kappa-B ligand (RANKL), bone morphogenetic proteins (BMPs) or sclerostin.[78] Besides calcium and vitamin D supplements, the most common therapy options include bisphosphonates like alendronate, which inhibit bone resorption by inducing apoptosis in osteoclasts by blocking either the mevalonate pathway[79] or being metabolized to a toxic ATP derivative.[80] They have shown to reduce fracture risk in patients by 50%, while being associated with severe side effects like osteonecrosis of the jaw or complications after either oral or intravenous application.[81] SERMs with an antagonistic profile on the breast and endometrium, but acting as agonists in the bone are used to treat osteoporosis, but are accompanied by side effects like venous thromboembolism.[82] Monoclonal antibodies such as denosumab are used to inhibit RANKL signaling to prevent osteoclast formation and survival[83], but can lead to osteonecrosis of the jaw or severe infections.[84,85] The mentioned drugs are considered anti-resorptive agents, being able to prevent future bone loss, but not stimulating formation of bone substance. Parathyroid hormone (PTH) or its analogues, like teriparatide, have been shown to have an anabolic effect on the bone when injected in low doses, despite the fact that constant high levels of endogenous PTH are associated over time with loss of bone substance, due to its stimulating effect on osteoclasts to release calcium from the bone, thus limiting its therapeutic usage.[86,87] Very recently, the FDA voted positive for the approval of the antibody romosozumab for the treatment of osteoporosis in postmenopausal women at high risk for fractures, after various positive phase III clinical trials of the drug. [88,89] This antibody targets sclerostin, an anti-osteoanabolic molecule secreted by osteocytes to inhibit osteoblastogenesis via inhibition of wnt signaling, and has therefore an anabolic effect on bone substance.[90]

Aside for treatment of osteoporosis for prevention of fractures, drugs targeting this disease could, in principle, also be applied in the process of fracture healing. Impaired fracture healing occurs in up to 20% of all patients and is accompanied by highly increased treatment duration and costs for the patient.[91] Various factors influence successful fracture healing, like age of the patient, smoking and alcohol abuse, nutrition, use of anti-inflammatory drugs or other comorbidities like diabetes, anemia, or hypothyroidism, but also the complexity of the fracture and the damage of the surrounding blood vessels play an important role in fracture healing.[92,93] Fracture healing is divided in different but subsequent and overlapping stages, here divided for clarity purposes. Directly after the fracture, an inflammatory response is triggered that leads to the formation of a hematoma between the two ends of the fractured bone, which is then vascularized by the surrounding blood capillaries. Both ends are then connected by the formation of a soft callus by fibroblasts and chondrocytes, serving as a template for ossification by osteoblasts and osteoclasts. This leads to an irregular woven, hard callus, which is highly vascularized. This hard callus is then remodeled to the actual shape and structure of the regular bone.[94] Anti-resorptive agents for osteoporosis, e.g. bisphosphonates, have so far not shown to have a beneficial effect on bone fracture healing.[87] Although, treatment of fractures with PTH or analogues has been successful in animal studies[95], clinical trials have so far led to conflicting results.[96] Bone morphogenetic proteins (BMPs) have been investigated as drugs for impaired bone fracture healing. They are a class of cytokines comprising 30 members, able to regulate a wide range of different cell types involved in bone regeneration. Concentrations of BMPs varies greatly during the different stages of bone fracture healing.[97] Local application of different BMPs on open fractures has shown to increase fracture healing in different animal models.[98] However, conflicting results in clinical trials, the need for local application of BMPs on carriers and the associated side effects strongly question applicability of this approach.[99]

As mentioned above, steroid hormones play an important role in healthy bone metabolism and preservation. Estradiol and Testosterone have shown to increase fracture healing in various animal models.[100–102] Their beneficial effect on bone formation and mass has been studied for a long time.[103] In fact, hormone replacement therapy has been used for decades to counteract the drop in physiological estradiol levels in elderly people to maintain a healthy bone metabolism and hence, prevent osteoporosis.[104] Nonetheless, severe side effects like cardiovascular diseases and an increased risk of breast cancer, originating from system application of estrogens, currently contraindicates this form of therapy for a large group of patients.[105] Targeted therapy for a local increase in estrogen levels is a promising way to make use of the beneficial effects of estrogens and androgens on the bone, while circumventing side effects following systemic application.

1.2.2. Role of 17β-HSDs in steroid metabolism

17β-Hydroxysteroid dehydrogenases (17β-HSDs) are a class of enzymes that catalyze the interconversion of the keto forms of steroids into the secondary alcohols at C17 of the steroid scaffold using either NADH or NADPH as cofactor, and are directly involved in the biotransformation of the active sex steroids estradiol and testosterone into their less active forms estrone and androstenedione (figure 6). Steroids are the main substrates of this enzyme class, but they are also involved in acyl-CoA, bile acid and retinoid metabolism.[106]

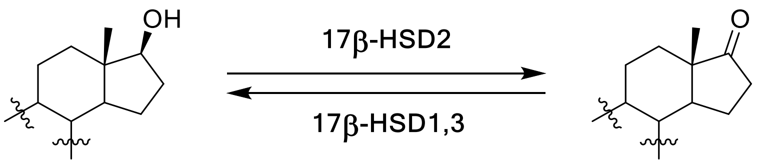

Figure 6: Oxidative/reductive reactions on steroid hormones catalyzed by 17β-HSDs

Until now, 12 different 17β-HSDs have been characterized in humans and have shown to belong to the class of short chain dehydrogenase/reductase enzyme family, except for 17β-HSD5, which belongs to the aldo-keto reductase family.[107] Despite being able to catalyze both reductive and oxidative reactions *in vitro*, the main metabolic direction *in vivo* is dictated by the abundance of their preferred cofactor at their location inside the cell. 17β-HSDs are expressed throughout the body, but the highest expression levels occur in androgen- and estrogen-sensitive tissues like prostate, testis, breasts, ovaries, placenta and endometrium, along with the liver and kidneys. As they are involved in either formation or inactivation of androgens and estrogens, depending on their reductive or oxidative nature on their steroid substrates, they directly modulate the activity of these hormones in their target tissue. Inhibition of these enzymes is hence a promising approach for targeted therapy of androgen- and estrogen-dependent diseases. Several reductive 17β-HSDs are of therapeutic interest for treatment of androgen- or estrogen-sensitive malignancies. 17β-HSD1 is the main enzyme that reduces estrone to estradiol and is expressed in the ovaries, breast, lung and placenta. It is directly involved in the pathogenesis of breast cancer[108], lung cancer[109], and endometriosis.[110] Furthermore, 17β-HSD5, which is expressed in the liver and prostate, has been found to be upregulated in androgen-independent prostate cancer types, being able to convert adrenal androstenedione to testosterone intratumorally in patients undergoing chemical castration.[111] Expression levels of the oxidizing, inactivating types of 17β-HSDs can be seen as a prognostic marker in different cancer types. High expression levels of 17β-HSD14 in estrogen receptor-positive breast cancer patients have been shown to be highly beneficial for the late progression of the disease.[112] The most studied oxidative enzyme of this class is 17β-HSD2. It catalyzes the NAD^+-dependent inactivation of estradiol to estrone and testosterone to androstenedione in estrogen- and androgen-sensitive tissues like ovaries, prostate, endometrium, breasts, placenta and bone, but is also expressed in the lungs, kidneys and the liver.[113] The enzyme (42.9 kDa) consists of 387 amino acids and it is bound to the membrane of the endoplasmic reticulum inside the cell, impeding crystallization of the enzyme.[114] The natural function of the enzyme is to protect tissues from excessive steroid action, like the breasts, endometrium or the uptake of maternal steroids through the placenta of an unborn child. Inhibition of 17β-HSD2 would therefore selectively elevate levels of estradiol and testosterone in tissues of expression, which would reduce side effects usually accompanied with systemic administration.[115] As 17β-HSD2 is expressed in osteoblasts, inhibition of the enzyme would be an attractive approach to treat estradiol-sensitive diseases like osteoporosis and impaired bone fracture healing.[116]

1.3. Outline

Targeted therapies describe the development of novel drugs, which utilize a deeper understanding of the pathogenesis of certain diseases developed over the last decades. This form of therapy aims to threat smaller amounts of people with “tailored” drugs that specifically interact with the underlying dysregulation. Novel cancer therapeutics are amongst the first of this new class of drugs, due to the high toxicity and lack of selectivity of the formerly state-of-the-art therapy options. Aberrations in signal transduction, gene transcription, immunosuppression, apoptotic stress, hormone production or angiogenesis are the drivers of cancerous growth and novel therapeutics, with partly revolutionary success, have been developed for cancer treatment. Angiogenesis plays a key role in cancer growth as every tissue is dependent on the supply of oxygen and nutrients. Current antiangiogenic therapies aim at disrupting the cytokine-kinase pathways such as VEGF by either interacting with the ligands/receptors on outside of the cell or by inhibiting kinase signal transduction intracellularly, but show limited long-term efficacy because the underlying pathways are redundant. The metalloprotease MT-MMP1 directly involved in the angiogenic and metastatic process by cleaving of ECM and enabling cellular migration of endothelial and cancer cells via various mechanisms, while remaining quiescent under physiological conditions, and is hence a novel target for antiangiogenic cancer therapy. The concept of targeted therapies cannot just be applied to cancer treatment, but also to endocrine diseases such as osteoporosis. This illness is characterized by a loss of bone density and increased fracture risk and occurs primarily in women after menopause, as the production of bone-preserving estradiol from the ovaries is highly decreased after that time point. The last step of estrogen biosynthesis is catalyzed by 17β-HSDs, which are expressed in estrogen-sensitive tissue, such as bone. Inhibition of 17β-HSD2, which oxidizes estradiol into its less active form estrone, is hence an attractive approach to increase estradiol levels in the bone, rather than altering systemic hormone levels, as traditional endocrine therapies do, hence minimizing side effects of the therapy. Inhibition of 17β-HSD2 is not only a promising approach for osteoporosis therapy, but also for increased bone fracture healing, as both processes are accomplished by similar biological mechanisms.

1.4. Literature-described inhibitors

1.4.1. MT-MMP1 inhibitors

Different types of inhibitors of MT-MMP1 have been developed, such as small molecules, peptides or antibodies.[117–120] However, clinical trials with MMP inhibitors for cancer treatment have so far led to disappointing results because of severe side effects such as musculoskeletal syndrome (MMS), or even worse clinical results for patients compared to control groups receiving traditional chemotherapeutics.[121] These side effects were attributed to the lack of selectivity of current MMP inhibitors, which inhibit this class of enzymes by blocking the active site via chelation of the zinc ion with a hydroxamate moiety. Taking into account the pro- and antiangiogenic effects of different MMPs at different time points of the angiogenesis process, optimal therapy onset and selectivity profile of the inhibitors is mandatory for a successful treatment.[121,122] Furthermore, the structure of the active site is highly conserved amongst the whole enzyme superfamily, called methzincins, which makes design of selective inhibitors targeting the active site of this enzyme class an incredibly difficult task.[123] A promising approach to circumvent the problems which are accompanied by promiscuous metalloprotease inhibition of the active site is the development of so called "exosite binders", compounds that target structurally less conserved domains of MMPs than the active site, but are essential for substrate binding, cleavage and other protein-protein interactions.[124] Recently, Remacle *et al* identified compound **A** (figure 7), an exosite binder and a potential inhibitor of MT-MMP1, by an *in silico* screening approach, docking a library into the tunnel at the center of the flat propeller-like structure of the PEX domain of MT-MMP1.[125]

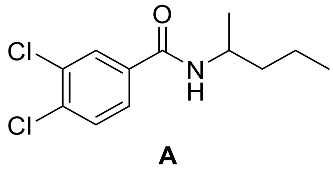

A

Figure 7: Literature desribed MT-MMP1 exosite binder

They could show that **A** does not inhibit catalytic cleavage of MT-MMP1 towards small peptide substrates and activation of pro-MMP2, but it does inhibit migration of cancer cells on a collagen matrix in a dose dependent manner, while being not cytotoxic. They conducted an *in vivo proof-of-principle* study with **A**, applying the compound intratumorally for three weeks in a mouse tumor xenograft model. The results were a significantly decreased tumor growth compared to vehicle controls, with the tumors showing a small fibrotic phenotype, similar to results obtained with a PEX deletant MT-MMP1 cancer cell mutant in the same study. These findings strongly support the development of novel MMP inhibitors with a new mechanism of action.

1.4.2. 17β-HSD2 inhibitors

Several classes of 17β-HSD2 inhibitors are described in literature (figure 8). The first 17β-HSD2 inhibitors were developed by the group of Poirier in 2001 and consisted structurally of a steroid scaffold with the C17 δ-spirolactone modified compound **B** being the most active one (IC_{50} = 6 nM).[126] However, steroidal inhibitors have considerable drawbacks like poor solubility and interference with steroid receptors, which might lead to adverse effects. The first non-steroidal 17β-HSD2 inhibitors were described by Wood and Gunn *et al* in 2005, who developed the *N*-methyl substituted *cis*-pyrrolidinone compound **C** with an IC_{50} of 50 nM.[127,128] The compound was further evaluated in a osteoporosis *proof-of-principle* study by Bagi *et al* using cynomolgus monkeys as investigated species.[129] They could show that after 23 weeks of daily oral administration of **C**, treated animals underwent a slight decrease in bone resorption, and an increase in bone formation, compared to ovariectomized vehicle controls, but the non-optimal pharmacokinetic profile of **C** led to greater variability of results in the study.

In our research group, several classes of non-steroidal 17β-HSD2 inhibitors have been developed. Hydroxyphenylnaphthyl derivative **D** was developed by Wetzel *et al* and shows a reasonable IC_{50} of 19 nM on the human enzyme, but only moderate inhibition on the mouse enzymes (72% at 1µM), which led to discontinuation of this class, since a high activity in the rodent is essential for further *in vivo* evaluation.[130] Perspicace *et al* developed the retro-*N*-methyl-sulfonamide **E** with an IC_{50} of 23 nM, but this class showed an even lower inhibition on the mouse enzyme (29% inhibition at 1µM).[131] Gargano *et al* developed the class of N-methyl-substituted aryl amide **F**, a compound with high *in vitro* metabolic stability in human liver S9 fraction ($t_{1/2}$ >60 min). Furthermore, the compound shows the highest inhibition value on the mouse 17β-HSD2 (IC_{50} = 140 nM) published so far, but the weak activity on the human enzyme (IC_{50} = 300 nM) convinced us not to investigate this class further in biological trials.[132] Recently, discovered in the field of 17β-HSD1 inhibitors, our group showed that the decoration on the benzoyl moiety of the highly active 17β-HSD1 class of arylthiophenyl methanones,[133] strongly influences activity on both 17β-HSD1 and 2, resulting in compound **G**.[134] This compound shows an outstanding IC_{50} of 1.4 nM and serves as an ideal hit compound for further optimization and biological evaluation studies, which will be further discussed in detail in this work.

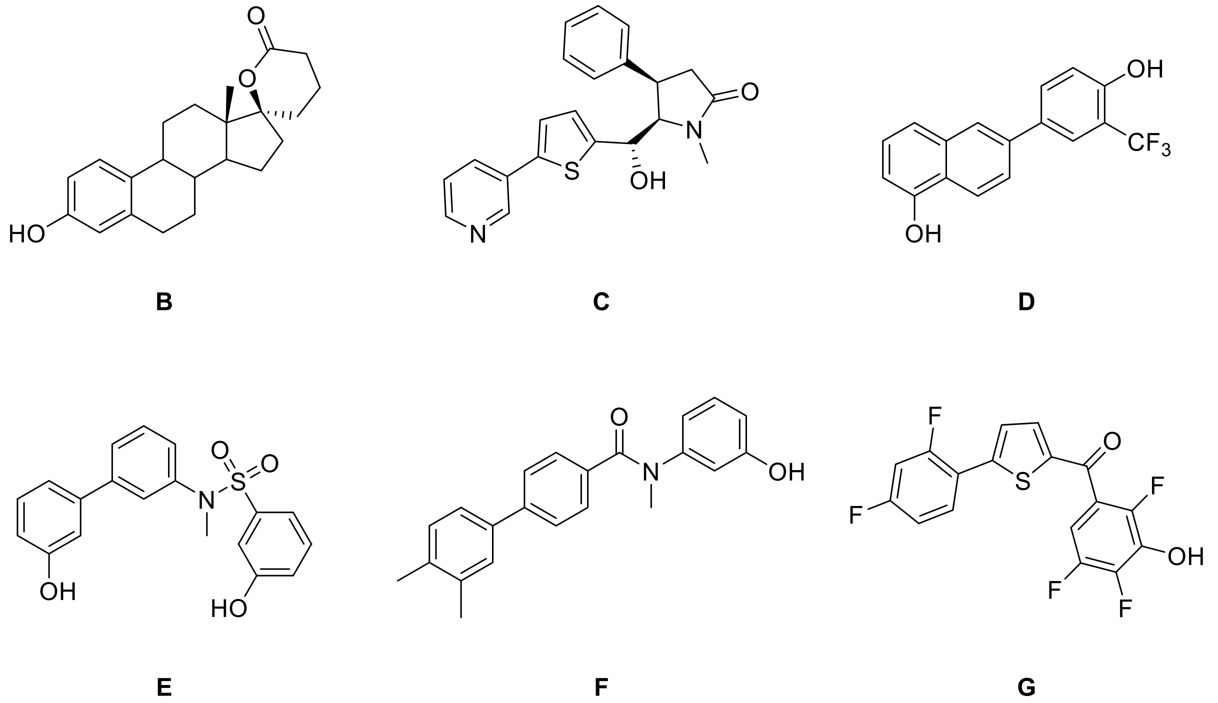
HO
O
O
B
OH
N
S
N
O
C
OH
CF3
OH
D
OH
HO
N
S
O
O
E
O
N
OH
F
F
F
S
O
F
OH
F
F
G

Figure 8: Steroidal and non-steroidal literature described 17β -HSD2 inhibitor classes

2. Aims of the thesis

Targeted therapy drugs are an emerging class which aim to specifically alter underlying mechanisms of various pathogenic conditions in smaller patient groups. Large research interest has already been put in the development of this kind of therapies for oncology, due to the heterogeneity of the disease and severe side effects of state-of-the-art treatment possibilities. Angiogenesis inhibitors are amongst the most promising concepts for this therapy form, as all types of cancer rely on nutrients and oxygen supply by their host body. Due to redundant pathways in angiogenesis signaling such as VEGF, novel targets for antiangiogenic therapy are an active field of research. MMPs play an important role in the angiogenic process and cancer cell migration. Especially MT-MMP1 has been identified as a key player in angiogenic sprouting of endothelial cells and metastasis formation. However, MMP inhibitors failed in clinical trials due to severe side effects caused by lack of selectivity towards other MMPs, due to high conservation of the inhibited active site of MMPs in the enzyme family. Targeting less conserved sites by small molecules is hence an attractive concept for the development of new antiangiogenic cancer drugs. The aim of the first part of this thesis is the development of inhibitors of MT-MMP1 that target the less-conserved PEX domain, based on a compound previously described in literature. A SAR of the compound class should be established by varying the two parts of the molecule. Therefore, two libraries of derivatives should be generated. On one hand, the activity of the newly synthesized compounds should be evaluated in a novel *in vitro* 3D migration assay using different kinds of cancer cells. On the other hand, the affinity of the compounds towards the recombinant PEX domain of MT-MMP1 should be proven using biophysical analysis methods, such as surface plasmon resonance spectroscopy. In a final step, selectivity of the newly synthesized active compounds towards other MMPs should be evaluated.

The second part of this work was aimed at the development of novel 17β-HSD2 inhibitors for the treatment of estrogen-dependent diseases such as delayed bone fracture healing and osteoporosis. The concept of targeted therapy should be transferred to this kind of diseases as well, as traditional therapies, such as systemic administration of estradiol, are accompanied with severe side effects like an increased risk of breast cancer and stroke. Therefore, an optimization procedure should be performed to obtain 17β-HSD2 inhibitors with high activity on both human and mouse enzyme. After assessment of *in vitro* metabolic stability using human liver S9 fraction, hepatic cytochrome P450 enzyme induction as well as affinity towards the estrogen receptor, the most promising compounds should be tested in a pharmacokinetic study in mice to evaluate plasma levels of the compounds after subcutaneous injection. The most suitable compound should be tested in a mouse *proof-of-principle* study for 14 days to investigate its bone fracture healing properties and hence validate the concept of targeted endocrine therapy. The readout of the experiments should be performed by biomechanical testing of bending stiffness of the bones, biochemical markers, as well as determination of circulating estradiol and testosterone levels in the animals.

In a next step, the previously described class of 17β-HSD2 inhibitors should be optimized for application as a potential osteoporosis medicine. For this kind of disease, peroral application of the drug is mandatory, as therapy duration often lasts several decades. Therefore, the compounds should be decreased in size and increased in solubility and *in vitro* metabolic stability, while at least maintaining the promising activity of this class. Based on SAR findings in the field of 17β-HSD1 inhibitors, the compound should be modified. Newly synthesized compounds should then be tested for their activity on both human and mouse 17β-HSD2 and 1, and the most promising compounds should be tested regarding their *in vitro* ADME profile. After metabolic stability evaluation in both human and mouse liver S9 fraction, solubility and CYP inhibition of the compounds should be evaluated. In a final step, the best compounds should be tested in a mouse PK study in mice following oral administration.

3. Results

3.1. Chapter I: Towards allosteric MMP inhibition: SAR studies of arylamides lead to selective MMP inhibitors for anti-angiogenic cancer therapy and beyond

The autor thanks the following coworkers for contributing in the experimental work described in this chapter:

Ingrid de Vries:	Performed the biological assays
Victor Hernandes-Olmos:	Performed parts of the synthetic chemical work and characterization of novel compounds
Sabrina Schnur:	Performed synthesis and purification of some compounds

INTRODUCTION

Cancer is generally characterized by the abnormal growth of malignant cells inside a specific tissue with the ability to spread to other parts of the body. As cancer cells grow, tumors are formed, whose growth rate is dependent on nutrient supply by the surrounding tissues. To achieve this optimal supply, tumors induce the growth of new vasculature, called the angiogenetic switch.[1] This phenomenon describes the shift towards pro angiogenic factors inside the tumor-host microenvironment in a para- or autocrine manner, resulting in breakdown of the basement membrane by endothelial cells. These cells themselves start to move through the extracellular matrix (ECM) and form new blood vessels towards the stimuli given by tumor[2], as do cancer cells move through the ECM towards blood capillaries or lymph nodes as metastases are formed.[3] Matrix – metalloproteinases (MMPs) are a class of multidomain - enzymes containing 28 members that proteolytically degrade all components of the ECM and are highly upregulated in various cancer types.[4] Recent findings have changed the understanding how these enzymes are involved in tumorigenesis. Besides their proteolytic activity on structural components of the ECM, e.g. collagen, these enzymes are also involved in the release of pro- and antiangiogenic factors and are now considered key players in modulation of the tumor microenvironment, with dysregulation driving tumor progression.[5] Furthermore, certain MMPs play a critical role in cell migration occurring in tumorigenesis.[6,7] The development of MMP inhibitors as angiostatic and anti-invasive agents is hence an attractive approach for novel cancer therapy and different broad spectrum inhibitor classes targeting the active site of the proteases have been identified.[8] However, all clinical trials of MMP inhibitors for cancer therapy so far have been unsuccessful, due to strong side effects, no measurable benefit or even worse patient outcome compared to control groups, threated with classical chemoterapeutics.[9] Besides inadequate study endpoints and therapy onset for different cancer types, lack of selectivity of the designed inhibitors towards other zinc proteases is the commonly accepted explanation for the negative outcomes of MMP inhibitor clinical trials.[10] These inhibitors bind to the catalytic domain (CAT) of the MMPs, which incorporates a Zn^{2+} ion. The structure of this active site is highly conserved amongst a whole superfamily of zinc proteases, so called metzincins[11], thus hampering the drug discovery process for selective MMP inhibitors. A potential approach to circumvent the selectivity issue is the development of so called “exosite binders”, compounds that inhibit MMPs in an allosteric manner by targeting other less structurally conserved domains as the CAT domain.[12] Amongst the whole metzincin metalloprotease family, the hemopexin domain (PEX) is only found in a subset of MMPs and it is structurally less conserved than the CAT domain, making this exosite a highly suitable binding site for a selective MMP inhibitor design approach. The domain is involved in various actions of MMPs, including triple helicase activity, dimerization, MMP activation, substrate binding and endocytosis activity.[13] Amongst the human MMPs bearing a PEX exosite, the membrane-bound MT1-MMP ((membrane type 1 – MMP) is considered an attractive target in anti-angiogenic drug discovery.[14] The PEX domain of MT1-MMP is involved in binding and activation of MMP2[15], resulting in degradation of the basement membrane by MMP2/9[16], which leads to tumor cell migration and angiogenesis.[17–19] It is also involved in shedding of gC1qR on the surface of proliferating cells, a receptor of complement component 1q, which, in a soluble form, impairs the immune response to cancer cells mediated by the complement system.[20] Furthermore, the PEX domain of MT1-MMP binds to CD44H, a receptor for ECM components on the cell surface, leading to colocalization of the MT1-MMP/CD44H complex to the invading edge of the cell.[21,22] Moreover, the PEX domain has shown to play an important role of MT1-MMP processing via clathrin mediated endocytosis[23] or tetraspanin mediated trafficking.[24] The PEX domain is also needed for cleavage of native collagen type I fibers by MT1-MMP, exerting triple helicase activity to unwind collagen fibers, making the substrate susceptible for proteolytic degradation.[25,26] Taken together, these findings underline the important role of the MT1-MMP PEX domain in cancer cell movement through tissue and angiogenesis.[14] Recently, Remacle et al identified a PEX binder of MT1-MMP (**A**, chart 1) by an *in silico* screening approach, docking a library provided by the NIH into the tunnel in the center of the PEX domain.[27] They showed that compound **A** does not inhibit catalytic activity of MT1-MMP towards a fluorescently labeled small peptide substrate and that intertumoral application of **A** in a mice xenograft model using MCF-7 cells caused small fibrotic tumors with similar phenotype compared to a ΔPEX mutant *in vivo*. However, the question remains doubtful whether the effect seen in the animal model originates from an interaction of **A** with the PEX domain of MT1-MMP or from an off-target effect. Furthermore, the low potency of the compound hinders further *in vivo* evaluation. In this study, we describe a two-step optimization process of compound **A** following a ligand-based approach. Utilizing a cellular 3D collagen invasion model with three different cancer cell lines yielded compounds with highly improved potency. Furthermore, screening against a panel of MMPs revealed a good selectivity profile towards other MMPs, enabling further *in vivo* studies.

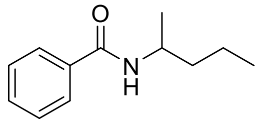

A

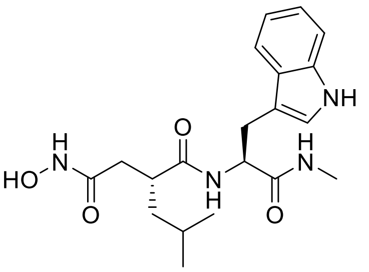

GM6001

Chart 1. Reference compounds used in this study: Literature described MMP14-PEX inhibitor **A** and active site hydroxamate MMP inhibitor **GM6001.**

DESIGN

Starting point of the study was Compound **A** (chart 1), which was identified by Remacle et al by an *in silico* screening approach.[27] They could show that intertumoral injection of **A** in a mouse xenograft model resulted in tumors significantly reduced in size compared to the control and in a tumor phenotype that resembles the ΔPEX mutant. Furthermore, they could show that **A** inhibits homodimerization of the PEX domain of MT1-MMP, cell migration and degradation of collagen type 1 (COL-I) *in vitro*, while not inhibiting the proteolytic activity of MT1-MMP towards small oligopeptidic substrates. However, low potency of **A** as well as poor solubility hinders further biological evaluation and so far, no SAR studies of this compound class have been reported. Therefore, we performed a ligand-based, two-step optimization process of **A**, resulting in compounds with highly improved potency. A combinatorial chemistry platform was used to generate two libraries (chart 2).

Chart 2. Designed & synthesized inhibitors

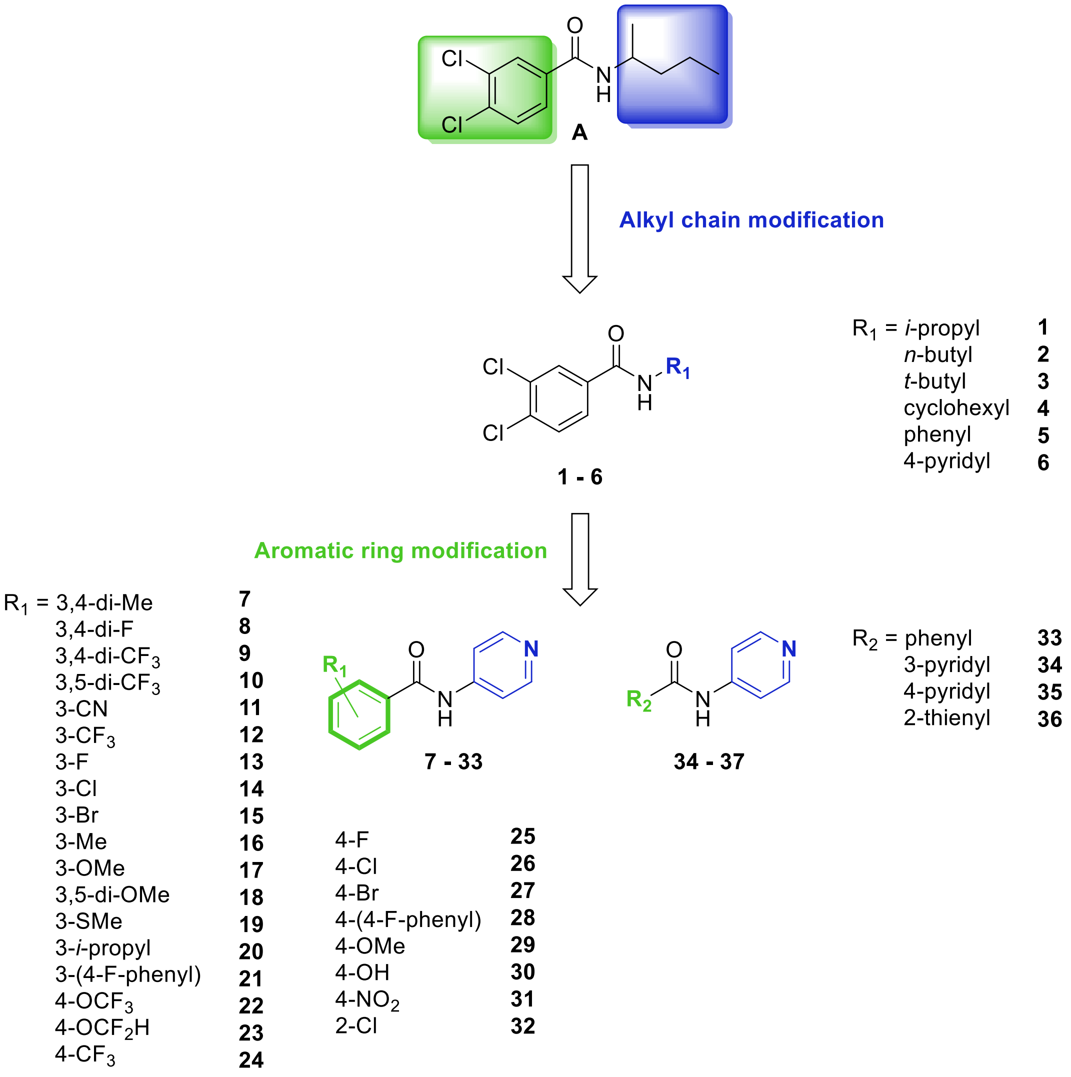

A

1 - 6

R$_1$ = *i*-propyl	**1**
n-butyl	**2**
t-butyl	**3**
cyclohexyl	**4**
phenyl	**5**
4-pyridyl	**6**

7 - 33

R$_1$ = 3,4-di-Me	**7**
3,4-di-F	**8**
3,4-di-CF$_3$	**9**
3,5-di-CF$_3$	**10**
3-CN	**11**
3-CF$_3$	**12**
3-F	**13**
3-Cl	**14**
3-Br	**15**
3-Me	**16**
3-OMe	**17**
3,5-di-OMe	**18**
3-SMe	**19**
3-*i*-propyl	**20**
3-(4-F-phenyl)	**21**
4-OCF$_3$	**22**
4-OCF$_2$H	**23**
4-CF$_3$	**24**
4-F	**25**
4-Cl	**26**
4-Br	**27**
4-(4-F-phenyl)	**28**
4-OMe	**29**
4-OH	**30**
4-NO$_2$	**31**
2-Cl	**32**

34 - 37

R$_2$ = phenyl	**33**
3-pyridyl	**34**
4-pyridyl	**35**
2-thienyl	**36**

The first one consists of molecules differing in size and branching of the alkyl chain, as well as saturated and aromatic six-membered rings (chart 2, compounds **1** – **6**). Evaluation of the compounds in a collagen 3D-invasion assay using HT1080 fibrosarcoma cells resulted in compounds with improved potency compared to **A**. In the second library, the aromatic moiety of **A** was modified with a broad structural diversity of the substituents, resulting in compounds **7 - 37**. Isosteric replacement of the chlorine substituents was performed and their positions on the phenyl ring were evaluated. Moreover, different hydrophilic substituents and heterocycles were introduced to gain deeper insight into the SAR of this compound class. Highly improved activity was achieved within the second library, depending on the substituent size and position, with **21** being ten times more potent than reference compound **A**.

CHEMISTRY

All described compounds were synthesized following a one-step to two-step reaction protocol. An EDC/HBTU utilized amide coupling procedure in DMF with 4-methylmorpholine as base was employed to generate the arylamides in high yields from commercially available arylcarboxylic acids and the corresponding alkyl- or arylamines. Compounds **21** and **28** were synthesized from their corresponding bromides **15** and **27** with 4-fluorophenyl boronic acid using a Suzuki coupling standard protocol.

BIOLOGY

Inhibition of HT1080 cell 3D collagen-I invasion

Compounds synthesized were tested for their inhibition of MT1-MMP activity using a HT1080 fibrosarcoma spheroid 3D invasion assay into a collagen-I matrix.[28] Besides the poor patient prognosis and hence the high need for drugs acting on this kind of cancer[29], this cell line thrives under *in vitro* conditions as spheroids in a 3D cellular culture, which allows assay conditions superior compared to conventional 2D culture techniques.[30] Moreover, HT1080 cells show high levels of MT1-MMP expression[31] and invasion of this cell into collagen matrices has been directly correlated with MT1-MMP activity via the PEX domain[28,32], which makes the assay highly suitable to study interactions of the described inhibitors with the PEX domain of MT1-MMP. In a first optimization step, the branched alkyl chain of **A** was subsequently modified to study the SAR of this part of the molecule (chart 2), the results at 100 µM inhibitor concentration are depicted in table 1.

Table 1. Activity data of Compounds **1 - 36**

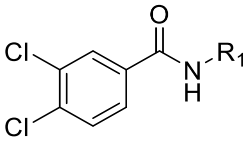

A, 1 - 6

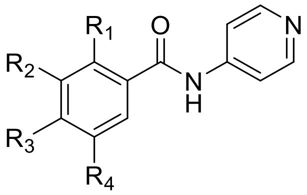

7 - 33

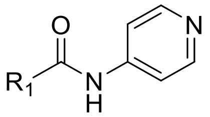

34 - 36

Cmpd	**R1**	**R2**	**R3**	**R4**	**Inhibition HT-1080**^{a,d}
A	2-pentyl				52 % (100 µM)
1	2-propyl				36 % (100 µM)
2	*n*-butyl				34 % (100 µM)
3	*t*-butyl				44 % (100 µM)
4	cyclohexyl				n.i.
5	phenyl				26 % (100 µM)
6	4-pyridyl				72 % (100 µM) 28 % (50 µM)
7		Me	Me	H	41 % (50 µM)
8		F	F	H	n.i.
9		CF_3	CF_3	H	32 % (50 µM)
10		CF_3	H	CF_3	49 % (50 µM)
11		CN	H	H	n.i.
12		CF_3	H	H	26 % (50 µM)
13		F	H	H	10 % (50 µM)
14		Cl	H	H	44 % (50 µM)
15		Br	H	H	57 % (50 µM)
16		Me	H	H	62 % (50 µM)
17		OMe	H	H	19 % (50 µM)
18		OMe	H	OMe	1.2 % (50 µM)
19		SMe	H	H	46 % (50 µM)

20		Isopropyl	H	H	53 % (50 μM)
21		4-F-Phenyl	H	H	52 % (10 μM)
22		H	OCF_3	H	2.5 % (50 μM)
23		H	OCF_2H	H	10 % (50 μM)
24		H	CF_3	H	19 % (50 μM)
25		H	F	H	24 % (50 μM)
26		H	Cl	H	19 % (100 μM)
27		H	Br	H	28 % (50 μM)
28		H	4-F-Phenyl	H	6.5 % (100 μM
29		H	OMe	H	6.0 % (50 μM)
30		H	OH	H	5.1 % (50 μM)
31		H	NO_2	H	5.5 % (50 μM)
32	Cl	H	H	H	40 % (100 μM)
33	H	H	H	H	8.6 % (100 μM)
34	3-pyridyl				n.i.
35	4-pyridyl				n.i.
36	2-thienyl				n.i.

[a]Mean value of at least two experiments. The deviations were <30%. [b]single value. [d]HT1080 collagen I invasion. [e]Cell viability > 85 %; n.t. not tested; n.i. inhibition, < 5 % at 100 μM;

Truncation of the alkyl chain to either a isopropyl- (**1**, 36%) or a linear butyl-residue (**2**, 34%) leads to a decrease in activity compared to the pentyl compound **A** (52%), as does further branching to the *tert*.-butyl compound (**3**, 44%). Introduction of the bulkier cyclohexyl residue (**4**, no inhibition) shows that there is limited space in the pocket at this side of the molecule. Exchange with the smaller phenyl analogue (**5**, 26%) is tolerated, but leads to a decrease in activity compared to **A** (52%). The increased activity of the 4-pyridyl compound (**6**, 72%) compared to **A** could be due to additional H-bond interactions deeper inside the pocket or favorable π-interactions of the pyridine ring. In the next optimization step, the role of the substituents on the phenyl ring of **A** were evaluated. Therefore, a library of 30 compounds was synthesized (chart 2), varying position, size and electronic properties of the substituents. For all newly synthesized compounds in this library, the 2-pentyl residue of **A** was exchanged with the 4-pyridyl moiety of **6**, based on the results of the first optimization step. Compounds have been tested at 50 µM concentration, the results are also depicted in table 1. Isosteric replacement of the two chlorine- to methyl- substituents (**7**, 41%) leads to increased activity compared to **6** (28%). Total loss of activity by exchange of chlorine by the smaller fluorine (**8**, no inhibition) points out the necessity of bigger, rather than electronegative substituents in these positions. Exchange by CF_3 (**9**, 32%) is tolerated by the enzyme compared to **6** (28%), but decreases activity compared to the methyl analogue (**7**, 41%). Moving the *p*-CF_3 to the second *m*-position increases activity compared to the *m,p*-substituted compound (**10**, 49% vs. **9**, 32%), indicating that substitution on the *m*-position is more important for activity than the *p*-position. Looking at the *m*-monosubstituted compounds, introduction of a nitrile group in *m*-position leads to a complete loss of activity (**11**, no inhibition) compared to the single substituted *m*-CF_3 (**12**, 26%), which is almost as active as the *m,p*-disubstituted compound **9** (32%). The loss of activity observed by the nitrile compound might be due to the necessity of a bigger, more lipophilic, rather than a hydrophilic electron-withdrawing substituent in this position. This observation can also be made when looking at the halogen compounds **13-15**, with the bromine-substituted compound (**15**, 57%) being the most active in this row. Switching to electron-donating moieties, the *m*-methyl compound **16** (62%) is so far the most active compound and more active than the di-methyl compound **7** (41%). Introduction of a methoxy- or di-methoxy residues is not well accepted by the enzyme (**17**, 19%, **18**, 1.2%), while the more lipophilic thioether **19** (46%) shows a high inhibition value, as well as the isopropyl derivative **20** (53%). Introduction of an additional phenyl ring in the *m*-position leads to the highly active compound **21** (52% at 10 µM), which is the most active one described in this study, with an activity ten times higher than reference compound **A** (52% at 100µM). Moving to the single *p*-substituted compounds, inside the halogen series **25-27**, the *p*-bromo compound is the most active one (**27**, 28%), but less active than its *m*-analogue (**15**, 57%), as this can also be seen for the chlorine (**26**, 19% at 100µM vs. **14**, 44% at 50 µM). In contrast to the *m*-substituted compounds, introduction of an additional phenyl ring in *p*-position does not lead to increased activity (**28**, 6.5% at 50µM vs **21**, 52% at 10 µM), indicating that the pocket is too small in this position for the substituent. Introduction of hydrophilic substituents in the *p*-position is also not accepted by the enzyme (**29**, 6%, **30**, 5.1%, **31**, 5.5%), as seen for the *m*-methoxy analogue (**17**, 19%). The lack of activity of the more fragment-like compounds **33-36** points out the necessity of an additional substituent on the phenyl ring (**33,** 8.6%, **34-36,** no inhibition).

Further biological investigation of MT1-MMP PEX inhibitors

To validate the applicability of the described MT1-MMP PEX inhibitors, collagen invasion of two other cancer cell lines expressing MT1-MMP in a 3D culture model was investigated. Incubation of compound **21** at 10 µM concentration with U87 cells, a cell line derived from glioblastoma multiforme, a highly aggressive brain cancer difficult to target with poor patient outcome[33], showed equally high inhibition values of collagen invasion as previously obtained results on the HT1080 cell line compared to DMSO controls (figure 1). Similar high activity of **21** was observed upon incubation with triple negative breast cancer cell line MBA-MD-231, also a form of cancer highly likely to metastasize with low survival rates. For the experiments, first-generation MMP inhibitor GM6001 was used as a positive control. These findings illustrate the potential of MT1-MMP PEX inhibitors not only to be employed by a small subset of cancer treatments, but to be utilized as more broad-spectrum agents for cancer therapy.

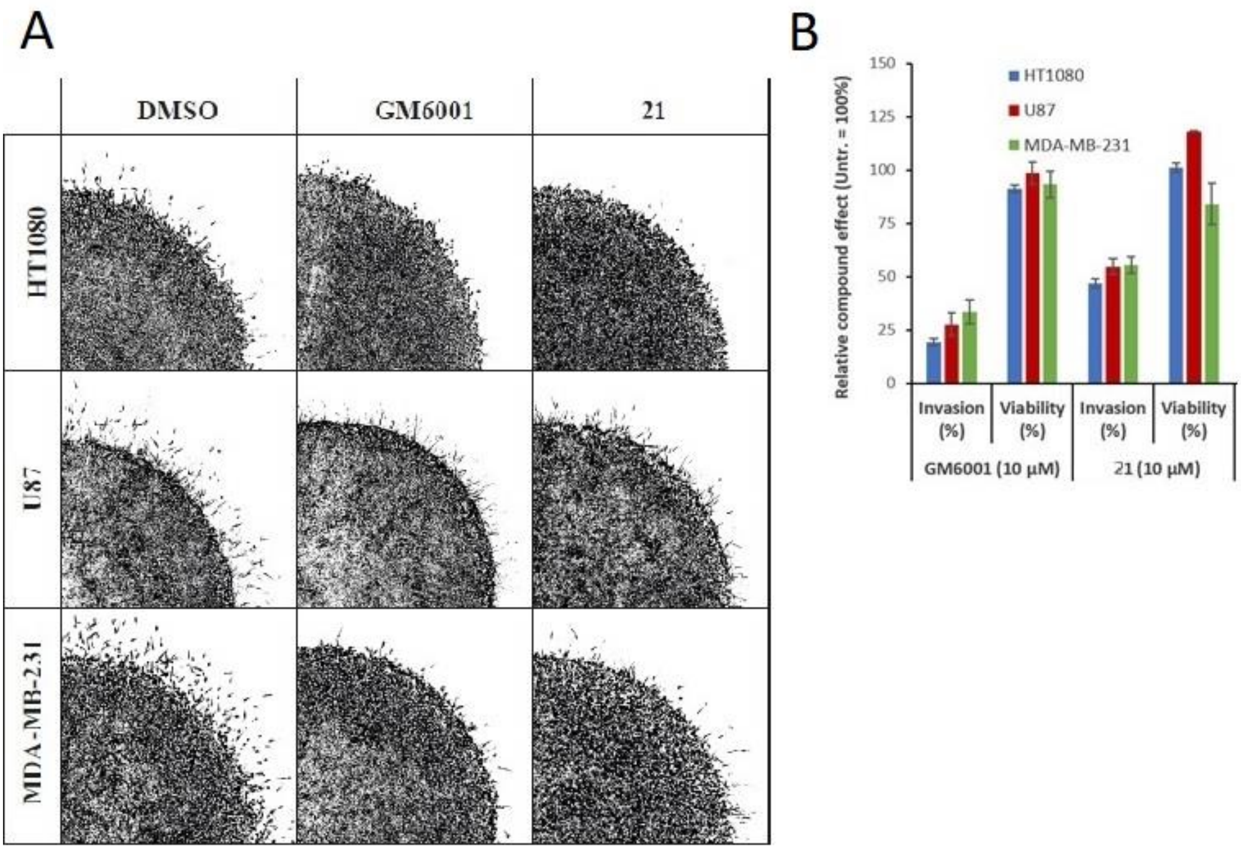

Figure 9 A. Newly identified MMP14 inhibitors inhibit the 3D collagen-I invasion of cell lines from different origin (HT1080 = fibrosarcoma, U87 = glioblastoma, MDA-MB-231 = breast carcinoma), proving the general applicability of these identified MMP14 inhibitors. **B.** Representative example of the invasion spots of cell lines from different origin, that were treated with 10 µM DMSO, GM6001 or **21.**

Inhibition of other MMPs

Lack of selectivity over other MMPs and other members of the methzincin enzyme superfamily is the main cause of failure of MMP inhbitiors in clinical trials so far.[34] The highly conserved active site makes the design of selective MMP inhibitors a difficult task and novel strategies are required to address this issue.[12] Targeting exosites, additional substrate binding sites, different than the active site, is a promising approach to inhibit MMPs in a highly selective allosteric manner.[35] Inhibition of MMP function by targeting the PEX domain can be seen as a superior strategy compared to active site inhibitors in multiple ways. Looking at the superfamily of methzincin enzymes, MMPs are the only family which feature a PEX domain, thus PEX inhibitors are MMP selective inside this superfamily of enzymes. Furthermore, only a fraction of MMPs incorporate a PEX domain[13], which further increases the selectivity of the approach. To further investigate selectivity of the described inhibitors amongst MMPs, we tested the inhibitory activity of selected compounds towards soluble MMPs with a narrow substrate profile compared to MT1-MMP (Table 2).

Table 2. Inhibition of other MMPs by compounds **A, 21- 28**

Cmpd	MMP1	MMP2	MMP8	MMP9	MMP13
A	n.t.	n.i. (10µM)	n.t.	n.i. (10µM)	5.8% (50µM)
21	n.i. (10µM)	3% (10µM[a]	n.i. (10µM)	2.2% (10µM)[a]	8.7% (10µM)[a]
22	n.i.	46%[a] 8.2%(10µM)	12.6%	4.2%[a]	91%[a] 47% (10µM)[a]
23	n.i.	60%	19%	13%	85%
24	n.i. (50µM)	30%	n.i. (50µM)	3.4%[a]	81%[b] 29% (10µM)
28	n.i. (10µM)	36% (10µM)[a]	n.i. (50µM)	n.i. (10µM)[a]	86% (10µM)[b]

single values; n.t. not tested; n.i. no inhibition < 1 % [a]Mean value of at least two experiments. The deviations were <10%; [b]S.D. > 15 %

Tested compounds did not inhibit the cleavage of a small peptide fragment by any of the investigated MMPs (data not shown), which is not surprising since the PEX domain is not needed for cleavage of such a small substrate. This finding points out the possibility of this compound class for selective inhibition of MMPs towards specific substrate types. In a next step, inhibition of compounds towards the cleavage of fluorescently labelled triple-helical COL-I, a substrate that can only be cleaved with the help of the triple helicase function of the PEX domain. Inhibition of the different MMPs at 100 µM inhibitor concentration or below was assessed, the results are depicted in table 2. Remarkably, *meta*-substituted compound **21**, the most active inhibitor of MT1-MMP described in this study, shows no to only very weak inhibition of the tested MMPs at 10µM, which is approximately its IC_{50} determined in the HT1080 invasion assay (MMP1 & 8, no inhibition, MMP2, 3%, MMP9, 2.2%, MMP13, 8.7% Inhibition), making **21** a highly selective compound. Moving to the *para*-substituted compounds **22-28**, these compounds show high inhibition values towards other MMPs. Trifluoromethylether-substituted **22** as well as its analogues **23** & **24** show high inhibition values towards MMP2 (**22**, 46%, **23**, 60%, **24**, 30%) and MMP13 (**22**, 91%, **23**, 85%, **24**, 91%) indicating that the more linear shape of these molecules is beneficial for binding to the PEX domain of these two MMPs. The *p*-substituted analogue of **21**, **28** shows a high inhibition value of MMP13 (86% at 10µM), being more potent on MMP13 than the *m*-substituted analogue **21** in the HT1080 invasion assay (52% at 10µM). MMP13 itself is a promising target for the treatment of osteoarthritis[36] and rheumatoid arthritis[37], but the issue is currently under investigation will be discussed in a different article. These findings underline the possibility of this compound class to inhibit different MMPs in a highly potent and selective manner, depending on the overall geometry of the molecule. Furthermore, by not inhibiting cleavage of substrates that don't require the PEX domain, selective inhibition towards different substrate types could be achieved.

CONCLUSION

MMPs are considered promising targets for cancer therapy.[5] Despite tremendous effort over decades to develop MMP inhibitors with high selectivity and potency, clinical trials with MMP inhibitors have so far not been successful due to promiscuous inhibition of various metalloproteases.[9] Recently, Remacle et al.[27] identified compound **A** by an *in silico* approach as a MT1-MMP PEX "exosite" binder to inhibit the enzyme in an allosteric manner. The aim of this study was to establish a structure-activity relationship of this compound class towards inhibition of MT1-MMP function, a MMP that is highly upregulated in different cancer types and considered a key player in cancer cell motility and angiogenic growth.[14] A HT1080 fibrosarcoma cell spheroid 3D-culture based invasion assay was used to assess the activity of newly synthesized compounds. Following a two-step optimization process of **A**, first the role of the alkyl chain of **A** was investigated, which could be substituted by a pyridine moiety, resulting in compound **6** with increased activity. In a second step the substituents on the aryl moiety were optimized, resulting in compound **21** with highly improved activity compared to **A** (52% at 100 µM vs 52% at 10µM). Furthermore, a SAR could be obtained depicting the role of the substituents upon MMP binding. Activity of **21** was validated by measuring inhibition of cell migration of glioblastoma U87 and triple negative breast cancer cell line MBA-MD-231, underlining the applicability of the studied MT1-MMP PEX inhibitors for different kinds of cancer. Screening of the studied inhibitors against a whole panel of MMPs revealed a good selectivity profile with the possibility of this compound class to selectively inhibit specific MMPs, as well as specific MMP substrate cleavage, which in the end could lead to highly selective MMP inhibitors for cancer treatment and other diseases like osteoarthritis.

CHEMICAL METHODS

Chemical names follow IUPAC nomenclature. Starting materials were purchased from Aldrich, Acros, Lancaster, Maybridge, Combi Blocks, Merk, or Fluka and were used without purification. In case of preparative HPLC purification the compounds were purified using a setup produced by Waters Corporation containing a 2767 Sample Manager, a 2545 binary gradient pump, a 2998 PDA detector and a 3100 electron spray mass spectrometer. The system has been used for a part of the analytical analysis as well as the preparative separation. In the latter case after separation the solvent flow has been split using a flow splitter and a 515 HPLC pump for makeup flow. Water containing 0.1% formic acid and acetonitrile containing 0.1%formic acid were used as solvents for the analysis and separation. A Machery-Nagel C18-ec column (C18, 150 x 4.6 mm, 5 µM) has been used with a flow of 1 ml/min for the analysis and a Waters X-Bridge column (C18, 150 x 19 mm, 5 µM) has been used with a flow of 20 ml/min for the separation.^{1}H NMR spectra were measured on a Bruker AM500 spectrometer (500 MHz) at 300 K or on a Bruker Fourier300 (300 MHz) at 295.5 K. Chemical shifts are reported in δ (parts per million: ppm), by reference to the hydrogenated residues of deuteriated solvent as internal standard ($CDCl_3$: δ = 7.24 ppm (^{1}H NMR) and δ = 77 ppm (^{13}C NMR), CD_3OD: δ = 3.31 ppm (^{1}H NMR) and δ = 49.3 ppm (^{13}C NMR), CD_3COCD_3: δ = 2.05 ppm (^{1}H NMR) and δ = 29.9 ppm (^{13}C NMR), CD_3SOCD_3 δ = 2.50 ppm (^{1}H NMR) and δ = 39.5 ppm (^{13}C NMR)). Signals are described as s, br. s, d, t, dd, ddd, m, dt, q, sep for singlet, broad singlet, doublet, triplet, doublet of doublets, doublet of doublets of doublets, multiplet, doublet of triplets, quadruplet, and septet respectively. All coupling constants (*J*) are given in hertz (Hz).Mass spectra (ESI) have been recorded on the system mentioned above. Tested compounds are >95% chemical purity as measured by HPLC.

General procedure for amide coupling (Method A)

In a dry flask with stirring bar, the corresponding benzoic acid (1 equiv.) and HBTU (1.5 equiv) were placed under argon and then dissolved in dry DMF (0.06 M). The corresponding amine (1.1 equiv.) and *N*-methylmorpholine (6 equiv.) were added at 0 °C and the reaction mixture was stirred for one hour at 0 °C. EDCCl (1.5 equiv) was added and the resulting solution was stirred at room temperature overnight. The mixture was diluted with water and extracted with ethyl acetate (3x). The combined organic layers were dried over $MgSO_4$, filtered and concentrated in vacuo to obtain the crude compounds, which were purified using either Biotage column chromatography or preparative HPLC.

BIOLOGICAL METHODS

Cellular 3D collagen-I invasion assays

Invasion of the cells into Col-I matrix was assed using a procedure similar to the literature described.[28] To describe the procedure briefly, cell-collagen spheroids were covered with a Col-I and preincubated at 37 °C. The assay was started by addition of medium containing either DMSO or the inhibitor. After 16h of incubation, invaded cells were stained using Hoechst 33342 dye for total cell number and propidium iodide for staining of dead cells, followed by PBS washing. Invading cells were then counted using fluorescence microscopy. In each experiment, GM6001 and DMSO were used as controls.

Inhibition of DQ-Col-I degradation by MMPs in cell-free assay

The assay was performed according to standard protocol similar described here.[38] Briefly, inhibitors in DMSO were diluted with reaction buffer (50 mM Tris-HCl, 150 mM NaCl, 5 mM $CaCl_2$, pH 7.6) to the desired concentration and fluorescently labeled DQ Collagen I in water was added to each well; Incubation was started by addition of the desired MMP in reaction buffer; Kinetic curves were recorded using a fluorescence microplate reader (495 nm absorption, 515 nm emission). Inhibitor GM6001 and pure DMSO were used as negative and positive controls.

3,4-Dichloro-*N*-isopropylbenzamide (1). The title compound was prepared by reaction of 3,4-dichlorobenzoic acid (95.5 mg, 0.5 mmol), *iso*-propylamine (32.5 mg, 0.55 mmol), HBTU (284 mg, 0.75 mmol), EDCCl (144 mg, 0.75 mmol) and *N*-methylmorpholine (303 mg, 3.00 mmol) according to method A. The product was purified by Biotage CC; yield: 76% (88.2 mg); ^1H NMR (300 MHz, $CDCl_3$, δ): 1.27 (d, J=6.5 Hz, 6 H) 4.26 (dt, J=7.7, 6.6 Hz, 1 H) 7.50 (d, J=8.4

Hz, 1 H) 7.57 (dd, J=8.4, 2.0 Hz, 1 H) 7.83 (d, J=2.0 Hz, 1 H).; MS (ESI): 232.1 $(M+H)^+$; UV λ (nm) = 234; Rf HPLC: 10.37 Min (13 Min 10 – 95% MeCN in water with 0.1% formic acid); Purity 99 %.

***N*-Butyl-3,4-dichlorobenzamide (2).** The title compound was prepared by reaction of 3,4-dichlorobenzoic acid (95.5 mg, 0.5 mmol), butylamine (40.2 mg, 0.55 mmol), HBTU (284 mg, 0.75 mmol), EDCCl (144 mg, 0.75 mmol) and *N*-methylmorpholine (303 mg, 3.00 mmol) according to method A. The product was purified by Biotage CC; yield: 69% (84.4 mg); ^1H NMR (300 MHz, $CDCl_3$, δ): 0.83 - 1.03 (m, 3 H) 1.31 - 1.48 (m, 2 H) 1.49 - 1.69 (m, 2 H) 3.45 (td, J=7.1, 5.8 Hz, 2 H) 6.04 (br. s., 1 H) 7.50 (d, J=8.2 Hz, 1 H) 7.58 (dd, J=8.2, 2.0 Hz, 1 H) 7.85 (d, J=2.0 Hz, 1 H); MS (ESI): 246.1 $(M+H)^+$; UV λ (nm) = 233; Rf HPLC: 11.38 Min (13 Min 10 – 95% MeCN in water with 0.1% formic acid); Purity 97 %.

***N*-(Tert-butyl)-3,4-dichlorobenzamide (3).** The title compound was prepared by reaction of 3,4-dichlorobenzoic acid (95.5 mg, 0.5 mmol), tert.butylamine (40.22 mg, 0.55 mmol), HBTU (284 mg, 0.75 mmol), EDCCl (144 mg, 0.75 mmol) and *N*-methylmorpholine (303 mg, 3.00 mmol) according to method A. The product was purified by Biotage CC; yield: 67% (82.9 mg); ^1H NMR (300 MHz, $CDCl_3$, δ): 1.47 (d, J=1.3 Hz, 9 H) 7.48 (d, J=1.0 Hz, 1 H) 7.53 (d, J=1.0 Hz, 1 H) 7.80 (s, 1 H); MS (ESI): 246.2 $(M+H)^+$; UV λ (nm) = 234, 280 (sh); Rf HPLC: 11.60 Min (13 Min 10 – 95% MeCN in water with 0.1% formic acid); Purity > 99 %.

3,4-Dichloro-*N*-cyclohexylbenzamide (4). The title compound was prepared by reaction of 3,4-dichlorobenzoic acid (95.5 mg, 0.5 mmol), cyclohexylamine (54.5 mg, 0.55 mmol), HBTU (284 mg, 0.75 mmol), EDCCl (144 mg, 0.75 mmol) and *N*-methylmorpholine (303 mg, 3.00 mmol) according to method A. The product was purified by Biotage CC; yield: 74% (100 mg); ^1H NMR (300 MHz, $CDCl_3$, δ): 1.09 - 1.33 (m, 3 H) 1.33 - 1.54 (m, 2 H) 1.54 - 1.86 (m, 3 H)

1.92 - 2.17 (m, 2 H) 3.81 - 4.12 (m, 1 H) 5.91 (br. s., 1 H) 7.49 (d, J=8.3, 1 H) 7.57 (d, J=8.3, 1.0 Hz, 1 H) 7.83 (s, 1 H); MS (ESI): 272.2 $(M+H)^+$; UV λ (nm) = 233; Rf HPLC: 12.21 Min (13 Min 10 – 95% MeCN in water with 0.1% formic acid); Purity 98 %.

3,4-Dichloro-*N*-phenylbenzamide (5). The title compound was prepared by reaction of 3,4-dichlorobenzoic acid (95.5 mg, 0.5 mmol), aniline (51.2 mg, 0.55 mmol), HBTU (284 mg, 0.75 mmol), EDCCl (144 mg, 0.75 mmol) and *N*-methylmorpholine (303 mg, 3.00 mmol) according to method A. The product was purified by Biotage CC; yield: 70% (93.6 mg); ^{1}H NMR (300 MHz, $CDCl_3$, δ): 7.13 - 7.22 (m, 1 H), 7.38 (t, J=7.9 Hz, 2 H), 7.52 - 7.66 (m, 3 H), 7.69 (dd, J=8.2, 1.9 Hz, 1 H), 7.76 (br. s., 1 H), 7.96 (d, J=1.9 Hz, 1 H); MS (ESI): 266.2 $(M+H)^+$; UV λ (nm) = 269; Rf HPLC: 11.89 Min (13 Min 10 – 95% MeCN in water with 0.1% formic acid); Purity 99 %.

3,4-Dichloro-*N*-(pyridin-4-yl)benzamide (6). The title compound was prepared by reaction of 3,4-dichlorobenzoic acid (57.3 mg, 0.3 mmol), 4-aminopyridine (31.1 mg, 0.33 mmol), HBTU (171 mg, 0.45 mmol), EDCCl (86.3 mg, 0.45 mmol) and *N*-methylmorpholine (182 mg, 1.8 mmol) according to method A. The product was purified by preparative HPLC; yield: 43 % (34.1 mg); ^{1}H NMR (300 MHz, MeOD, δ): 8.65 (d, *J* = 5.7 Hz, 2 H), 8.34 (d, *J* = 5.7 Hz, 2 H), 8.22 (d, *J* = 2.1 Hz, 1 H), 7.95 (dd, *J* = 8.4, 2.1 Hz, 1 H), 7.76 (t, *J* = 8.4 Hz, 1 H); MS (ESI): 267.2 $(M+H)^+$; UV λ (nm) = 279; Rf HPLC: 5.98 Min (13 Min 10 – 95% MeCN in water with 0.1% formic acid); Purity 99 %.

3,4-Dichloro-*N*-(pyridin-4-yl)benzamide (7). The title compound was prepared by reaction of 3,4-dimethylbenzoic acid (45.1 mg, 0.3 mmol), 4-aminopyridine (31.1 mg, 0.33 mmol), HBTU (171 mg, 0.45 mmol), EDCCl (86.3 mg, 0.45 mmol) and *N*-methylmorpholine (182 mg, 1.8 mmol) according to method A. The product was purified by preparative HPLC; yield: 24 % (19.5 mg, formiate salt); ^{1}H NMR (300 MHz, MeOD, δ): 8.45 (d, *J* = 3.6 Hz, 2 H), 8.16 (br s, 1 H), 7.90 (d, *J* = 5.4 Hz, 1 H), 7.75 (s, 1 H), 7.69 (d, *J* = 8.1 Hz, 1 H), 7.29 (d, *J* = 8.1 Hz, 1 H), 2.36 (s, 3 H), 2.35 (s, 3 H); MS (ESI): 225.2 $(M-H)^+$; UV λ (nm) = 283; Rf HPLC: 5.48 Min (13 Min 10 – 95% MeCN in water with 0.1% formic acid); Purity ≥99 %.

3,4-Difluoro-*N*-(pyridin-4-yl)benzamide (8). The title compound was prepared by reaction of 3,4-difluorobenzoic acid (47.4 mg, 0.3 mmol), 4-aminopyridine (31.1 mg, 0.33 mmol), HBTU (171 mg, 0.45 mmol), EDCCl (86.3 mg, 0.45 mmol) and *N*-methylmorpholine (182 mg, 1.8 mmol) according to method A. The product was purified by preparative HPLC; yield: 64 % (45.2 mg); ^{1}H NMR (300 MHz, MeOD, δ): 8.65 (d, *J* = 6.9 Hz, 2 H), 8.32 (d, *J* = 7.2 Hz, 2 H), 8.03-7.96 (m, 1 H), 7.92-7.88 (m, 1 H), 7.54-7.45 (m, 1 H); MS (ESI): 235.2 $(M+H)^+$; UV λ (nm) = 278; Rf HPLC: 4.88 Min (13 Min 10 – 95% MeCN in water with 0.1% formic acid); Purity 95 %.

***N*-(pyridin-4-yl)-3,4-bis(trifluoromethyl)benzamide (9).** The title compound was prepared by reaction of 3,4-bis(trifluoromethyl)benzoic acid (77.4 mg, 0.3 mmol), 4-aminopyridine (31.1 mg, 0.33 mmol), HBTU (171 mg, 0.45 mmol), EDCCl (86.3 mg, 0.45 mmol) and *N*-methylmorpholine (182 mg, 1.8 mmol) according to method A. The product was purified by preparative HPLC; yield: 61 % (61.0 mg); ^{1}H NMR (300 MHz, MeOD, δ): 8.58 (br s, 2 H), 8.48 (d, *J* = 5.4 Hz, 2 H), 8.24 (s, 1 H), 7.88 (d, *J* = 5.1 Hz, 1 H); MS (ESI): 335.2 $(M+H)^+$; UV λ (nm) = 274; Rf HPLC: 6.98 Min (13 Min 10 – 95% MeCN in water with 0.1% formic acid); Purity 95 %.

***N*-(pyridin-4-yl)-3,5-bis(trifluoromethyl)benzamide (10).** The title compound was prepared by reaction of 3,4-bis(trifluoromethyl)benzoic acid (77.4 mg, 0.3 mmol), 4-aminopyridine (31.1 mg, 0.33 mmol), HBTU (171 mg, 0.45 mmol), EDCCl (86.3 mg, 0.45 mmol) and *N*-methylmorpholine (182 mg, 1.8 mmol) according to method A. The product was purified by preparative HPLC; yield: 51 % (50.9 mg); ^{1}H NMR (300 MHz, MeOD, δ): 8.09 - 8.19 (m, 2 H) 8.28 (s, 1 H) 8.61 (m, 4 H); MS (ESI): 335.3 $(M+H)^+$; UV λ (nm) = 274; Rf HPLC: 6.98 Min (13 Min 10 – 95% MeCN in water with 0.1% formic acid); Purity 99 %.

3-Cyano-*N*-(pyridin-4-yl)benzamide (11). The title compound was prepared by reaction of 3-cyanobenzoic acid (44.1 mg, 0.3 mmol), 4-aminopyridine (31.1 mg, 0.33 mmol), HBTU (171 mg, 0.45 mmol), EDCCl (86.3 mg, 0.45 mmol) and *N*-methylmorpholine (182 mg, 1.8 mmol) according to method A. The product was purified by preparative HPLC; yield: 61 % (40.8 mg); ^{1}H NMR (300 MHz, MeOD, δ): 7.71 - 7.78 (m, 1 H) 7.95 - 8.04 (m, 3 H) 8.27 (dt, J=7.92, 1.49 Hz, 1 H) 8.35 (t, J=1.44 Hz, 1 H) 8.53 (br. s., 2 H); MS (ESI): 224.2 $(M+H)^+$; UV λ (nm) = 276; Rf HPLC: 4.09 Min (13 Min 10 – 95% MeCN in water with 0.1% formic acid); Purity 98 %.

***N*-(pyridin-4-yl)-3-(trifluoromethyl)benzamide (12).** The title compound was prepared by reaction of 3-(trifluoromethyl)benzoic acid (57.0 mg, 0.3 mmol), 4-aminopyridine (31.1 mg, 0.33 mmol), HBTU (171 mg, 0.45 mmol), EDCCl (86.3 mg, 0.45 mmol) and *N*-methylmorpholine (182 mg, 1.8 mmol) according to method A. The product was purified by preparative HPLC; yield: 73 % (58.2 mg); ^{1}H NMR (300 MHz, MeOD, δ): 8.67 (d, J = 7.2 Hz, 2 H), 8.39-8.35 (m, 3 H), 8.29 (d, J = 7.8 Hz, 1 H), 7.99 (d, J = 7.8 Hz, 1 H), 7.80 (t, J = 7.8 Hz, 1 H); MS (ESI): 267.2 $(M+H)^+$; UV λ (nm) = 230, 276; Rf HPLC: 5.59 Min (13 Min 10 – 95% MeCN in water with 0.1% formic acid); Purity 98 %.

3-Fluoro-*N*-(pyridin-4-yl)benzamide (13). The title compound was prepared by reaction of 3-fluorobenzoic acid (42.0 mg, 0.3 mmol), 4-aminopyridine (31.1 mg, 0.33 mmol), HBTU (171 mg, 0.45 mmol), EDCCl (86.3 mg, 0.45 mmol) and *N*-methylmorpholine (182 mg, 1.8 mmol) according to method A. The product was purified by preparative HPLC; yield: 67 % (43.5 mg); ^{1}H NMR (300 MHz, MeOD, δ): = 7.29 - 7.45 (m, 1 H) 7.57 (td, J=8.01, 5.68 Hz, 1 H) 7.67 - 7.76 (m, 1 H) 7.77 - 7.84 (m, 1 H) 7.94 (br. s., 2 H) 8.50 (br. s., 2 H); MS (ESI): 217.2 $(M+H)^+$; UV λ (nm) = 276; Rf HPLC: 4.48 Min (13 Min 10 – 95% MeCN in water with 0.1% formic acid); Purity 95 %.

3-Chloro-*N*-(pyridin-4-yl)benzamide (14). The title compound was prepared by reaction of 3-chlorobenzoic acid (47.0 mg, 0.3 mmol), 4-aminopyridine (31.1 mg, 0.33 mmol), HBTU (171 mg, 0.45 mmol), EDCCl (86.3 mg, 0.45 mmol) and *N*-methylmorpholine (182 mg, 1.8 mmol) according to method A. The product was purified by preparative HPLC; yield: 58 % (40.2 mg); ^{1}H NMR (300 MHz, MeOD, δ): = 7.54 (t, J=7.87 Hz, 1 H) 7.60 - 7.69 (m, 1 H) 7.91 (dt, J=7.75, 1.34 Hz, 1 H) 7.96 - 8.08 (m, 3 H) 8.52 (br. s., 2 H); MS (ESI): 233.2 $(M+H)^+$; UV λ (nm) = 276; Rf HPLC: 5.14 Min (13 Min 10 – 95% MeCN in water with 0.1% formic acid); Purity 95 %.

3-Bromo-*N*-(pyridin-4-yl)benzamide (15). The title compound was prepared by reaction of 3-bromobenzoic acid (133 mg, 0.67 mmol), 4-aminopyridine (69.4 mg, 0.74 mmol), HBTU (380 mg, 1.00 mmol), EDCCl (192 mg, 1.00 mmol) and *N*-methylmorpholine (405 mg, 4.00 mmol) according to method A. The product was purified by preparative HPLC; yield: 98 % (179 mg); ^{1}H NMR (300 MHz, MeOD, δ): = 8.45-8.43 (m, 2 H), 8.13 (s, 1 H), 7.93 (d, J = 6.9 Hz, 1 H), 7.84-7.82 (m, 2 H), 7.77 (d, J = 8.1 Hz, 1 H), 7.46 (t, J = 7.8 Hz, 1 H); MS (ESI): 277.2 $(M+H)^+$; UV λ (nm) = 276; Rf HPLC: 5.34 Min (13 Min 10 – 95% MeCN in water with 0.1% formic acid); Purity 99 %.

3-Methyl-*N*-(pyridin-4-yl)benzamide (16). The title compound was prepared by reaction of 3-methylbenzoic acid (40.8 mg, 0.3 mmol), 4-aminopyridine (31.1 mg, 0.33 mmol), HBTU (171 mg, 0.45 mmol), EDCCl (86.3 mg, 0.45 mmol) and *N*-methylmorpholine (182 mg, 1.8 mmol) according to method A. The product was purified by preparative HPLC; yield: 65 % (41.3 mg); ^{1}H NMR (300 MHz, MeOD, δ): = 2.45 (s, 3 H) 7.36 - 7.51 (m, 2 H) 7.74 - 7.88 (m, 2 H) 8.22 (br. s., 2 H); MS (ESI): 213.2 $(M+H)^+$; UV λ (nm) = 279; Rf HPLC: 4.89 Min (13 Min 10 – 95% MeCN in water with 0.1% formic acid); Purity 99 %.

3-Methoxy-*N*-(pyridin-4-yl)benzamide (17). ^{1}H NMR (500 MHz, MeOD, δ): = 3.87 (s, 3 H) 7.17 (dd, *J*=8.16, 2.52 Hz, 1 H) 7.43 (t, *J*=7.93 Hz, 1 H) 7.47 - 7.55 (m, 2 H) 7.83 (d, *J*=6.26 Hz, 2 H) 8.43 (d, *J*=6.26 Hz, 2 H); MS (ESI): 229.2 $(M+H)^+$; UV λ (nm) = 278; Rf HPLC: 4.54 Min (13 Min 10 – 95% MeCN in water with 0.1% formic acid); Purity 97 %.

3,5-Dimethoxy-*N*-(pyridin-4-yl)benzamide (18). ^{1}H NMR (500 MHz, MeOD, δ): = 3.85 (s, 6 H) 6.71 (t, *J*=1.98 Hz, 1 H) 7.10 (d, *J*=1.98 Hz, 2 H) 7.83 (d, *J*=5.65 Hz, 2 H) 8.44 (br. s., 2 H); MS (ESI): 259.3 $(M+H)^+$; UV λ (nm) = 281 325 (sh); Rf HPLC: 4.93 Min (13 Min 10 – 95% MeCN in water with 0.1% formic acid); Purity > 99 %.

3-(Methylthio)-*N*-(pyridin-4-yl)benzamide (19). The title compound was prepared by reaction of 3-(methylthio)benzoic acid (50.5 mg, 0.3 mmol), 4-aminopyridine (31.1 mg, 0.33 mmol), HBTU (171 mg, 0.45 mmol), EDCCl (86.3 mg, 0.45 mmol) and *N*-methylmorpholine (182 mg, 1.8 mmol) according to method A. The product was purified by preparative HPLC; yield: 75 % (55.0 mg); ^{1}H NMR (300 MHz, MeOD, δ): = 2.56 (s, 3 H) 7.39 - 7.56 (m, 2 H) 7.71 (dt, J=7.33, 1.55 Hz, 1 H) 7.84 (t, J=1.63 Hz, 1 H) 8.00 (br. s., 2 H) 8.51 (br. s., 2 H); MS (ESI): 246.2 $(M+H)^+$; UV λ (nm) = 276, 325; Rf HPLC: 5.22 Min (13 Min 10 – 95% MeCN in water with 0.1% formic acid); Purity 99 %.

3-Isopropyl-*N*-(pyridin-4-yl)benzamide (20). The title compound was prepared by reaction of 3-isopropylbenzoic acid (49.3 mg, 0.3 mmol), 4-aminopyridine (31.1 mg, 0.33 mmol), HBTU (171 mg, 0.45 mmol), EDCCl (86.3 mg, 0.45 mmol) and *N*-methylmorpholine (182 mg, 1.8 mmol) according to method A. The product was purified by preparative HPLC; yield: 38 % (27.5 mg); ^{1}H NMR (300 MHz, MeOD, δ): = 1.31 (d, J=6.98 Hz, 6 H) 3.02 (dt, J=13.85, 6.90 Hz, 1 H) 7.39 - 7.55 (m, 2 H) 7.77 (dt, J=7.45, 1.63 Hz, 1 H) 7.85 (t, J=1.77 Hz, 1 H) 7.99 (br. s., 2 H); MS (ESI): 241.2 $(M+H)^+$; UV λ (nm) = 279; Rf HPLC: 6.14 Min (13 Min 10 – 95% MeCN in water with 0.1% formic acid); Purity 98 %.

4'-Fluoro-*N*-(pyridin-4-yl)-[1,1'-biphenyl]-3-carboxamide (21). The title compound was prepared according to the following procedure: a mixture of 3-bromo-*N*-(pyridin-4-yl)benzamide (83.1 mg, 0.3 mmol), 4-fluorophenylboronic acid (46.2 mg, 0.33 mmol), cesium carbonate (342 mg, 1.05 mmol) and tetrakis(triphenylphosphine) palladium (12.1 mg, 0.0105 mmol) was suspended in an oxygen-free toluene/DME/water (0.7 ml / 0.9 ml / 2 ml) solution and heated under argon atmosphere to 85 °C for 16 h. The reaction mixture was cooled to room temperature. Water was added and the aqueous layer was extracted with ethyl acetate three times. The combined organic layers were dried over magnesium sulfate, filtered and concentrated to dryness. The product was purified by preparative HPLC; 58 % (57.5 mg); ^{1}H NMR (300 MHz, DMSO-d6, δ): = 10.66 (s, 1 H), 8.50 (d, J = 6.0 Hz, 1 H), 8.20 (t, J = 1.8 Hz, 1 H), 8.14 (s, 1 H), 7.96-7.89 (m, 2 H), 7.85-7.79 (m, 4 H), 7.65 (t, J = 7.8 Hz, 1 H), 7.35 (t, J = 8.7 Hz, 2 H). MS (ESI): 246.2 $(M+H)^+$; UV λ (nm) = 238, 278; Rf HPLC: 6.83 Min (13 Min 10 – 95% MeCN in water with 0.1% formic acid); Purity ≥ 99 %.

***N*-(Pyridin-4-yl)-4-(trifluoromethoxy)benzamide (22).** The title compound was prepared by reaction of 4-(trifluoromethoxy)benzoic acid (68.0 mg, 0.33 mmol), 4-aminopyridine (34.2 mg, 0.363 mmol), HBTU (190 mg, 0.5 mmol), EDCCl (96.0 mg, 0.45 mmol) and *N*-methylmorpholine (202 mg, 1.8 mmol) according to method A. The product was purified by preparative HPLC; yield: 97 % (90.0 mg); ^{1}H NMR (300 MHz, DMSO-d6, δ): = 11.04 (s, 1 H), 8.61 (d, *J* = 5.7 Hz, 2 H), 8.12 (d, *J* = 9.0 Hz, 2 H), 7.98 (d, *J* = 6.6 Hz, 2 H), 7.58 (d, *J* = 7.8 Hz, 2 H); MS (ESI): 241.2 $(M+H)^+$; UV λ (nm) = 278; Rf HPLC: 6.09 Min (13 Min 10 – 95% MeCN in water with 0.1% formic acid); Purity 96 %.

4-(Difluoromethoxy)-*N*-(pyridin-4-yl)benzamide (23). The title compound was prepared by reaction of 4-(difluoromethoxy)benzoic acid (62.1 mg, 0.33 mmol), 4-aminopyridine (34.2 mg, 0.363 mmol), HBTU (190 mg, 0.5 mmol), EDCCl (96.0 mg, 0.5 mmol) and *N*-methylmorpholine (202 mg, 1.8 mmol) according to method A. The product was purified by preparative HPLC; yield: 89 % (91.3 mg, formiate salt); ^{1}H NMR (300 MHz, DMSO-d6, δ): = 11.03 (s, 1 H), 8.63 (d, *J* = 4.8 Hz, 2 H), 8.08 (d, *J* = 8.7 Hz, 2 H), 8.04 (d, *J* = 6.6 Hz, 2 H), 7.41 (t, *J* = 73.5 Hz, 1 H), 7.37 (d, *J* = 8.7 Hz, 2 H); MS (ESI): 265.2 $(M+H)^+$; UV λ (nm) = 281; Rf HPLC: 5.27 Min (13 Min 10 – 95% MeCN in water with 0.1% formic acid); Purity 98 %.

***N*-(Pyridin-4-yl)-4-(trifluoromethyl)benzamide (24).** The title compound was prepared by reaction of 4-(trifluoromethyl)benzoic acid (57.0 mg, 0.3 mmol), 4-aminopyridine (31.1 mg, 0.33 mmol), HBTU (171 mg, 0.45 mmol), EDCCl (86.3 mg, 0.45 mmol) and *N*-methylmorpholine (182 mg, 1.8 mmol) according to method A. The product was purified by preparative HPLC; yield: 54 % (43.5 mg); ^{1}H NMR (300 MHz, MeOD, δ): = 8.68 (d, *J* = 6.9 Hz, 2 H), 8.37 (d, *J* = 6.9 Hz, 2 H), 8.19 (d, *J* = 7.8 Hz, 2 H), 7.90 (d, *J* = 8.1 Hz, 2 H); MS (ESI): 267.2 $(M+H)^+$; UV λ (nm) =227 (sh), 281; Rf HPLC: 5.74 Min (13 Min 10 – 95% MeCN in water with 0.1% formic acid); Purity ≥ 99 %.

4-fluoro-*N*-(pyridin-4-yl)benzamide (25). MS (ESI): 217.2 $(M+H)^+$; UV λ (nm) =279; Rf HPLC: 4.26 Min (13 Min 10 – 95% MeCN in water with 0.1% formic acid); Purity ≥ 99 %.

4-Chloro-*N*-(pyridin-4-yl)benzamide (26). The title compound was prepared by reaction of 4-chlorobenzoic acid (47.0 mg 0.3 mmol), 4-aminopyridine (31.1 mg, 0.33 mmol), HBTU (171 mg, 0.45 mmol), EDCCl (86.3 mg, 0.45 mmol) and *N*-methylmorpholine (182 mg, 1.8 mmol) according to method A. The product was purified by preparative HPLC; yield: quantitative (70.3 mg); ^{1}H NMR (300 MHz, MeOD, δ): = 7.49 - 7.61 (m, 2 H) 7.83 (d, J=5.87 Hz, 2 H) 7.88 - 8.02 (m, 2 H) 8.45 (br. s., 2 H); MS (ESI): 233.2 $(M+H)^+$; UV λ (nm) =281; Rf HPLC: 5.18 Min (13 Min 10 – 95% MeCN in water with 0.1% formic acid); Purity 99 %.

4-Bromo-*N*-(pyridin-4-yl)benzamide (27). The title compound was prepared by reaction of 4-bromobenzoic acid (402 mg 2.0 mmol), 4-aminopyridine (207 mg, 2.2 mmol), HBTU (1.14 g, 3.0 mmol), EDCCl (575 mg, 3.0 mmol) and *N*-methylmorpholine (1.21 g, 12 mmol) according to method A. The product was purified by Biotage CC; yield: quantitative (584 mg); ^{1}H NMR (300 MHz, MeOD, δ): = 8.43 (d, J = 6.6 Hz, 2 H), 7.87-7.82 (m, 4 H), 7.69 (d, J = 8.7 Hz, 2 H); MS (ESI): 279.2 $(M+H)^+$; UV λ (nm) =281; Rf HPLC: 5.40 Min (13 Min 10 – 95% MeCN in water with 0.1% formic acid); Purity ≥ 99 %.

4'-Fluoro-*N*-(pyridin-4-yl)-[1,1'-biphenyl]-4-carboxamide (28). The title compound was prepared according to the following procedure: a mixture of 4-bromo-*N*-(pyridin-4-yl)benzamide (139 mg, 0.5 mmol), 4-fluorophenylboronic acid (77.0 mg, 0.55 mmol), cesium carbonate (569 mg, 1.75 mmol) and tetrakis(triphenylphosphine) palladium (20.2 mg, 0.0175 mmol) was suspended in an oxygen-free toluene/DME/water (1.3 ml / 1.7 ml / 3.7 ml) solution and heated under argon atmosphere to 85 °C for 15 h. The reaction mixture was cooled to room temperature. Water was added and the aqueous layer was extracted with ethyl acetate three times. The combined organic layers were dried over magnesium sulfate, filtered and concentrated to dryness. The product was purified by preparative HPLC; 12 % (17.9 mg); MS (ESI): 315.3 $(M+Na)^+$; UV λ (nm) = 298; Rf HPLC: 7.59 Min (13 Min 10 – 95% MeCN in water with 0.1% formic acid); Purity 91 %.

4-Methoxy-*N*-(pyridin-4-yl)benzamide (29). ^{1}H NMR (500 MHz, MeOD, δ): = 3.88 (s, 3 H) 7.01 - 7.08 (m, 2 H) 7.82 (d, *J*=6.41 Hz, 2 H) 7.90 - 7.99 (m, 2 H) 8.42 (d, *J*=6.26 Hz, 2 H); MS (ESI): 229.2 $(M+H)^+$; UV λ (nm) =295; Rf HPLC: 4.47 Min (13 Min 10 – 95% MeCN in water with 0.1% formic acid); Purity $\geq$ 99 %.

4-Hydroxy-*N*-(pyridin-4-yl)benzamide (30). The title compound was prepared according to the following procedure: To a solution of 4-methoxy-*N*-(pyridin-4-yl)benzamide (300 mg, 1.31 mmol) in 20 mL DCM (dry) was added dropwise BBr_3 (1 M in DCM, 3.93 ml, 3.93 mmol) at -95°C. The mixture was stirred at room temperature for 3h. 1 M HCl was added to quench the reaction. The pH was adjusted to 8 with NaHCO(sat) and the mixture was extracted with EtOAc. The combined organic layers were washed with brine, dried with magnesium sulphate and concentrated in vacuo to afford the crude product, which was purified by preparative HPLC; ^{1}H NMR (300 MHz, DMSO-d6, δ): = 10.31 (s, 1 H), 8.44 (d, *J* = 5.4 Hz, 2 H), 7.87 (d, *J* = 8.7 Hz, 2 H), 7.76 (d, *J* = 6.0 Hz, 2 H), 6.88 (d, *J* = 8.7 Hz, 2 H); MS (ESI): 215.2 $(M+H)^+$;

UV λ (nm) =276; Rf HPLC: 3.48 Min (13 Min 10 – 95% MeCN in water with 0.1% formic acid); Purity ≥ 99 %.

4-Nitro-*N*-(pyridin-4-yl)benzamide (31). The title compound was prepared by reaction of 4-nitrobenzoic acid (50.1 mg, 0.3 mmol), 4-aminopyridine (31.1 mg, 0.33 mmol), HBTU (171 mg, 0.45 mmol), EDCCl (86.3 mg, 0.45 mmol) and *N*-methylmorpholine (182 mg, 1.8 mmol) according to method A. The product was purified by preparative HPLC; yield: 50 % (36.3 mg); ^{1}H NMR (300 MHz, MeOD, δ): = 8.69 (d, J = 7.2 Hz, 2 H), 8.43-8.37 (m, 4 H), 8.23 (d, J = 9.0 Hz, 2 H); MS (ESI): 244.2 $(M+H)^+$; UV λ (nm) =281; Rf HPLC: 4.60 Min (13 Min 10 – 95% MeCN in water with 0.1% formic acid); Purity 95 %.

2-Chloro-*N*-(pyridin-4-yl)benzamide (32). The title compound was prepared by reaction of 2-chlorobenzoic acid (47.0 mg, 0.3 mmol), 4-aminopyridine (31.1 mg, 0.33 mmol), HBTU (171 mg, 0.45 mmol), EDCCl (86.3 mg, 0.45 mmol) and *N*-methylmorpholine (182 mg, 1.8 mmol) according to method A. The product was purified by preparative HPLC; yield: 68 % (47.8 mg); ^{1}H NMR (300 MHz, MeOD, δ): = 7.46 - 7.59 (m, 1 H) 7.60 - 7.68 (m, 1 H) 7.91 (dt, J=7.87, 1.37 Hz, 1 H) 7.95 - 8.07 (m, 3 H) 8.52 (br. s., 2 H); MS (ESI): 233.2 $(M+H)^+$; UV λ (nm) =272; Rf HPLC: 4.37 Min (13 Min 10 – 95% MeCN in water with 0.1% formic acid); Purity 99 %.

***N*-(pyridin-4-yl)benzamide (33).** The title compound was prepared by reaction of benzoic acid (36.6 mg, 0.3 mmol), 4-aminopyridine (31.1 mg, 0.33 mmol), HBTU (171 mg, 0.45 mmol), EDCCl (86.3 mg, 0.45 mmol) and *N*-methylmorpholine (182 mg, 1.8 mmol) according to method A. The product was purified by preparative HPLC; yield: 83 % (49.4 mg); ^{1}H NMR (300 MHz, MeOD, δ): = 8.64 (d, *J* = 6.6 Hz, 2 H), 8.37 (d, *J* = 6.6 Hz, 2 H), 8.02 (d, *J* = 7.5 Hz, 2 H), 7.68 (t, *J* = 7.2 Hz, 1 H), 7.57 (t, *J* = 7.5 Hz, 2 H); MS (ESI): 199.2 $(M+H)^+$; UV λ (nm) =278; Rf HPLC: 4.09 Min (13 Min 10 – 95% MeCN in water with 0.1% formic acid); Purity ≥ 99 %.

***N*-(pyridin-4-yl)nicotinamide (34).** ^{1}H NMR (500 MHz, MeOD, δ): = 7.60 (dd, *J*=8.01, 4.96 Hz, 1 H) 7.84 (d, *J*=6.56 Hz, 2 H) 8.37 (dd, *J*=7.93, 1.68 Hz, 1 H) 8.46 (d, *J*=6.26 Hz, 2 H) 8.72 - 8.78 (m, 1 H) 9.10 (d, *J*=2.29 Hz, 1 H); MS (ESI): 200.1 (M+H)$^+$; UV λ (nm) =276; Rf HPLC: 2.45 Min (13 Min 10 – 95% MeCN in water with 0.1% formic acid); Purity 99 %.

***N*-(Pyridin-4-yl)isonicotinamide (35).** ^{1}H NMR (500 MHz, MeOD, δ): = 7.85 (d, *J*=6.41 Hz, 2 H) 7.90 (d, *J*=5.80 Hz, 2 H) 8.47 (d, *J*=6.10 Hz, 2 H) 8.76 (d, *J*=5.95 Hz, 2 H); MS (ESI): 200.1 (M+H)$^+$; UV λ (nm) =274; Rf HPLC: 2.19 Min (13 Min 10 – 95% MeCN in water with 0.1% formic acid); Purity 82 %.

***N*-(pyridin-4-yl)thiophene-2-carboxamide (36).** The title compound was prepared by reaction of thiophene-2-carboxylic acid (38.4 mg, 0.3 mmol), 4-aminopyridine (31.1 mg, 0.33 mmol), HBTU (171 mg, 0.45 mmol), EDCCl (86.3 mg, 0.45 mmol) and *N*-methylmorpholine (182 mg, 1.8 mmol) according to method A. The product was purified by preparative HPLC; yield: 87 % (53.3 mg); ^{1}H NMR (300 MHz, MeOD, δ): = 7.50 - 7.58 (m, 1 H) 7.61 - 7.68 (m, 1 H) 7.91 (dt, J=7.87, 1.37 Hz, 1 H) 7.96 - 8.05 (m, 3 H) 8.52 (br. s., 2 H); MS (ESI): 205.1 (M+H)$^+$; UV λ (nm) = 255 (sh), 298; Rf HPLC: 3.89 Min (13 Min 10 – 95% MeCN in water with 0.1% formic acid); Purity 97 %.

ASSOCIATED CONTENT

AUTHOR INFORMATION

Corresponding Author

* For **R.W. H.**: Phone: +(49) 681 98806 2000. E-Mail: rolf.hartmann@helmholtz-hzi.de.

ACKNOWLEDGMENTS

The authors thank Nadja Weber and Christopher Hörnesfor their help with synthesizing the compounds. Furthermore, the authors thank Drs. Chris van Koppen and Jens Burkhart for their help in this project.

ABBREVIATIONS

CAT, Catalytic domain; Col, Collagen; ECM, Extracellular matrix; EDC, 1-Ethyl-3-(3-dimethylaminopropyl)carbodiimide; HBTU, Hexafluorophosphate Benzotriazole Tetramethyl Uronium; MMP, Matrixmetalloprotease; MT1-MMP, Membrane Type 1 – MMP; PEX, Hemopexin; SAR, Structure – Activity – relationship;

REFERENCES

(1) Bergers, G.; Benjamin, L. E. Tumorigenesis and the Angiogenic Switch. *Nature Reviews Cancer*. Nature Publishing Group June 1, 2003, pp 401–410.

(2) Gupta, M. K.; Qin, R. Y. Mechanism and Its Regulation of Tumor-Induced Angiogenesis. *World Journal of Gastroenterology*. Baishideng Publishing Group Inc June 2003, pp 1144–1155.

(3) Friedl, P.; Alexander, S. Cancer Invasion and the Microenvironment: Plasticity and Reciprocity. *Cell*. Elsevier November 23, 2011, pp 992–1009.

(4) Mittal, R.; Patel, A. P.; Debs, L. H.; Nguyen, D.; Patel, K.; Grati, M.; Mittal, J.; Yan, D.; Chapagain, P.; Liu, X. Z. Intricate Functions of Matrix Metalloproteinases in Physiological and Pathological Conditions. *J. Cell. Physiol.* **2016**.

(5) Kessenbrock, K.; Plaks, V.; Werb, Z. Matrix Metalloproteinases: Regulators of the Tumor Microenvironment. *Cell*. Elsevier April 2, 2010, pp 52–67.

(6) Nabeshima, K.; Inoue, T.; Shimao, Y.; Sameshima, T. Matrix Metalloproteinases in Tumor Invasion: Role for Cell Migration. *Pathology International*. Blackwell Science Pty April 1, 2002, pp 255–264.

(7) Michaelis, U. R. Mechanisms of Endothelial Cell Migration. *Cell. Mol. Life Sci.* **2014**, *71* (21), 4131–4148.

(8) Verma, R. P.; Hansch, C. Matrix Metalloproteinases (MMPs): Chemical-Biological Functions and (Q)SARs. *Bioorganic and Medicinal Chemistry*. 2007, pp 2223–2268.

(9) Coussens, L. M.; Fingleton, B.; Matrisian, L. M. Matrix Metalloproteinase Inhibitors and Cancer: Trials and Tribulations. *Science*. American Association for the Advancement of Science March 29, 2002, pp 2387–2392.

(10) Overall, C. M.; Kleifeld, O. Validating Matrix Metalloproteinases as Drug Targets and Anti-Targets for Cancer Therapy. *Nature Reviews Cancer*. Nature Publishing Group March 1, 2006, pp 227–239.

(11) Gomis-Rüth, F. X. Structural Aspects of the Metzincin Clan of Metalloendopeptidases. *Applied Biochemistry and Biotechnology - Part B Molecular Biotechnology*. Humana Press 2003, pp 157–202.

(12) Sela-Passwell, N.; Rosenblum, G.; Shoham, T.; Sagi, I. Structural and Functional Bases for Allosteric Control of MMP Activities: Can It Pave the Path for Selective Inhibition? *Biochimica et Biophysica Acta - Molecular Cell Research*. Elsevier January 1, 2010, pp 29–38.

(13) Piccard, H.; Van den Steen, P. E.; Opdenakker, G. Hemopexin Domains as Multifunctional Liganding Modules in Matrix Metalloproteinases and Other Proteins. *J. Leukoc. Biol.* **2007**, *81* (4), 870–892.

(14) Itoh, Y. MT1-MMP: A Key Regulator of Cell Migration in Tissue. *IUBMB Life (International Union Biochem. Mol. Biol. Life)* **2006**, *58* (10), 589–596.

(15) Itoh, Y.; Takamura, A.; Ito, N.; Maru, Y.; Sato, H.; Suenaga, N.; Aoki, T.; Seiki, M. Homophilic Complex Formation of MT1-MMP Facilitates ProMMP-2 Activation on the Cell Surface and Promotes Tumor Cell Invasion. *EMBO J.* **2001**, *20* (17), 4782–4793.

(16) Toth, M.; Chvyrkova, I.; Bernardo, M. M.; Hernandez-Barrantes, S.; Fridman, R. Pro-MMP-9 Activation by the MT1-MMP/MMP-2 Axis and MMP-3: Role of TIMP-2 and Plasma Membranes. *Biochem. Biophys. Res. Commun.* **2003**, *308* (2), 386–395.

(17) Zeng, Z. S.; Cohen, A. M.; Guillem, J. G. Loss of Basement Membrane Type IV Collagen Is Associated with Increased Expression of Metalloproteinases 2 and 9 (MMP-2 and MMP-9) during Human Colorectal Tumorigenesis. *Carcinogenesis* **1999**, *20* (5), 749–755.

(18) Murakami, M.; Sakai, H.; Kodama, A.; Yanai, T.; Mori, T.; Maruo, K.; Masegi, T. Activation of Matrix Metalloproteinase (MMP)-2 by Membrane Type 1-MMP and Abnormal Immunolocalization of the Basement Membrane Components Laminin and Type IV Collagen in Canine Spontaneous Hemangiosarcomas. *Histol. Histopathol.* **2009**, *24* (4), 437–446.

(19) Zheng, H.; Takahashi, H.; Murai, Y.; Cui, Z.; Nomoto, K.; Niwa, H.; Tsuneyama, K.; Takano, Y. Expressions of MMP-2, MMP-9 and VEGF Are Closely Linked to Growth, Invasion, Metastasis and Angiogenesis of Gastric Carcinoma. *Anticancer Res.* **2006**, *26* (5 A), 3579–3583.

(20) Rozanov, D. V; Ghebrehiwet, B.; Postnova, T. I.; Eichinger, A.; Deryugina, E. I.; Strongin, A. Y. The Hemopexin-like C-Terminal Domain of Membrane Type 1 Matrix Metalloproteinase Regulates Proteolysis of a Multifunctional Protein, GC1qR. *J. Biol. Chem.* **2002**, *277* (11), 9318–9325.

(21) Mori, H.; Tomari, T.; Koshikawa, N.; Kajita, M.; Itoh, Y.; Sato, H.; Tojo, H.; Yana, I.; Seiki, M. CD44 Directs Membrane-Type 1 Matrix Metalloproteinase to Lamellipodia by Associating with Its Hemopexin-like Domain. *EMBO J.* **2002**, *21* (15), 3949–3959.

(22) Suenaga, N.; Mori, H.; Itoh, Y.; Seiki, M. CD44 Binding through the Hemopexin-like

Domain Is Critical for Its Shedding by Membrane-Type 1 Matrix Metalloproteinase. *Oncogene* **2005**, *24* (5), 859–868.

(23) Lafleur, M. A.; Mercuri, F. A.; Ruangpanit, N.; Seiki, M.; Sato, H.; Thompson, E. W. Type I Collagen Abrogates the Clathrin-Mediated Internalization of Membrane Type 1 Matrix Metalloproteinase (MT1-MMP) via the MT1-MMP Hemopexin Domain. *J. Biol. Chem.* **2006**, *281* (10), 6826–6840.

(24) Schröder, H. M.; Hoffmann, S. C.; Hecker, M.; Korff, T.; Ludwig, T. The Tetraspanin Network Modulates MT1-MMP Cell Surface Trafficking. *Int. J. Biochem. Cell Biol.* **2013**, *45* (6), 1133–1144.

(25) Tam, E. M.; Wu, Y. I.; Butler, G. S.; Sharon Stack, M.; Overall, C. M. Collagen Binding Properties of the Membrane Type-1 Matrix Metalloproteinase (MT1-MMP) Hemopexin C Domain: The Ectodomain of the 44-KDa Autocatalytic Product of MT1-MMP Inhibits Cell Invasion by Disrupting Native Type I Collagen Cleavage. *J. Biol. Chem.* **2002**, *277* (41), 39005–39014.

(26) Tam, E. M.; Moore, T. R. B.; Butler, G. S.; Overall, C. M. Characterization of the Distinct Collagen Binding, Helicase and Cleavage Mechanisms of Matrix Metalloproteinase 2 and 14 (Gelatinase A and MT1-MMP): The Differential Roles of the MMP Hemopexin C Domains and the MMP-2 Fibronectin Type II Modules in Collage. *J. Biol. Chem.* **2004**, *279* (41), 43336–43344.

(27) Remacle, A. G.; Golubkov, V. S.; Shiryaev, S. A.; Dahl, R.; Stebbins, J. L.; Chernov, A. V.; Cheltsov, A. V.; Pellecchia, M.; Strongin, A. Y. Novel MT1-MMP Small-Molecule Inhibitors Based on Insights into Hemopexin Domain Function in Tumor Growth. *Cancer Res.* **2012**, *72* (9), 2339–2349.

(28) Evensen, N. A.; Li, J.; Yang, J.; Yu, X.; Sampson, N. S.; Zucker, S.; Cao, J.; Hanahan,

D.; Weinberg, R.; Normanno, N.; et al. Development of a High-Throughput Three-Dimensional Invasion Assay for Anti-Cancer Drug Discovery. *PLoS One* **2013**, *8* (12), e82811.

(29) Augsburger, D.; Nelson, P. J.; Kalinski, T.; Udelnow, A.; Knösel, T.; Hofstetter, M.; Qin, J. W.; Wang, Y.; Gupta, A. Sen; Bonifatius, S.; et al. Current Diagnostics and Treatment of Fibrosarcoma -Perspectives for Future Therapeutic Targets and Strategies. *Oncotarget* **2017**, *8* (61), 104638–104653.

(30) Gaebler, M.; Silvestri, A.; Haybaeck, J.; Reichardt, P.; Lowery, C. D.; Stancato, L. F.; Zybarth, G.; Regenbrecht, C. R. A. Three-Dimensional Patient-Derived In Vitro Sarcoma Models: Promising Tools for Improving Clinical Tumor Management. *Front. Oncol.* **2017**, *7*, 203.

(31) Partridge, J. J.; Madsen, M. A.; Ardi, V. C.; Papagiannakopoulos, T.; Kupriyanova, T. A.; Quigley, J. P.; Deryugina, E. I. Functional Analysis of Matrix Metalloproteinases and Tissue Inhibitors of Metalloproteinases Differentially Expressed by Variants of Human HT-1080 Fibrosarcoma Exhibiting High and Low Levels of Intravasation and Metastasis. *J. Biol. Chem.* **2007**, *282* (49), 35964–35977.

(32) Takino, T.; Miyamori, H.; Watanabe, Y.; Yoshioka, K.; Seiki, M.; Sato, H. Membrane Type 1 Matrix Metalloproteinase Regulates Collagen-Dependent Mitogen-Activated Protein/Extracellular Signal-Related Kinase Activation and Cell Migration. *Cancer Res.* **2004**, *64* (3), 1044–1049.

(33) Pearson, J. R. D.; Regad, T. Targeting Cellular Pathways in Glioblastoma Multiforme. *Signal Transduct. Target. Ther.* **2017**, *2*, 17040.

(34) Winer, A.; Adams, S.; Mignatti, P. Matrix Metalloproteinase Inhibitors in Cancer Therapy: Turning Past Failures Into Future Successes. *Mol. Cancer Ther.* **2018**, *17* (6),

1147–1155.

(35) Overall, C. M. Molecular Determinants of Metalloproteinase Substrate Specificity: Matrix Metalloproteinase Substrate Binding Domains, Modules, and Exosites. *Mol. Biotechnol.* **2002**, *22* (1), 051–086.

(36) Li, H.; Wang, D.; Yuan, Y.; Min, J. New Insights on the MMP-13 Regulatory Network in the Pathogenesis of Early Osteoarthritis. *Arthritis Res. Ther.* **2017**, *19* (1), 248.

(37) Jüngel, A.; Ospelt, C.; Lesch, M.; Thiel, M.; Sunyer, T.; Schorr, O.; Michel, B. A.; Gay, R. E.; Kolling, C.; Flory, C.; et al. Effect of the Oral Application of a Highly Selective MMP-13 Inhibitor in Three Different Animal Models of Rheumatoid Arthritis. *Ann. Rheum. Dis.* **2010**, *69* (5), 898–902.

(38) Della Porta, P.; Soeltl, R.; Krell, H. W.; Collins, K.; O'Donoghue, M.; Schmitt, M.; Krüger, A. Combined Treatment with Serine Protease Inhibitor Aprotinin and Matrix Metalloproteinase Inhibitor Batimastat (BB-94) Does Not Prevent Invasion of Human Esophageal and Ovarian Carcinoma Cells in Vivo. *Anticancer Res.* **1999**, *19* (5 B), 3809–3816.

3.2. Chapter II: Targeted Endocrine Therapy: Design, Synthesis, and Proof-of-Principle of 17β-Hydroxysteroid Dehydrogenase Type 2 Inhibitors in Bone Fracture Healing

Abdelsamie, A. S.; Herath, S.; Biskupek, Y.; Börger, C.; Siebenbürger, L.; Salah, M.; Scheuer, C.; Marchais-Oberwinkler, S.; Frotscher, M.; Pohlemann, T.; Menger, M. D.; Hartmann, R. W.; Laschke, M. W.; van Koppen, C. J.;

Reprinted with permission from *J. Med. Chem.* **2019***, 62, 3,* 1362-1372*.*

DOI: 10.1021/acs.jmedchem.8b01493

Copyright (2019) American Chemical Society

Journal of Medicinal Chemistry

Article

Cite This: J. Med. Chem. 2019, 62, 1362−1372

pubs.acs.org/jmc

Targeted Endocrine Therapy: Design, Synthesis, and *Proof-of-Principle* of 17β-Hydroxysteroid Dehydrogenase Type 2 Inhibitors in Bone Fracture Healing

Ahmed S. Abdelsamie,[†,‡,○] Steven Herath,[§,○] Yannik Biskupek,[§] Carsten Börger,[∥] Lorenz Siebenbürger,[∥] Mohamed Salah,[⊥] Claudia Scheuer,[#] Sandrine Marchais-Oberwinkler,[¶] Martin Frotscher,[⊥] Tim Pohlemann,[§] Michael D. Menger,[#] Rolf W. Hartmann,[⊥,∇] Matthias W. Laschke,[#] and Chris J. van Koppen*[,†,⊥]

[†] ElexoPharm GmbH, Im Stadtwald, Building A1.2, 66123 Saarbrücken, Germany

[‡] Chemistry of Natural and Microbial Products Department, National Research Centre, Dokki, 12622 Cairo, Egypt

[§] Department of Trauma, Hand and Reconstructive Surgery, and [#] Institute of Clinical & Experimental Surgery, Saarland University, 66421 Homburg/Saar, Germany

[∥] PharmBioTec GmbH, 66123 Saarbrücken, Germany

[⊥] Department of Pharmaceutical and Medicinal Chemistry, Saarland University, 66123 Saarbrücken, Germany

[¶] Institute of Pharmaceutical Chemistry, Philipps-University, 35032 Marburg, Germany

[∇] Department of Drug Design and Optimization, Helmholtz Institute for Pharmaceutical Research Saarland (HIPS), 66123 Saarbrücken, Germany

Supporting Information

ABSTRACT: Current therapies of steroid hormone-dependent diseases predominantly alter steroid hormone concentrations (or their actions) in plasma, in target and nontarget tissues alike, rather than in target organs only. Targeted therapy through the inhibition of steroidogenic enzymes may pose an attractive alternative with much less side effects. Here, we describe the design of a nanomolar potent 17β-hydroxysteroid dehydrogenase type 2 (17β-HSD2) inhibitor (compound **15**) and successful targeted intracrine therapy in a mouse bone fracture model. Blockade of 17β-HSD2 in bone is thought to increase intracellular estradiol (E2) and testosterone (T), which thereby inhibits bone resorption by osteoclasts and stimulates bone formation by osteoblasts, respectively. Administration of compound **15** in the mouse fracture model strongly increases the mechanical stability of the healing fractured bone because of a larger periosteal callus with newly formed bone without changing the plasma E2 and T concentrations. Steroidogenic 17β-HSD2 inhibition thus enables targeted intracrine therapy.

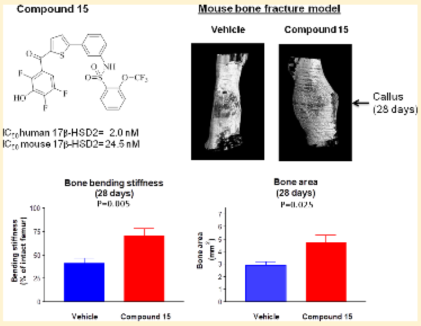

INTRODUCTION

Current therapies of steroid hormone-dependent diseases, like osteoporosis and endometriosis, involve primarily treatment with drugs that alter the steroid hormone concentrations (or their actions) in plasma, in target and nontarget tissues alike, rather than in the target organs only. As a consequence, these treatments most often are accompanied with highly undesirable side effects.[1] Local intracrine inhibition of steroidogenic enzymes, affecting the intracellular concentrations in the target organs only, represents an attractive, alternative therapeutic paradigm with much less side effects and disturbances of the hypothalamus−pituitary organ axes. Unfortunately, successful *proof-of-principle* studies with steroidogenic enzyme inhibitors, which do not change systemic hormone concentrations, have been rather infrequent. These include 5α-reductase inhibitors to treat patients with benign prostatic hyperplasia,[2] 11β-HSD1 inhibitors,[3] and 17β-HSD1 inhibitors in an endometrial hyperplasia animal model.[4] In the present study, we have developed novel nanomolar potent 17β-HSD2 inhibitors and successfully performed a *proof-of-principle* study in a mouse bone fracture healing model. Approximately 10% of the patients with bone fractures suffer from serious nonunion or delayed/impaired bone fracture healing.[5] Inadequate bone healing is not only difficult to treat, with the therapeutic options being very limited,[6−8] but the demand for novel drugs with fewer side effects is also increasing rapidly because of the relatively high prevalence of bone fractures, the anticipated

Received: September 25, 2018
Published: January 15, 2019

© 2019 American Chemical Society

DOI: 10.1021/acs.jmedchem.8b01493
J. Med. Chem. 2019, 62, 1362−1372

worldwide increase in postmenopausal osteoporosis-related bone fractures, and the growing elderly population. 17β-HSD2 in bone tissue converts the biologically active steroid hormones, estradiol (E2) and T, into the much less active estrone and androstenedione. The blockade of 17β-HSD2 in bone thus increases intracellular E2 and T, and, through estrogen and androgen receptor stimulation, inhibits bone resorption by osteoclasts and stimulates bone formation by osteoblasts,[9−11] respectively. The expression and activity of 17β-HSD2 in human bone tissue are superior over that of 17β-HSD1, 17β-HSD3, and 17β-HSD4,[12−14] the enzymes that catalyze the synthesis and degradation of E2 and T. A previous study in ovariectomized cynomolgus monkeys showed that a 17β-HSD2 inhibitor increases the so-called ultimate bone strength, that is, the maximum stress that an intact bone specimen can sustain.[15] Here, we developed a nanomolar potent, metabolically sufficiently stable, nontoxic 17β-HSD2 inhibitor and tested this compound for activity in an established mouse bone fracture healing model[16] during a *proof-of-principle* study of 28 days. Mouse bone cells express active 17β-HSD2 as demonstrated by 17β-HSD2 immunohistochemistry, using a validated antimouse 17β-HSD2 antibody (Figure S1, Supporting Information), and shown by enzymatic determination,[17] together with androgen and estrogen receptors (ERs).[12−14]

■ RESULTS AND DISCUSSION

As bicyclic substituted hydroxyphenylmethanones (BSHs) bearing a sulfonamide moiety were originally designed as inhibitors of human 17β-HSD1, most members show selectivity toward 17β-HSD1 over 17β-HSD2.[18] In addition, BSHs display low metabolic stability, precluding their use in an in vivo *proof-of-principle* study. Thus, a rational two-stage drug design strategy focusing on rings A and D (Charts 1 and 2, see also Supporting Information for details) was applied that, on the one hand, aimed at improving the metabolic stability and, on the other, at enhancing the potency and selectivity for *human* and *murine* 17β-HSD2 (h + m17β-HSD2), resulting in a small library of 16 compounds. As a starting point, the nonsubstituted scaffold structure (compound **A**) was chosen.

Chart 1. Lead Compound A and Designed Compounds 1−8

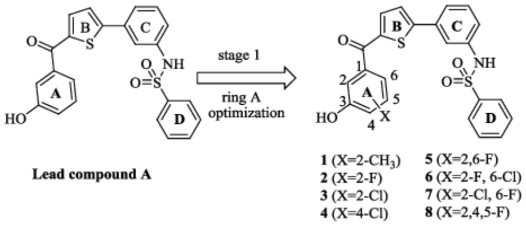

Chart 2. Lead Compound 8 and Designed Compounds 9−16

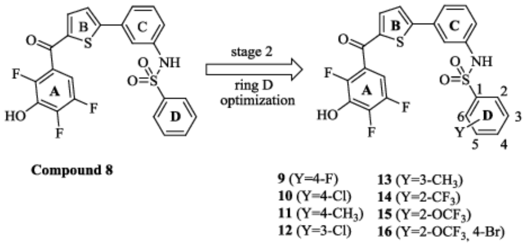

Previous investigations revealed that the low metabolic stability of the BSHs was primarily due to phase II biotransformation of the phenolic OH group, which is essential for activity.[19] Therefore, stage 1 of the design strategy, aiming at the improvement of metabolic stability, consisted in the introduction of small substituents on the hydroxyphenyl moiety (ring A) of compound **A**. These groups could protect the OH functionality from biotransformation by the electron withdrawal effect and/or steric hindrance (Chart 1, compounds **1**−**8**).

Compound **8** showed an enhanced metabolic stability and was chosen as a starting point for the optimization of the substitution pattern of the D-ring (stage 2 of the design strategy). Only such groups were selected to be introduced that were likely to maintain potency toward both human and mouse 17β-HSD2.[18] We aimed for a slight (three- to — fourfold) selectivity over the h17β-HSD1 enzyme (Chart 2, **9**−**16**). On the one hand, a highly selective 17β-HSD2 inhibitor would induce an undesirable increase in intracellular E2 in tissues that express similar levels of 17β-HSD2 and 17β-HSD1 and prone to E2-dependent proliferation (i.e., breast[20,21] and endometrium[22]), whereas on the other hand, a nonselective 17β-HSD2/1 inhibitor would likely affect the role of 17β-HSD1 in regulating the endometrium cyclicity in women of childbearing age.[22]

The starting point for the syntheses of compounds **1**−**16** was a Friedel−Crafts reaction of 2-bromothiophene with the appropriate benzoyl chloride, which in case of the chlorinated **3b** and **4b** had to be prepared from the corresponding benzoic acids. The obtained intermediates **1b**−**8b** were subjected to Suzuki cross-coupling reactions with 3-aminophenylboronic acid to afford anilines **1a**−**8a**. The latter were reacted with the sulfonamides using the appropriately substituted sulfonic acid chloride, giving direct access to compound **1**. Ether cleavage using BBr$_3$ in dichloromethane yielded the final compounds **2**−**16** (Scheme 1).

The introduction of an electron-donating methyl group on ring A (Table 1, **1**) led to a twofold decrease in inhibitory potency toward h17β-HSD2 compared to lead **A**. In contrast, the presence of an electron-withdrawing fluorine or chlorine atom in the same position strongly increased the activity; see **1** versus **2** and **3**.

The beneficial effect of electron-withdrawing substituents on the inhibitory activity was also apparent for **4**−**8**, in agreement with the observations made recently for the BSHs lacking the sulfonamide moiety.[22] Metabolic stability was determined for **3**, **7**, and **8** as these compounds displayed selectivity over 17β-HSD1 and nanomolar potency toward m17β-HSD2. The trifluoro substitution pattern of **8** resulted in an improved metabolic stability and was therefore maintained in the subsequent optimization of ring D. All eight compounds of this second series (**9**−**16**) showed a strong inhibition of *human* and *mouse* 17β-HSD2 as well as a low activity toward m17β-HSD1. Compounds **14** and **15** were especially interesting as they displayed moderate h17β-HSD2 selectivity, which was aimed at, as well as improved metabolic stability.

Because of their favorable potency, selectivity, and metabolic stability properties, **14** and **15** were selected for testing for potential cytotoxicity. Both **14** and **15** were not toxic in the MTT assay with HEK293 cells (i.e., <20% reduction in cell

Scheme 1. Synthetic Route to 1−16

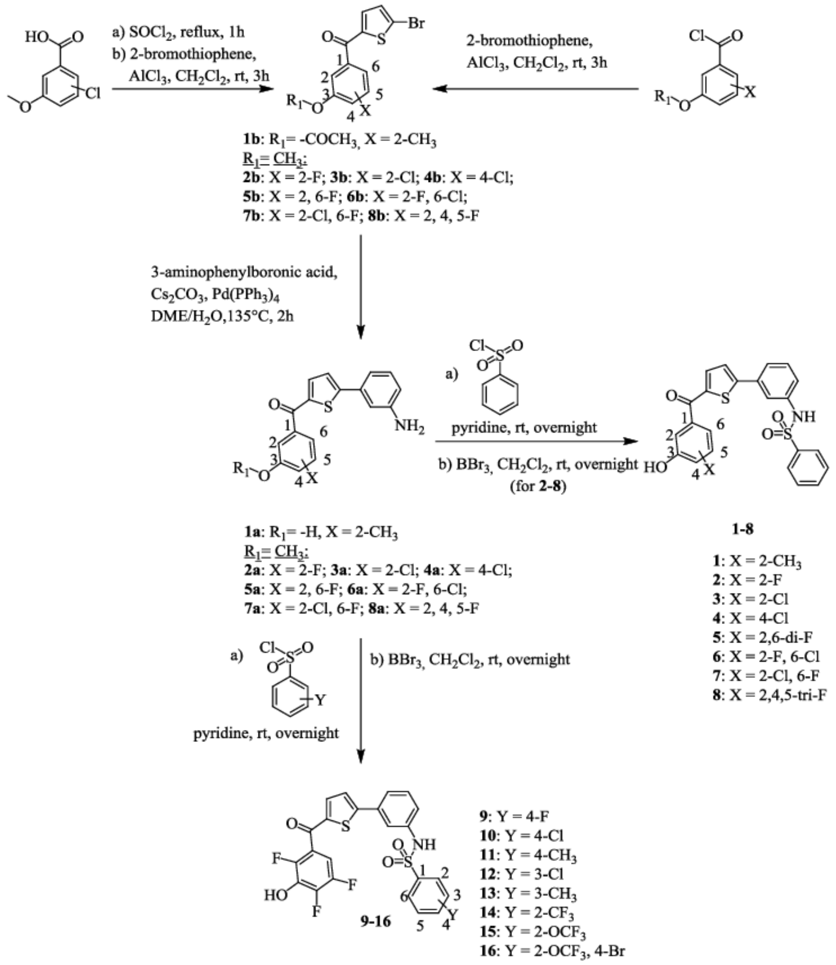
a) $SOCl_2$, reflux, 1h
b) 2-bromothiophene, $AlCl_3$, CH_2Cl_2, rt, 3h
2-bromothiophene, $AlCl_3$, CH_2Cl_2, rt, 3h
1b: R_1= -$COCH_3$, X = 2-CH_3
R_1= CH_3:
2b: X = 2-F; 3b: X = 2-Cl; 4b: X = 4-Cl;
5b: X = 2, 6-F; 6b: X = 2-F, 6-Cl;
7b: X = 2-Cl, 6-F; 8b: X = 2, 4, 5-F
3-aminophenylboronic acid, Cs_2CO_3, $Pd(PPh_3)_4$ DME/H_2O,135°C, 2h
a) pyridine, rt, overnight
b) BBr_3, CH_2Cl_2, rt, overnight (for 2-8)
1a: R_1= -H, X = 2-CH_3
R_1= CH_3:
2a: X = 2-F; 3a: X = 2-Cl; 4a: X = 4-Cl;
5a: X = 2, 6-F; 6a: X = 2-F, 6-Cl;
7a: X = 2-Cl, 6-F; 8a: X = 2, 4, 5-F
1-8
1: X = 2-CH_3
2: X = 2-F
3: X = 2-Cl
4: X = 4-Cl
5: X = 2,6-di-F
6: X = 2-F, 6-Cl
7: X = 2-Cl, 6-F
8: X = 2,4,5-tri-F
a) pyridine, rt, overnight
b) BBr_3, CH_2Cl_2, rt, overnight
9-16
9: Y = 4-F
10: Y = 4-Cl
11: Y = 4-CH_3
12: Y = 3-Cl
13: Y = 3-CH_3
14: Y = 2-CF_3
15: Y = 2-OCF_3
16: Y = 2-OCF_3, 4-Br

viability over 66 h) up to concentrations that were approximately 11 000-fold over the respective *h*17*β*-HSD2 IC_{50} value.

We also checked whether **14** and **15** do not bind to ERs at relevant concentrations to avoid E2 being blocked from activating ER receptors in bone. Compound **15** displayed negligible ER*α* and ER*β* binding, whereas **14** showed a higher ER binding (i.e., 28 and 21% inhibition of E2 binding in the presence of a 1000-fold excess of **15** over E2 vs 64 and 49% inhibition in the presence of 1000-fold excess of **14**, respectively). Compound **15** was able to inhibit endogenously expressed 17*β*-HSD2 in the cellular assay (human MDA-MB 231 cells) with an IC_{50} of 2.4 nM, which is very similar to the IC_{50} of 2.0 nM in the 17*β*-HSD2 cell-free assay (Table 1). This indicates that compound **15** readily enters cells at pharmacologically relevant concentrations.

We thus selected **15** for further profiling and investigated in vitro whether **15** does not induce the expression of hepatic CYP450 enzymes, which otherwise may reduce the plasma concentrations of **15** during repetitive dosing in the bone fracture healing study. At 3.16 *μ*M, **15** did neither activate the aryl hydrocarbon receptor, constitutive androstane receptor, nor the pregnane X receptor (<5% activation). These nuclear receptors are the transcription factors of the CYP1, CYP2, and CYP3 families of CYP450 hepatic enzymes, respectively. We next investigated whether or not the pharmacokinetic profile of **15** would allow *proof-of-principle* testing in a well-established, reproducible bone fracture model in mice.[16,24,25] For this, **15** was administered subcutaneously in C57BL/6 mice (50 mg/kg body weight) as a suspension in 0.5% gelatine/5% mannitol in water. Compound **15** showed a stable plasma concentration over 24 h after a single-dose administration: 264 nM at 2 h, 175 nM at 18 h, and 191 nM at 24 h, all ~10-fold higher than the *m*17*β*-HSD2 IC_{50} of 25 nM and thus sufficiently high to block *m*17*β*-HSD2 by >90% in vitro during 24 h. This corresponds to the fairly high metabolic stability measured in mouse liver S9 fraction ($t_{1/2}$ of 46 min).

Next, to analyze bone fracture repair, C57BL/6 male mice received **15** subcutaneously once daily (50 mg/kg) or vehicle (0.5% gelatine/5% mannitol in water) for 14 or 28 days, starting immediately following fracturing of the femur under anesthesia. Bending stiffness of fractured bones, relative to the contralateral unfractured bones in the same animal, is the upmost important functional recovery parameter at the site of the fracture in bone fracture healing.[16,24,25] After 14 and 28 days, the bending stiffness of the fractured femurs of the

DOI: 10.1021/acs.jmedchem.8b01493
J. Med. Chem. 2019, 62, 1362−1372

Table 1. Inhibition of 17β-HSD2 and 17β-HSD1 by A and 1−16

			IC$_{50}$ (nM)[a]			IC$_{50}$ (nM)[a]	% inh.@500 nM[a]	metabolic stability $t_{1/2}$ (min)
Cmpd	X	Y	h17β-HSD2	h17β-HSD1	s.f.[b]	m17β-HSD2	m17β-HSD1	human liver S9
A			111	21	0.2	n.i.[c]	n.i.[c]	<5
1	2-CH$_3$	−H	231	306	1.3	n.i.[c]	n.i.[c]	n.d.[d]
2	2-F	−H	6.9	7.2	1	81.6	12	n.d.[d]
3	2-Cl	−H	0.9	20.3	22.5	2.7	26	<5
4	4-Cl	−H	13.8	8.2	0.6	303.5	22	n.d.[d]
5	2,6-di-F	−H	5.6	1.4	0.3	30.5	43	n.d.[d]
6	2-F,6-Cl	−H	8.5	1.7	0.2	8.9	54	n.d.[d]
7	2-Cl,6-F	−H	6.7	15.6	2.3	2.7	25	<5
9	2,4,5-tri-F	4-F	1.2	1.2	1	27.3	24	32
10	2,4,5-tri-F	4-Cl	0.4	0.7	1.8	6.2	31	40
11	2,4,5-tri-F	4-CH$_3$	0.2	0.1	0.5	9.9	30	32
12	2,4,5-tri-F	3-Cl	0.4	0.8	2	5.6	28	42
13	2,4,5-tri-F	3-CH$_3$	0.2	0.1	0.5	7.9	49	28
14	2,4,5-tri-F	2-CF$_3$	1.4	4.8	3.4	11.6	30	51
15	2,4,5-tri-F	2-OCF$_3$	2.0	6.0	3	24.5	25 (1764 nM)[e]	60
16	2,4,5-tri-F	2-OCF$_3$,4-Br	1.8	2.4	1.3	14.0	30	n.d.[d]

[a]Mean value of at least two determinations, standard deviation less than 20%. [b]s.f.: selectivity factor = hIC$_{50}$(17β-HSD1)/hIC$_{50}$(17β-HSD2). [c]n.i.: no inhibition@1 μM. [d]n.d.: not determined. [e]mIC$_{50}$(17β-HSD1). Final concentration of E1 and E2 in h17β-HSD1 and h17β-HSD2 assay: 500 and 500 nM, respectively. Final concentration of E1 and E2 in m17β-HSD1 and m17β-HSD2 assay: 10 and 10 nM, respectively.

vehicle-treated animals was 27.6 and 40.9% of the stiffness determined in the nonfractured femurs of the same animal, respectively. These values are similar to those reported previously in C57BL/6 mice.[24] After 14 days, no difference in bending stiffness could be discerned between the **15**- and vehicle-treated animals (Figure 1 and Table S1) or in the periosteal area of the callus (i.e., the area that represents the newly formed tissue around the fracture) (Figure 2A and Table S1). However, after 28 days, the bending stiffness of the fractured bones in animals treated with **15** was almost twice as high as the bending stiffness of the fractured bones of vehicle-treated animals (P = 0.005) (Figure 1 and Table S1). The strong increase in bending stiffness was accompanied with a 61% larger periosteal area of the callus (P = 0.026) in **15**-treated animals at 28 days (Figure 2A and Table S1). Representative photographs of the callus of healing fractured femurs after 28 days of treatment with **15** and vehicle are shown in Figure 2B.

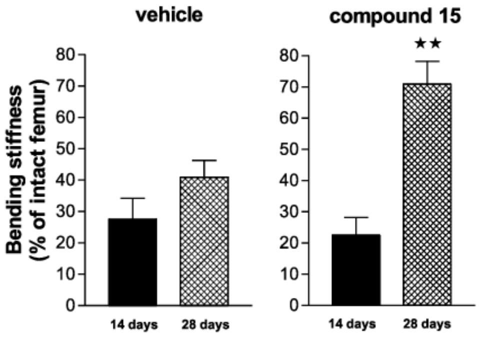

Figure 1. Effect of compound **15** on the bending stiffness of the fractured femurs of C57BL/6 male mice after 14 and 28 days of treatment. **indicates $P < 0.01$ in bone bending stiffness between the vehicle- and **15**-treated animals at 28 days (Student's t test).

The periosteal area in the callus of **15**-treated animals consisted of a larger bone area than in the vehicle-treated animals after 28 days (Figure 2C and Table S2, P = 0.025), whereas the cartilage and fibrous tissue areas in the periosteal callus area were not different (Table S2). Bone mineralization, that is, the rise in the so-called high-density bone (from ~7% at 14 days to ~18% at 28 days), and increase in bone mineral density (from ~0.24 g/cm^3 at 14 days to ~0.32 g/cm^3 at 28 days) proceeded normally (Tables S3 and S4). The same holds true for the trabecular number, trabecular thickness, and trabecular separation in the callus (Table S4). Compound **15** does not affect bone mineral density, trabecular number, trabecular thickness, and trabecular separation in the nonfractured (intact) femurs of the animals (Table S5). Compound **15** also does not influence the normal cortical bone distant from the fracture: the diameter measurements of the femurs demonstrate comparable values in the **15**-treated animals and vehicle controls (Table S6). These results indicate that 17β-HSD2 inhibition stimulates bone formation in the callus. As resorption of "old" bone at the fracture site precedes new bone formation, we also investigated whether or not **15** increases the expression of osteoprotegerin (OPG), a biomarker of the inhibition of bone resorption. OPG is an E2-inducible, antiresorptive decoy receptor for the receptor activator of nuclear factor κB ligand (RANKL), which in turn promotes bone resorption.[26] Indeed, treatment with **15** for 14 days increased the expression of OPG in callus by 55% (P = 0.048) compared to vehicle treatment, whereas the expression of RANKL in callus did not differ (−1% change). These data are consistent with our working hypothesis that 17β-HSD2 inhibition leads to both E2-mediated suppression of bone resorption and T-mediated stimulation of bone formation and demonstrate the target engagement of the 17β-HSD2 inhibitor. These data also demonstrate that despite a lack of change in the bending stiffness of the fractured bone after 14 days (Figure 1), biochemical changes do occur (i.e., increase in OPG expression) within the first 14 days of treatment with **15**. The process of remodeling in the **15** group is apparently not completed at day 28 (compared to the vehicle group), as indicated by the still larger callus, which might be because of both these underlying E2- and T-mediated processes.

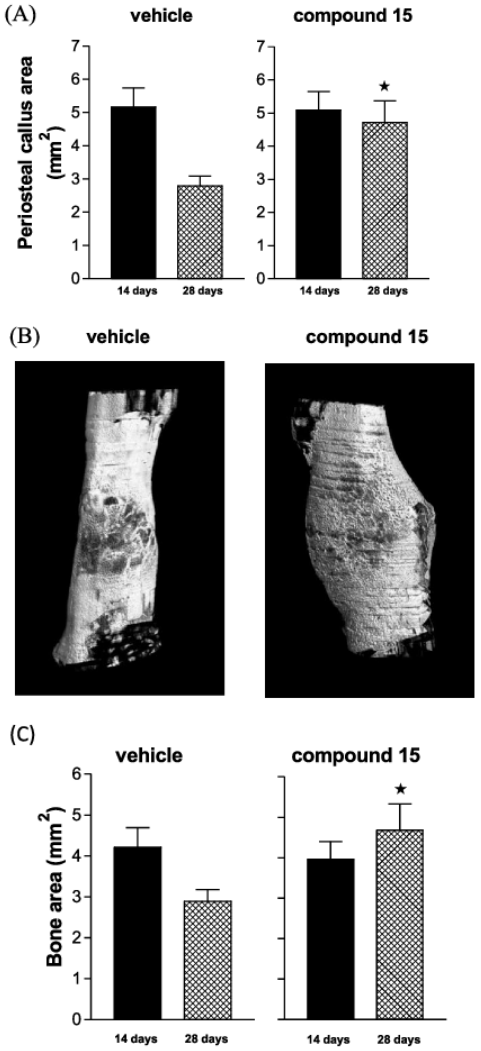

Figure 2. Effect of compound **15** on the periosteal callus area (A), callus size (B), and bone area (C) of the fractured femurs of C57BL/6 male mice after 14 and 28 days of treatment. * indicates $P < 0.05$ regarding the difference in the periosteal callus area and bone area between the vehicle- and **15**-treated animals at 28 days (Student's *t* test).

Notwithstanding the incomplete remodeling at day 28, this target engagement results in a markedly higher biomechanical stability of the healing fracture without affecting the bone quality. Importantly, 28 days of treatment with **15** did not change the plasma concentrations of E2 and T (Table S7). This is in full accordance with the working hypothesis that 17β-HSD2 regulates predominantly intracellular concentrations of E2 and T. In support, the weight of seminal vesicles, which is known to be highly sensitive to the changes in plasma testosterone,[11,27] was not different between **15**- and vehicle-treated animals after 14 or 28 days (Table S8). We cannot exclude completely that **15** acts via another unknown mechanism, independent of 17β-HSD2, or inhibits an unknown 17β-HSD2 function which is independent of E2 and T. However, this seems highly unlikely. First, our data are commensurate with 17β-HSD2 inhibition: the plasma concentrations of **15** are sufficiently high (and not too high) to block mouse 17β-HSD2, and our bone E2-inducible biomarker OPG is upregulated in the callus of **15**-treated animals. Second, 17β-HSD2 expression in bone tissue is superior over that of 17β-HSD1, 17β-HSD3, and 17β-HSD4: the enzymes that are structurally and functionally the most similar to 17β-HSDS2 and which catalyze the synthesis and degradation of E2 and T. Third, **15** does not markedly bind to E2 receptors, ruling out that **15** acts by stimulating E2 receptors. Fourth, no effects on (control) bone parameters (bone strength and diameter, trabecular number, separation, and thickness), no change in plasma E2 and T, no effect on liver, testicles, seminal vesicles, or body weight (Table S9), and no change in animal behavior during the 28 days of treatment were observed.

■ CONCLUSIONS

In summary, this study provides for the first time *proof-of-principle* of a 17β-HSD2 inhibitor: inhibition of 17β-HSD2 strongly increases the mechanical stability of the fractured bone because of a larger callus with a newly formed bone without changing the plasma E2 and T concentrations and disturbance of the hypothalamus−pituitary−testes axis. In follow-up studies toward *Proof of Concept* in human patients, compound **15** should be tested for in vivo safety and pharmacokinetic properties in nonrodents, including nonhuman primates (monkeys), and for confirmation of its bone fracture healing efficacy in larger animals. As low-molecular-weight 17β-HSD2 inhibitors shorten the period of immobility during bone fracture healing, 17β-HSD2 inhibitors thus represent a highly attractive, targeted endocrine therapy to treat fractures of fragile bones in patients with osteoporosis and in the elderly.

■ EXPERIMENTAL SECTION

Chemical Methods. Chemical names follow IUPAC nomenclature. The starting materials were purchased from Aldrich, Acros, Combi-Blocks, or Fluorochem and were used without purification. Gravity-flow column chromatography (CC) was performed on silica gel (70−200 μm), and the reaction progress was monitored by TLC on Alugram SIL G/UV254 (Macherey-Nagel). Visualization was accomplished with UV light. The ^{1}H nuclear magnetic resonance (NMR), ^{13}C NMR, and ^{19}F NMR spectra were measured on a Bruker AM500 spectrometer (at 500 MHz, 125, and 470 MHz, respectively) at 300 K and on a Bruker Fourier 300 (at 300 and 75 MHz, respectively) at 300 K. Chemical shifts are reported in δ (parts per million: ppm), by reference to the hydrogenated residues of deuterated solvents as internal standards: 2.05 ppm (^{1}H NMR) and 29.8 and 206.3 ppm (^{13}C NMR) for acetone-d_6, 2.50 ppm (^{1}H NMR) and 39.52 ppm (^{13}C NMR) for dimethyl sulfoxide (DMSO)-d_6. In case of ^{19}F NMR, trifluoroacetic acid (TFA) was added as an internal standard: δ −76.5 ppm ($CF_{3,TFA}$). The signals are described as br (broad), s (singlet), d (doublet), t (triplet), dd (doublet of doublets), ddd (doublet of doublet of doublets), dt (doublet of triplets), and m (multiplet). All coupling constants (*J*) are given in Hertz (Hz). Mass spectrometry was performed on a TSQ Quantum (Thermo Fisher, Dreieich, Germany). The triple quadrupole mass spectrometer was equipped with an electrospray interface. The purity of compounds was determined by liquid chromatography−mass spectrometry (LCMS) using the area percentage method on the UV trace, recorded at a wavelength of 254 nm, and found to be >95%. The Surveyor LC system consisted of a pump, an autosampler, and a PDA detector. The system was operated by the standard software Xcalibur. An RP C18 NUCLEODUR 100-5 (3 mm) column (Macherey-Nagel

DOI: 10.1021/acs.jmedchem.8b01493
J. Med. Chem. 2019, 62, 1362−1372

GmbH, Düren, Germany) was used as the stationary phase. All solvents were high-pressure liquid chromatography (HPLC) grade. In a gradient run, using acetonitrile and water, the percentage of acetonitrile (containing 0.1% trifluoroacetic acid) was increased from an initial concentration of 0% at 0 min to 100% at 13 min and kept at 100% for 2 min. The injection volume was 15 μL and the flow rate was set to 800 μL/min. MS analysis was carried out at a needle voltage of 3000 V and a capillary temperature of 350 °C. Mass spectra were acquired in positive mode, using the electron spray ionization (ESI) method, from 100 to 1000 m/z, and the UV spectra were recorded at the wavelength of 254 nm and in some cases at 360 nm. High-resolution mass spectrometry (HRMS) measurements were recorded on a SpectraSystems-MSQ LCMS system (Thermo Fisher, Dreieich, Germany).

Method A: General Procedure for Friedel–Crafts Acylation. An ice-cooled mixture of arylcarbonyl chloride (1 equiv), monosubstituted thiophene derivative (1.5 equiv), and aluminum trichloride (1 equiv) in anhydrous dichloromethane (10 mL/mmol of arylcarbonyl chloride) was warmed to room temperature and stirred for 2−4 h. A 10 mL of HCl (1 M) was used to quench the reaction. The aqueous layer was extracted with dichloromethane (3 × 50 mL). The combined organic layers were washed with brine, dried over magnesium sulfate, filtered, and concentrated to dryness. The product was used directly in the subsequent reaction without further purification.

Method B: General Procedure for Suzuki–Miyaura Coupling. A mixture of arylbromide (1 equiv), boronic acid derivative (1.2 equiv), cesium carbonate (4 equiv) and tetrakis(triphenylphosphine) palladium (0.05 equiv) was suspended in an oxygen-free dimethyl ether/water (1:1, v/v, 15 mL/mmol of arylbromide) solution and refluxed under a nitrogen atmosphere. The reaction mixture was cooled to room temperature. The aqueous layer was extracted with ethyl acetate (3 × 50 mL). The organic layer was washed once with brine and once with water, dried over $MgSO_4$, filtered, and the solution was concentrated under reduced pressure. The product was purified by CC.

Method C: General Procedure for Sulfonamide Coupling. The amino phenyl derivative (1 equiv) was dissolved in absolute pyridine (10 mL/mmol of reactant), and sulfonyl chloride (1.2 equiv) was added. The reaction mixture was stirred overnight at room temperature. The reaction was quenched by adding 10 mL of 2 M HCl and extracted with ethyl acetate (3 × 50 mL). The organic layers were washed with saturated $NaHCO_3$ and brine, dried over magnesium sulfate, filtered, and concentrated to dryness. The product was used directly in the subsequent reaction without further purification.

Method D: General Procedure for Ether Cleavage. To a solution of respective methoxyaryl compound (1 equiv) in dry dichloromethane (20 mL/mmol of reactant), boron tribromide, 1 M solution in dichloromethane (3 equiv), was added dropwise at 0 °C and stirred overnight at room temperature. After the completion of the reaction, the mixture was diluted with water. The aqueous layer was extracted with dichloromethane (3 × 50 mL). The combined organic layers were washed with brine, dried over magnesium sulfate, and evaporated to dryness under reduced pressure. The product was purified by CC.

*Acetic Acid 3-(5-Bromo-thiophene-2-carbonyl)-2-methyl-phenyl Ester (**1b**).* The title compound was prepared by the reaction of 2-bromothiophene (1150 mg, 7.05 mmol), 3-acetyloxy-2-methylbenzoyl chloride (1000 mg, 4.70 mmol), and aluminum chloride (627 mg, 4.70 mmol) according to method A. The crude product was used directly in the subsequent reaction without further purification [750 mg; MS (ESI) m/z: 338.9 (M + H)$^+$, $C_{14}H_{12}BrO_3S^+$ calcd 338.90].

*[5-(3-Aminophenyl)thiophen-2-yl](3-hydroxy-2-methylphenyl)-methanone (**1a**).* The title compound was prepared by the reaction of acetic acid 3-(5-bromo-thiophene-2-carbonyl)-2-methyl-phenyl ester (**1b**) (750 mg, 2.21 mmol), 3-aminophenylboronic acid (365 mg, 2.65 mmol), cesium carbonate (2875 mg, 8.84 mmol), and tetrakis(triphenylphosphine) palladium (128 mg, 111 μmol) according to method B. The product was purified by CC (petroleum ether/ethyl acetate 1:1); yield: 33% (230 mg). ^{1}H NMR (500 MHz, acetone-d_6): δ 8.72 (s, 1H), 7.70 (ddd, J = 11.8, 5.2, 3.2 Hz, 1H), 7.65−7.60 (m, 2H), 7.42 (t, J = 3.9 Hz, 1H), 7.39 (t, J = 3.5 Hz, 1H), 7.19−7.11 (m, 1H), 6.96−6.93 (m, 1H), 6.78−6.68 (m, 1H), 4.89 (s, 2H), 2.17 (s, 3H). MS (ESI) m/z: 310.1 (M + H)$^+$, $C_{18}H_{16}NO_2S^+$ calcd 310.0.

N-{3-[5-(3-Hydroxy-2-methylbenzoyl)thiophen-2-yl]phenyl}-benzenesulfonamide (1). The title compound was prepared by the reaction of [5-(3-aminophenyl)thiophen-2-yl](3-hydroxy-2-methylphenyl)methanone (**1a**) (230 mg, 0.74 mmol) and benzenesulfonyl chloride (156 mg, 0.88 mmol) according to method C. The product was purified by CC (dichloromethane/methanol 99:1); yield: 25% (85 mg). ^{1}H NMR (500 MHz, acetone-d_6): δ 9.24 (s, 1H), 8.67 (s, 1H), 7.93−7.79 (m, 2H), 7.61 (m, 2H), 7.57−7.52 (m, 2H), 7.51−7.47 (m, 1H), 7.45 (d, J = 4.0 Hz, 1H), 7.41 (d, J = 4.0 Hz, 1H), 7.36 (t, J = 7.9 Hz, 1H), 7.28 (ddt, J = 8.1, 2.0, 0.9 Hz, 1H), 7.19−7.13 (m, 1H), 7.06−7.02 (m, 1H), 6.96 (dd, J = 7.5, 1.1 Hz, 1H), 2.18 (s, 3H). ^{13}C NMR (125 MHz, acetone-d_6): δ 190.3, 156.7, 152.9, 144.7, 141.1, 139.7, 137.3, 135.0, 133.9, 133.9, 131.1, 130.0, 128.0, 127.0, 125.7, 123.0, 121.9, 119.8, 118.7, 117.4, 117.3, 12.9. MS (ESI) t_R 8.31 min, m/z: 450.0 (M + H)$^+$, $C_{24}H_{20}NO_4S_2^+$ calcd 450.0; HRMS m/z: 450.08099 ([M + H]$^+$, $C_{24}H_{20}NO_4S_2^+$ calcd 450.08280).

*N-{3-[5-(2-Fluoro-3-hydroxy-benzoyl)-thiophen-2-yl]-phenyl}-benzenesulfonamide (**2**).* The title compound was prepared by the reaction of [5-(3-aminophenyl)thiophen-2-yl](2-fluoro-3-methoxyphenyl)methanone (**2a**) (400 mg, 1.22 mmol) and benzenesulfonyl chloride (259 mg, 1.46 mmol) according to method C. The crude product was reacted with boron tribromide (3 equiv) according to method D. The product was purified by CC (dichloromethane/methanol 99:1); yield over two steps: 14% (80 mg). ^{1}H NMR (500 MHz, acetone-d_6): δ 9.27 (s, 1H), 9.13 (s, 1H), 7.93−7.82 (m, 2H), 7.60 (dd, J = 10.5, 4.2 Hz, 2H), 7.55 (dt, J = 14.7, 4.4 Hz, 3H), 7.49 (t, J = 6.2 Hz, 2H), 7.37 (t, J = 7.9 Hz, 1H), 7.32−7.27 (m, 1H), 7.23 (td, J = 8.1, 1.7 Hz, 1H), 7.18 (t, J = 7.8 Hz, 1H), 7.09−7.03 (m, 1H). ^{13}C NMR (125 MHz, acetone-d_6): δ 184.9, 153.4, 149.3 (d, J = 245.9 Hz), 146.3 (d, J = 12.9 Hz), 143.7, 140.6, 139.8, 137.6, 134.9, 133.9, 131.1, 130.0, 128.7 (d, J = 13.0 Hz), 128.0, 125.9, 125.4 (d, J = 4.2 Hz), 123.0, 122.0, 121.3 (d, J = 2.9 Hz), 120.6, 118.7. MS (ESI) t_R 8.31 min, m/z: 454.0 (M + H)$^+$, $C_{23}H_{17}FNO_4S_2^+$ calcd 454.0; HRMS m/z: 454.05588 (M + H)$^+$, $C_{23}H_{17}FNO_4S_2^+$ calcd 454.05775.

*(5-Bromothiophen-2-yl)(2-chloro-3-methoxyphenyl)methanone (**3b**).* 2-Chloro-3-methoxy-benzoic acid (400 mg, 2.14 mmol, 1 equiv) was dissolved in thionyl chloride (4320 mg, 36.4 mmol, 17 equiv) and stirred under reflux for 1 h. The solution was concentrated in vacuum, and the crude product was reacted with 2-bromothiophene (523 mg, 3.21 mmol) and aluminum chloride (285 mg, 2.14 mmol) according to method A. In slight variation, the mixture was stirred at room temperature overnight. The crude product was used directly in the subsequent reaction without further purification [500 mg; MS (ESI) m/z: 330.96 (M + H)$^+$, $C_{12}H_9BrClO_2S^+$ calcd 330.9].

*N-{3-[5-(2-Chloro-3-hydroxy-benzoyl)-thiophen-2-yl]-phenyl}-benzenesulfonamide (**3**).* The title compound was prepared by the reaction of [5-(3-aminophenyl)thiophen-2-yl](2-chloro-3-methoxyphenyl)methanone (**3a**) (450 mg, 1.30 mmol) and benzenesulfonyl chloride (277 mg, 1.57 mmol) according to method C. The crude product was reacted with boron tribromide (3 equiv) according to method D. The product was purified by CC (dichloromethane/methanol 99:1); yield over two steps: 19% (100 mg). ^{1}H NMR (500 MHz, acetone-d_6): δ 9.26 (s, 1H), 9.22 (s, 1H), 7.87 (ddd, J = 7.0, 3.2, 1.8 Hz, 2H), 7.64−7.58 (m, 2H), 7.57−7.52 (m, 2H), 7.50 (ddd, J = 7.7, 1.7, 1.0 Hz, 1H), 7.47 (d, J = 4.0 Hz, 1H), 7.42 (d, J = 4.0 Hz, 1H), 7.37 (t, J = 7.9 Hz, 1H), 7.33 (dd, J = 8.1, 7.5 Hz, 1H), 7.29 (ddd, J = 8.1, 2.1, 0.9 Hz, 1H), 7.20 (dd, J = 8.2, 1.5 Hz, 1H), 7.03 (dd, J = 7.5, 1.5 Hz, 1H). ^{13}C NMR (125 MHz, acetone-d_6): δ 187.0, 154.4, 153.6, 143.3, 140.6, 140.5, 139.8, 137.8, 134.9, 133.9, 131.1, 130.0, 128.7, 128.0, 125.9, 123.0, 122.0, 120.4, 118.9, 118.7, 117.9. MS (ESI) t_R 8.30 min, m/z: 470.0 (M + H)$^+$, $C_{23}H_{17}ClNO_4S_2^+$ calcd 470.0; HRMS m/z: 470.02643 ([M + H]$^+$, $C_{23}H_{17}ClNO_4S_2^+$ calcd 470.02820).

*N-{3-[5-(4-Chloro-3-hydroxybenzoyl)thiophen-2-yl]phenyl}benzenesulfonamide (**4**).* The title compound was prepared by the reaction of [5-(3-aminophenyl)thiophen-2-yl](4-chloro-3-methoxyphenyl)methanone (**4a**) (450 mg, 1.30 mmol) and benzenesulfonyl chloride (277 mg, 1.57 mmol) according to method C. The crude product was reacted with boron tribromide (3 equiv) according to method D. The product was purified by CC (dichloromethane/methanol 99:1); yield over two steps: 23% (120 mg). ^{1}H NMR (500 MHz, acetone-d_6): δ 9.36 (s, 1H), 9.28 (s, 1H), 7.90–7.85 (m, 2H), 7.72 (d, *J* = 4.0 Hz, 1H), 7.64–7.59 (m, 2H), 7.57–7.53 (m, 3H), 7.52–7.49 (m, 3H), 7.41–7.35 (m, 2H), 7.28 (ddd, *J* = 8.1, 2.1, 1.0 Hz, 1H). ^{13}C NMR (125 MHz, acetone-d_6): δ 186.6, 154.0, 152.6, 143.1, 140.6, 139.7, 138.5, 137.0, 134.9, 133.9, 131.1, 131.0, 130.0, 128.0, 125.7, 125.6, 123.0, 122.0, 121.9, 118.7, 117.6. MS (ESI) t_R 8.74 min, *m/z*: 470.0 (M + H)$^+$, $C_{23}H_{17}ClNO_4S_2^+$ calcd 470.0; HRMS *m/z*: 470.02631 ([M + H]$^+$, $C_{23}H_{17}ClNO_4S_2^+$ calcd 470.02820).

*N-{3-[5-(2,6-Difluoro-3-hydroxybenzoyl)thiophen-2-yl]phenyl}benzenesulfonamide (**5**).* The title compound was prepared by the reaction of [5-(3-aminophenyl)thiophene-2-yl](3-methoxy-2,6-difluorophenyl)methanone (**5a**) (390 mg, 0.83 mmol) and benzenesulfonyl chloride (177 mg, 0.99 mmol) according to method C. The crude product was reacted with boron tribromide (3 equiv) according to method D. The product was purified by CC (dichloromethane/methanol 99:1) followed by washing with petroleum ether/diethyl ether 2:1; yield over two steps: 28% (150 mg). ^{1}H NMR (500 MHz, acetone-d_6): δ 9.26 (s, 1H), 9.06 (s, 1H), 7.91–7.84 (m, 2H), 7.65–7.58 (m, 3H), 7.58–7.50 (m, 4H), 7.41–7.36 (m, 1H), 7.30 (ddd, *J* = 8.1, 2.1, 1.0 Hz, 1H), 7.25–7.18 (m, 1H), 7.07–7.00 (m, 1H). ^{13}C NMR (125 MHz, acetone-d_6): δ 180.6, 154.5, 152.5 (dd, *J* = 240.5, 5.8 Hz), 148.4 (dd, *J* = 245.8, 7.7 Hz), 143.4, 142.6 (dd, *J* = 12.9, 3.1 Hz), 140.6, 139.8, 138.2, 134.7, 133.9, 131.2, 130.0, 128.0, 126.2, 123.1, 122.2, 120.3 (dd, *J* = 9.1, 3.8 Hz), 118.8, 118.0 (dd, *J* = 23.9, 19.7 Hz), 112.4 (dd, *J* = 22.8, 3.9 Hz). MS (ESI) t_R 8.37 min, *m/z*: 472.0 (M + H)$^+$, $C_{23}H_{16}F_2NO_4S_2^+$ calcd 472.0; HRMS *m/z*: 472.04626 ([M + H]$^+$, $C_{23}H_{16}F_2NO_4S_2^+$ calcd 472.04833).

*N-{3-[5-(6-Chloro-2-fluoro-3-hydroxybenzoyl)thiophen-2-yl]phenyl}benzenesulfonamide (**6**).* The title compound was prepared by the reaction of [5-(3-aminophenyl)thiophen-2-yl](6-chloro-2-fluoro-3-methoxyphenyl)methanone (**6a**) (380 mg, 1.05 mmol) and benzenesulfonyl chloride (223 mg, 1.26 mmol) according to method C. The crude product was reacted with boron tribromide (3 equiv) according to method D. The product was purified by CC (dichloromethane/methanol 99:1) followed by washing with petroleum ether/diethyl ether 2:1; yield over two steps: 22% (115 mg). ^{1}H NMR (500 MHz, acetone-d_6): δ 9.38 (s, 1H), 9.27 (s, 1H), 7.91–7.82 (m, 2H), 7.64–7.59 (m, 2H), 7.57–7.50 (m, 5H), 7.38 (dd, *J* = 12.0, 4.2 Hz, 1H), 7.30 (ddd, *J* = 8.1, 2.1, 1.0 Hz, 1H), 7.25 (dd, *J* = 8.8, 1.4 Hz, 1H), 7.19 (t, *J* = 8.9 Hz, 1H). ^{13}C NMR (125 MHz, acetone-d_6): δ 182.5, 154.5, 149.0 (d, *J* = 244.9 Hz), 145.2 (d, *J* = 12.9 Hz), 142.9, 140.6, 139.8, 138.1, 134.7, 133.9, 131.2, 130.0, 128.4 (d, *J* = 19.6 Hz), 128.0, 126.6 (d, *J* = 3.7 Hz), 126.3, 123.1, 122.2, 120.8 (d, *J* = 4.2 Hz), 120.5 (d, *J* = 3.5 Hz), 118.8. MS (ESI) t_R 8.65 min, *m/z*: 488.0 (M + H)$^+$, $C_{23}H_{16}ClFNO_4S_2^+$ calcd 488.0; HRMS *m/z*: 488.01669 ([M + H]$^+$, $C_{23}H_{16}ClFNO_4S_2^+$ calcd 488.01878).

*N-{3-[5-(2-Chloro-6-fluoro-3-hydroxybenzoyl)thiophen-2-yl]phenyl}benzenesulfonamide (**7**).* The title compound was prepared by the reaction of [5-(3-aminophenyl)thiophen-2-yl](2-chloro-6-fluoro-3-methoxyphenyl)methanone (**7b**) (450 mg, 1.24 mmol) and benzenesulfonyl chloride (264 mg, 1.49 mmol) according to method C. The crude product was reacted with boron tribromide (3 equiv) according to method D. The product was purified by CC (dichloromethane/methanol 99:1) followed by washing with petroleum ether/diethyl ether 2:1; yield: 25% (150 mg). ^{1}H NMR (500 MHz, acetone-d_6): δ 9.28 (s, 1H), 7.91–7.80 (m, 2H), 7.65–7.59 (m, 2H), 7.57–7.49 (m, 5H), 7.38 (t, *J* = 7.9 Hz, 1H), 7.30 (d, *J* = 7.5 Hz, 1H), 7.23–7.15 (m, 2H). ^{13}C NMR (125 MHz, acetone-d_6): δ 182.6, 154.4, 153.1 (d, *J* = 239.4 Hz), 151.0 (d, *J* = 13.5 Hz), 142.9, 140.6 (d, *J* = 7.5 Hz), 139.8 (d, *J* = 9.6 Hz), 137.9, 134.7, 133.9, 131.2, 130.0, 128.3 (d, *J* = 23.6 Hz), 128.0, 126.2, 123.1 (d, *J* = 1.5 Hz), 122.2 (d, *J* = 3.7 Hz), 118.9 (d, *J* = 11.4 Hz), 118.8 (d, *J* = 3.3 Hz), 116.1, 115.9. MS (ESI) t_R 8.44 min, *m/z*: 488.0 (M + H)$^+$, $C_{23}H_{16}ClFNO_4S_2^+$ calcd 488.0; HRMS *m/z*: 488.01669 ([M + H]$^+$, $C_{23}H_{16}ClFNO_4S_2^+$ calcd 488.01878).

*N-{3-[5-(2,4,5-Trifluoro-3-hydroxy-benzoyl)-thiophen-2-yl]-phenyl}-benzenesulfonamide (**8**).* The title compound was prepared by the reaction of [5-(3-aminophenyl)thiophen-2-yl](2,4,5-trifluoro-3-methoxyphenyl)methanone (**8a**) (300 mg, 0.82 mmol) and benzenesulfonyl chloride (177 mg, 0.99 mmol) according to method C. The crude product was reacted with boron tribromide (3 equiv) according to method D. The product was purified by CC (dichloromethane/methanol 99:1) followed by washing with petroleum ether/diethyl ether 2:1; yield over two steps: 25% (100 mg). ^{1}H NMR (500 MHz, acetone-d_6): δ 10.02 (s, 1H), 9.24 (s, 1H), 7.87–7.81 (m, 2H), 7.64 (dd, *J* = 4.0, 1.7 Hz, 1H), 7.61–7.56 (m, 2H), 7.52 (t, *J* = 7.6 Hz, 2H), 7.50–7.46 (m, 2H), 7.35 (t, *J* = 7.9 Hz, 1H), 7.25 (dd, *J* = 8.1, 1.3 Hz, 1H), 7.09 (ddd, *J* = 9.9, 8.2, 5.7 Hz, 1H). ^{13}C NMR (125 MHz, acetone-d_6): δ 182.8, 154.0, 148.0 (ddd, *J* = 244.2, 11.1, 3.1 Hz), 147.0 (ddd, *J* = 245.1, 12.3, 3.7 Hz), 143.6 (ddd, *J* = 248.3, 15.8, 5.8 Hz), 142.9, 140.6, 139.8, 138.3 (d, *J* = 1.9 Hz), 137.1 (ddd, *J* = 15.8, 12.8, 2.3 Hz), 134.7, 133.9, 131.2, 130.0, 128.0, 126.0, 123.1, 123.2–122.8 (m), 122.1, 118.7, 106.9 (dd, *J* = 21.1, 2.9 Hz). MS (ESI) t_R 8.64 min, *m/z*: 490.0 (M + H)$^+$, $C_{23}H_{15}F_3NO_4S_2^+$ calcd 490.0; HRMS *m/z*: 490.03586 ([M + H]$^+$, $C_{23}H_{15}F_3NO_4S_2^+$ calcd 490.03891).

*4-Fluoro-N-{3-[5-(2,4,5-trifluoro-3-hydroxy-benzoyl)-thiophen-2-yl]-phenyl}-benzenesulfonamide (**9**).* The title compound was prepared by the reaction of [5-(3-aminophenyl)thiophen-2-yl](2,4,5-trifluoro-3-methoxyphenyl)methanone (**8a**) (300 mg, 0.82 mmol) and 4-fluorobenzene-1-sulfonyl chloride (194 mg, 0.99 mmol) according to method C. The crude product was reacted with boron tribromide (3 equiv) according to method D. The product was purified by CC (dichloromethane/methanol 97:3) followed by washing with petroleum ether/diethyl ether 2:1; yield over two steps: 12% (50 mg). ^{1}H NMR (500 MHz, acetone-d_6): δ 10.00 (s, 1H), 9.27 (s, 1H), 7.97–7.89 (m, 2H), 7.67 (dd, *J* = 4.1, 1.8 Hz, 1H), 7.63 (t, *J* = 1.8 Hz, 1H), 7.53 (ddd, *J* = 5.4, 2.9, 1.9 Hz, 2H), 7.39 (t, *J* = 7.9 Hz, 1H), 7.35–7.30 (m, 2H), 7.29 (ddd, *J* = 8.1, 2.1, 0.9 Hz, 1H), 7.12 (ddd, *J* = 9.9, 8.1, 5.6 Hz, 1H). ^{13}C NMR (125 MHz, acetone-d_6): δ 181.9, 165.1 (d, *J* = 252.6 Hz), 153.0, 147.1 (ddd, *J* = 244.1, 11.0, 3.1 Hz), 146.1 (ddd, *J* = 244.1, 4.1, 2.9 Hz), 142.7 (ddd, *J* = 248.5, 15.8, 5.8 Hz), 142.1, 138.7, 137.4 (d, *J* = 2.1 Hz), 136.1 (ddd, *J* = 18.2, 12.8, 3.0 Hz), 135.9 (d, *J* = 3.1 Hz), 133.9, 130.3, 130.1 (d, *J* = 9.6 Hz), 125.2, 122.4, 122.1 (ddd, *J* = 15.4, 6.5, 3.8 Hz), 121.4, 118.1, 116.2 (d, *J* = 22.9 Hz), 106.0 (dd, *J* = 21.1, 3.0 Hz). MS (ESI) t_R 8.78 min, *m/z*: 508.0 (M + H)$^+$, $C_{23}H_{14}F_4NO_4S_2^+$ calcd 508.0; HRMS *m/z*: 508.02756 ([M + H]$^+$, $C_{23}H_{14}F_4NO_4S_2^+$ calcd 508.02949).

*4-Chloro-N-{3-[5-(2,4,5-trifluoro-3-hydroxy-benzoyl)-thiophen-2-yl]-phenyl}-benzenesulfonamide (**10**).* The title compound was prepared by the reaction of [5-(3-aminophenyl)-thiophen-2-yl](2,4,5-trifluoro-3-methoxyphenyl)methanone (**8a**) (400 mg, 1.1 mmol) and 4-chlorobenzene-1-sulfonyl chloride (279 mg, 1.32 mmol) according to method C. The crude product was reacted with boron tribromide (3 equiv) according to method D. The product was purified by CC (dichloromethane/methanol 99:1); yield over two steps: 13% (75 mg). ^{1}H NMR (500 MHz, acetone-d_6): δ 9.40 (s, 1H), 7.89–7.84 (m, 2H), 7.66 (dd, *J* = 4.1, 1.8 Hz, 1H), 7.64 (t, *J* = 1.8 Hz, 1H), 7.60–7.56 (m, 2H), 7.54–7.50 (m, 2H), 7.39 (t, *J* = 7.9 Hz, 1H), 7.30 (ddd, *J* = 8.1, 2.1, 1.0 Hz, 1H), 7.11 (ddd, *J* = 9.9, 8.1, 5.6 Hz, 1H). ^{13}C NMR (125 MHz, acetone-d_6): δ 182.8, 153.9, 148.0 (ddd, *J* = 244.1, 11.0, 3.2 Hz), 147.0 (ddd, *J* = 244.2, 4.2, 2.9 Hz), 143.6 (ddd, *J* = 248.6, 15.8, 5.8 Hz), 143.0, 139.6, 139.5, 139.4, 138.2 (d, *J* = 2.0 Hz), 137.1 (ddd, *J* = 18.0, 12.7, 3.0 Hz), 134.8, 131.2, 130.2, 129.8, 126.1, 123.4, 123.0 (ddd, *J* = 15.4, 6.5, 3.8 Hz), 122.4, 119.0, 106.9 (dd, *J* = 21.1, 3.0 Hz). MS (ESI) t_R 9.10 min, *m/z*: 523.9 (M + H)$^+$, $C_{23}H_{14}ClF_3NO_4S_2^+$ calcd 523.9; HRMS *m/z*: 523.99725 ([M + H]$^+$, $C_{23}H_{14}ClF_3NO_4S_2^+$ calcd 523.99994).

*4-Methyl-N-{3-[5-(2,4,5-trifluoro-3-hydroxy-benzoyl)-thiophen-2-yl]-phenyl}-benzenesulfonamide (**11**).* The title compound was prepared by the reaction of [5-(3-aminophenyl)thiophen-2-yl](2,4,5-trifluoro-3-methoxyphenyl)methanone (**8a**) (400 mg, 1.1 mmol) and 4-methylbenzene-1-sulfonyl chloride (252 mg, 1.32 mmol) according to method C. The crude product was reacted with boron tribromide (3 equiv) according to method D. The product was purified by CC (dichloromethane/methanol 99:1) followed by washing with petroleum ether/diethyl ether 2:1; yield over two steps: 22% (120 mg). ^{1}H NMR (500 MHz, acetone-d_6): δ 10.04 (s, 1H), 9.19 (s, 1H), 7.77–7.73 (m, 2H), 7.67 (dd, J = 4.1, 1.8 Hz, 1H), 7.63 (dd, J = 2.9, 1.0 Hz, 1H), 7.53–7.49 (m, 2H), 7.40–7.33 (m, 3H), 7.29 (ddd, J = 8.1, 2.1, 1.0 Hz, 1H), 7.13 (ddd, J = 9.9, 8.1, 5.6 Hz, 1H), 2.35 (s, 3H). ^{13}C NMR (125 MHz, acetone-d_6): δ 182.8, 154.1, 148.1 (ddd, J = 243.9, 11.0, 2.9 Hz), 147.0 (ddd, J = 244.1, 4.1, 3.1 Hz), 144.7, 143.6 (ddd, J = 248.5, 15.8, 5.9 Hz), 142.9, 140.0, 138.2 (d, J = 1.9 Hz), 137.82, 137.0 (ddd, J = 18.3, 12.8, 3.1 Hz), 134.7, 131.1, 130.5, 128.0, 126.0, 123.0 (ddd, J = 15.9, 6.7, 4.1 Hz), 122.9, 121.9, 118.5, 106.9 (dd, J = 21.0, 3.0 Hz), 21.3. MS (ESI) t_R 8.90 min, m/z: 503.9 $(M + H)^+$, $C_{24}H_{17}F_3NO_4S_2^+$ calcd 504.0; HRMS m/z: 504.05258 ($[M + H]^+$, $C_{24}H_{17}F_3NO_4S_2^+$ calcd 504.05456).

*3-Chloro-N-{3-[5-(2,4,5-trifluoro-3-hydroxy-benzoyl)-thiophen-2-yl]-phenyl}-benzenesulfonamide (**12**).* The title compound was prepared by the reaction of [5-(3-aminophenyl)thiophen-2-yl](2,4,5-trifluoro-3-methoxyphenyl)methanone (**8a**) (300 mg, 0.82 mmol) and 3-chlorobenzene-1-sulfonyl chloride (211 mg, 1.00 mmol) according to method C. The crude product was reacted with boron tribromide (3 equiv) according to method D. The product was purified by CC (dichloromethane/methanol 99:1) followed by washing with petroleum ether/diethyl ether 2:1; yield over two steps: 42% (180 mg). ^{1}H NMR (500 MHz, acetone-*d6*): δ ^{1}H NMR (500 MHz, acetone-d_6): δ 10.10 (s, 1H), 9.35 (s, 1H), 7.70–7.64 (m, 2H), 7.63 (m, 2H), 7.63 (m, 1H), 7.59 (t, J = 7.9 Hz, 1H), 7.56 (dd, J = 7.8, 0.7 Hz, 1H), 7.53 (d, J = 4.0 Hz, 1H), 7.42 (t, J = 7.9 Hz, 1H), 7.30 (dd, J = 8.1, 1.2 Hz, 1H), 7.13 (ddd, J = 9.8, 8.2, 5.7 Hz, 1H). ^{13}C NMR (125 MHz, acetone-d_6): δ 182.8, 153.8, 148.1 (ddd, J = 244.4, 11.1, 3.1 Hz), 148.1–145.9 (m), 144.9–142.5 (m), 143.0, 142.4, 139.3, 138.2 (d, J = 2.0 Hz), 137.4–136.7 (m), 135.5, 134.9, 133.9, 131.9, 131.3, 127.7, 126.5, 126.1, 123.5, 123.0 (ddd, J = 15.3, 6.6, 3.8 Hz), 122.5, 119.1, 106.9 (dd, J = 21.1, 3.0 Hz). MS (ESI) t_R 9.07 min, m/z: 523.8 $(M + H)^+$, $C_{23}H_{14}ClF_3NO_4S_2^+$ calcd 523.9; HRMS m/z: 523.99823 ($[M + H]^+$, $C_{23}H_{14}ClF_3NO_4S_2^+$ calcd 523.99994).

*3-Methyl-N-{3-[5-(2,4,5-trifluoro-3-hydroxy-benzoyl)-thiophen-2-yl]-phenyl}-benzenesulfonamide (**13**).* The title compound was prepared by the reaction of [5-(3-aminophenyl)-thiophen-2-yl](2,4,5-trifluoro-3-methoxyphenyl)methanone (**8a**) (250 mg, 0.68 mmol) and 3-methylbenzene-1-sulfonyl chloride (157 mg, 0.82 mmol) according to method C. The crude product was reacted with boron tribromide (3 equiv) according to method D. The product was purified by CC (dichloromethane/methanol 99:1) followed by washing with petroleum ether/diethyl ether 2:1; yield over two steps: 26% (90 mg). ^{1}H NMR (500 MHz, acetone-d_6): δ 10.00 (s, 1H), 9.21 (s, 1H), 7.70 (s, 1H), 7.69–7.64 (m, 2H), 7.62 (t, J = 1.8 Hz, 1H), 7.54–7.49 (m, 2H), 7.45–7.40 (m, 2H), 7.38 (t, J = 7.9 Hz, 1H), 7.28 (ddd, J = 8.1, 2.1, 0.9 Hz, 1H), 7.16–7.09 (m, 1H), 2.37 (s, 3H). ^{13}C NMR (125 MHz, acetone-d_6): δ 182.8, 154.1, 149.1–146.9 (m), 148.2–145.9 (m), 143.6 (ddd, J = 248.5, 15.8, 5.8 Hz), 142.9, 140.6, 140.2, 139.9, 138.2 (d, J = 2.0 Hz), 137.0 (ddd, J = 18.1, 12.8, 3.0 Hz), 134.7, 134.5, 131.1, 129.9, 128.3, 126.0, 125.1, 123.3–123.0 (m), 122.98, 122.04, 118.61, 106.9 (dd, J = 21.1, 3.0 Hz), 21.24. MS (ESI) t_R 8.89 min, m/z: 503.9 $(M + H)^+$, $C_{24}H_{17}F_3NO_4S_2^+$ calcd 504.0; HRMS m/z: 504.05252 ($[M + H]^+$, $C_{24}H_{17}F_3NO_4S_2^+$ calcd 504.05456).

*N-{3-[5-(2,4,5-Trifluoro-3-hydroxybenzoyl)thiophen-2-yl]-phenyl}-2-trifluoro-methylbenzenesulfonamide (**14**).* The title compound was prepared by the reaction of [5-(3-aminophenyl)-thiophen-2-yl](2,4,5-trifluoro-3-methoxyphenyl)methanone (**8a**) (260 mg, 0.72 mmol) and 2-trifluoromethylbenzenesulfonyl chloride (177 mg, 0.72 mmol) according to method C. The crude product was reacted with boron tribromide (3 equiv) according to method D. The product was purified by CC (dichloromethane/methanol 99.5:0.5); yield over two steps: 19% (75 mg); ^{1}H NMR (500 MHz, acetone-d_6): δ 9.97 (s, 1H), 9.40 (s, 1H), 8.30–8.23 (m, 1H), 8.04–7.98 (m, 1H), 7.89–7.82 (m, 2H), 7.67 (dd, J = 4.1, 1.8 Hz, 1H), 7.66 (t, J = 1.8 Hz, 1H), 7.53 (ddd, J = 7.8, 1.8, 1.0 Hz, 1H), 7.51 (d, J = 4.1 Hz, 1H), 7.40 (t, J = 7.9 Hz, 1H), 7.31 (ddd, J = 8.1, 2.2, 1.0 Hz, 1H), 7.12 (ddd, J = 9.9, 8.1, 5.6 Hz, 1H); ^{13}C NMR (125 MHz, acetone-d_6): δ 182.8, 153.9, 148.0 (ddd, J = 243.6, 11.1, 3.4 Hz), 148.3–145.5 (m), 144.8–142.3 (m), 143.0, 139.1, 138.2 (d, J = 2.1 Hz), 137.0 (ddd, J = 10.1, 8.0, 5.8 Hz), 134.9, 134.4, 133.8, 132.7, 131.3, 129.5 (q, J = 6.4 Hz), 128.4, 128.1, 126.1, 125.0, 123.3, 122.8, 122.0, 118.6, 106.9 (dd, J = 21.1, 3.0 Hz). MS (ESI) t_R 8.39 min, m/z: 558.0 $(M + H)^+$, $C_{24}H_{14}F_6NO_4S_2^+$ calcd 558.0; HRMS m/z: 558.02411 ($[M + H]^+$, $C_{24}H_{14}F_6NO_4S_2^+$ calcd 558.02629).

*N-{3-[5-(2,4,5-Trifluoro-3-hydroxybenzoyl)thiophen-2-yl]-phenyl}-2-trifluoromethoxybenzenesulfonamide (**15**).* The title compound was prepared by the reaction of [5-(3-aminophenyl)-thiophen-2-yl](2,4,5-trifluoro-3-methoxyphenyl)methanone (**8a**) (260 mg, 0.72 mmol) and 2-trifluoromethoxybenzenesulfonyl chloride (189 mg, 0.72 mmol) according to method C. The crude product was reacted with boron tribromide (3 equiv) according to method D. The product was purified by CC (dichloromethane/methanol 99.5:0.5); yield over two steps: 38% (154 mg); ^{1}H NMR (500 MHz, acetone-d_6): δ 9.98 (s, 1H), 9.52 (s, 1H), 8.13–8.09 (m, 1H), 7.78 (ddd, J = 8.4, 7.5, 1.7 Hz, 1H), 7.66 (ddd, J = 4.3, 3.1, 1.1 Hz, 2H), 7.58–7.53 (m, 2H), 7.52–7.50 (m, 2H), 7.38 (td, J = 7.9, 0.4 Hz, 1H), 7.31 (ddd, J = 8.1, 2.2, 1.0 Hz, 1H), 7.12 (ddd, J = 9.9, 8.1, 5.6 Hz, 1H). ^{13}C NMR (125 MHz, acetone-d_6): δ 181.9, 153.0, 147.1 (ddd, J = 244.2, 11.1, 2.9 Hz), 147.0 (ddd, J = 244.3, 4.1, 2.9 Hz), 145.9, 142.7 (ddd, J = 248.3, 15.7, 5.9 Hz), 142.1, 138.2, 137.3 (d, J = 1.5 Hz), 136.1 (ddd, J = 17.5, 12.9, 2.8 Hz), 135.4, 133.9, 131.6, 131.3, 130.3, 127.1, 125.1, 122.3, 122.1 (ddd, J = 15.6, 6.6, 4.1 Hz), 120.9, 120.6 (d, J = 1.3 Hz), 120.3 (q, J = 259.2 Hz), 117.5, 106.0 (dd, J = 21.1, 2.8 Hz). ^{19}F NMR (470 MHz, acetone-d6): δ −56.4, −76.5 ($CF_{3,TFA}$), −138.6, −142.0 to −142.3 (m), −152.5 to −153.5 (m). MS (ESI) t_R 10.40 min, m/z: 574.0 $(M + H)^+$, $C_{24}H_{14}F_6NO_5S_2^+$ calcd 574.0; HRMS m/z: 574.01880 ($[M + H]^+$, $C_{24}H_{14}F_6NO_5S_2^+$ calcd 574.02121).

*4-Bromo-N-{3-[5-(2,4,5-trifluoro-3-hydroxybenzoyl)thiophen-2-yl]phenyl}-2-trifluoromethoxybenzenesulfonamide (**16**).* The title compound was prepared by the reaction of [5-(3-aminophenyl)-thiophen-2-yl](2,4,5-trifluoro-3-methoxyphenyl)methanone (**8a**) (260 mg, 0.72 mmol) and 4-bromo-2-trifluoromethoxybenzenesulfonyl chloride (243 mg, 0.72 mmol) according to method C. The crude product was reacted with boron tribromide (3 equiv) according to method D. The product was purified by CC (dichloromethane/methanol 99.5:0.5); yield over two steps: 41% (190 mg); ^{1}H NMR (500 MHz, acetone-d_6): δ 9.97 (s, 1H), 9.61 (s, 1H), 8.03 (d, J = 8.5 Hz, 1H), 7.77 (dd, J = 8.5, 1.8 Hz, 1H), 7.74 (d, J = 1.6 Hz, 1H), 7.67 (dd, J = 4.1, 1.8 Hz, 1H), 7.67–7.65 (m, 1H), 7.54 (ddd, J = 7.8, 1.8, 1.0 Hz, 1H), 7.52 (d, J = 4.1 Hz, 1H), 7.42–7.37 (m, 1H), 7.31 (ddd, J = 8.1, 2.2, 1.0 Hz, 1H), 7.12 (ddd, J = 9.9, 8.1, 5.6 Hz, 1H); ^{13}C NMR (125 MHz, acetone-d_6): δ 182.85, 153.86, 148.10 (ddd, J = 244.2, 10.9, 3.2 Hz), 148.23–145.93 (m), 146.95 (d, J = 1.8 Hz), 143.65 (ddd, J = 248.6, 15.8, 5.8 Hz), 143.09, 138.84, 138.25, 138.23, 137.08 (ddd, J = 18.3, 12.9, 3.0 Hz), 134.94, 133.83, 131.82, 131.46, 131.32, 129.11, 126.14, 124.91 (d, J = 1.9 Hz), 123.53, 123.07 (ddd, J = 15.7, 6.8, 3.9 Hz), 122.07, 118.76, 106.96 (dd, J = 21.1, 3.0 Hz). MS (ESI) t_R 9.70 min, m/z: 651.9 $(M + H)^+$, $C_{24}H_{13}BrF_6NO_5S_2^+$ calcd 651.9; HRMS m/z: 651.92902 ($[M + H]^+$, $C_{24}H_{13}BrF_6NO_5S_2^+$ calcd 651.93172).

Biochemical Assays. Human and mouse 17β-HSD2 preparations were obtained by isolating the microsomal fractions of human placenta and mouse liver homogenates, respectively, according to the described methods.[19] Incubations were run with [^{3}H]-E2 (human: 500 nM; mouse: 10 nM), cofactor NAD$^+$, and inhibitor. Human 17β-HSD1 was prepared from the cytosolic fractions of human placenta, whereas recombinant mouse 17β-HSD1 cDNA (Origene, USA) was transiently expressed in HEK293 cells and prepared by ammonium

DOI: 10.1021/acs.jmedchem.8b01493
J. Med. Chem. 2019, 62, 1362–1372

sulfate precipitation essentially as described for human 17β-HSD1 preparation.[19] The enzyme preparations were incubated with [^{3}H]-E1 (human: 500 nM; mouse: 10 nM), cofactor, and inhibitor.[19] The separation and measurement of the substrate and product were accomplished by radio-HPLC. The cellular *h*17β-HSD2 inhibitory activity was measured using the breast cancer cell line MDA-MB-231 (17β-HSD1 activity negligible) with 200 nM [^{3}H]-E2 as the substrate and incubated with **15** for 6 h at 37 °C.[29] After ether extraction, the substrate and product were separated and measured as described above. ERα/ERβ binding affinity assays, and MTT cell viability assays in HEK293 cells, were performed as described previously.[19,23] The metabolic stabilities in human and mouse liver S9 fractions were determined in the presence of the cofactors NADPH, UDPGA, and PAPS, as described earlier.[23] Aryl hydrocarbon receptor agonist assays were performed as described earlier.[28] Agonist activity on the pregnane X receptor and constitutive androstane receptors were performed at CEREP (now Eurofins) in a cofactor recruitment cell-free assay.

Immunohistochemistry. The expression of 17β-HSD2 in mouse bone was investigated in 6 μm longitudinal cryosections of C57BL/6 mouse femur fixed in 4% paraformaldehyde. Immunohistochemistry was performed with the rabbit polyclonal antimouse 17β-HSD2 antibody M-165 (sc-135042; Santa Cruz Biotechnology, Heidelberg, Germany; 1:50 dilution) as the primary antibody and an Alexa 555-conjugated goat antirabbit IgG (Thermo Fisher, Kandel, Germany; 1:200 dilution) as the secondary antibody. Negative control represents incubation with secondary antibody only. The cell nuclei were stained with 4′,6-diamidino-2-phenylindole.

Western Blot Analysis of Biomarkers in Callus Protein. The expression of OPG and RANKL in callus was analyzed in five animals per group after 28 days of treatment following sodium dodecyl sulfate polyacrylamide gel electrophoresis and western blotting using rabbit polyclonal antimouse OPG (1:100, Santa Cruz Biotechnology Inc.) and rabbit polyclonal antimouse RANKL (1:100, Abcam, Cambridge, UK), as described in detail previously.[23] The signals were densitometrically assessed and normalized to β-actin signals to correct for unequal loading.[23] Comparison between the groups was performed using the Student's *t* test. *P* values were calculated using GraphPad Prism QuickCalcs.

E2 and T Plasma Analysis. To determine the effect of 17β-HSD2 inhibition on the plasma levels of E2 and T, at day 28 after fracture, 100 μL of plasma was collected from the vena cava for the determination of the plasma levels of E2 and T by ELISA after the extraction of the steroids from the plasma, according to the manufacturer's protocol (DRG, Marburg, Germany).

Animal Procedures. All animal experiments in C57BL/6 mice were approved by the local governmental animal care committee and were conducted in accordance with the European legislation on protection of animals and the *NIH Guidelines for the Care and Use of Laboratory Animals* (NIH Publication #85-23 Rev. 1985). Experiments were conducted on mature C57BL/6 mice (body weight 27 ± 3 g, mean ± SD).

Mouse Subcutaneous Pharmacokinetics. Compound **15** was subcutaneously administered at a dose of 50 mg/kg body weight per animal (*n* = 3). Thirty minutes before administration, suspensions of **15** were freshly prepared in an ultrasonic water bath for 10 minutes. Before the application of the suspension (4 mL/kg body weight), female C57BL/6 mice were anesthetized with 2% isoflurane. At 2, 18, and 24 h, blood samples of 50 μL were taken from the tail vein and collected in 0.2 mL Eppendorf tubes containing 5 μL of 106 mM sodium citrate buffer as an anticoagulant. After centrifugation at 5000 rpm at 4 °C, the plasma samples were immediately frozen at −20 °C, and within 24 h, all were stored at −80 °C. For bioanalysis, the plasma samples were thawed, and 10 μL of plasma was added to 50 μL of acetonitrile containing diphenhydramine (500 nM) as the internal standard. The samples and calibration standards (in mouse plasma) were centrifuged at 15 000 rpm for 5 min at 4 °C. The solutions were transferred to fresh vials for HPLC-MS/MS analysis (Accucore RP-MS, TSQ Quantum triple quadrupole mass spectrometer, ESI interface). After injection of 10 μL (performed in duplicate), the data were analyzed based on the ratio of the peak areas of compound **15** and the internal standard. The detection limit of **15** in plasma was 1.2 nM. In the bone fracture study, the plasma level of **15** was also determined in nine animals at day 28 of treatment (i.e., 24 h after the last dosing at day 27), at sacrifice under anesthetics: the plasma levels of **15** were 498 ± 81 nM (mean ± SEM).

Surgical Procedures. Male mice were anesthetized by an intraperitoneal injection of xylazine (15 mg/kg body weight) and ketamine (75 mg/kg body weight) before fracture and surgery. The surgical procedure was performed as described in detail earlier.[23] For analgesia, the mice received tramadol hydrochloride in the drinking water (2.5 mg/100 mL) from day 1 before surgery until day 3 after surgery. The suspensions of **15** in vehicle were made fresh each time during the treatment period of 14 or 28 days. A treatment period of 28 days was chosen because this period covers the most critical (and sensitive) phases in bone fracture healing (i.e., initial inflammation because of tissue injury, callus formation, neovascularization, restoration of bending stiffness, and start of bone remodeling).

Histomorphometrical Analysis. To determine the influence of **15** on the course of bone healing, histomorphometric analysis of the callus was performed at 14 and 28 days of fracture healing after resection of the healed femora and removal of the implant, fixation of the femur in formaldehyde, bone decalcification in ethylenediaminetetraacetic acid, trichrome staining (Masson−Goldner), and light microscopy according to the nomenclature and units of the recommendations of the *American Society of Bone and Mineral Research* (*ASBMR*), as described in detail previously.[15]

Biomechanical Analysis. For biomechanical analysis, the resected femora were freed from the soft tissue. After removing the implants, the bending stiffness of the callus was measured with a nondestructive bending test using a 3-point bending device, as described in detail previously.[15] To account for the differences in bone stiffness of the individual animals, the nonfractured femora were also analyzed, serving as internal control. All values of the fractured femora are given as percentage of the corresponding nonfractured femora.

Radiological Analysis. At the end of the bone healing period of 14 and 28 days, the complete callus area of the fractured femurs was analyzed using a high-resolution micro-CT imaging system, as described in detail previously.[23] By this method, the following parameters were determined: tissue volume, bone volume, the ratio of bone volume to tissue volume, trabecular thickness, trabecular number, and trabecular separation.

■ ASSOCIATED CONTENT

Ⓢ Supporting Information

The Supporting Information is available free of charge on the ACS Publications website at DOI: 10.1021/acs.jmedchem.8b01493.

> Synthesis of intermediates **2b**, **4b**−**8b**, and **2a**−**8a**; NMR spectra, HRMS, and LC−MS of compounds **1**−**16**, **8a**, and **8b**; and additional biological results of **15** (immunofluorescence microscopy of 17β-HSD2 expression in mouse cortical bone; ; E2 and T plasma analysis; histomorphometrical, biomechanical, and radiological bone analysis; body, liver, seminal vesicles, testicles weights) (PDF)
>
> Molecular formula strings of all final compounds (CSV)

■ AUTHOR INFORMATION

Corresponding Author

*E-mail: vankoppen@elexopharm.de. Phone: +49 681 910 2893.

ORCID

Ahmed S. Abdelsamie: 0000-0002-5326-4400
Mohamed Salah: 0000-0002-9535-6741

Sandrine Marchais-Oberwinkler: 0000-0001-9941-7233
Martin Frotscher: 0000-0003-1777-8890
Rolf W. Hartmann: 0000-0002-5871-5231
Chris J. van Koppen: 0000-0003-2799-6728

Author Contributions

○A.S.A. and S.H. contributed equally to the work.

Notes

The authors declare the following competing financial interest(s): The authors: Ahmed S. Abdelsamie, Carsten Börger, Lorenz Siebenbürger, Sandrine Marchais-Oberwinkler, Martin Frotscher, Rolf W. Hartmann and Chris J. van Koppen are inventors of a patent application, which covers the respective compound class. ElexoPharm GmbH is the owner of this patent application. Rolf W. Hartmann is the CEO of ElexoPharm GmbH. Chris van Koppen is an employee of ElexoPharm GmbH.

■ ACKNOWLEDGMENTS

This research was supported by a *KMU-innovativ-12* grant of the *Bundesministerium für Bildung und Forschung* (031A467). We thank Janine Becker and Julia Parakening for excellent technical assistance.

■ ABBREVIATIONS

E2, estradiol; ER, estrogen receptor; *h*, human; *m*, mouse; T testosterone17β-HSD, testosterone17β-HSD17β-hydroxysteroid dehydrogenase

■ REFERENCES

(1) Brunton, L. L.; Chabner, B. A.; Knollmann, B. C. *Goodman & Gilman. The Pharmacological Basis of Therapeutics*, 13th Edition; McGraw-Hill: New York, 2017.

(2) Edwards, J.; Moore, R. A. Finasteride in the treatment of clinical benign prostatic hyperplasia: a systematic review of randomised trials. *BMC Urol.* **2002**, *2*, 14.

(3) Hermanowski-Vosatka, A.; Balkovec, J. M.; Cheng, K.; Chen, H. Y.; Hernandez, M.; Koo, G. C.; Le Grand, C. B.; Li, Z.; Metzger, J. M.; Mundt, S. S.; Noonan, H.; Nunes, C. N.; Olson, S. H.; Pikounis, B.; Ren, N.; Robertson, N.; Schaeffer, J. M.; Shah, K.; Springer, M. S.; Strack, A. M.; Strowski, M.; Wu, K.; Wu, T.; Xiao, J.; Zhang, B. B.; Wright, S. D.; Thieringer, R. 11β-HSD1 inhibition ameliorates metabolic syndrome and prevents progression of atherosclerosis in mice. *J. Exp. Med.* **2005**, *202*, 517−527.

(4) Saloniemi, T.; Järvensivu, P.; Koskimies, P.; Jokela, H.; Lamminen, T.; Ghaem-Maghami, S.; Dina, R.; Damdimopoulou, P.; Mäkelä, S.; Perheentupa, A.; Kujari, H.; Brosens, J.; Poutanen, M. Novel Hydroxysteroid (17β) Dehydrogenase 1 Inhibitors Reverse Estrogen-Induced Endometrial Hyperplasia in Transgenic Mice. *Am. J. Pathol.* **2010**, *176*, 1443−1451.

(5) Aspenberg, P.; Genant, H. K.; Johansson, T.; Nino, A. J.; See, K.; Krohn, K.; García-Hernández, P. A.; Recknor, C. P.; Einhorn, T. A.; Dalsky, G. P.; Mitlak, B. H.; Fierlinger, A.; Lakshmanan, M. C. Teriparatide for acceleration of fracture repair in humans: a prospective, randomized, double-blind study of 102 postmenopausal women with distal radial fractures. *J. Bone Miner. Res.* **2010**, *25*, 404−414.

(6) Fujita, N.; Matsushita, T.; Ishida, K.; Sasaki, K.; Kubo, S.; Matsumoto, T.; Kurosaka, Y.; Tabata, Y.; Kuroda, R. An analysis of bone regeneration at a segmental bone defect by controlled release of bone morphogenetic protein 2 from a biodegradable sponge composed of gelatin and β-tricalcium phosphate. *J. Tissue Eng. Regener. Med.* **2012**, *6*, 291−298.

(7) Woo, E. J. Adverse events after recombinant human BMP2 in nonspinal orthopaedic procedures. *Clin. Orthop. Relat. Res.* **2013**, *471*, 1707−1711.

(8) Bhandari, M.; Jin, L.; See, K.; Burge, R.; Gilchrist, N.; Witvrouw, R.; Krohn, K. D.; Warner, M. R.; Ahmad, Q. I.; Mitlak, B. Does teriparatide improve femoral neck fracture healing: results from a randomized placebo-controlled trial. *Clin. Orthop. Relat. Res.* **2016**, *474*, 1234−1244.

(9) Wu, L.; Einstein, M.; Geissler, W.M.; Chan, H.K.; Elliston, K.O.; Andersson, S. Expression cloning and characterization of human 17 beta-hydroxysteroid dehydrogenase type 2, a microsomal enzyme possessing 20 alpha-hydroxysteroid dehydrogenase activity. *J. Biol. Chem.* **1993**, *268*, 12964−12969.

(10) Lu, M.-L.; Huang, Y.-W.; Lin, S.-X. Purification, Reconstitution, and Steady-state Kinetics of the Trans-membrane 17β-Hydroxysteroid Dehydrogenase 2. *J. Biol. Chem.* **2002**, *277*, 22123−22130.

(11) Vanderschueren, D.; Vandenput, L.; Boonen, S.; Lindberg, M. K.; Bouillon, R.; Ohlsson, C. Androgens and bone. *Endocr. Rev.* **2004**, *25*, 389−425.

(12) Purohit, A.; Flanagan, A. M.; Reed, M. J. Estrogen synthesis by osteoblast cell lines. *Endocrinology* **1992**, *131*, 2027−2029.

(13) Janssen, J. M. M. F.; Bland, R.; Hewison, M.; Coughtrie, M. W. H.; Sharp, S.; Arts, J.; Pols, H. A. P.; van Leeuwen, J. P. T. M. Estradiol formation by human osteoblasts via multiple pathways: relation with osteoblast function. *J. Cell. Biochem.* **1999**, *75*, 528−537.

(14) Dong, Y.; Qiu, Q. Q.; Debear, J.; Lathrop, W. F.; Bertolini, D. R.; Tamburini, P. P. 17β-hydroxysteroid dehydrogenases in human bone cells. *J. Bone Miner. Res.* **1998**, *13*, 1539−1546.

(15) Bagi, C. M.; Wood, J.; Wilkie, D.; Dixon, B. Effect of 17beta-hydroxysteroid dehydrogenase type 2 inhibitor on bone strength in ovariectomized cynomolgus monkeys. *J. Musculoskelet. Neuronal Interact.* **2008**, *8*, 267−280.

(16) Holstein, J. H.; Matthys, R.; Histing, T.; Becker, S. C.; Fiedler, M.; Garcia, P.; Meier, C.; Pohlemann, T.; Menger, M. D. Development of a Stable Closed Femoral Fracture Model in Mice. *J. Surg. Res.* **2009**, *153*, 71−75.

(17) Milewich, L.; Garcia, R. L.; Gerrity, L. W. 17β-Hydroxysteroid oxidoreductase: A ubiquitous enzyme. Interconversion of estrone and estradiol-17β in mouse tissues. *Metabolism* **1985**, *34*, 938−944.

(18) Abdelsamie, A. S.; Bey, E.; Gargano, E. M.; van Koppen, C. J.; Empting, M.; Frotscher, M. Towards the evaluation in an animal disease model: Fluorinated 17β-HSD1 inhibitors showing strong activity towards both the human and the rat enzyme. *Eur. J. Med. Chem.* **2015**, *103*, 56−68.

(19) Abdelsamie, A. S.; Bey, E.; Hanke, N.; Empting, M.; Hartmann, R. W.; Frotscher, M. Inhibition of 17β-HSD1: SAR of bicyclic substituted hydroxyphenylmethanones and discovery of new potent inhibitors with thioether linker. *Eur. J. Med. Chem.* **2014**, *82*, 394−406.

(20) Miettinen, M. M.; Mustonen, M. V. J.; Poutanen, M. H.; Isomaa, V. V.; Vihko, R. K. Human 17β-hydroxysteroid dehydrogenase type 1 and type 2 isoenzymes have opposite activities in cultured cells and characteristic cell- and tissue-specific expression. *Biochem. J.* **1996**, *314*, 839−845.

(21) Speirs, V.; Green, A. R.; Atkin, S. L. Activity and gene expression of 17β-hydroxysteroid dehydrogenase type I in primary cultures of epithelial and stromal cells derived from normal and tumourous human breast tissue: the role of IL-8. *J. Steroid Biochem. Mol. Biol.* **1998**, *67*, 267−274.

(22) Huhtinen, K.; Desai, R.; Ståhle, M.; Salminen, A.; Handelsman, D. J.; Perheentupa, A.; Poutanen, M. Endometrial and endometriotic concentrations of estrone and estradiol are determined by local metabolism rather than circulating levels. *J. Clin. Endocrinol. Metab.* **2012**, *97*, 4228−4235.

(23) Abdelsamie, A. S.; van Koppen, C. J.; Bey, E.; Salah, M.; Börger, C.; Siebenbürger, L.; Laschke, M. W.; Menger, M. D.; Frotscher, M. Treatment of estrogen-dependent diseases: Design, synthesis and profiling of a selective 17β-HSD1 inhibitor with sub-nanomolar IC 50 for a proof-of-principle study. *Eur. J. Med. Chem.* **2017**, *127*, 944−957.

(24) Histing, T.; Andonyan, A.; Klein, M.; Scheuer, C.; Stenger, D.; Holstein, J. H.; Veith, N. T.; Pohlemann, T.; Menger, M. D. Obesity

does not affect the healing of femur fractures in mice. *Injury* **2016**, *47*, 1435−1444.

(25) Histing, T.; Stenger, D.; Scheuer, C.; Metzger, W.; Garcia, P.; Holstein, J. H.; Klein, M.; Pohlemann, T.; Menger, M. D. Pantoprazole, a proton pump inhibitor, delays fracture healing in mice. *Calcif. Tissue Int.* **2012**, *90*, 507−514.

(26) Bord, S.; Ireland, D. C.; Beavan, S. R.; Compston, J. E. The effects of estrogen on osteoprotegerin, RANKL, and estrogen receptor expression in human osteoblasts. *Bone* **2003**, *32*, 136−141.

(27) Rivero-Müller, A.; Chou, Y.-Y.; Ji, I.; Lajic, S.; Hanyaloglu, A. C.; Jonas, K.; Rahman, N.; Ji, T. H.; Huhtaniemi, I. Rescue of defective G protein-coupled receptor function in vivo by intermolecular cooperation. *Proc. Natl. Acad. Sci. U.S.A.* **2010**, *107*, 2319−2324.

(28) Emmerich, J.; van Koppen, C. J.; Burkhart, J. L.; Hu, Q.; Siebenbürger, L.; Boerger, C.; Scheuer, C.; Laschke, M. W.; Menger, M. D.; Hartmann, R. W. Lead optimization generates CYP11B1 inhibitors of pyridylmethyl isoxazole type with improved pharmacological profile for the treatment of Cushing's disease. *J. Med. Chem.* **2017**, *60*, 5086−5098.

(29) Gargano, E. M.; Allegretta, G.; Perspicace, E.; Carotti, A.; Van Koppen, C.; Frotscher, M.; Marchais-Oberwinkler, S.; Hartmann, R. W. 17*β*-Hydroxysteroid Dehydrogenase Type 2 Inhibition: Discovery of Selective and Metabolically Stable Compounds Inhibiting Both the Human Enzyme and Its Murine Ortholog. *PLoS One* **2015**, *10*, No. e0134754.

3.3. Chapter III: Highly Potent 17β-HSD2 Inhibitors with a Promising Pharmacokinetic Profile for Targeted Osteoporosis Therapy

Siebenbürger, L.; Hernandez-Olmos, V.; Abdelsamie, A. S.; Frotscher, M.; van Koppen, C. J.; Marchais-Oberwinkler, S.; Scheuer, C.; Laschke, M. W.; Menger, M. D.; Börger, C.; Hartmann, R. W.;

Reprinted with permission from *J. Med. Chem.* **2018***, 61,* 10724−10738*.*

DOI: 10.1021/acs.jmedchem.8b01373

Copyright (2018) American Chemical Society

Journal of Medicinal Chemistry

Article

Cite This: J. Med. Chem. 2018, 61, 10724−10738

pubs.acs.org/jmc

Highly Potent 17β-HSD2 Inhibitors with a Promising Pharmacokinetic Profile for Targeted Osteoporosis Therapy

Lorenz Siebenbuerger,[†] Victor Hernandez-Olmos,[‡] Ahmed S. Abdelsamie,[§,∥] Martin Frotscher,[∥] Chris J. van Koppen,[⊥] Sandrine Marchais-Oberwinkler,[#] Claudia Scheuer,[¶] Matthias W. Laschke,[¶] Michael D. Menger,[¶] Carsten Boerger,[†] and Rolf W. Hartmann*[,∥,∇]

[†]PharmBioTec GmbH, Science Park 1, 66123 Saarbrücken, Germany

[‡]Fraunhofer Institute for Molecular Biology and Applied Ecology IME, Branch for Translational Medicine and Pharmacology TMP, Theodor-Stern-Kai 7, 60596 Frankfurt am Main, Germany

[§]Chemistry of Natural and Microbial Products Department, National Research Centre, Dokki, 12622 Cairo, Egypt

[∥]Department of Pharmacy, Saarland University, Campus C2.3, 66123 Saarbrücken, Germany

[⊥]Elexopharm GmbH, Campus A1, 66123 Saarbrücken, Germany

[#]Institute for Pharmaceutical Chemistry, Philipps University Marburg, 35032 Marburg, Germany

[¶]Institute for Clinical and Experimental Surgery, Saarland University, 66421 Homburg/Saar, Germany

[∇]Department of Drug Design and Optimization, Helmholtz Institute for Pharmaceutical Research Saarland (HIPS), Campus E8.1, 66123 Saarbrücken, Germany

Supporting Information

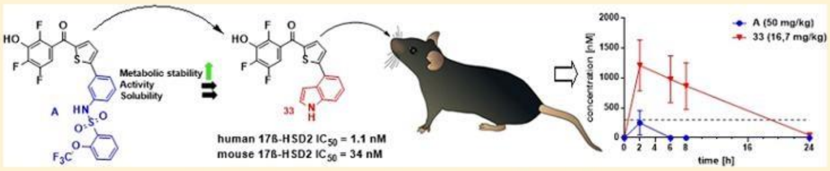

ABSTRACT: Intracellular elevation of E2 levels in bone by inhibition of 17β hydroxysteroid dehydrogenase type 2 (17β-HSD2) without affecting systemic E2 levels is an attractive approach for a targeted therapy against osteoporosis, a disease which is characterized by loss of bone mineral density. Previously identified inhibitor **A** shows high potency on human and mouse 17β-HSD2, but poor pharmacokinetic properties when applied perorally in mice. A combinatorial chemistry approach was utilized to synthesize truncated derivatives of **A**, leading to highly potent compounds with activities in the low nanomolar to picomolar range. Compound **33**, comparable to **A** in terms of inhibitor potency against both human and mouse enzymes, displays high in vitro metabolic stability in human and mouse liver S9 fraction as well as low toxicity and moderate hepatic CYP inhibition. Thus, compound **33** showed a highly improved peroral pharmacokinetic profile in comparison to **A**, making **33** a promising candidate for further development.

■ INTRODUCTION

Healthy bone is primarily maintained by two different cell types, osteoblasts (OBs) and osteoclasts (OCs). OBs are responsible for the formation of new bone matrix and OCs for its degradation. An imbalance in the activities of these cell types in favor of matrix degradation, as it is often the case in elderly people, leads to osteoporosis. Osteoporosis is characterized by decreased bone mineral density and impaired bone microarchitecture, resulting in an increased risk of bone fractures.[1] Osteoporosis is directly associated with a decrease of the plasma levels of the steroid hormone 17β-estradiol (E2), as it occurs in women after menopause.[2] Furthermore, a decrease of testosterone (T) has been linked to osteoporosis in elderly men.[3] 17β-Hydroxysteroid dehydrogenase type 2 (17β-HSD2) catalyzes the NAD$^+$-dependent oxidation of E2 into estrone (E1) and of T into 4-androstene-3,17-dione (A-dione). The resulting oxidized steroid hormones are much less active on the estrogen receptors α and β (ERα and ERβ) and the androgen receptor than their reduced forms. Systemic administration of E2 leads to prevention of osteoporosis, but is accompanied by serious side effects such as an increased risk of venous emboli and breast cancer. As 17β-HSD2 is expressed in bone OBs,[4] inhibition of this enzyme leads to increased E2 and T levels inside OBs, making 17β-HSD2 inhibition a promising approach for a targeted therapy. Bagi et al. validated the beneficial effect of 17β-HSD2 inhibitors on bone quality in an ovariectomized monkey model.[5] However, only a minor effect was seen on bone mass, which might be due to the poor pharmacokinetic (PK) profile of the administered compound

Received: September 3, 2018
Published: November 27, 2018

© 2018 American Chemical Society

DOI: 10.1021/acs.jmedchem.8b01373
J. Med. Chem. 2018, 61, 10724−10738

Chart 1. Reported Nonsteroidal 17β-HSD2 Inhibitors[25,28]

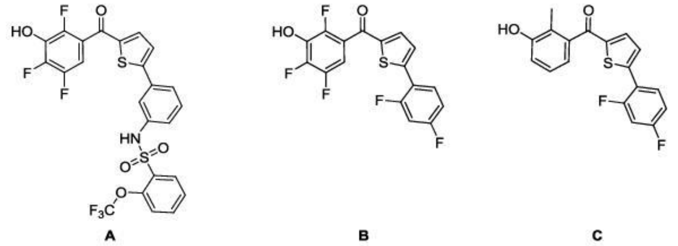

A
hHSD2:IC_{50} = 2 nM
hHSD1:IC_{50} = 6nM (SF: 3)
mHSD2:IC_{50} = 25 nM

B
hHSD2:IC_{50} = 1.4 nM
hHSD1:IC_{50} = 7nM (SF: 5)
mHSD2:C_{50} = 85 % @ 250 nM

C
hHSD2:IC_{50} = 299 nM
hHSD1:IC_{50} = 3427 nM (SF: 11)
mHSD2:IC_{50} = 18 % @ 1 μM

or its moderate potency. Therefore, the development of novel potent inhibitors with improved in vivo efficacy is highly desirable. Both steroidal[6−8] and nonsteroidal[9−18] inhibitors of 17β-HSD2 have been described in the literature. Different scaffolds of 17β-HSD2 inhibitors have been identified and optimized,[11−20] resulting in compounds with strong 17β-HSD2 inhibition and high selectivity toward 17β-hydroxysteroid dehydrogenase type 1 (17β-HSD1). 17β-HSD1 on the other hand is an attractive target for the treatment of endometriosis and breast cancer.[19−24] Very recently, lead compound **A**, a highly active 17β-HSD2 inhibitor (Chart 1, human IC_{50} = 2 nM, mouse IC_{50} = 25 nM, human liver S9 $t_{1/2}$ = 60 min, mouse liver S9 $t_{1/2}$ = 46 min), was administered subcutaneously to mice in a proof-of-principle model for bone fracture healing.[25] Strong efficacy of the compound was observed by histological and biomechanical testing because of the large formed callus and bone formation at the site of the fracture compared to vehicle controls. These findings underline the beneficial effect of 17β-HSD2 inhibitors on the formation of new bone substance. However, compound **A** is not suitable for osteoporosis therapy because of its poor PK properties after oral administration (Figure 1), which is regarded a prerequisite for long-term therapy of osteoporosis. It is important that newly designed inhibitors should also inhibit the mouse 17β-HSD2 ortholog because this species is appropriate for the evaluation of compounds in an osteoporosis model.[26] As there is no 17β-HSD1 detectable in OBs,[4] no selectivity toward 17β-HSD1 is required to increase E2 levels inside the bone. In fact, nonselective compounds might be favorable because in contrast to nonselective inhibitors, selective inhibitors will increase E2 levels in tissues where both 17β-HSD2 and 17β-HSD1 are present. In the breast tissue,[27] for example, both reductive and oxidative activities of 17β-HSDs are equally present and inhibition of the oxidative activity by 17β-HSD2 inhibitors could therefore lead to increased E2 concentrations inside the breast, which leads to an increased risk for breast cancer. In addition to sufficient inhibitory potency on the target, compounds should show good in vitro and in vivo ADME-Tox properties such as metabolic stability, aqueous solubility, as well as low cytotoxicity and CYP inhibition. Plasma concentrations should be in the range of the IC_{90} in order to show efficacy in a rodent proof-of-principle model. Furthermore, the compound should be suitable for oral applications because this route of administration is the most adequate for long-term osteoporosis therapy. In this study, we describe the design, synthesis, and biological assessment of novel 17β-HSD2 inhibitors. The obtained compounds show the highest in vitro inhibition values of both human and mouse 17β-HSD2 described so far for osteoporosis therapy. Furthermore, the compounds show good metabolic stability in human and mouse liver S9 fraction, thus toward phase 1 and phase 2 metabolizing enzymes. Finally, high plasma concentrations of the compounds are reached for a considerable length of time in a mouse PK study after oral administration.

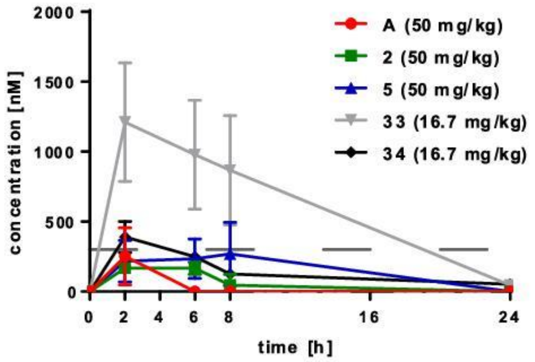

Figure 1. Mean profile (±) S.E.M. of plasma concentration [nM] in C57Bl/6 mice vs time after oral application of compounds **A**, **2**, **5**, **33**, and **34** in single dosing experiments (n = 3). Dashed line represents the in vitro 17β-HSD2 IC_{90} value for **33** in mouse.

■ DESIGN

Starting point of this study was the sulfonamide compound **A** (Chart 1), which has recently been shown to be a suitable candidate for a bone fracture healing proof-of-principle study, showing high potency on the human and murine 17β-HSD2, as well as moderate aqueous solubility and metabolic stability.[25] Subcutaneous application of compound **A** in high dose (50 mg/kg) to mice is necessary to achieve sufficiently high plasma concentrations to inhibit mouse 17β-HSD2 for at least 24 h after a single dose. However, compound **A** is not suitable for peroral applications, as **A** in a single dose of 50 mg/kg is cleared entirely from the plasma after 6 h (Figure 1). Compounds **B** and **C**, designed as 17β-HSD1 inhibitors,[28] show that the sulfonamide moiety is not required to achieve high potency on both human 17β-HSD2 and 17β-HSD1 when compared to **A**. Compound **B** shows high potency on human 17β-HSD2 and moderate potency on the murine 17β-HSD enzyme, as well as moderate selectivity toward 17β-HSD1. Compound **C** shows moderate activity on the human 17β-HSD2 and an increased selectivity over 17β-HSD1 compared to **B**, making **B** and **C** promising optimized hit compounds for

DOI: 10.1021/acs.jmedchem.8b01373
J. Med. Chem. 2018, 61, 10724−10738

Chart 2. Designed and Synthesized 17β-HSD2 Inhibitors

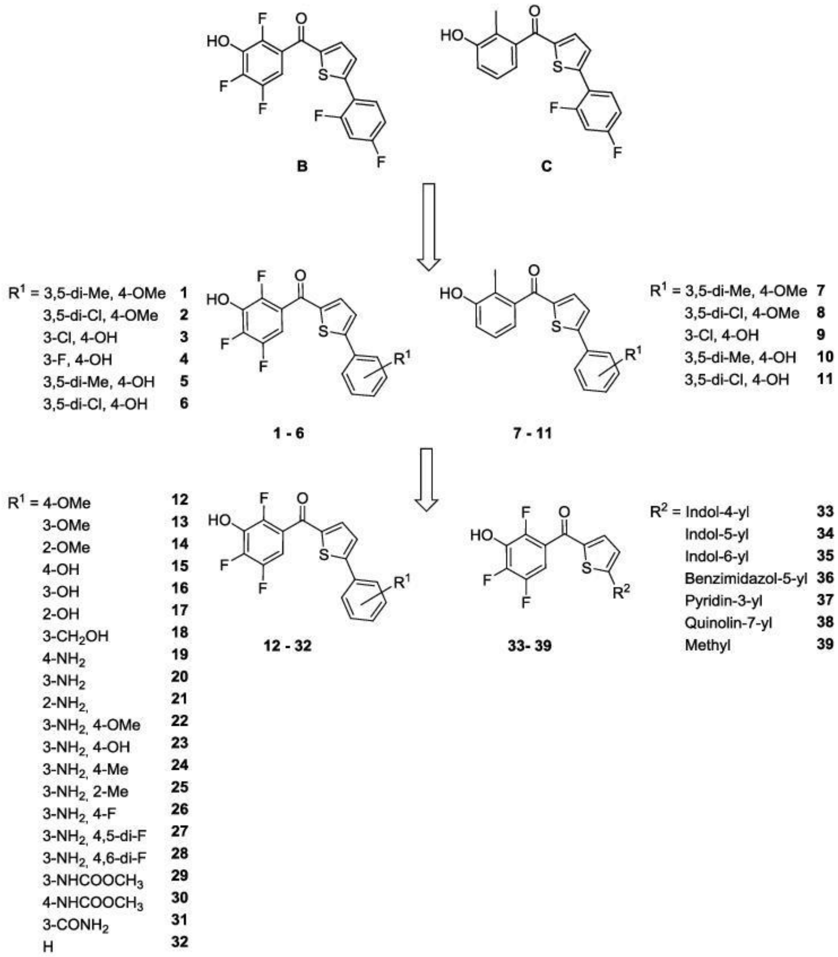
B
C
R1 = 3,5-di-Me, 4-OMe 1
3,5-di-Cl, 4-OMe 2
3-Cl, 4-OH 3
3-F, 4-OH 4
3,5-di-Me, 4-OH 5
3,5-di-Cl, 4-OH 6
1 - 6
7 - 11
R1 = 3,5-di-Me, 4-OMe 7
3,5-di-Cl, 4-OMe 8
3-Cl, 4-OH 9
3,5-di-Me, 4-OH 10
3,5-di-Cl, 4-OH 11
R1 = 4-OMe 12
3-OMe 13
2-OMe 14
4-OH 15
3-OH 16
2-OH 17
3-CH2OH 18
4-NH2 19
3-NH2 20
2-NH2 21
3-NH2, 4-OMe 22
3-NH2, 4-OH 23
3-NH2, 4-Me 24
3-NH2, 2-Me 25
3-NH2, 4-F 26
3-NH2, 4,5-di-F 27
3-NH2, 4,6-di-F 28
3-NHCOOCH3 29
4-NHCOOCH3 30
3-CONH2 31
H 32
12 - 32
33- 39
R2 = Indol-4-yl 33
Indol-5-yl 34
Indol-6-yl 35
Benzimidazol-5-yl 36
Pyridin-3-yl 37
Quinolin-7-yl 38
Methyl 39

further optimization. Furthermore, they showed that a *p*-methoxy or a hydroxy group, flanked by one or two *m*-chloro or methyl substituents on the phenyl ring, leads to an increased activity on both human 17β-HSDs (results not shown).[28] Newly designed compounds should show similar or improved potency on both human and mouse 17β-HSD2, as well as improved solubility and metabolic stability compared to reference compound **A**. A ligand-based approach using combinatorial chemistry methods was employed in order to synthesize new compounds. In a first step, we investigated whether the structure–activity relationship (SAR) obtained from the 17β-HSD1 inhibitor class[28] could be transferred to the tri-F- and methyl-scaffold of **B** and **C**, respectively. These hit compounds already show high to moderate potency on 17β-HSD2 as well as selectivity over 17β-HSD1 and serve as ideal templates for further SAR studies. Therefore, a set of mono- and disubstituted *p*-methoxy and *p*-hydroxy derivatives combined with the benzoyl moieties of **B** and **C** have been synthesized (Chart 2, compounds **1**–**11**) and tested for their activity on human and murine 17β-HSD1 and 17β-HSD2. The newly designed compounds show similar or increased inhibitory potency on human 17β-HSD2 compared to the reference compounds **A**, **B**, and **C**. Regarding activity on mouse 17β-HSD2, an increased potency compared to **B** and **C** was achieved, but not compared to compound **A**. Because of the close structural similarity of compounds **1**–**11** of the first library, a second, structurally more diverse library (**12**–**39**, Chart 2) was designed and synthesized in order to gain deeper insight into the SAR of the compounds concerning both human and mouse 17β-HSD2 inhibition. In this library, phenyl rings bearing different hydrophilic electron-donating substituents and different heterocyclic moieties were combined with the tri-F benzoyl thiophene motif of **B**. Compounds of both libraries that showed best inhibitory activities on human and mouse 17β-HSD2 were tested for metabolic stability in human and murine liver S9 fraction. On the basis of the testing results, a SAR regarding potency and selectivity on both human and murine 17β-HSD2 as well as metabolic stability was obtained. Selected compounds were further evaluated for other ADME-Tox parameters. Finally, the compounds with the highest metabolic stability were tested in a mouse PK study.

■ RESULTS AND DISCUSSION

Chemistry. The synthesis of compounds **1**–**39** was achieved following a two- to four-step reaction sequence (Scheme 1) with derivatization occurring mostly at the last two

DOI: 10.1021/acs.jmedchem.8b01373
J. Med. Chem. 2018, 61, 10724–10738

Scheme 1. Synthesis of Compounds 1−39[a]

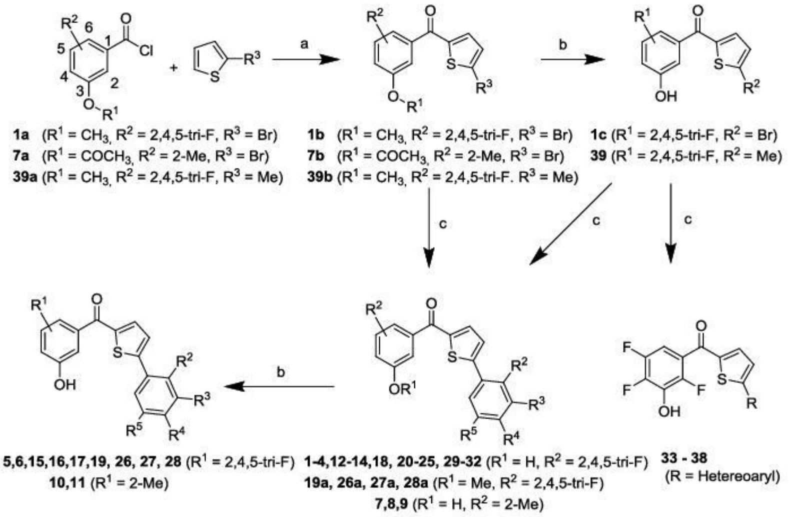
a
b
c
c
c
b
1a (R¹ = CH₃, R² = 2,4,5-tri-F, R³ = Br)
7a (R¹ = COCH₃, R² = 2-Me, R³ = Br)
39a (R¹ = CH₃, R² = 2,4,5-tri-F, R³ = Me)
1b (R¹ = CH₃, R² = 2,4,5-tri-F, R³ = Br)
7b (R¹ = COCH₃, R² = 2-Me, R³ = Br)
39b (R¹ = CH₃, R² = 2,4,5-tri-F. R³ = Me)
1c (R¹ = 2,4,5-tri-F, R² = Br)
39 (R¹ = 2,4,5-tri-F, R² = Me)
5,6,15,16,17,19, 26, 27, 28 (R¹ = 2,4,5-tri-F)
10,11 (R¹ = 2-Me)
1-4,12-14,18, 20-25, 29-32 (R¹ = H, R² = 2,4,5-tri-F)
19a, 26a, 27a, 28a (R¹ = Me, R² = 2,4,5-tri-F)
7,8,9 (R¹ = H, R² = 2-Me)
33 - 38
(R = Hetereoaryl)

[a]Reagents and conditions: (a) method A, $AlCl_3$, anhydrous CH_2Cl_2, 0 °C, 0.5 h and then rt, 3 h. (b) Method B, BBr_3, CH_2Cl_2, −93 °C to rt, overnight. (c) Method C1, corresponding boronic acid for **1−37**, Cs_2CO_3, $Pd(PPh_3)_4$, toluene/DME/water (0.7:0.9:2), 85 °C, 16 h. Method C2 for **38**, Na_2CO_3 (2 M), $Pd(PPh_3)_4$, toluene/ethanol (1:1), reflux, overnight.

steps. The tri-F and methyl thiophene scaffolds of **B** and **C** can be easily prepared as their 2-bromothiophene intermediates. Mild Suzuki coupling conditions (method C1) can be applied to introduce a large number of aromatic rings to the thiophene core, which makes the reaction scheme ideal for combinatorial chemistry on a robotic synthesis platform. Starting from the commercially available substituted benzoyl chlorides **1a** and **7a**, a Friedel−Crafts acylation using a standard protocol (method A) was performed on 2-bromothiophene to obtain **1b** and **7b** or on 2-methylthiophene to obtain **39b**, respectively. Ether cleavage of **1b** and **39b** with BBr_3 under anhydrous conditions yielded intermediate **1c** and final compound **39** (method B). The bromo compound **1c** was then converted to final compounds **1−4**, **12−14**, and **18−38** in a Suzuki−Miyaura cross-coupling reaction with the corresponding boronic acids using tetrakis(triphenylphosphine) palladium(0) as a catalyst with cesium carbonate in oxygen-free toluene/1,2-dimethoxyethane (DME)/water at 85 °C for 16 h (method C1).[28] Compound **38** was obtained using a similar Suzuki coupling procedure with toluene/ethanol as a solvent and sodium carbonate as a base (method C2).[28] In the case of compounds **22**, **23**, **25**, **33**, and **38**, the corresponding boronic acid pinacol esters **22a**, **23a**, **25a**, **33a**, and **38a** were synthesized by Miyaura borylation reaction[29] before the Suzuki coupling was performed (see the Supporting Information). Suzuki coupling of **7b** with the corresponding boronic acids yielded the final hydroxy compounds **7−9**. The dihydroxy derivatives **5**, **6**, **10**, **11**, and **15−17** were obtained by the cleavage of the respective methylethers with BBr_3 in dichloromethane (DCM) at low temperature (method B).

Inhibition of 17*β*-HSD2 and 17*β*-HSD1. All final compounds have been tested for their inhibitory activities on both human 17*β*-HSD2 and 17*β*-HSD1. The results are presented in Table 1.

The inhibition values of compounds **1−11** are similar to those already obtained from compounds **B** and **C**. Compounds bearing the 2,4,5-tri-F motif (**1−6**, IC_{50} = 1.3−11 nM) show increased inhibition values compared to their 2-methyl analogues (**7−11**, 20−46% inhibition at 100 nM) by a factor of approximately 100 or higher, whereas in general, the di-*m*-Cl/Me, *p*-OH/OMe motif (**1−6**, IC_{50} = 1.3−11 nM) does not lead to an increase in potency compared to **A** (IC_{50} = 2 nM) and **B** (IC_{50} = 1.4 nM). Because of the low potency of **7−11**, only compounds **1−6** were tested for their inhibition of the murine enzymes m17*β*-HSD2 and m17*β*-HSD1 at concentrations of 50 and 1000 nM, respectively. All compounds show decreased activity on the murine 17*β*-HSD1 compared to m17*β*-HSD2. IC_{50} values were determined for compounds showing the highest inhibition on m17*β*-HSD2. In general, all tested compounds show strongly decreased activity on the murine enzymes compared to the human ones. The best two compounds are two and four times less active on the m17*β*-HSD2 with IC_{50} values of 58 nM for **5** and 89 nM for **2**, respectively, compared to compound **A** (IC_{50} = 25 nM).

This discrepancy between the inhibition values on human and mouse 17*β*-HSDs led to a second design step to establish a SAR on both human and murine 17*β*-HSDs. To this end, a set of isosteres of the hydroxy group, different cyclic moieties, and a methyl group were introduced to the tri-F scaffold, resulting in compounds **12−39**. In general, the compounds of this series showed increased or similar activity on the human 17*β*-HSD2 when compared to sulfonamide compound **A**, with IC_{50} values in the picomolar to lower nanomolar range. Selectivity factors of up to 24 were reached within these compounds.

Comparing the monosubstituted methoxy derivatives **12−14** (IC_{50} = 1.1−2.3 nM) with the hydroxy derivatives **15−17** (IC_{50} = 0.32−1.1 nM), the former show slightly decreased activity on human 17*β*-HSD2. A possible explanation is the lack of an H-bond donor in the case of the methoxy compounds. **15−17** represents the most active 17*β*-HSD2 inhibitors described with the *p*-hydroxy **15** (IC_{50} = 0.32 nM) as the most potent one with a sixfold increase in activity compared to **A** (IC_{50} = 2 nM). The increased or similar potency of the plain *para* OMe or OH substituted compounds

Table 1. Inhibition of Human and Murine 17β-HSD2 and 17β-HSD1 by Compounds 1−39

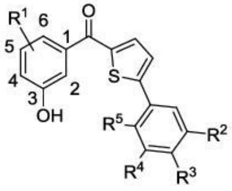

A, B, C, 1 -11

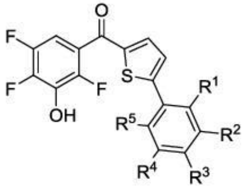

12 - 32

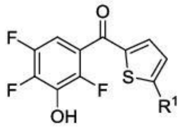

33 - 39

Cmd	R^1	R^2	R^3	R^4	R^5	IC_{50} [nM][a,c,d]		SF[e]	% inhibition[a,f,g]	
						h17β-HSD2	h17β-HSD1		m17β-HSD2@50 nM (IC_{50})	m17β-HSD1@1000 nM[b]
A	2,4,5-tri-F	$NHSO_2(2\text{-}OCF_3Phe)$	H	H	H	2.0	6.0	3	81 (25 nM)	47
B	2,4,5-tri-F	H	F	H	F	1.4	7.0	5	85@250 nM	27.5
C	2-Me	H	F	H	F	299	3427	11	18@1 μM	n.d.
1	2,4,5-tri-F	Me	OMe	Me	H	2.3	1.2	0.5	22.4	26.8
2	2,4,5-tri-F	Cl	OMe	Cl	H	1.6	0.4	0.25	37.6 (89 nM)	39.5
3	2,4,5-tri-F	Cl	OH	H	H	2.6	1.7[b]	0.7	28.4	32.7
4	2,4,5-tri-F	F	OH	H	H	2.7	3.1	1.1	30.9	13.7
5	2,4,5-tri-F	Me	OH	Me	H	1.3	0.9	0.7	49.3[b] (58 nM)	58.8
6	2,4,5-tri-F	Cl	OH	Cl	H	11	4.7	2	12	14
7	2-Me	Me	OMe	Me	H	23%[h]	32%[i]			
8	2-Me	Cl	OMe	Cl	H	20%[h]	45%[i]			
9	2-Me	Cl	OH	H	H	31%[h]	59%[i]			
10	2-Me	Me	OH	Me	H	46%[h]	62%[i]			
11	2-Me	Cl	OH	Cl	H	45%[h]	16%[i]			
12	H	H	OMe	H	H	2.3	15	7	42	33
13	H	OMe	H	H	H	1.8	7.3	4	22	22
14	OMe	H	H	H	H	1.1	6.8	6	33	35
15	H	H	OH	H	H	0.32	7.0	22	47	32
16	H	OH	H	H	H	1.1	3.3	3	34	30
17	OH	H	H	H	H	0.63	5.2	8	38	27
18	H	CH_2OH	H	H	H	4.4	5.9	1	21	22
19	H	H	NH_2	H	H	9.2	27	3	22[b]	6
20	H	NH_2	H	H	H	5.4	49	9	22	6
21	NH_2	H	H	H	H	4.0	92	23	19	19
22	H	NH_2	OMe	H	H	7.1	84	12	20	17
23	H	NH_2	OH	H	H	3.4	13.0	4	28	7
24	H	NH_2	Me	H	H	10	49	5	48	47
25	Me	NH_2	H	H	H	6.0	76	13	35	24
26	H	NH_2	F	H	H	8.9	35	4	37	20
27	H	NH_2	F	F	H	2.2	5.3	3	24	19
28	H	NH_2	F	H	F	5.8	27	5	35	34
29	H	$NHCOCH_3$	H	H	H	4.5	30	7	41	24
30	H	H	$NHCOCH_3$	H	H	10	235	24	24	22

Table 1. continued

						IC$_{50}$ [nM][a,c,d]		SF[e]	% inhibition[a,f,g]	
Cmd	R^1	R^2	R^3	R^4	R^5	h17β-HSD2	h17β-HSD1		m17β-HSD2@50 nM (IC$_{50}$)	m17β-HSD1@1000 nM[b]
31	H	CONH$_2$	H	H	H	5.4	50	9	18	10
32	H	H	H	H	H	0.85	6.7	8	27	25
33	indol-4-yl					1.1	1.5	1	63 (34 nM)	42
34	indol-5-yl					1.3	5.8	4.5	69 (34 nM)	14
35	indol-6-yl					3.8	21	6	43	35
36	benzimidazol-5-yl					5.2	48[b]	9	10	37
37	pyridin-3-yl					6.3	96	15	0	11
38	quinolin-7-yl					3.1	53	17	10	33
39	methyl					56%[h]	13%[b,h]			

[a]Mean value of at least two experiments. The deviations were <30%. [b]Single value. [c]Human placental, microsomal fraction, substrate E2 500 nM, cofactor NAD$^+$, 1500 μM. [d]Human placental, cytosolic fraction, substrate E1 500 nM, cofactor NADH 500 μM. [e]SF: IC$_{50}$ 17β-HSD1/IC$_{50}$ 17β-HSD2. [f]Mouse liver, microsomal fraction, substrate E2 10 nM, cofactor NAD$^+$ 1500 μM. [g]Recombinant enzyme, substrate E1 500 nM, cofactor NADPH 500 μM. [h]Tested at 100 nM. [i]Tested at 500 nM.

12 (IC$_{50}$ = 2.3 nM) and **15** (IC$_{50}$ = 0.32 nM) compared to the *p*-OH/OMe-*m*-Me/Cl compounds **1**−**6** (IC$_{50}$ = 1.3−11 nM) shows that for the tri-F compound class, the meta substituent does not lead to an enhanced potency on human 17β-HSD2, as observed in the SAR of the closely related di-F class.[28] Substitution of the hydroxy or methoxy oxygen by an amino function as seen in compounds **19**−**21** (IC$_{50}$ = 4−9.2 nM) leads to decreased potency on the human 17β-HSD2 compared to their oxygen analogues **12**−**17** (IC$_{50}$ = 0.32−2.3 nM). A combination of both, an amino function with an OMe or OH group (**22**, IC$_{50}$ = 7.1 nM, **23**, IC$_{50}$ = 3.4 nM), does not restore the activity as seen for **12** (IC$_{50}$ = 2.3 nM) and **15** (IC$_{50}$ = 0.32 nM). Introduction of F or Me on the ring to the most active aniline **20** (IC$_{50}$ = 5.4 nM) is tolerated well by the enzyme and leads to equipotent or slightly less potent compounds **24**−**28** (IC$_{50}$ = 2.2−10 nM). Cyclization to the corresponding indole compounds **33**−**35** (IC$_{50}$ = 1.1−3.8 nM) results in comparable to slightly increased potency compared to the aniline derivatives **18** (IC$_{50}$ = 4.4 nM) and **19** (IC$_{50}$ = 9.2 nM). The plain phenyl−substituted compound **32** (IC$_{50}$ = 0.85 nM, SF 8) shows one of the highest inhibition values for 17β-HSD2 with moderate 17β-HSD1 activity, indicating that no additional substituent is required for this class to achieve high potency on the human 17β-HSD2 as well as moderate selectivity. Different heterocyclic moieties **33**−**38** (IC$_{50}$ = 1.1−6.3 nM) are also tolerated by the enzyme, but lead to a decreased potency compared to **32** (IC$_{50}$ = 0.85 nM), except the indole derivatives **33** (IC$_{50}$ = 1.1 nM) and **34** (IC$_{50}$ = 1.3 nM), which are equipotent on the target enzyme. The highly decreased potency of the truncated molecule **39** (56% at 100 nM for human 17β-HSD2 vs 13% at 100 nM for 17β-HSD1) compared to **32** (IC$_{50}$ = 0.85 nM) not only illustrates the necessity of a bulkier group on the right side of the molecule connected to the thiophene to achieve high potency on human 17β-HSD2 but also points out that the tri-F-benzoyl thiophene moiety alone is already 17β-HSD2 selective. These findings demonstrate clearly that a wide range of different substituted phenyl moieties is tolerated by human 17β-HSD2 within this compound class and no bigger sulfonamide tail, as seen in **A**, is needed for high potency.

The compounds of the second library **12**−**37** were tested for their inhibition of the murine 17β-HSD2 at 50 nM and HSD1 at 1 μM. IC$_{50}$ values were obtained for compounds showing more than 50% inhibition at 50 nM. The compounds show strongly decreased potency compared to their human ortholog as well as selectivity over murine 17β-HSD1, as observed for the first library (compounds **1**−**11**) before. However, some properties observed in the SAR of **12**−**38** on the human 17β-HSD2 can also be seen on the murine enzyme. The amino derivatives **19**−**21** (**19**, 22%, **20**, 22%, and **21**, 19% inhibition of murine 17β-HSD2) show decreased activity compared to their hydroxy analogues (**15**, 47%, **16**, 34%, and **17**, 38% inhibition of murine 17β-HSD2). On contrary to the findings on the human enzyme, addition of methyl or fluorine on the phenyl ring (**24**, 48%, **25**, 35%, **26**, 37%, and **28**, 35% inhibition of murine 17β-HSD2) leads to an increase in activity compared to unsubstituted *m*-aniline **20** (22% inhibition of murine 17β-HSD2). Furthermore, the unsubstituted phenyl (**32**, 27% inhibition of murine 17β-HSD2) is only weakly active, as are most of the heterocyclic compounds **36**−**38** as well. An exception are the bulkier indole derivatives **33**−**35** (**33**, 63%, **34**, 69%, **35**, 43% inhibition of murine 17β-HSD2) which show the same trend in activity regarding their substitution pattern as observed for the human enzyme. Especially, compounds **33** (m17β-HSD2 IC_{50} = 34 nM) and **34** (m17β-HSD2 IC_{50} = 34 nM) show the highest inhibition values on the mouse enzyme obtained in this study, being equipotent to reference compound **A** (m17β-HSD2 IC_{50} = 25 nM).

■ FURTHER IN VITRO BIOLOGICAL EVALUATION

Cytotoxicity. In order to identify suitable candidates for applications in vivo, it was necessary for the administered compounds to be nontoxic. Therefore, the most active compounds toward potency on mouse 17β-HSD2 (**2**, **5**, **33**, and **34**) were evaluated in a cellular toxicity MTT assay over 66 hours using HEK293 cells. All compounds showed safety factors (LC_{20}/IC_{50} human 17β-HSD2) >1000 and, thus, are regarded as nontoxic.

Aqueous Solubility and Metabolic Stability. In order to achieve a sufficient plasma concentration for a sufficient period of time following peroral administration of the compound, aqueous solubility and metabolic stability are two important factors for good oral absorption and low clearance of the drug. Solubility of the compounds in aqueous solution and in vitro metabolic half-life using human and mouse liver S9 fraction have been determined. The results are depicted in Table 2. Both compounds **2** and **5** show increased solubility (>200 μM) compared to **A** (50−100 μM), whereas the solubility of the indole derivatives **33** and **34** (50−100 μM) is in the same range as seen for reference **A** (50−100 μM). Comparing metabolic stability in human liver S9 fraction, the most newly synthesized compounds (**2**, $t_{1/2}$ = 19 min, **5**, $t_{1/2}$ = 32 min, and **34**, $t_{1/2}$ = 34 min) show two to four times decreased half-life times compared to **A** ($t_{1/2}$ = 60 min). Only the half-life time of compound **33** (51 min) is similar to that of **A** ($t_{1/2}$ = 60 min). Having a look at the stability in murine liver S9 fraction, most of the tested compounds (**2**, $t_{1/2}$ = 70 min, **33**, $t_{1/2}$ ≫ 60 min, **34**, 49 min) are more or equally stable than **A** ($t_{1/2}$ = 46 min), except **5** ($t_{1/2}$ = 18 min), which is three times less stable than **A**. It is noted that **33** shows the highest metabolic stability both in human and mouse liver S9 fraction.

Table 2. Aqueous Solubility and Metabolic Stability of Selected Compounds

Cmpd	aq solubility[a,d] (μM)	$t_{1/2}$ human S9[b,d] (min)	$t_{1/2}$ mouse S9[c,d] (min)
A	50−100	60	46
2	>200	19	70
5	>200	32[e]	18[e]
33	50−100	51	≫60
34	50−100	34	49[e]

[a] Solubility of compound in phosphate-buffered saline, pH 7.2, containing 2% DMSO. [b] Pooled human liver S9 fraction (1 mg/mL), 2 mM NADPH regenerating system, 1 mM UDPGA, 0.1 mM PAPS, 1 μM test compound at 37 °C for 0, 15, and 60 min. [c] Pooled mouse liver S9 fraction (1 mg/mL), 2 mM NADPH regenerating system, 1 mM UDPGA, 0.1 mM PAPS, 1 μM test compound at 37 °C for 0, 15, and 60 min. [d] Mean value of two determinations, SD < 15%. [e] Single value.

■ IN VIVO EVALUATION OF PLASMA CONCENTRATION IN MICE

Osteoporosis is a disease affecting mostly elderly persons, and therapy often occurs over decades. For a drug that is to be administered frequently, the oral route is preferred. Thus, the two compounds showing the highest in vitro potency and metabolic stability, **2** and **5** of the first and **33** and **34** of the second library, were tested in a PK study in C57Bl/6 mice. **2** and **5** were applied at a single dose of 50 mg/kg, **33** and **34** at a three times lower dose of 16.7 mg/kg. The obtained concentration curves are depicted in Figure 1. The obtained PK parameters are listed in Table 3. All compounds show bigger area-under-the-curve values (AUC) than **A**. Compound **33** had the highest value with a 13-fold increase in AUC compared to **A**. **33** also shows the highest plasma concentrations with a C_{max} of 1211 nM. Furthermore, both indole derivatives **33** and **34** can still be detected after 24 h (46 and 53 nM, respectively), enabling accumulation of the drug after multiple dosing, each once-a-day. The most likely desirable inhibitor concentration should be around the IC_{90}, which is assumed as 10 times the IC_{50}, based on the in vitro inhibition curves of **33**. During the course of the day, only **33** is likely to reach this concentration for 19 h (dotted line, 300 nM for **33**), which makes **33** a suitable candidate for an in vivo proof-of-principle study.

Table 3. PK Parameters of Selected Compounds[a,b]

Cmpd	dose [mg/kg]	C_{max} [nM]	T_{max} [h]	C_{24h} [nM]	$AUC_{0-\infty}$ [ng·h/mL]
A	50	252	2	ND	434
2	50	167	6	ND	609
5	50	269	8	ND	1428
33	16.7	1211	2	46	5503
34	16.7	390	2	53	1293

[a] Data are mean values. [b] Abbreviations: C_{max}, highest plasma concentration of a drug after administration; T_{max}, time to reach C_{max}; C_{24h}, plasma concentration at 24 h timepoint, AUC, area under the concentration−time curve. ND, nondetectable (below lowest level of detection); methods were validated, CV was below 20%, in rare cases higher; GraphPadPrism 6 was used for AUC calculation.

Inhibition of Human Hepatic CYP Enzymes. To analyze the potential risk of drug−drug interaction, inhibition of **33** toward human hepatic CYP enzymes CYP2C19, CYP2D6, and CYP3A4 was evaluated. Compound **33** was tested at 1.2 μM and showed no or moderate inhibition (22, 0, and 41%).

■ CONCLUSIONS

17β-HSD2 has been shown to be a suitable target for the treatment of osteoporosis.[5] Originating from the closely related field of 17β-HSD1 inhibitors,[28] the potent 17β-HSD2 inhibitor **A** was developed and successfully tested in a bone fracture model in mice when applied subcutaneously.[25] However, this compound shows an unfavorable oral PK profile administered in mice and therefore is not a suitable candidate to be evaluated in an osteoporosis proof-of-principle model. The aim of this work was to develop a low molecular weight compound with similar potency on both human and mouse 17β-HSD2 and with increased aqueous solubility and metabolic stability with regards to **A** to increase plasma concentrations. In a first design step, different phenol-derived moieties were synthesized. Among these, **2** and **5** showed decreased potency on the mouse 17β-HSD2, but increased solubility and metabolic stability compared to **A**. The decreased potency on the mouse enzyme led to the synthesis of a second library, introducing different hydrophilic substituents as well as different aromatic moieties to gain deeper insights into the SAR of the mouse 17β-HSD2, resulting in compounds **12**−**39**. In this series, compound **15** is the most potent 17β-HSD2 inhibitor (IC_{50} = 320 pmolar) currently described in the literature for osteoporosis therapy and the most selective of its compound class (22-fold). The highest murine 17β-HSD2 inhibitory activities are shown by compounds **29**, **33**, and **34** which are equipotent to compound **A**. These findings clearly demonstrate that the sulfonamide moiety of **A** does not significantly contribute to the binding to the enzyme of this compound class and can therefore be omitted. Taking into account principles for the design of orally bioavailable compounds,[30,31] the decreased molecular weight below 500 should facilitate permeability via passive diffusion of the compounds through the gastro-intestinal barrier and hence increase absorption of the drug. The compounds show comparable or increased aqueous solubility and metabolic stability with **33** showing better profile than **A**. The best two compounds of each library, **2** and **5** of the first and **33** and **34** of the second library, were tested in a mouse oral PK study. All tested compounds showed an increase in AUC compared to **A**, with **33** showing a 13-fold increase. Furthermore, **33** is able to maintain a pharmacologically relevant plasma concentration for much longer than **A**, lasting for at least 8 hours after a single dose. In summary, **33** was identified as a highly potent inhibitor of human and mouse 17β-HSD2 with a superior pharmacological profile and is therefore a promising candidate for an in vivo proof-of-principle study in a mouse osteoporosis model.

■ EXPERIMENTAL SECTION

Chemical Methods. Chemical names follow IUPAC nomenclature. Starting materials were purchased from Aldrich, Acros, Lancaster, Maybridge, Combi Blocks, Merk, or Fluka and were used without purification.

Column chromatography (CC) was performed on silica gel (70−200 μm), and reaction progress was monitored by thin-layer chromatography on Alugram SIL G UV_{254} (Macherey-Nagel).

All Suzuki couplings have been conducted according to method C1 on a combinatorial chemistry synthesis platform (Chemspeed Isynth, Chemspeed AG, Füllinsdorf, Switzerland). In the case of preparative high-performance liquid chromatography (HPLC) purification, the compounds were purified using a setup produced by Waters Corporation containing a 2767 Sample Manager, a 2545 binary gradient pump, a 2998 PDA detector, and a 3100 electron spray mass spectrometer. The system has been used for a part of the analytical analysis as well as the preparative separation. In the latter case after separation, the solvent flow has been split using a flow splitter and a 515 HPLC pump for makeup flow. Water containing 0.1% formic acid and acetonitrile containing 0.1% formic acid were used as solvents for the analysis and separation. A Waters X-Bridge column (C18, 150 × 4.6 mm, 5 μM) has been used with a flow of 1 mL/min for the analysis, and a Waters X-Bridge column (C18, 150 × 19 mm, 5 μM) has been used with a flow of 20 mL/min for the separation. ^{1}H NMR spectra were measured on a Bruker AM500 spectrometer (500 MHz) at 300 K or on a Bruker Fourier 300 (300 MHz) at 295.5 K. Chemical shifts are reported in δ (parts per million: ppm), by reference to the hydrogenated residues of the deuterated solvent as an internal standard [$CDCl_3$: δ = 7.24 ppm (^{1}H NMR) and δ = 77 ppm (^{13}C NMR), CD_3OD: δ = 3.35 ppm (^{1}H NMR) and δ = 49.3 ppm (^{13}C NMR), CD_3COCD_3: δ = 2.05 ppm (^{1}H NMR) and δ = 29.9 ppm (^{13}C NMR), CD_3SOCD_3 δ = 2.50 ppm (^{1}H NMR) and δ = 39.5 ppm (^{13}C NMR)]. Signals are described as s, br s, d, t, dd, ddd, m, dt, q, and sep for singlet, broad singlet, doublet, triplet, doublet of doublets, doublet of doublets of doublets, multiplet, doublet of triplets, quadruplet, and septet, respectively. All coupling constants (*J*) are given in hertz (Hz). Melting points have been recorded on a SMP40 apparatus (Stuart-Equipment, Staffordshire, United Kingdom.) Mass spectra (ESI) have been recorded on the system mentioned above. Tested compounds were recrystallized from acetonitrile/water +0.1% formic acid and are of >95% chemical purity as measured by HPLC unless otherwise stated. MS/MS measurements were performed on a TSQ Quantum Acess Max (ThermoFisher, Dreieich, Germany) coupled to an Acella UHPLC system. An electrospray interface (ESI) was used as an ion source. The Acella-LC-system consisted of a pump and an auto sampler. The system was operated by the standard software Xcalibur. All solvents were HPLC grade. All newly synthetized compounds passed an in silico PAINS filter.

General Procedure for Friedel−Crafts Acylation (Method A). An ice-cooled mixture of monosubstituted thiophene derivate (1 or 1.5 equiv), arylcarbonyl chloride (1 equiv), and aluminumtrichloride (1 equiv) in anhydrous dichloromethane was warmed to room temperature and stirred for 2−4 h. HCl (1 M) was used to quench the reaction. The aqueous layer was extracted with ethyl acetate. The combined organic layers were washed with brine, dried over magnesium sulfate, filtered, and concentrated to dryness. The product was purified by CC.

General Procedure for Ether Cleavage (Method B). To a solution of methoxybenzene derivative (1 equiv) in anhydrous dichloromethane at −78 °C (dry ice/acetone bath), boron tribromide in dichloromethane (1 M, 3 equiv per methoxy function) was added dropwise. The reaction mixture was stirred overnight at room temperature under nitrogen atmosphere. Water was added to quench the reaction, and the aqueous layer was extracted with ethyl acetate. The combined organic layers were washed with brine, dried over magnesium sulfate, filtered, and concentrated to dryness. The product was purified by CC.

General Procedure for Suzuki Coupling (Method C1). A mixture of arylbromide (1 equiv), boronic acid derivative (1.1 equiv), cesium carbonate (3.5 equiv), and tetrakis(triphenylphosphine) palladium (0.035 equiv) was suspended in an oxygen-free toluene/DME/water (0.7:0.9:2) solution and heated under argon atmosphere to 85 °C for 16 h. The reaction mixture was cooled to room temperature. Water was added, and the aqueous layer was extracted with ethyl acetate three times. The combined organic layers were dried over magnesium sulfate, filtered, and concentrated to dryness. The product was purified by preparative HPLC.

Method C2. A mixture of arylbromide (1 equiv), boronic acid derivative (1.2 equiv), sodium carbonate (2 equiv), and tetrakis(triphenylphosphine) palladium (0.01 equiv) was suspended in an oxygen-free toluene/ethanol (1:1) solution and was refluxed for 20 h under nitrogen atmosphere. The aqueous layer was extracted with ethyl acetate. The combined organic layers were washed with brine, dried over magnesium sulfate, filtered, and concentrated to dryness. The product was purified by CC.

Biological Methods. [2,4,6,7-^{3}H]-E2 and [2,4,6,7-^{3}H]-E1 were obtained from PerkinElmer, Boston. A Quickszint Flow 302 scintillator fluid was purchased from Zinsser Analytic, Frankfurt. Other chemicals were bought from Sigma, Roth, Merck, or Santa Cruz Biotechnology.

Ethics Statement. Placental samples were obtained anonymously from Saarbrücken-Dudweiler Hospital's Department of Gynecology. None of the authors involved in this study has received any information about the patients. The microsomal fraction of the mouse enzyme (m17β-HSD2) was obtained from mouse livers, which were purchased from Pharmacelsus GmbH (Saarbrücken, Germany). All animal experiments were approved by the local governmental animal protection committee (Landesamt für Verbraucherschutz, Abteilung C Lebensmittel-und Veterinärwesen, Saarbrücken, Germany) and were conducted in accordance with the European legislation on protection of animals (Guide line 2016/63/EU) and the National Institutes of Health Guidelines for the Care and Use of Laboratory

Animals (http://oacu.od.nih.gov/regs/index.htm. Eighth Edition; 2011).

Preparation of h17β-HSD1 and h17β-HSD2 Enzymes. Cytosolic (h17β-HSD1) and microsomal (h17β-HSD2) fractions were obtained from human placenta similar to previously described procedures.[23,32] The placenta was homogenized, and the enzymes were separated by fractional centrifugation at 1000*g*, 10 000*g*, and 150 000*g*. The pellet containing the microsomal h17β-HSD2 fraction was used for the determination of h17β-HSD2 inhibition, whereas h17β-HSD1 was obtained by ammonium sulfate precipitation from the cytosolic fraction. Aliquots of the enzyme were stored at −78 °C.

m17β-HSD2 Enzyme Preparation and Inhibition. The microsomal fraction (m17β-HSD2) was obtained from mouse liver similar to the procedure described for h17β-HSD2. Inhibitory activities were evaluated by a method identical to the one described for the human enzyme.

m17β-HSD1 Enzyme Preparation. Recombinant m17β-HSD1 enzyme was produced by transfection of HEK293 cells with an 17β-HSD1 expression plasmid (coding sequence of NM_010475 in pCMV6Entry vector, OriGene Technologies, Inc.) according to a described procedure.[33] Transfected cells were homogenized after 48 h by sonication (3 × 10 s) in a 40 mM Tris buffer containing 250 mM saccharose, 5 mM ethylenediaminetetraacetic acid (EDTA), 7 mM DTT, 1 mM phenylmethylsulfonyl fluoride, pH 7.5. Cell lysate was centrifuged (1000*g*, 15 min, 4 °C), and 20% glycerol was added to the supernatant before aliquots were frozen and stored at −70 °C.

Inhibition of h17β-HSD2 and m17β-HSD2 in Cell-free Assay. Inhibitory activities were evaluated following an established method with minor modifications.[34] Briefly, the enzyme preparation was incubated with NAD$^+$ (1500 μM) in the presence of potential inhibitors at 37 °C in a phosphate buffer (50 mM), pH 7.4 supplemented with 20% of glycerol and 1 mM EDTA. Inhibitor stock solutions were prepared in DMSO. Final concentration of DMSO was adjusted to 1% in all samples. The enzymatic reaction was started by the addition of a mixture of unlabeled- and [^{3}H]-E2 (final concentration: 500 nM, 0.11 μCi). After 20 min, the incubation was stopped with 100 mM $HgCl_2$ and the mixture was extracted with ether. After evaporation, the steroids were dissolved in acetonitrile/water (45:55). E1 and E2 were separated using acetonitrile/water (45:55) as a mobile phase in a C18 RP chromatography column connected to a HPLC system (Agilent 1100 Series, Agilent Technologies, Waldbronn). Detection and quantification of the steroids were performed using a radio-flow detector (Berthold Technologies, Bad Wildbad). The conversion rate was calculated according to the following equation: % conversion = (% E1/(% E1 + % E2)) × 100. Each value was calculated from at least two independent experiments. In each experiment, a reference compound was included.

Inhibition of h17β-HSD1 and m17β-HSD1 in Cell-Free Assay. The 17β-HSD1 inhibition assay was performed similarly to the h17β-HSD2 test. The human enzyme was incubated with NADH (500 μM), whereas the mouse recombinant enzyme was incubated with NADPH (500 μM). Test compound and a mixture of nonlabeled- and [^{3}H]-E1 (final concentration: 500 nM, 0.15 μCi) were added and mixed for 10 min at 37 °C. Further treatment of the samples and HPLC separation was carried out as-mentioned above for h17β-HSD2. In each experiment, a reference compound was included.

MTT Cytotoxicity Assay. In general, the assay was performed similar to a protocol described in the literature.[35] HEK293 cells (2 × 10^5 cells per well, 1 mL per well) were seeded in 96-well flat-bottom plates. Culturing of cells, incubations, and OD measurements were performed as described previously with minor modifications. In short, 4 h after seeding the cells, the incubation was started by the addition of compounds (100, 50, 25, 12.5, and 6.25 μM) in a final DMSO concentration of 1% or vehicle (DMSO) in quadruplicates. After 66 h, 50 μL of 5 mg/mL MTT (3-(4,5-dimethylthiazol-2-yl)-2,5-diphenyltetrazolium bromide) solution in phosphate-buffered saline is added to the medium and cells were then incubated for 30 min at 37 °C in a CO_2 incubator. After this, the medium was removed by suction and 250 μL of DMSO containing 10% SDS and 0.5% acetic acid was added to dissolve the cells and MTT crystals. Then, fluorescence was measured in a BioTek Synergy 2 plate reader. The decrease in fluorescence (at 570 nm) in the presence of the test compound compared to the fluorescence in the presence of the vehicle control (1% DMSO) was determined followed by the calculation of IC_{20} values using GraphpadPrism 6 curve fitting. In each experiment, a reference compound was included.

Aqueous Solubility Determination. Aqueous solubility was evaluated as previously described.[36] Final concentrations of 5, 15, 50, 100, and 200 μM of **A**, **2**, **5**, **33**, and **34** in an aqueous solution containing 2% DMSO were prepared, and the solution clarity and potential compound precipitation were determined by eye after 1 and 24 h at room temperature. In each experiment, a reference compound was included.

Metabolic Stability in a Cell-Free Assay. Compounds were tested according to an established method.[37] For evaluation of phases I and II metabolic stability, 1 μM compound was incubated with 1 mg/mL pooled mammalian (human or mouse) liver S9 fraction (BD Gentest), 2 mM NADPH regenerating system, 1 mM UDPGA, and 0.1 mM PAPS at 37 °C for 0, 5, 15, and 60 min at a final volume of 100 μL. The incubation was stopped by precipitation of S9 enzymes with 2 volumes of ice-cold acetonitrile containing diphenhydramine as an internal standard. Concentration of the remaining test compound at different time points was analyzed by LC-MS/MS and used to determine half-life ($t_{1/2}$). In each experiment, a reference compound was included.

Inhibition of Human Hepatic CYP Enzymes. Inhibition of hepatic CYP enzymes CYP2B6, CYP2C19, and CYP3A4 by the test compound (1.2 μM) was measured in baculosomes expressing the recombinant human enzymes according to the manufacturer's instruction (Life Technologies). In each experiment, a reference compound was included.

PK Experiments. Experiments were conducted on female C57BL/6 mice (body weight 20−25 g). Compounds were orally administered at a dose of 50 mg/kg ($n = 3$) or 16.7 mg/kg ($n = 3$) per animal. The administered suspensions of solid inhibitors were prepared by mixing them with 0.5% gelatin and 5% mannitol (w/w) in water. Blood samples were collected in citrate tubes from the tail vein at 2, 4, 8, and 24 h. Obtained blood samples (50 μL blood + 5 μL citrate buffer) were centrifuged at 3000 rpm. Subsequently, 10 μL of mouse plasma was added to 50 μL of acetonitrile containing diphenhydramine as an internal standard, and obtained samples were stored at −20 °C until HPLC-MS/MS analysis. Samples and calibration standards were centrifuged at 15 000 rpm for 5 min at 4 °C. The solution was transferred into fresh vials for HPLC-MS/MS analysis (Accucore RP-MS, TSQ Quantum triple quadrupole mass spectrometer, electrospray interface). After injection of 10 μL, data were analyzed based on the ratio of the peak areas of analyte and internal standard.

*(5-(4-Methoxy-3,5-dimethylphenyl)thiophen-2-yl)(2,4,5-trifluoro-3-hydroxyphenyl)methanone (**1**).* The title compound was prepared by reaction of (5-bromothiophen-2-yl) (2,4,5-trifluoro-3-hydroxyphenyl)methanone (**1b**) (96.0 mg, 0.285 mmol), (4-methoxy-3,5-dimethylphenyl)boronic acid (54.0 mg, 0.300 mmol), cesium carbonate (326 mg, 1.00 mmol), and tetrakis(triphenylphosphine) palladium (11.5 mg, 9.95 μmol) according to method C1. The product was purified by preparative HPLC; yield: 73% (81.5 mg); mp 162−164 °C; ^{1}H NMR (300 MHz, $CDCl_3$, δ): 7.49 (dd, J = 3.9, 1.7 Hz, 1H), 7.34 (s, 2H), 7.24−7.27 (m, 1H), 6.99 (td, J = 8.7, 6.1 Hz, 1H), 3.76 (s, 3H), 2.38 (s, 6H); MS (ESI): 393.2 (M + H)$^+$; UV λ (nm) = 250, 355; RT HPLC: 13.48 min (13 min 10−95% MeCN in water with 0.1% formic acid); purity >99%.

*(5-(3,5-Dichloro-4-methoxyphenyl)thiophen-2-yl)(2,4,5-trifluoro-3-hydroxyphenyl)methanone (**2**).* The title compound was prepared by the reaction of (5-bromothiophen-2-yl)(2,4,5-trifluoro-3-hydroxyphenyl)methanone (**1b**) (96.0 mg, 0.285 mmol), (3,5-dichloro-4-methoxyphenyl)boronic acid (66.3 mg, 0.300 mmol), cesium carbonate (326 mg, 1.00 mmol), and tetrakis-(triphenylphosphine)palladium (11.5 mg, 9.95 μmol) according to method C1. The product was purified by preparative HPLC; yield: 59% (73.2 mg); mp 156−158 °C; ^{1}H NMR (300 MHz, acetone-d_6,

δ): 7.86 (s, 2H), 7.71–7.69 (m, 2H), 7.13 (ddd, *J* = 10.0, 8.1, 5.7 Hz, 1H), 3.95 (s, 3H); MS (ESI): 431.0 $(M - H)^-$; UV λ (nm) = 340; RT f HPLC: 14.14 min (13 min 10–95% MeCN in water with 0.1% formic acid); purity >99%.

*(5-(3-Chloro-4-hydroxyphenyl)thiophen-2-yl)(2,4,5-trifluoro-3-hydroxyphenyl)methanone (**3**).* The title compound was prepared by the reaction of (5-bromothiophen-2-yl)(2,4,5-trifluoro-3-hydroxyphenyl)methanone (**1b**) (96.0 mg, 0.285 mmol), (3-chloro-4-hydroxyphenyl)boronic acid (51.7 mg, 0.300 mmol), cesium carbonate (326 mg, 1.00 mmol), and tetrakis(triphenylphosphine) palladium (11.5 mg, 9.95 μmol) according to method C1. The product was purified by preparative HPLC; yield: 40% (43.4 mg); mp 107–110 °C; ^{1}H NMR (300 MHz, acetone-d_6, δ): 9.61 (br s, 1H), 7.82 (d, *J* = 2.2 Hz, 1H), 7.68–7.59 (m, 2H), 7.53 (d, *J* = 4.1 Hz, 1H), 7.13 (d, *J* = 8.6 Hz, 1H), 7.18–7.04 (m, 1H), 7.13 (d, *J* = 8.6 Hz, 1H); MS (ESI): 385.1 $(M + H)^+$; UV λ (nm) = 250, 361; Rf HPLC: 11.04 min (13 min 10–95% MeCN in water with 0.1% formic acid); purity 95%.

*(5-(3-Fluoro-4-hydroxyphenyl)thiophen-2-yl)(2,4,5-trifluoro-3-hydroxyphenyl)methanone (**4**).* The title compound was prepared by the reaction of (5-bromothiophen-2-yl)(2,4,5-trifluoro-3-hydroxyphenyl)methanone (**1b**) (96.0 mg, 0.285 mmol), (3-fluoro-4-hydroxyphenyl)boronic acid (46.8 mg, 0.300 mmol), cesium carbonate (326 mg, 1.00 mmol), and tetrakis(triphenylphosphine) palladium (11.5 mg, 9.95 μmol) according to method C1. The product was purified by preparative HPLC; yield: 29% (30.8 mg); mp 164–166 °C; ^{1}H NMR (300 MHz, acetone-d_6, δ): 9.55 (br s, 1H), 7.65 (dd, *J* = 4.1, 1.5 Hz, 1H), 7.60 (dd, *J* = 11.9, 2.2 Hz, 1H), 7.52–7.48 (m, 1H), 7.51 (d, *J* = 4.1 Hz, 1H), 7.14–7.06 (m, 1H), 7.11 (t, *J* = 8.8 Hz, 1H); MS (ESI-): 367.1 $(M - H)^-$; UV λ (nm) = 363; Rf HPLC: 10.97 min (13 min 10–95% MeCN in water with 0.1% formic acid); purity 98%.

*(5-(4-Hydroxy-3,5-dimethylphenyl)thiophen-2-yl)(2,4,5-trifluoro-3-hydroxyphenyl)methanone (**5**).* The title compound was prepared by the reaction of (5-(4-methoxy-3,5-dimethylphenyl)thiophen-2-yl)(2,4,5-trifluoro-3-hydroxyphenyl)methanone (**1**) (51 mg, 0.13 mmol), and boron tribromide (0.39 mmol, 3.0 equiv) according to method B. The product was purified by CC; yield: 98% (51 mg); mp 198–200 °C; ^{1}H NMR (300 MHz, $CDCl_3$, δ): 7.48 (dd, *J* = 4.1, 2.0 Hz, 1H), 7.32 (br s, 2H), 7.22 (d, *J* = 4.1 Hz, 1H), 6.98 (ddd, *J* = 9.6, 8.1, 5.8 Hz, 1H), 4.90 (s, 1H), 2.30 (s, 6H); MS (ESI): 379.10 $(M + H)^+$; UV λ (nm) = 377; Rf HPLC: 11.28 min (13 min 10–95% MeCN in water with 0.1% formic acid); purity >99%.

*(5-(3,5-Dichloro-4-hydroxyphenyl)thiophen-2-yl)(2,4,5-trifluoro-3-hydroxyphenyl)methanone (**6**).* The title compound was prepared by the reaction of (5-(3,5-dichloro-4-methoxyphenyl)thiophen-2-yl)(2,4,5-trifluoro-3-hydroxyphenyl)methanone (**2**) (48 mg, 0.11 mmol), and boron tribromide (0.34 mmol, 3.0 equiv) according to method B. The product was purified by CC; yield: quantitative (84 mg); mp 212–214 °C; ^{1}H NMR (300 MHz, acetone-d_6, δ): 9.92 (s, 1 H); 9.30 (s, 1 H); 7.81 (s, 2 H); 7.68 (dd, *J* = 1.8, 4.1 Hz, 1 H); 7.65–7.61 (m, 1 H); 7.13 (ddd, *J* = 5.6, 8.1, 10.0 Hz, 1 H); MS (ESI): 419.20 $(M + H)^+$; UV λ (nm) = 355; Rf HPLC: 11.54 min (13 min 10–95% MeCN in water with 0.1% formic acid). Purity 98%.

*(3-Hydroxy-2-methylphenyl)(5-(4-methoxy-3,5-dimethylphenyl)-thiophen-2-yl)methanone (**7**).* The title compound was prepared by the reaction of (3-(5-bromothiophene-2-carbonyl)-2-methylphenyl acetate (**7b**) (84.8 mg, 0.250 mmol), 4-methoxy-3,5-dimethylphenyl)-boronic acid (54.0 mg, 0.300 mmol), cesium carbonate (326 mg, 1.00 mmol), and tetrakis(triphenylphosphine)palladium (11.5 mg, 9.95 μmol) according to method C1. The product was purified by preparative HPLC; yield: 26% (23.0 mg); mp 194–196 °C; ^{1}H NMR (300 MHz, acetone-d_6, δ): 8.57 (br s, 1H), 7.47 (s, 2H), 7.44 (d, *J* = 3.9 Hz, 1H), 7.39 (d, *J* = 3.9 Hz, 1H), 7.16 (t, *J* = 7.8 Hz, 1H), 7.02 (dd, *J* = 8.1, 1.2 Hz, 1H), 6.95 (dd, *J* = 7.5, 1.2 Hz, 1H), 3.75 (s, 3H), 2.32 (s, 6H), 2.18 (s, 3H); MS (ESI): 353.21 $(M + H)^+$; UV λ (nm) = 236, 348; Rf HPLC: 13.83 min (13 min 10–95% MeCN in water with 0.1% formic acid); purity >99%.

*(5-(3,5-Dichloro-4-methoxyphenyl)thiophen-2-yl)(3-hydroxy-2-methylphenyl)methanone (**8**).* The title compound was prepared by the reaction of (3-(5-bromothiophene-2-carbonyl)-2-methylphenyl acetate (**7b**) (84.8 mg, 0.250 mmol), (3,5-dichloro-4-methoxyphenyl))boronic acid (66.3 mg, 0.300 mmol), cesium carbonate (326 mg, 1.00 mmol), and tetrakis(triphenylphosphine) palladium (11.5 mg, 9.95 μmol) according to method C1. The product was purified by preparative HPLC; yield: 61% (59.9 mg); mp 209–211 °C; ^{1}H NMR (300 MHz, acetone-d_6, δ): 8.60 (br s, 1H), 7.84 (s, 2H), 7.64 (d, *J* = 3.9 Hz, 1H), 7.45 (d, *J* = 4.2 Hz, 1H), 7.17 (t, *J* = 7.5 Hz, 1H), 7.04 (dd, *J* = 8.1, 1.2 Hz, 1H), 6.98 (dd, *J* = 7.5, 1.2 Hz, 1H), 3.94 (s, 3H), 2.19 (s, 3H); MS (ESI): 393.12 $(M + H)^+$; UV λ (nm) = 334; Rf HPLC: 14.42 min (13 min 10–95% MeCN in water with 0.1% formic acid); purity 98%.

*(5-(3-Chloro-4-hydroxyphenyl)thiophen-2-yl)(3-hydroxy-2-methylphenyl)methanone (**9**).* The title compound was prepared by the reaction of (3-(5-bromothiophene-2-carbonyl)-2-methylphenyl acetate (**7b**) (84.8 mg, 0.250 mmol), (3-chloro-4-hydroxyphenyl))-boronic acid (51.7 mg, 0.300 mmol), cesium carbonate (326 mg, 1.00 mmol), and tetrakis(triphenylphosphine)palladium (11.5 mg, 9.95 μmol) according to method C1. The product was purified by preparative HPLC; yield: 3.5% (3.00 mg); mp 106–108 °C; ^{1}H NMR (300 MHz, acetone-d_6, δ): 7.79 (d, *J* = 2.1 Hz, 1H), 7.60 (dd, *J* = 8.4, 2.1 Hz, 1H), 7.47 (d, *J* = 3.9 Hz, 1H), 7.39 (d, *J* = 4.2 Hz, 1H), 7.18–7.11 (m, 2H), 7.03 (dd, *J* = 7.8, 0.9 Hz, 1H), 6.95 (dd, *J* = 7.5, 0.9 Hz, 1H), 2.18 (s, 3H).; MS (ESI): 345.11 $(M + H)^+$; UV λ (nm) = 233, 355; Rf HPLC: 10.90 min (13 min 10–95% MeCN in water with 0.1% formic acid); purity 99%.

*(3-Hydroxy-2-methylphenyl)(5-(4-hydroxy-3,5-dimethylphenyl)-thiophen-2-yl)methanone (**10**).* The title compound was prepared by the reaction of (3-hydroxy-2-methylphenyl)(5-(4-methoxy-3,5-dimethylphenyl)thiophen-2-yl)methanone (**7**) (16 mg, 0.045 mmol), and boron tribromide (0.14 mmol, 3.0 equiv) according to method B. The product was purified by preparative HPLC; yield 66%: (10.0 mg); mp 180–183 °C; ^{1}H NMR (300 MHz, methanol-d_4, δ): 7.25–7.39 (m, 4 H), 7.08–7.17 (m, 1 H), 6.88 (d, *J* = 7.6 Hz, 1 H), 6.93 (d, *J* = 7.9 Hz, 1 H), 2.26 (s, 6 H), 2.16 (s, 3 H); MS (ESI): 339.3 $(M + H)^+$; UV λ (nm) = 363; Rf HPLC: 10.98 min (13 min 10–95% MeCN in water with 0.1% formic acid); purity 99%.

*(5-(3,5-Dichloro-4-hydroxyphenyl)thiophen-2-yl)(3-hydroxy-2-methylphenyl)methanone (**11**).* The title compound was prepared by the reaction of (5-(3,5-dichloro-4-methoxyphenyl)thiophen-2-yl)(3-hydroxy-2-methylphenyl)methanone (**8**) (34.0 mg, 0.086 mmol) and boron tribromide (0.23 mmol, 3.0 equiv) according to method B. The product was purified by preparative HPLC; yield 92%: (30.0 mg). ^{1}H NMR (300 MHz, methanol-d_4, δ): 7.66 (s, 2 H), 7.32–7.43 (m, 2 H), 7.06–7.19 (m, 1 H), 6.82–6.98 (m, 2 H), 2.15 (s, 3 H); MS (ESI): 365.2 $(M + H)^+$; UV λ (nm) = 347, 246 (sh); Rf HPLC: 11.29 min (13 min 10–95% MeCN in water with 0.1% formic acid); purity >99%.

*(5-(4-Methoxyphenyl)thiophen-2-yl)(2,4,5-trifluoro-3-hydroxyphenyl)methanone (**12**).* The title compound was prepared by the reaction of (5-bromothiophen-2-yl)(2,4,5-trifluoro-3-hydroxyphenyl)methanone (**7b**) (94.8 mg, 0.281 mmol), 4-methoxyphenylboronic acid (45.6 mg, 0.300 mmol), cesium carbonate (326 mg, 1.00 mmol), and tetrakis(triphenylphosphine)-palladium (11.6 mg, 10.0 μmol) according to method C1. The product was purified by preparative HPLC; yield: 40% (40.7 mg); mp 150–152 °C; ^{1}H NMR (300 MHz, acetone-d_6, δ): 7.81–7.70 (m, 2H), 7.64 (dd, *J* = 4.1, 1.8 Hz, 1H), 7.48 (d, *J* = 4.1 Hz, 1H), 7.17–6.99 (m, 3H), 3.87 (s, 3H); MS (ESI): 365.2 $(M + H)^+$. UV λ (nm) = 363; Rf HPLC: 12.14 min (13 min 10–95% MeCN in water with 0.1% formic acid); purity 98%.

*(5-(3-Methoxyphenyl)thiophen-2-yl)(2,4,5-trifluoro-3-hydroxyphenyl)methanone (**13**).* The title compound was prepared by the reaction of (5-bromothiophen-2-yl)(2,4,5-trifluoro-3-hydroxyphenyl)methanone (**1b**) (94.8 mg, 0.281 mmol), 3-methoxyphenylboronic acid (45.6 mg, 0.300 mmol), cesium carbonate (326 mg, 1.00 mmol), and tetrakis(triphenylphosphine) palladium (11.6 mg, 10.0 μmol) according to method C1. The product was purified by preparative HPLC; yield: 43% (44.0 mg); mp 161–163 °C; ^{1}H NMR (300 MHz, MeOH-d^4, δ): 7.81–7.48 (m,

2H), 7.46–7.26 (m, 3H), 7.09–6.95 (m, 2H), 3.89 (s, 3H); MS (ESI): 365.2 (M + H)$^+$; UV λ (nm) = 345; RT HPLC = 12.30 min (13 min 10–95% MeCN in water with 0.1% formic acid); purity >98%.

*(5-(2-Methoxyphenyl)thiophen-2-yl)(2,4,5-trifluoro-3-hydroxyphenyl)methanone (**14**).* The title compound was prepared by the reaction of (5-bromothiophen-2-yl)(2,4,5-trifluoro-3-hydroxyphenyl)methanone (**1b**) (94.8 mg, 0.281 mmol), 2-methoxyphenylboronic acid (45.6 mg, 0.300 mmol), cesium carbonate (326 mg, 1.00 mmol), and tetrakis(triphenylphosphine)-palladium (11.6 mg, 10.0 μmol) according to method C1. The product was purified by preparative HPLC; yield: 68% (70.0 mg); mp 167–169 °C; ^{1}H NMR (300 MHz, acetone-d_6, δ): 7.87 (dd, J = 7.8, 1.7 Hz, 1H), 7.71 (d, J = 4.2 Hz, 1H), 7.63 (dd, J = 4.2, 1.8 Hz, 1H), 7.43 (ddd, J = 8.5, 7.2, 1.6 Hz, 1H), 7.24–7.19 (m, 1H), 7.15–7.05 (m, 2H), 4.03 (s, 3H); MS (ESI): 365.2 (M + H)$^+$; UV λ (nm) = 359; RT HPLC = 12.16 min (13 min 10–95% MeCN in water with 0.1% formic acid); purity 97%.

*(5-(4-Hydroxyphenyl)thiophen-2-yl)(2,4,5-trifluoro-3-hydroxyphenyl)methanone (**15**).* The title compound was prepared by the reaction of (5-(4-methoxyphenyl)thiophen-2-yl)(2,4,5-trifluoro-3-hydroxyphenyl)methanone (**12**) (20.0 mg, 54.9 μmol) and boron tribromide (0.165 mmol, 3.0 equiv) according to method B. The product was purified by preparative HPLC; yield: 18% (3.50 mg); mp 145–148 °C; ^{1}H NMR (300 MHz, acetone-d_6, δ): 7.70–7.63 (m, 2H), 7.61 (dd, J = 4.1, 1.9 Hz, 1H), 7.43 (d, J = 4.1 Hz, 1H), 7.05–6.91 (m, 3H); MS (ESI): 351.2 (M + H)$^+$; UV λ (nm) = 365; RT HPLC = 10.15 min (13 min 10–95% MeCN in water with 0.1% formic acid); purity 96%.

*(5-(3-Hydroxyphenyl)thiophen-2-yl)(2,4,5-trifluoro-3-hydroxyphenyl)methanone (**16**).* The title compound was prepared by the reaction of (5-(3-methoxyphenyl)thiophen-2-yl)(2,4,5-trifluoro-3-hydroxyphenyl)methanone (**13**) (26.2 mg, 71.9 μmol) and boron tribromide (0.216 mmol, 3.0 equiv) according to method B. The product was purified by preparative HPLC; yield: 83% (21.0 mg); mp 215–218 °C; ^{1}H NMR (500 MHz, acetone-d_6, δ): 7.66 (dd, J = 3.9, 1.7 Hz, 1H), 7.54 (d, J = 4.1 Hz, 1H), 7.33–7.26 (m, 2H), 7.25–7.23 (m, 1H), 7.11 (ddd, J = 10.0, 8.1, 5.5 Hz, 1H), 6.95–6.91 (m, 1H); MS (ESI): 351.3 (M + H)$^+$; UV λ (nm) = 264 (sh), 348; RT HPLC = 10.22 min (C18, 13 min 10–95% MeCN in water with 0.1% formic acid); purity 98%.

*(5-(2-Hydroxyphenyl)thiophen-2-yl)(2,4,5-trifluoro-3-hydroxyphenyl)methanone (**17**).* The title compound was prepared by the reaction of (5-(2-methoxyphenyl)thiophen-2-yl)(2,4,5-trifluoro-3-hydroxyphenyl)methanone (**14**) (34.3 mg, 94.1 μmol) and boron tribromide (0.282 mmol, 3.0 equiv) according to method B. The product was purified by preparative HPLC; yield: 45% (14.7 mg). ^{1}H NMR (300 MHz, acetone-d_6, δ): 7.82 (dd, J = 7.9, 1.5 Hz, 1H), 7.75 (d, J = 4.2 Hz, 1H), 7.64 (dd, J = 4.1, 1.6 Hz, 1H), 7.31–7.21 (m, 1H), 7.15–7.03 (m, 2H), 6.98 (t, J = 7.5 Hz, 1H); MS (ESI): 351.2 (M + H)$^+$; UV λ (nm) = 265 (sh), 290 (sh), 363; RT HPLC = 10.56 min (13 min 10–95% MeCN in water with 0.1% formic acid); purity >99%.

*(5-(3-(Hydroxymethyl)phenyl)thiophen-2-yl)(2,4,5-trifluoro-3-hydroxyphenyl)methanone (**18**).* The title compound was prepared by the reaction of (5-bromothiophen-2-yl)(2,4,5-trifluoro-3-hydroxyphenyl)methanone (**1b**) (96.0 mg, 0.285 mmol), (3-(hydroxymethyl)phenyl)boronic acid (45.6 mg, 0.300 mmol), cesium carbonate (326 mg, 1.00 mmol), and tetrakis(triphenylphosphine) palladium (11.5 mg, 9.95 μmol) according to method C1. The product was purified by preparative HPLC; yield: 24% (25.1 mg); mp 170–172 °C; ^{1}H NMR (300 MHz, MeOH-d^4, δ): 7.75 (s, 1H), 7.65 (d, J = 6.7 Hz, 1H), 7.58 (dd, J = 4.0, 1.8 Hz, 1H), 7.51 (d, J = 4.1 Hz, 1H), 7.47–7.37 (m, 2H), 6.97 (ddd, J = 9.7, 8.1, 5.7 Hz, 1H), 4.67 (s, 2H); MS (APCI$^-$): 364.1 (M − H)$^-$; UV λ (nm) = 345; Rf HPLC: 10.61 min (13 min 10–95% MeCN in water with 0.1% formic acid); purity 99%.

*(5-(4-Aminophenyl)thiophen-2-yl)(2,4,5-trifluoro-3-hydroxyphenyl)methanone (**19**).* The title compound was prepared by the reaction of (5-(4-aminophenyl)thiophen-2-yl)(2,4,5-trifluoro-3-methoxyphenyl)methanone (**19a**) (300 mg, 0.82 mmol) and boron tribromide (4.17 mmol) according to method B. The product was purified by CC (dichloromethane/methanol 99:1); yield: 31% (90 mg); ^{1}H NMR (500 MHz, acetone-d_6, δ) 9.79 (s, 1H, OH), 7.63 (ddd, J = 41.7, 4.1, 1.8 Hz, 1H), 7.57–7.52 (m, 2H), 7.36 (d, J = 4.1 Hz, 1H), 7.07 (ddd, J = 10.0, 8.2, 5.6 Hz, 1H), 6.83–6.74 (m, 3H), 4.94 (s, 2H); UV λ (nm) = 399, 260 (sh); RT HPLC = 10.02 (13 min 10–95% MeCN in water with 0.1% formic acid); purity 99%.

*(5-(3-Aminophenyl)thiophen-2-yl)(2,4,5-trifluoro-3-hydroxyphenyl)methanone (**20**).* The title compound was prepared by the reaction of (5-bromothiophen-2-yl)(2,4,5-trifluoro-3-hydroxyphenyl)methanone (**1b**) (96.0 mg, 0.285 mmol), (3-aminophenyl)boronic acid (41.1 mg, 0.300 mmol), cesium carbonate (326 mg, 1.00 mmol), and tetrakis(triphenylphosphine)palladium (11.5 mg, 9.95 μmol) according to method C1. The product was purified by preparative HPLC; yield: 24% (25.1 mg); mp 182–184 °C; ^{1}H NMR (300 MHz, MeOH-d^4, δ): 7.57–7.53 (m, 1H), 7.44–7.41 (m, 1H), 7.20–7.14 (m, 1H), 7.09–6.93 (m, 3H), 6.78–6.74 (m, 1H); MS (ESI): 350.2 (M + H)$^+$; UV λ (nm) = 343; RT HPLC = 10.19 min (13 min 10–95% MeCN in water with 0.1% formic acid); purity 96%.

*(5-(2-Aminophenyl)thiophen-2-yl)(2,4,5-trifluoro-3-hydroxyphenyl)methanone (**21**).* The title compound was prepared by the reaction of (5-bromothiophen-2-yl)(2,4,5-trifluoro-3-hydroxyphenyl)methanone (**1b**) (94.8 mg, 0.281 mmol), (2-aminophenyl)boronic acid (41.1 mg, 0.300 mmol), cesium carbonate (326 mg, 1.00 mmol), and tetrakis(triphenylphosphine)palladium (11.6 mg, 10.0 μmol) according to method C1. The product was purified by preparative HPLC; yield: 53% (52.1 mg); mp 216–218 °C; ^{1}H NMR (300 MHz, MeOH-d^4, δ): 7.64 (dd, J = 3.8, 1.7 Hz, 1H), 7.45–7.38 (m, 1H), 7.33 (dd, J = 7.7, 1.5 Hz, 1H), 7.26–7.14 (m, 1H), 7.11–6.95 (m, 1H), 6.90 (d, J = 8.1 Hz, 1H), 6.84–6.71 (m, 1H); MS (ESI): 350.2 (M + H)$^+$; UV λ (nm) = 281, 316, 377; Rf = 10.98 min (13 min 10–95% MeCN in water with 0.1% formic acid); purity >99%.

*(5-(3-Amino-4-methoxyphenyl)thiophen-2-yl)(2,4,5-trifluoro-3-hydroxyphenyl)methanone (**22**).* The title compound was prepared by the reaction of (5-bromothiophen-2-yl)(2,4,5-trifluoro-3-hydroxyphenyl)methanone (**1b**) (94.8 mg, 0.281 mmol), 2-methoxy-5-(4,4,5,5-tetramethyl-1,3,2-dioxaborolan-2-yl)aniline (**22a**) (74.7 mg, 0.300 mmol), cesium carbonate (326 mg, 1.00 mmol), and tetrakis(triphenylphosphine)palladium (11.6 mg, 10.0 μmol) according to method C1. The product was purified by preparative HPLC; yield: 31% (33.3 mg); mp 181–183 °C; ^{1}H NMR (300 MHz, MeOH-d^4, δ): 7.61–7.52 (m, 1H), 7.29 (d, J = 3.9 Hz, 1H), 7.22–7.10 (m, 1H), 7.05–6.86 (m, 1H), 6.78 (d, J = 8.1 Hz, 1H), 4.61 (br s, 2H), 3.94 (s, 3H); MS (ESI): 380.3 (M + H)$^+$; UV λ (nm) = 285 (sh), 380; RT HPLC = 10.54 min (13 min 10–95% MeCN in water with 0.1% formic acid); purity >99%.

*(5-(3-Amino-4-hydroxyphenyl)thiophen-2-yl)(2,4,5-trifluoro-3-hydroxyphenyl)methanone (**23**).* The title compound was prepared by the reaction of (5-bromothiophen-2-yl)(2,4,5-trifluoro-3-hydroxyphenyl)methanone (**1b**) (94.8 mg, 0.281 mmol), 5-(4,4,5,5-tetramethyl-1,3,2-dioxaborolan-2-yl)benzo[*d*]oxazole (**23a**) (73.5 mg, 0.300 mmol), cesium carbonate (326 mg, 1.00 mmol), and tetrakis(triphenylphosphine)palladium (11.6 mg, 10.0 μmol) according to method C1. The product was purified by preparative HPLC; yield: 35% (35.7 mg). ^{1}H NMR (300 MHz, MeOH-d^4, δ): 7.58–7.51 (m, 1H), 7.33 (d, J = 3.9 Hz, 1H), 7.17 (d, J = 1.5 Hz, 1H), 7.04 (dd, J = 8.0, 2.1 Hz, 1H), 7.01–6.92 (m, 1H), 6.78 (d, J = 8.1 Hz, 1H); MS (ESI): 366.2 (M + H)$^+$; UV λ (nm) = 285 (sh), 365; RT HPLC = 8.32 min (13 min 10–95% MeCN in water with 0.1% formic acid); purity >99%.

*(5-(3-Amino-4-methylphenyl)thiophen-2-yl)(2,4,5-trifluoro-3-hydroxyphenyl)methanone (**24**).* The title compound was prepared by the reaction of (5-bromothiophen-2-yl)(2,4,5-trifluoro-3-hydroxyphenyl)methanone (**1b**) (94.8 mg, 0.281 mmol), 3-amino-4-methylphenylboronic acid (45.3 mg, 0.300 mmol), cesium carbonate (326 mg, 1.00 mmol), and tetrakis(triphenylphosphine) palladium (11.6 mg, 10.0 μmol) according to method C1. The

product was purified by preparative HPLC; yield: 15% (15.7 mg); mp 208−210 °C; ^{1}H NMR (300 MHz, MeOH-d^4, δ): 7.61 (d, J = 2.2 Hz, 1H), 7.14 (d, J = 3.9 Hz, 1H), 7.11−6.97 (m, 2H), 6.86 (d, J = 7.8 Hz, 1H), 6.80 (d, J = 7.5 Hz, 1H), 2.22 (s, 3H); MS (ESI): 364.2 (M + H)$^+$; UV λ (nm) = 323; RT HPLC = 12.23 min (13 min 10−95% MeCN in water with 0.1% formic acid); purity >99%.

*(5-(3-Amino-2-methylphenyl)thiophen-2-yl)(2,4,5-trifluoro-3-hydroxyphenyl)methanone (**25**).* The title compound was prepared by the reaction of (5-bromothiophen-2-yl)(2,4,5-trifluoro-3-hydroxyphenyl)methanone (**1b**) (94.8 mg, 0.281 mmol), 2-methyl-3-(4,4,5,5-tetramethyl-1,3,2-dioxaborolan-2-yl)aniline (**25a**) (69.9 mg, 0.300 mmol), cesium carbonate (326 mg, 1.00 mmol), and tetrakis(triphenylphosphine)palladium (11.6 mg, 10.0 μmol) according to method C1. The product was purified by preparative HPLC; yield: 7% (7.60 mg); mp 201−203 °C; ^{1}H NMR (300 MHz, MeOH-d^4, δ): 7.58 (dd, J = 3.9, 1.8 Hz, 1H), 7.43 (d, J = 4.0 Hz, 1H), 7.19−6.88 (m, 4H), 2.22 (s, 3H); MS (ESI): 364.2 (M + H)$^+$; UV λ (nm) = 280 (sh), 353; RT HPLC = 10.97 min (13 min 10−95% MeCN in water with 0.1% formic acid); purity 97%.

*(5-(3-Amino-4-fluorophenyl)thiophen-2-yl)(2,4,5-trifluoro-3-hydroxyphenyl)methanone (**26**).* The title compound was prepared by the reaction of (5-(3-amino-4-fluorophenyl)thiophen-2-yl)(2,4,5-trifluoro-3-methoxyphenyl)methanone (**26a**) (150 mg, 0.53 mmol) and boron tribromide (1.97 mmol) according to method B. The product was purified by CC (dichloromethane/methanol 99.5:0.5); yield: 31% (45 mg). ^{1}H NMR (500 MHz, acetone-d_6, δ) 9.79 (s, 1H, OH), 7.64 (dd, J = 4.1, 1.8 Hz, 1H), 7.44 (d, J = 4.0 Hz, 1H), 7.31−7.27 (m, 1H), 7.14–7.02 (m, 3H), 5.32 (s, 2H); MS (ESI): 368.3 (M + H)$^+$; UV λ (nm) = 276 (sh), 348; RT HPLC = 10.91 min (13 min 10−95% MeCN in water with 0.1% formic acid); purity 95%.

*(5-(3-Amino-4,5-difluorophenyl)thiophen-2-yl)(2,4,5-trifluoro-3-hydroxyphenyl)methanone (**27**).* The title compound was prepared by the reaction of (5-(3-amino-4,5-difluorophenyl)thiophen-2-yl)-(2,4,5-trifluoro-3-methoxyphenyl)methanone (**27a**) (100 mg, 0.25 mmol) and boron tribromide (1.25 mmol) according to method B. The product was purified by CC (dichloromethane/methanol 99.5:0.5); yield: 46% (45 mg). ^{1}H NMR (500 MHz, acetone-d_6 δ) 9.77 (s, 1H, OH), 7.67 (dd, J = 4.1, 1.8 Hz, 1H), 7.52 (d, J = 4.1 Hz, 1H), 7.16−7.09 (m, 2H), 6.98 (ddd, J = 11.1, 6.6, 2.2 Hz, 1H), 5.39 (s, 2H); MS (ESI): 386.2 (M + H)$^+$; UV λ (nm) = 270 (sh), 343; RT HPLC = 11.29 min (13 min 10−95% MeCN in water with 0.1% formic acid); purity 98%.

*(5-(3-Amino-4,6-difluorophenyl)thiophen-2-yl)(2,4,5-trifluoro-3-hydroxyphenyl)methanone (**28**).* The title compound was prepared by the reaction of (5-(3-amino-4-fluorophenyl)thiophen-2-yl)(2,4,5-trifluoro-3-methoxyphenyl)methanone (**28a**) (150 mg, 0.53 mmol) and boron tribromide (1.97 mmol) according to method B. The product was purified by CC (dichloromethane/methanol 99.5:0.5); yield: 31% (45 mg). ^{1}H NMR (500 MHz, acetone-d_6 δ) 9.76 (s, 1H, OH), 7.69 (ddd, J = 4.1, 1.8, 1.0 Hz, 1H), 7.52 (dd, J = 4.1, 1.0 Hz, 1H), 7.35−7.07 (m, 3H), 5.29 (s, 2H); MS (ESI): 386.3 (M + H)$^+$; UV λ (nm) = 283 (sh), 341; RT HPLC = 11.29 min (13 min 10−95% MeCN in water with 0.1% formic acid); purity 90%.

*N-(3-(5-(2,4,5-Trifluoro-3-hydroxybenzoyl)thiophen-2-yl)-phenyl)acetamide (**29**).* The title compound was prepared by the reaction of (5-bromothiophen-2-yl) (2,4,5-trifluoro-3-hydroxyphenyl)methanone (**1b**) (94.8 mg, 0.281 mmol), 3-acetylamidophenylboronic acid (53.7 mg, 0.300 mmol), cesium carbonate (326 mg, 1.00 mmol), and tetrakis(triphenylphosphine) palladium (11.6 mg, 10.0 μmol) according to method C1. The product was purified by preparative HPLC; yield: 8% (8.72 mg); ^{1}H NMR (300 MHz, acetone-d_6, δ): 9.31 (br s, 1H), 8.21−8.14 (m, 1H), 7.72−7.60 (m, 2H), 7.60−7.34 (m, 3H), 7.12 (ddd, J = 10.0, 8.1, 5.6 Hz, 1H), 3.31 (s, 3H); MS (ESI): 392.3 (M + H)$^+$; UV λ (nm) = 255 (sh), 346; RT HPLC = 12.16 min (13 min 10−95% MeCN in water with 0.1% formic acid); purity >99%.

*N-(4-(5-(2,4,5-Trifluoro-3-hydroxybenzoyl)thiophen-2-yl)-phenyl)acetamide (**30**).* The title compound was prepared by the reaction of (5-bromothiophen-2-yl)(2,4,5-trifluoro-3-hydroxyphenyl)-methanone (**1b**) (94.8 mg, 0.281 mmol), 4-acetylamidophenylboronic acid (53.7 mg, 0.300 mmol), cesium carbonate (319 mg, 0.979 mmol), and tetrakis(triphenylphosphine)palladium (11.3 mg, 9.78 μmol) according to method C1. The product was purified by preparative HPLC; yield: 12% (12.9 mg); mp 264 °C (decomposition); ^{1}H NMR (300 MHz, DMSO-d_6 δ): 10.16 (s, 1H) 7.76 (d, J = 8.9 Hz, 2H), 7.69 (d, J = 8.8 Hz, 2H), 7.64 (dd, J = 4.1, 1.5 Hz, 1H), 7.61−7.56 (m, 1H), 7.19−7.07 (m, 1H), 2.07 (s, 3H); MS (ESI): 392.2 (M + H)$^+$; UV λ (nm) = 257 (sh), 363; RT HPLC: 9.91 min (13 min 10−95% MeCN in water with 0.1% formic acid); purity 86%.

*3-(5-(2,4,5-Trifluoro-3-hydroxybenzoyl)thiophen-2-yl)benzamide (**31**).* The title compound was prepared by the reaction of (5-bromothiophen-2-yl)-(2,4,5-trifluoro-3-hydroxyphenyl)methanone (**1b**) (96.0 mg, 0.285 mmol), (3-carbamoylphenyl)boronic acid (49.5 mg, 0.300 mmol), cesium carbonate (326 mg, 1.00 mmol), and tetrakis(triphenylphosphine)palladium (11.5 mg, 9.95 μmol) according to method C1. The product was purified by preparative HPLC giving the formiate of the title compound; yield: 21% (25.7 mg); mp 260 °C (decomposition); ^{1}H NMR (300 MHz, DMSO-d_6 δ): 11.35 (br s, 1H), 8.28 (t, J = 1.8 Hz, 1H), 8.16 (br s, 1H), 8.00−7.92 (m, 2H), 7.77 (d, J = 4.3 Hz, 1H), 7.73 (dd, J = 4.3, 1.7 Hz, 1H), 7.66−7.50 (m, 3H), 7.28−7.20 (m, 1H); MS (ESI$^-$): 376.1 (M − H)$^-$; UV λ (nm) = 341; Rf HPLC: 9.14 min (13 min 10−95% MeCN in water with 0.1% formic acid); purity >99%.

*(5-Phenylthiophen-2-yl)(2,4,5-trifluoro-3-hydroxyphenyl)-methanone (**32**).* The title compound was prepared by the reaction of (5-bromothiophen-2-yl)(2,4,5-trifluoro-3-hydroxyphenyl)-methanone (**1b**) (94.8 mg, 0.281 mmol), phenylboronic acid (36.6 mg, 0.300 mmol), cesium carbonate (326 mg, 1.00 mmol), and tetrakis(triphenylphosphine)palladium (11.6 mg, 10.0 μmol) according to method C1. The product was purified by preparative HPLC; yield: 51% (47.9 mg); mp 214−216 °C; ^{1}H NMR (300 MHz, acetone-d_6, δ): 9.91 (br s, 1H), 7.87−7.77 (m, 2H), 7.69 (dd, J = 4.1, 1.8 Hz, 1H), 7.61 (d, J = 4.1 Hz, 1H), 7.55−7.39 (m, 3H), 7.12 (ddd, J = 10.0, 8.1, 5.7 Hz, 1H); MS (ESI): 335.2 (M + H)$^+$; UV λ (nm) = 336; RT HPLC = 12.23 min (13 min 10−95% MeCN in water with 0.1% formic acid); purity >99%.

*(5-(1H-Indol-4-yl)thiophen-2-yl)(2,4,5-trifluoro-3-hydroxyphenyl)methanone (**33**).* The title compound was prepared by the reaction of (5-bromothiophen-2-yl)(2,4,5-trifluoro-3-hydroxyphenyl)methanone (**1b**) (94.8 mg, 0.281 mmol), 4-(4,4,5,5-tetramethyl-1,3,2-dioxaborolan-2-yl)-1*H*-indole (**33a**) (72.9 mg, 0.300 mmol), cesium carbonate (319 mg, 0.979 mmol), and tetrakis(triphenylphosphine)palladium (11.3 mg, 9.78 μmol) according to method C1. The product was purified by preparative; yield: 95% (99.6 mg); mp 204−208 °C; ^{1}H NMR (300 MHz, acetone-d_6, δ): 10.67 (br s, 1H), 7.73 (dd, J = 4.0, 1.8 Hz, 1H), 7.67 (d, J = 4.1 Hz, 2H), 7.60−7.52 (m, 2H), 7.48 (dd, J = 7.4, 0.9 Hz, 1H), 7.28−7.20 (m, 1H), 7.15 (ddd, J = 10.0, 8.1, 5.6 Hz, 1H), 6.96 (ddd, J = 3.2, 2.0, 1.0 Hz, 1H); MS (ESI): 374.3 (M + H)$^+$; UV λ (nm) = 276. 374; RT HPLC = 10.22 min (13 min 10−95% MeCN in water with 0.1% formic acid); purity >99%.

*(5-(1H-Indol-5-yl)thiophen-2-yl)(2,4,5-trifluoro-3-hydroxyphenyl)methanone (**34**).* The title compound was prepared by the reaction of (5-bromothiophen-2-yl)(2,4,5-trifluoro-3-hydroxyphenyl)methanone (**1g**) (94.8 mg, 0.281 mmol), (1*H*-indol-5-yl)boronic acid (48.3 mg, 0.300 mmol), cesium carbonate (326 mg, 1.00 mmol), and tetrakis(triphenylphosphine)palladium (11.6 mg, 10.0 μmol) according to method C1. The product was purified by preparative HPLC; yield: 49% (51.6 mg). ^{1}H NMR (500 MHz, acetone-d_6, δ): 8.09 (dd, J = 1.9, 0.6 Hz, 1H), 7.65 (dd, J = 4.1, 1.9 Hz, 1H), 7.60−7.51 (m, 3H), 7.47−7.41 (m, 1H), 7.11 (ddd, J = 10.1, 8.2, 5.7 Hz, 1H), 6.63−6.57 (m, 1H); MS (ESI): 374.3 (M + H)$^+$; UV λ (nm) = 265 (sh), 380; Rf = 11.27 min (13 min 10−95% MeCN in water with 0.1% formic acid); purity >99%.

*(5-(1H-Indol-6-yl)thiophen-2-yl)(2,4,5-trifluoro-3-hydroxyphenyl)methanone (**35**).* The title compound was prepared by the reaction of (5-bromothiophen-2-yl)(2,4,5-trifluoro-3-hydroxyphenyl)methanone (**1b**) (96.0 mg, 0.285 mmol), (1*H*-indol-6-yl)boronic acid (48.3 mg, 0.300 mmol), cesium carbonate (326 mg,

DOI: 10.1021/acs.jmedchem.8b01373
J. Med. Chem. 2018, 61, 10724−10738

1.00 mmol), and tetrakis(triphenylphosphine)palladium (11.5 mg, 9.95 μmol) according to method C1. The product was purified by preparative HPLC; yield: 81% (85.7 mg); ^{1}H NMR (300 MHz, acetone-d_6, δ): 10.50 (br s, 1H), 7.91 (m, 1H), 7.67 (d, J = 8.4 Hz, 1H), 7.64 (dd, J = 4.1, 1.9 Hz, 1H), 7.53 (d, J = 4.1 Hz, 1H), 7.51–7.46 (m, 2H), 7.13–7.05 (m, 1H), 6.56–6.52 (m, 1H); MS (ESI-): 372.1 (M − H)$^-$; UV λ (nm) = 271, 389; Rf HPLC: 11.81 min (13 min 10–95% MeCN in water with 0.1% formic acid); purity 96%.

(5-(1H-Benzo[d]imidazole-5-yl)thiophen-2-yl)(2,4,5-trifluoro-3-hydroxyphenyl)methanone (36). The title compound was prepared by the reaction of (5-bromothiophen-2-yl)(2,4,5-trifluoro-3-hydroxyphenyl)methanone (**1b**) (94.8 mg, 0.281 mmol), 1*H*-benzimidazole-5-boronic acid pinacol ester (73.2 mg, 0.300 mmol), cesium carbonate (320 mg, 0.984 mmol), and tetrakis(triphenylphosphine)palladium (40.4 mg, 35.0 μmol) according to method C1. The product was purified by preparative HPLC; yield: 7% (7.60 mg). ^{1}H NMR (300 MHz, DMSO-d_6 δ): 12.58 (br s, 1H), 8.32 (s, 1H), 8.04 (br s, 1H), 7.70–7.64 (m, 4H), 7.19–7.11 (m, 1H); MS (ESI): 375.2 (M + H)$^+$; UV λ (nm) = 347; RT HPLC = 7.02 min (C18, 13 min 10–95% MeCN in water with 0.1% formic acid); purity >99%.

(5-(Pyridin-3-yl)thiophen-2-yl)(2,4,5-trifluoro-3-hydroxyphenyl)methanone (37). The title compound was prepared by the reaction of (5-bromothiophen-2-yl)(2,4,5-trifluoro-3-hydroxyphenyl)methanone (**1b**) (94.8 mg, 0.281 mmol), pyridine-3-boronic acid (36.9 mg, 0.300 mmol), cesium carbonate (326 mg, 1.00 mmol), and tetrakis(triphenylphosphine)palladium (11.3 mg, 9.78 μmol) according to method C1. The product was purified by preparative HPLC; yield: 15% (14.2 mg); mp 133–135 °C; ^{1}H NMR (500 MHz, DMSO-d_6 δ): 9.05 (d, J = 2.0 Hz, 1H), 8.63 (dd, J = 4.8, 1.4 Hz, 1H), 8.22 (dt, J = 8.0, 1.9 Hz, 1H), 7.81 (d, J = 4.1 Hz, 1H), 7.74 (dd, J = 4.1, 1.4 Hz, 1H), 7.67–7.48 (m, 1H), 7.24 (ddd, J = 10.0, 8.2, 5.7 Hz, 1H); MS (ESI): 336.3 (M + H)$^+$; UV λ (nm) = 331; RT HPLC = 9.23 min (13 min 10–95% MeCN in water with 0.1% formic acid); purity 92%.

(5-(Quinolin-7-yl)thiophen-2-yl)(2,4,5-trifluoro-3-hydroxyphenyl)methanone (38). The title compound was prepared by the reaction of (5-bromothiophen-2-yl)(2,4,5-trifluoro-3-hydroxyphenyl)methanone (**1b**) (94.8 mg, 0.281 mmol), 7-(4,4,5,5-tetramethyl-1,3,2-dioxaborolan-2-yl)quinoline (**38a**) (76.5 mg, 0.300 mmol), sodium carbonate (74.2 mg, 0.700 mmol), and tetrakis(triphenylphosphine)palladium (3.24 mg, 2.80 μmol) according to method C2. The product was purified by preparative HPLC; yield: 5% (5.9 mg). ^{1}H NMR (300 MHz, DMSO-d_6 δ): 8.97 (dd, J = 4.2, 1.7 Hz, 1H), 8.46–8.38 (m, 2H), 8.20–8.02 (m, 2H), 7.94 (d, J = 4.0 Hz, 1H), 7.74 (dd, J = 4.1, 1.5 Hz, 1H), 7.58 (dd, J = 8.1, 4.2 Hz, 1H), 7.13 (d, J = 6.2 Hz, 1H); MS (ESI): 386.2 (M + H)$^+$; UV λ (nm) = 355; RT HPLC = 10.45 min (13 min 10–95% MeCN in water with 0.1% formic acid); purity 84%.

(5-Methylthiophen-2-yl)(2,4,5-trifluoro-3-hydroxyphenyl)methanone (39). The title compound was prepared by the reaction of (5-methylthiophen-2-yl)(2,4,5-trifluoro-3-methoxyphenyl)methanone (**39a**) (121 mg, 0.423 mmol) and boron tribromide (1.38 mmol, 3.3 equiv) according to method B. The product was purified by preparative HPLC; yield: 55% (63.1 mg). ^{1}H NMR (300 MHz, MeOH-d^4, δ) 7.47–7.43 (m, 1H), 7.02–6.90 (m, 2H), 2.62 (s, 3H); MS (ESI): 273.2 (M + H)$^+$; UV λ (nm) = 260 (sh), 309; RT HPLC = 10.33 min (13 min 10–95% MeCN in water with 0.1% formic acid); purity 95%.

■ ASSOCIATED CONTENT

Ⓢ Supporting Information

The Supporting Information is available free of charge on the ACS Publications website at DOI: 10.1021/acs.jmedchem.8b01373.

Molecular formula strings of all final compounds (CSV)

Synthetic procedure for intermediates **1b**, **1c**, **19a**, **22a**, **23a**, **25a**, **26a**, **27a**, **28a**, **33a**, **38a**, and **39b** (PDF)

■ AUTHOR INFORMATION

Corresponding Author

*E-mail: rolf.hartmann@helmholtz-hzi.de. Phone: +(49) 681 98806 2000.

ORCID

Martin Frotscher: 0000-0003-1777-8890
Chris J. van Koppen: 0000-0003-2799-6728
Sandrine Marchais-Oberwinkler: 0000-0001-9941-7233
Rolf W. Hartmann: 0000-0002-5871-5231

Notes

The authors declare the following competing financial interest(s): L.S., V.H.-O., A.S.A., M.F., C.J.v.K., S.M.-O., C.B., and R.W.H. are inventors of a patent application, which covers the respective compound class. ElexoPharm GmbH is the owner of this patent application. R.W.H. is CEO of ElexoPharm GmbH.

■ ACKNOWLEDGMENTS

The authors thank Nadja Weber, Christopher Hörnes, Birgit Wiegand, Isabella Mang, and Jannine Ludwig for their help with the in vitro tests, Julia Parakenings for her help with the animal experiments, and Jennifer Pham and Anke Kaiser for their help with synthesizing the compounds. Furthermore, the authors thank Dr. Emmanuel Bey for his help within the project. The research project has been financially supported by the federal ministry for education and research under the sign 031A467. The authors are responsible for the content of the publication.

■ ABBREVIATIONS

OBs, osteoblasts; OCs, osteoclasts; E2, estradiol; T, testosterone; 17β-HSD2, 17β-hydroxysteroid dehydrogenase type 2; E1, estrone; A-dione, androstenedione; 17β-HSD1, 17β-hydroxysteroid dehydrogenase type 1; PK, pharmacokinetic; SAR, structure–activity relationship; MTT, 3-(4,5-dimethylthiazol-2-yl)-2,5-diphenyltetrazolium bromide; DCM, dichloromethane

■ REFERENCES

(1) Compston, J. E. Sex Steroids and Bone. *Physiol. Rev.* **2001**, *81*, 419–447.

(2) Riggs, B. L.; Khosla, S.; Melton, L. J. A Unitary Model for Involutional Osteoporosis: Estrogen Deficiency Causes Both Type I and Type II Osteoporosis in Postmenopausal Women and Contributes to Bone Loss in Aging Men. *J. Bone Miner. Res.* **1998**, *13*, 763–773.

(3) Chin, K.-Y.; Ima-Nirwana, S. Sex Steroids and Bone Health Status in Men. *Int. J. Endocrinol.* **2012**, *2012*, 208719.

(4) Dong, Y.; Qiu, Q. Q.; Debear, J.; Lathrop, W. F.; Bertolini, D. R.; Tamburini, P. P. 17Beta-Hydroxysteroid Dehydrogenases in Human Bone Cells. *J. Bone Miner. Res.* **2009**, *13*, 1539–1546.

(5) Bagi, C. M.; Wood, J.; Wilkie, D.; Dixon, B. Effect of 17β-Hydroxysteroid Dehydrogenase Type 2 Inhibitor on Bone Strength in Ovariectomized Cynomolgus Monkeys. *J. Musculoskeletal Neuronal Interact.* **2008**, *8*, 267–280.

(6) Bydal, P.; Auger, S.; Poirier, D. Inhibition of Type 2 17beta-Hydroxysteroid Dehydrogenase by Estradiol Derivatives Bearing a Lactone on the D-Ring: Structure-Activity Relationships. *Steroids* **2004**, *69*, 325–342.

(7) Tremblay, M. R.; Luu-The, V.; Leblanc, G.; Noël, P.; Breton, E.; Labrie, F.; Poirier, D. Spironolactone-Related Inhibitors of Type II 17β-Hydroxysteroid Dehydrogenase: Chemical Synthesis, Receptor Binding Affinities, and Proliferative/Antiproliferative Activities. *Bioorg. Med. Chem.* **1999**, *7*, 1013–1023.

(8) Poirier, D.; Bydal, P.; Tremblay, M. R.; Sam, K.-M.; Luu-The, V. Inhibitors of Type II 17β-Hydroxysteroid Dehydrogenase. *Mol. Cell. Endocrinol.* **2001**, *171*, 119–128.

(9) Vuorinen, A.; Engeli, R.; Meyer, A.; Bachmann, F.; Griesser, U. J.; Schuster, D.; Odermatt, A. Ligand-Based Pharmacophore Modeling and Virtual Screening for the Discovery of Novel 17β-Hydroxysteroid Dehydrogenase 2 Inhibitors. *J. Med. Chem.* **2014**, *57*, 5995–6007.

(10) Wood, J.; Bagi, C. M.; Akuche, C.; Bacchiocchi, A.; Baryza, J.; Blue, M.-L.; Brennan, C.; Campbell, A.-M.; Choi, S.; Cook, J. H.; et al. 4,5-Disubstituted Cis-Pyrrolidinones as Inhibitors of Type II 17β-Hydroxysteroid Dehydrogenase. Part 3. Identification of Lead Candidate. *Bioorg. Med. Chem. Lett.* **2006**, *16*, 4965–4968.

(11) Perspicace, E.; Cozzoli, L.; Gargano, E. M.; Hanke, N.; Carotti, A.; Hartmann, R. W.; Marchais-Oberwinkler, S. Novel, Potent and Selective 17β-Hydroxysteroid Dehydrogenase Type 2 Inhibitors as Potential Therapeutics for Osteoporosis with Dual Human and Mouse Activities. *Eur. J. Med. Chem.* **2014**, *83*, 317–337.

(12) Perspicace, E.; Giorgio, A.; Carotti, A.; Marchais-Oberwinkler, S.; Hartmann, R. W. Novel N-Methylsulfonamide and Retro-N-Methylsulfonamide Derivatives as 17β-Hydroxysteroid Dehydrogenase Type 2 (17β-HSD2) Inhibitors with Good ADME-Related Physicochemical Parameters. *Eur. J. Med. Chem.* **2013**, *69*, 201–215.

(13) Marchais-Oberwinkler, S.; Xu, K.; Wetzel, M.; Perspicace, E.; Negri, M.; Meyer, A.; Odermatt, A.; Möller, G.; Adamski, J.; Hartmann, R. W. Structural Optimization of 2,5-Thiophene Amides as Highly Potent and Selective 17β-Hydroxysteroid Dehydrogenase Type 2 Inhibitors for the Treatment of Osteoporosis. *J. Med. Chem.* **2013**, *56*, 167–181.

(14) Al-Soud, Y. A.; Marchais-Oberwinkler, S.; Frotscher, M.; Hartmann, R. W. Synthesis and Biological Evaluation of Phenyl Substituted 1H-1,2,4-Triazoles as Non-Steroidal Inhibitors of 17β-Hydroxysteroid Dehydrogenase Type 2. *Arch. Pharm.* **2012**, *345*, 610–621.

(15) Wetzel, M.; Gargano, E. M.; Hinsberger, S.; Marchais-Oberwinkler, S.; Hartmann, R. W. Discovery of a New Class of Bicyclic Substituted Hydroxyphenylmethanones as 17β-Hydroxysteroid Dehydrogenase Type 2 (17β-HSD2) Inhibitors for the Treatment of Osteoporosis. *Eur. J. Med. Chem.* **2012**, *47*, 1–17.

(16) Wetzel, M.; Marchais-Oberwinkler, S.; Perspicace, E.; Möller, G.; Adamski, J.; Hartmann, R. W. Introduction of an Electron Withdrawing Group on the Hydroxyphenylnaphthol Scaffold Improves the Potency of 17β-Hydroxysteroid Dehydrogenase Type 2 (17β-HSD2) Inhibitors. *J. Med. Chem.* **2011**, *54*, 7547–7557.

(17) Wetzel, M.; Marchais-Oberwinkler, S.; Hartmann, R. W. 17β-HSD2 Inhibitors for the Treatment of Osteoporosis: Identification of a Promising Scaffold. *Bioorg. Med. Chem.* **2011**, *19*, 807–815.

(18) Xu, K.; Wetzel, M.; Hartmann, R. W.; Marchais-Oberwinkler, S. Synthesis and Biological Evaluation of Spiro-δ-Lactones as Inhibitors of 17β-Hydroxysteroid Dehydrogenase Type 2 (17β-HSD2). *Lett. Drug Des. Discovery* **2011**, *8*, 406–421.

(19) Miralinaghi, P.; Schmitt, C.; Hartmann, R. W.; Frotscher, M.; Engel, M. 6-Hydroxybenzothiophene Ketones: Potent Inhibitors of 17β-Hydroxysteroid Dehydrogenase Type 1 (17β-HSD1) Owing to Favorable Molecule Geometry and Conformational Preorganization. *ChemMedChem* **2014**, *9*, 2294–2308.

(20) Spadaro, A.; Negri, M.; Marchais-Oberwinkler, S.; Bey, E.; Frotscher, M. Hydroxybenzothiazoles as New Nonsteroidal Inhibitors of 17b-Hydroxysteroid Dehydrogenase Type 1 (17b- HSD1). *PLoS One* **2012**, *7*, No. e29252.

(21) Henn, C.; Einspanier, A.; Marchais-Oberwinkler, S.; Frotscher, M.; Hartmann, R. W. Lead Optimization of 17β-HSD1 Inhibitors of the (Hydroxyphenyl)Naphthol Sulfonamide Type for the Treatment of Endometriosis. *J. Med. Chem.* **2012**, *55*, 3307–3318.

(22) Spadaro, A.; Frotscher, M.; Hartmann, R. W. Optimization of Hydroxybenzothiazoles as Novel Potent and Selective Inhibitors of 17β-HSD1. *J. Med. Chem.* **2012**, *55*, 2469–2473.

(23) Marchais-Oberwinkler, S.; Wetzel, M.; Ziegler, E.; Kruchten, P.; Werth, R.; Henn, C.; Hartmann, R. W.; Frotscher, M. New Drug-like Hydroxyphenylnaphthol Steroidomimetics as Potent and Selective 17β-Hydroxysteroid Dehydrogenase Type 1 Inhibitors for the Treatment of Estrogen-Dependent Diseases. *J. Med. Chem.* **2011**, *54*, 534–547.

(24) Oster, A.; Klein, T.; Werth, R.; Kruchten, P.; Bey, E.; Negri, M.; Marchais-Oberwinkler, S.; Frotscher, M.; Hartmann, R. W. Novel Estrone Mimetics with High 17β-HSD1 Inhibitory Activity. *Bioorg. Med. Chem.* **2010**, *18*, 3494–3505.

(25) van Koppen, C.; Abdelsamie, A.; Herath, S.; Biskupek, Y.; Boerger, C.; Siebenbürger, L.; Salah, M.; Scheuer, C.; Marchais-Oberwinkler, S.; Frotscher, M.; Pohlemann, T.; Menger, M. D.; Hartmann, R. W.; Laschke, M. W.; van Koppen, C. J. Targeted Endocrine Therapy: Design, Synthesis and Proof-of-Principle of 17ß-Hydroxysteroid Dehydrogenase Type 2 Inhibitors in Bone Fracture Healing. *J. Med. Chem.* **2018**, submitted.

(26) Watanabe, K.; Hishiya, A. Mouse Models of Senile Osteoporosis. *Mol. Aspects Med.* **2005**, *26*, 221–231.

(27) Martel, C.; Rhéaume, E.; Takahashi, M.; Trudel, C.; Couët, J.; Luu-The, V.; Simard, J.; Labrie, F. Distribution of 17ß-Hydroxysteroid Dehydrogenase Gene Expression and Activity in Rat and Human Tissues. *J. Steroid Biochem. Mol. Biol.* **1992**, *41*, 597–603.

(28) Abdelsamie, A. S.; van Koppen, C. J.; Bey, E.; Salah, M.; Börger, C.; Siebenbürger, L.; Laschke, M. W.; Menger, M. D.; Frotscher, M. Treatment of Estrogen-Dependent Diseases: Design, Synthesis and Profiling of a Selective 17β-HSD1 Inhibitor with Sub-Nanomolar IC50 for a Proof-of-Principle Study. *Eur. J. Med. Chem.* **2017**, *127*, 944–957.

(29) Ishiyama, T.; Murata, M.; Miyaura, N. Palladium(0)-Catalyzed Cross-Coupling Reaction of Alkoxydiboron with Haloarenes: A Direct Procedure for Arylboronic Esters. *J. Org. Chem.* **1995**, *60*, 7508–7510.

(30) Lipinski, C. A.; Lombardo, F.; Dominy, B. W.; Feeney, P. J. Experimental and Computational Approaches to Estimate Solubility and Permeability in Drug Discovery and Development Settings1PII of Original Article: S0169-409X(96)00423-1. The Article Was Originally Published in Advanced Drug Delivery Reviews 23 (1997) 3. *Adv. Drug Delivery Rev.* **2001**, *46*, 3–26.

(31) Navia, M. A.; Chaturvedi, P. R. Design Principles for Orally Bioavailable Drugs. *Drug Discovery Today*; Elsevier Current Trends, May 1, 1996; pp 179–189.

(32) Zhu, D.-W.; Lee, X.; Breton, R.; Ghosh, D.; Pangborn, W.; Duax, W. L.; Lin, S.-X. Crystallization and Preliminary X-Ray Diffraction Analysis of the Complex of Human Placental 17β-Hydroxysteroid Dehydrogenase with NADP+. *J. Mol. Biol.* **1993**, *234*, 242–244.

(33) Sam, K. M.; Boivin, R. P.; Tremblay, M. R.; Auger, S.; Poirier, D. C16 and C17 Derivatives of Estradiol as Inhibitors of 17 Beta-Hydroxysteroid Dehydrogenase Type 1: Chemical Synthesis and Structure-Activity Relationships. *Drug Des. Discovery* **1998**, *15*, 157–180.

(34) Kruchten, P.; Werth, R.; Marchais-Oberwinkler, S.; Frotscher, M.; Hartmann, R. W. Development of a Biological Screening System for the Evaluation of Highly Active and Selective 17β-HSD1-Inhibitors as Potential Therapeutic Agents. *Mol. Cell. Endocrinol.* **2009**, *301*, 154–157.

(35) Emmerich, J.; van Koppen, C. J.; Burkhart, J. L.; Hu, Q.; Siebenbürger, L.; Boerger, C.; Scheuer, C.; Laschke, M. W.; Menger, M. D.; Hartmann, R. W. Lead Optimization Generates CYP11B1 Inhibitors of Pyridylmethyl Isoxazole Type with Improved Pharmacological Profile for the Treatment of Cushing's Disease. *J. Med. Chem.* **2017**, *60*, 5086–5098.

(36) Lu, C.; Kirsch, B.; Maurer, C. K.; de Jong, J. C.; Braunshausen, A.; Steinbach, A.; Hartmann, R. W. Optimization of Anti-Virulence PqsR Antagonists Regarding Aqueous Solubility and Biological Properties Resulting in New Insights in Structure–activity Relationships. *Eur. J. Med. Chem.* **2014**, *79*, 173–183.

(37) Gargano, E. M.; Perspicace, E.; Hanke, N.; Carotti, A.; Marchais-Oberwinkler, S.; Hartmann, R. W. Metabolic Stability Optimization and Metabolite Identification of 2,5-Thiophene Amide

17β-Hydroxysteroid Dehydrogenase Type 2 Inhibitors. *Eur. J. Med. Chem.* **2014**, *87*, 203−219.

4. Final discussion

Aim of this study was the development of novel drug-like molecules for targeted therapy. This form of therapy directly addresses biochemical pathways which are altered in the target disease through a specific action of the drug, in contrast to unspecific medications. The first part of the study dealt with the development of MT-MMP1 inhibitors as novel angiogenesis inhibitors for cancer treatment. The novel idea consisted here in developing compounds able to bind to structurally less conserved sites of the enzyme with the aim to increase the selectivity and therefore, decrease severe side effects which commonly accompany *state-of-the-art* broad-spectrum MMP inhibitors. The second part of this study dealt with the development of novel 17β-HSD2 inhibitors for the treatment of estrogen-dependent diseases such as impaired bone fracture healing and osteoporosis. In this case, we applied a new pharmacological strategy aimed at selectively increasing estradiol inside the bone to enhance bone formation and reduce side effects which are normally associated to systemic administration of estradiol. In a follow-up study, the described compound class was optimized for the treatment of osteoporosis, a disease that requires drugs to be orally bioavailable due to the long duration of the therapy. For both parts of the study, a ligand-based approach was utilized to generate compounds with improved properties.

4.2. PEX binders as a promising approach for the development of next-generation MMP inhibitors

Antiangiogenic cancer therapy is a widely used form of targeted therapy to treat nearly all forms of cancer today. In order to grow, tumors rely on the supply of oxygen and nutrients coming from the surrounding tissue and thus induce the growth of blood vessels via the release of cytokines such as VEGF. Current forms of antiangiogenic therapy aim at the blockage of the cytokine-receptor interactions or the signal transduction inside the cell.[135] This angiogenic signaling represents a signaling network rather than one isolated pathway, and hence resistance is a widespread result of this form of therapy as the tumor has the possibility reactivate a suppressed pathway from a number of side streets.[136] The MT-MMP1 family constitutes an attractive target for the development of novel antiangiogenic drugs, as it is considered a key regulator of angiogenic sprouting of endothelial cells and metastasis formation.[43] Inhibition of this class of enzymes via “exosite binders”, using compounds that target less conserved domains rather than the catalytic, is a promising approach for the design of novel MMP inhibitors.[124,137] In this context, PEX binder **I.A** was identified through an *in silico* approach and was already tested in an *in vivo* PoP model, as described in literature.[125] We performed the first SAR study on this compound class which exploited modifications of **I.A** in a two-step approach, resulting first in compound **I.6** and finally, after a second optimization round, to a 10-fold increase in activity over **I.A** with compound **I.21** (figure 9). The SAR obtained so far for this compound class can be summarized as follows, rigidization of the *iso*-pentyl moiety to 4-pyridyl is favored in terms of activity on the target, as do lipophilic isosteric substituents of the chlorine in *meta* position on the aromatic core structure, significantly increasing the activity. The most active compounds are depicted in figure 10.

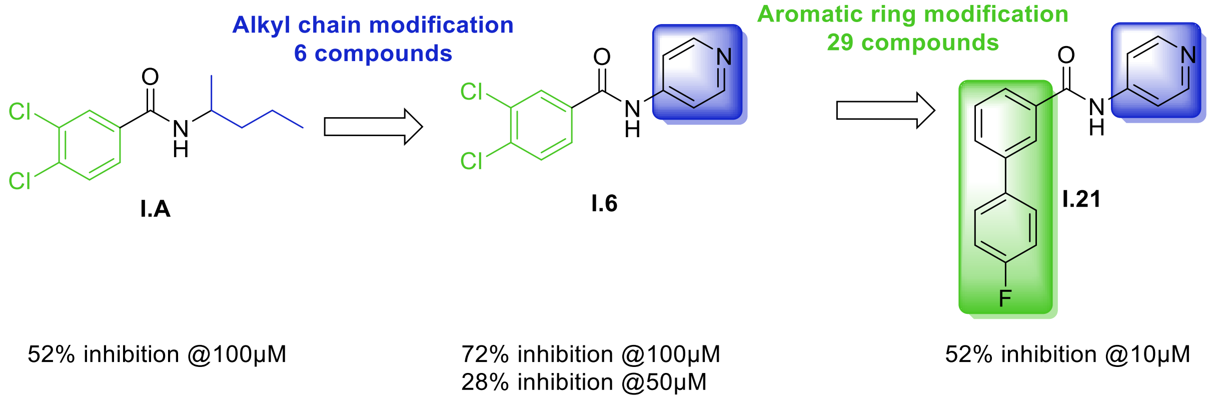

Figure 10: Design strategy of newly developed MT-MMP1 PEX binders

The newly synthesized compounds showed ten times increased activity compared to reference **I.A** in a novel cellular collagen I invasion assay, which utilizes HT1080 fibrosarcoma cell spheroids invading a collagen I matrix. We used this advanced assay technique because it has several benefits over classical proteolytic enzyme activity assays, as it is more reflective of the *in vivo* situation than enzymatic cleavage of a small peptide substrate surrogate.[138] Furthermore, the ability of this cell line to invade a collagen matrix has been directly linked to the PEX domain of MT-MMP1, which is highly expressed on the cell surface.[139] The applicability of the described MT-MMP1 inhibitors to inhibit cellular movement was validated over two additional cancer cell lines, U87 glioblastoma *multiforme* and MDA-MD-231 breast cancer. These cancer types are considered highly aggressive and associated with poor survival rates in patients.[23,140] This finding clearly highlights the possibility to apply the approach to different kinds of cancer that are difficult to treat with *state-of-the-art* therapy options.

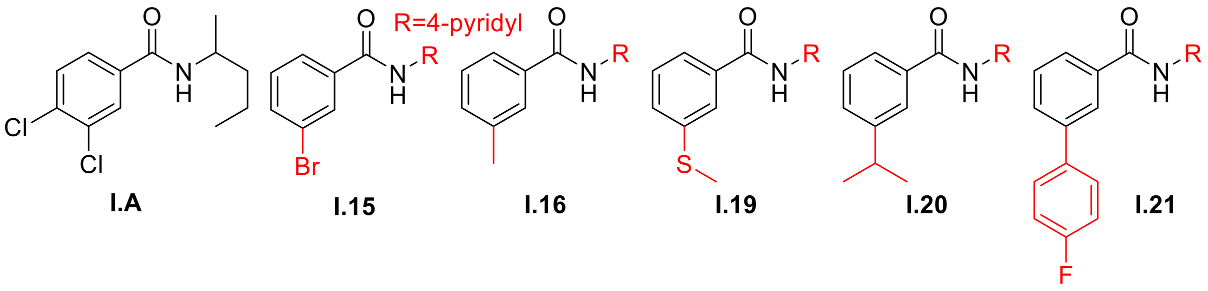

I.A 52% (100μM)

I.15 57% (50μM)

I.16 62% (50μM)

I.19 46% (50μM)

I.20 53% (50μM)

I.21 52% (10 μM)

Figure 11: Structures of the most active newly synthesized compounds and reference **I.A**, their inhibition values in the invasion assay, tested inhibitor concentration in brackets

As aforementioned, one of the aims of this thesis is to prove the interaction of the novel MT-MMP1 inhibitors using biophysical analysis methods such as surface plasmon resonance spectroscopy. Upon screening of the synthesized compounds **I.1-35**, at 100 µM concentration against the immobilized PEX domain of MT-MMP1, signal intensities could be correlated to the SAR obtained from the invasion assay using the HT1080 cell line (data not shown). However, the determination of K_d values of these compounds failed due to the fact that upon binding, the compounds decrease the obtained signal compared to the reference channel. On the other hand, with increased inhibitor concentration, non-specific interaction of the inhibitors with the matrix increases signal in the reference channel, making it impossible to obtain proper binding curves with this measurement technique. To overcome this issue and obtain a parameter of direct binding, other biophysical techniques such as isothermal titration calorimetry or thermal-shift assay could be employed, but were not performed so far due to the limited availability of the recombinant PEX domain of MT-MMP1.

194 Metalloproteases are described in humans, of which 64 belong to the metzincin enzyme family, including MMPs, ADAMs and ADAMTs.[141] Given the high structural similarity of the active site of this enzyme class, the development of selective classical active site MMP inhibitors is a difficult task;[123] in fact, discontinued clinical trials have shown that the probability of off-target effects with these inhibitors is tremendously high.[142] Targeting the PEX domain, a domain for protein–protein interactions has superior advantages, as only MMPs bear this domain amongst the methzincin protease superfamily.[123] Furthermore, not all MMPs share this domain, increasing the *per se* selectivity of the approach and limiting the space for possible off-target effects (figure 11). Taking into account the decreased structural conservation of the domain

among MMPs, the development of binders to this domain is a highly promising approach for development of next-generation MMP inhibitors.[39]

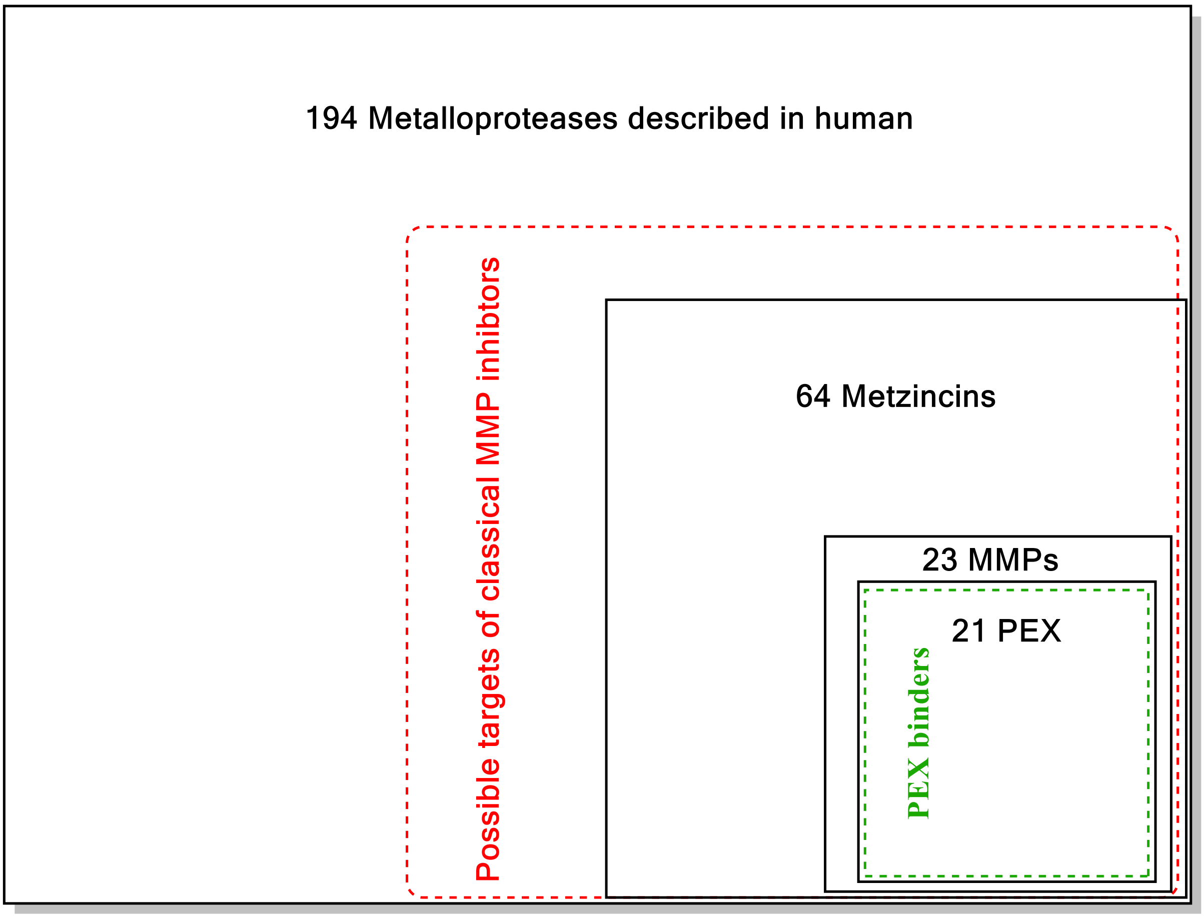
194 Metalloproteases described in human
Possible targets of classical MMP inhibitors
64 Metzincins
23 MMPs
21 PEX
PEX binders

Figure 12: Structural space of Metalloproteases and possible overlapping targets of MMP inhibitors

Selectivity over other MMPs is the key element for a promising pharmacological profile of novel MMP inhibitors. For this reason, we tested a large set of the newly synthesized compounds towards degradation of a small peptidic substrate by the gelatinases MMP2 and 9, as well as the collagenases MMP1, 8 and 13. None of the synthesized inhibitors was able to block the degradation of the substrate by these enzymes, which emphasizes the advantages of exosite binders as highly selective MMP inhibitors. Subsequently, the compounds ability to inhibit the degradation of a fluorescently labeled collagen I substrate was additionally evaluated. Under physiological conditions, the PEX domain of these enzymes has triple helicase activity towards fibrillar collagen, making the substrate prone to cleavage via the active site of the enzyme.[39] Compound **I.21** at 10 µM concentration did not significantly inhibit any of the enzymes (table 1), making it a highly selective and, hence, promising compound for further evaluation. Besides this highly interesting finding regarding the selectivity of the most active compound described in this study, a screening of the compounds against the panel of MMPs revealed that other compounds of this class were selectively active against other MMPs, such as MMP13 or MMP2. The small *p*-OCF_3 substituted compound **I.22** shows high inhibition of MMP13 (47% at 10 µM, table 1), as does the *p*-4-F-phenyl compound **I.28** (86% at 10 µM, table 1). This proves the possibility of this class to selectively inhibit other types of MMPs, depending on their molecular structure. MMP13 is a promising target for rheumatoid and osteoarthritis, two inflammatory diseases in which cartilage is excessively degraded primarily in the joints, leading to limb stiffness and excessive pain.[143,144] As these diseases can often be treated only symptomatically, the development of novel drugs constitutes a highly interesting field of research. To summarize the findings of this chapter, the here described compound class was proven to inhibit collagenolytic activity of a set of different MMPs, depending on the structure of the inhibitors. Based on a novel mechanism of action, presumably by interacting with the PEX domain, this class of inhibitors holds the potential for selective MMP inhibition, thus enabling a plethora of possible novel MMP targeted-therapy drugs.

Table 1: Inhibition values of selected compounds towards a larger set of MMPs

Cmpd	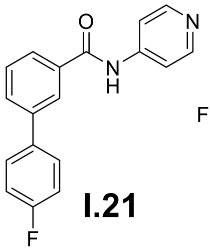 **I.21**	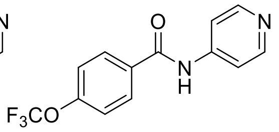 **I.22**	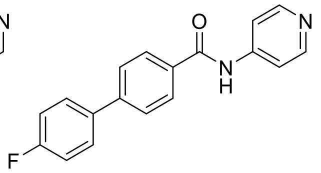 **I.28**
Inhibition of HT1080 invasion (MT-MMP1)[a,b]	52%[a]	2.5%[c]	6.5%[b]
MMP1	n.i.[a]	n.i.[b]	n.i.[a]
MMP2	3%[a]	8.2%[a]	36%[a]
MMP8	n.i.[a]	12.6%[b]	n.i.[c]
MMP9	2.2%[a]	4.2%[b]	n.i.[a]
MMP13	8.7%[a]	47%[a]	86%[a]

[a]tested at 10 µM inhibitor concentration. [b]tested at 100 µM inhibitor concentration. [c]tested at 50 µM inhibitor concentration.

4.3. Development and *Proof-of-Principle* evaluation of 17β-HSD2 inhibitors for bone fracture healing

The second part of this thesis dealt with the development of novel agents for targeted endocrine therapy. Misbalance in steroid hormone concentrations in hormone-sensitive tissues nurtures pathologic conditions such as prostate cancer, breast cancer, or osteoporosis.[145] Traditional therapies against such diseases often alter steroid concentrations or their actions systemically in body, hence leading to severe side effects and disturbance of the hypothalamus–pituitary–organ axis.[146,147] The aim of targeted endocrine therapy would be to specifically alter hormone concentrations in the target tissue of the disease, thereby reducing the side effects of the therapy (figure 12).

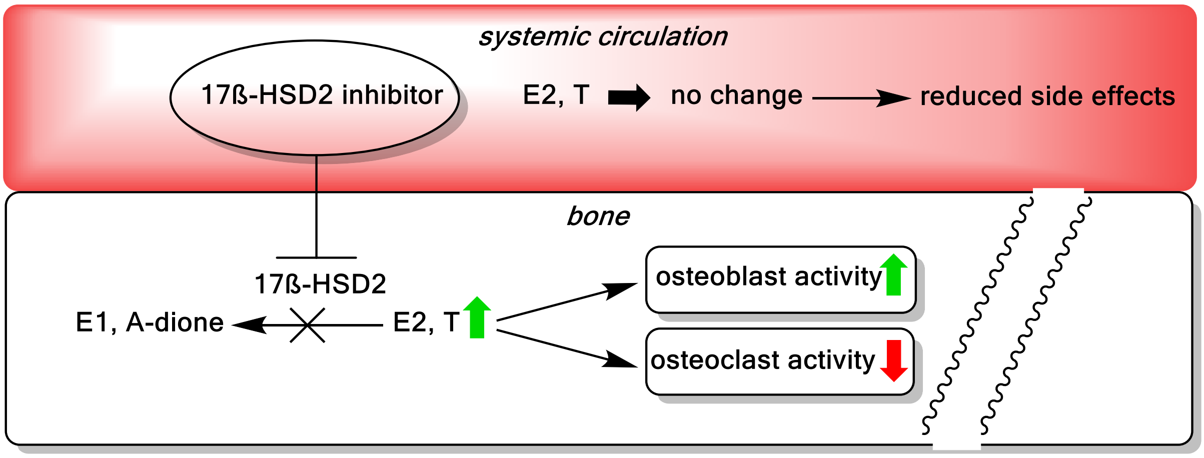

Figure 13: Working hypothesis of 17β-HSD2 inhibitors for targeted endocrine therapy in bone

Inhibition of 17β-HSD2, an enzyme which deactivates estradiol and testosterone, is a promising approach for targeted endocrine therapy, as it would increase hormone concentration in the target bone tissue in an intracrine manner.[148] The concept had previously been validated in literature, showing that treatment of ovariectomized monkeys with a 17β-HSD2 inhibitor significantly increased bone strength.[129] The first part of this 17β-HSD2 inhibitor study dealt with the applicability of this concept to decreased bone fracture healing, as the underlying biological mechanisms for fracture healing are highly similar to osteoporosis.[87]

For this purpose, we took compound **II.A**, originating from the field of highly potent 17β-HSD1 inhibitors for treatment of estrogen-excessive diseases such as breast cancer or endometriosis[149], and subjected it to a two-step optimization process (figure 13). The moderately active compound (IC_{50} = 111 nM) shows a very low *in vitro* metabolic stability in human liver S9 fraction, which is attributed to a facile phase II conjugation reaction on the hydroxyl moiety of the benzoyl part of the molecule, as well as no inhibition of murine 17β-HSD2. The first optimization step aimed at reducing electron density of the phenolic OH on the benzoyl moiety, thereby decreasing nucleophilicity and increasing steric hindrance on the group, thus potentially reducing phase II metabolism.

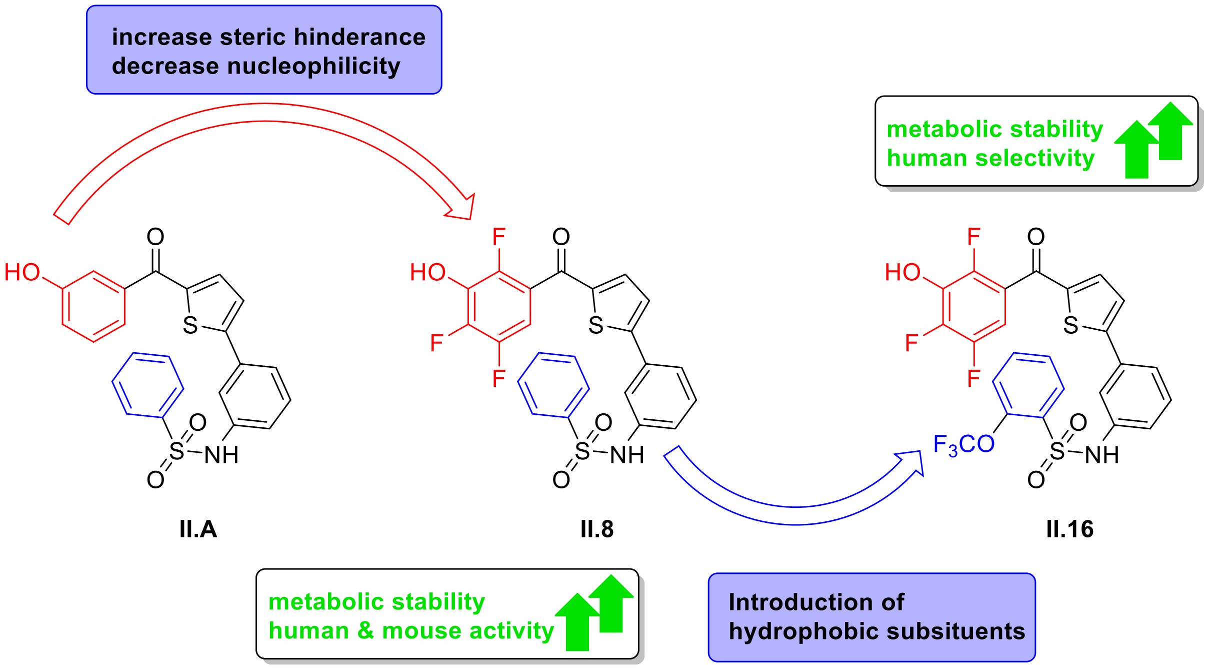
increase steric hinderance
decrease nucleophilicity
metabolic stability
human selectivity
HO
O
S
O
S
NH
O
F
F
F
F3CO
II.A
II.8
II.16
metabolic stability
human & mouse activity
Introduction of
hydrophobic subsituents

Figure 14: Design strategy of novel 17-HSD2 inhibitors for bone fracture healing

This could be proven to be successful as a strong increase in *in vitro* metabolic stability could be seen when introducing two fluorine substituents in *ortho* to the phenolic hydroxy group (**II.8**, $t_{1/2}$ = 25 min vs **II.A**, $t_{1/2} \leq 5$ min). A single substituent on the *o*-position does not lead to this effect (**II.3**, $t_{1/2} \leq 5$ min). A similar observation was made for the 2,6-di-F substituted compounds in the 17β-HSD1 project (data not shown).[149] Furthermore, these modifications with an electron-withdrawing group on the benzoyl moiety led to a 10 to 100-fold increase in activity, with the 2-chlorine substituted **II.3** being the most active compound in this series (IC_{50} = 0.9 nM vs. 111 nM), probably due to the increased acidity of the phenolic OH. The conformational restriction induced by substitution at the 2-position, together with the increased acidity, also led to increased inhibition of the mouse 17β-HSD2, the second main goal of the study. A single substitution in the 2-position with fluorine or chlorine led to highly active compounds on the mouse enzyme (**II.3** and **II.7**, IC_{50} = 2.7 nM), but showed a disappointing metabolic stability profile ($t_{1/2} \leq 5$ min) due to the missing substituent on position 4. A combination of the two features, the 2,4,5-tri-F motif, led to an even higher increase in activity on the human and murine 17β-HSD2 (**II.8**, 0.5 nM and 17.5 nM) and a highly increased metabolic stability ($t_{1/2}$ = 25 min), and was thus kept for further optimization.

Another aim of the study was to obtain a compound with slight selectivity over 17β-HSD1 (s.f 2–5). A highly selective 17β-HSD2 inhibitor would highly increase estradiol concentrations in tissue where both 17β-HSD1 and 2 are present like breast and endometrium[150], and a non-selective 17β-HSD2/1 inhibitor would affect the regulating role of 17β-HSD1 in the menstrual cycle of female patients. Therefore, we performed modifications on the aromatic sulfonamide moiety, as the thiophene- and aniline-derived parts of the molecules had already been optimized in previous studies in the 17β-HSD projects and had shown to not significantly contribute to the selectivity profile of this compound class.[133,151] The SAR on the sulfonamide part of the molecule is relatively flat, as all compound **II.9-16** share the high activity and metabolic stability previously seen. The two CF_3 substituted compounds **II.14** and **II.15** were further profiled, as they showed the desired high activity, selectivity profile (s.f. 3 and 3.4) as well as an increased metabolic stability ($t_{1/2}$ = 51&60 min) compared to **II.8** (s.f.1, $t_{1/2}$ = 25 min), the major goals of the study. The low activity of all tested compounds in this study on mouse 17β-HSD1 shows that the mouse is not a suitable organism for the development of novel 17β-HSD1 inhibitors with this compound class. Compound **II.14** and **II.15** showed no toxicity in an *in vitro* cytotoxicity assay as well as negligible binding to the estrogen receptors ERα and β. This finding highlights the advantage of this non-steroid derived compound class compared to compounds with a steroid backbone, which are more likely to interact with steroid receptors. **II.15** inhibited estradiol production in MDA-MB231 cells with a IC_{50} value comparable to the cell-free assay (2 nM vs 2.4 nM), which proves that this compound class is able to pass cellular membrane in pharmacologically active amounts, an essential feature for a successful *in vivo* efficacy study.

Having increased the metabolic stability of our inhibitors, we subjected **II.15** to a pharmacokinetic study in mice, using subcutaneous application at a dose of 50 mg/kg bodyweight of the animals. This application form was chosen as it is suitable for the treatment of decreased bone fracture healing, as patients are bed ridden and the time span of application is relatively short. Plasma concentrations of **II.15** were stable in the analyzed mice for up to 24h after a single injection with an average of

210 nM, which is roughly ten times its mouse 17β-HSD2 IC_{50} and is high enough to inhibit the enzyme in a pharmacologically active way. Upon these highly promising results, the *proof-of-principle* study was performed in mice, which received **II.15** once daily at a dose of 50 mg/kg after application of the femur fraction model under anesthesia.[152] Animals were studies 14 and 28 days after the surgery. Bending stiffness of the fractured bone served as the most important readout, as mechanical stability is closely correlated with less pain and improved quality of life of the patients after fracture.[153] Treated animals showed now significant difference of bending stiffness after 14 days of treatment, but almost twice as high stiffness after 28 days compared to vehicle treated animals. Histological investigation revealed that **II.15**-treated animals showed a 61% larger area of the newly formed callus tissue around the fracture, while its composition, *e.g.* bone mineral density, structure and cartilage content did not change in the studied groups. These findings prove that the 17β-HSD2 inhibition does not cause the bone to grow in an irregular manner, but increases the amount of newly formed tissue. Inhibition of 17β-HSD2 also leads to a decreased bone resorption during fracture healing, as levels of osteoprotegerin, a biomarker of decreased bone formation[154], were elevated in the callus by 55% compared to vehicle controls after 14 days of treatment.

This shows that despite the lack of increased mechanical strength after 14 days of treatment, a change in biochemical signaling of the healing process is already visible. Taken together, the hypothesis of 17β-HSD2 inhibitors to decrease estradiol-mediated bone resorption and to increase testosterone-induced bone formation is clearly depicted in the increased callus size and biochemical markers, which results in the superior stability of the fractured bone after 28 days upon treatment with **II.15.** Investigation of serum estradiol and testosterone levels in the treated animals showed no difference in the two groups studied, highlighting that 17β-HSD2 inhibitors alter intracellular concentrations of estradiol and testosterone in target tissue, validating the concept of targeted-endocrine therapeutic agents. This is further supported by no weight difference of the seminal vesicles of the two studies animal groups, a tissue highly sensitive to fluctuating testosterone levels.[155]

4.4. Development of highly active 17β-HSD2 inhibitors for targeted osteoporosis therapy

The second part of the here described 17β-HSD2 inhibitor study, and the third part of this thesis, dealt with the development of novel 17β-HSD2 inhibitors for the treatment of osteoporosis. This disease is characterized by a loss of bone mineral density and is accompanied by an increased risk of fractures in elderly people.[103] While women after menopause are the primary subjects affected by the disease, due to the highly decreased production of estradiol in the ovaries, a decreased in testosterone levels in elderly men has also been associated with the disease.[76,156] The biological mechanisms are closely related to those of decreased bone fracture healing, as both diseases show a misbalance in bone metabolism, mediated by osteoblasts and osteoclasts.[87] Nonetheless, the pharmacological properties of novel inhibitors differ significantly for these two diseases, as osteoporosis treatment requires the novel drugs to be sufficiently orally bioavailable due to the long duration of treatment, which can last from decades to the end of the patient lifetime. The applicability and efficacy of 17β-HSD2 inhibitors to treat osteoporosis had already been shown in a *proof-of-principle* study in ovariectomized monkeys in literature[129], but so far, no inhibitor of the compound class described in this study has been tested in an osteoporosis animal model. Aim of the present study was to reduce the molecular weight of compound **II.15/III.A** while increasing its *in vitro* metabolic stability and solubility to enhance oral absorption and, hence, its oral bioavailability. Nevertheless, all beneficial properties such as the high potency on human and mouse 17β-HSD2 should be retained (figure 14).

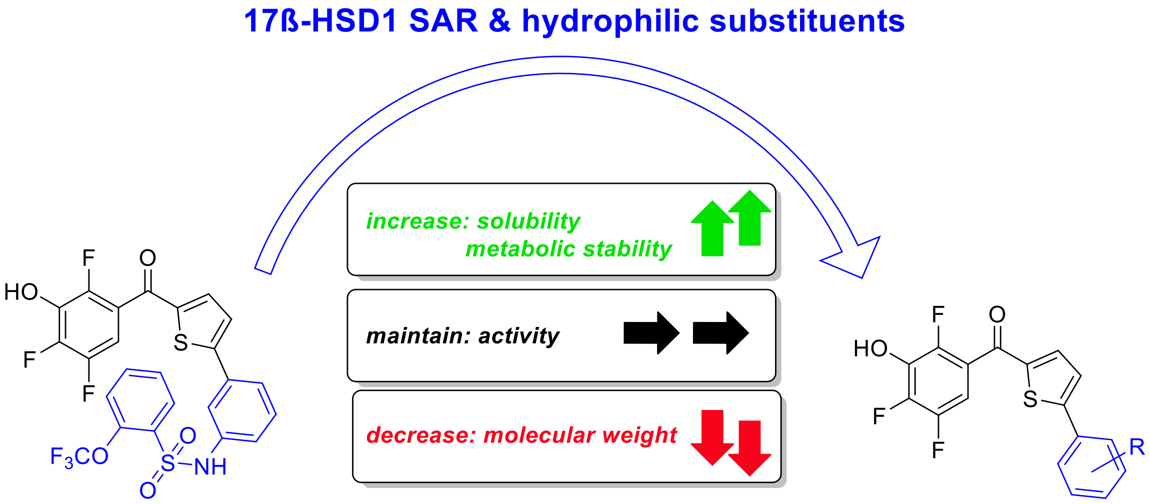

II.15/III.A

III.1-39

Figure 15: Design strategy to increase oral absorption of novel 17β -HSD2 inhibitors

We aimed at replacing the large aryl sulfonamide tail with more hydrophilic substituents to increase the solubility and metabolic stability, while reducing the molecular weight. Recently, it was shown, that, for 17β-HSD1 inhibitors bearing the 2,6-di-F motif on the benzoyl moiety, the sulfonamide tail can be omitted without losing activity on human 17β-HSDs (**II.15/III.A**, 17β-HSD2 IC_{50} = 2 nM, vs **III.B**, 1.4 nM).[149] We transferred the SAR to the 2,4,5-tri-F scaffold, which led to highly active compounds on the human 17β-HSD2, but disappointing activity on the mouse 17β-HSD2, due to the missing interactions provided by the sulfonamide tail. For this reason, we decided to introduce a more structurally diverse set of substituents on the scaffold, resulting in compounds with two-digit nanomolar to three-digit picomolar activity on human 17β-HSD2. The SAR on the human enzyme is extremely flat, allowing for the introduction of almost any aromatic moiety. The plain phenyl derivative **III.32** is one of the most potent compounds described in the study (human 17β-HSD2 IC_{50} = 0.85 nM) and shows that no additional decoration is necessary to achieve high activity.In previous studies of this compound class, it was hypothesized that the *p*-hydroxy moiety, as seen in **III.5** or **III.15** (table 2), could have a key interaction within the binding pocket of the 17β-HSD1.[133,149] This could be rejected for the 2,4,5-tri-F class as the single substituted *p*-hydroxy compound **III.15** is the most active 17β-HSD2 inhibitor so far described in literature (human 17β-HSD2 IC_{50} = 320 pM) and the most selective of its class for 17β-HSD2 over 17β-HSD1 (s.f. 22). However, it is unknown whether such selectivity is necessary, as 17β-HSD1 is not present in the bone.[116] Additionally, a selective inhibition would enhance hormone concentrations in tissues where both 17β-HSD1&2 are present like the breasts, therefore increasing the risk of side-effects as seen with systemic estradiol application.[113] We are happy to show that both profiles, highly active selective and non-selective, are represented within this inhibitor class (table 2). Regarding activity on the mouse 17β-HSD2, it turned out to be more difficult to obtain potent inhibitors compared to the study described in Chapter II, highlighting the beneficial role of the sulfonamide tail for activity on this particular enzyme. The most active compounds found are the indole-derivatives **III.33** and **III.34,** which are equipotent to reference compound **II.15/III.A** (table 2).

Table 2: Activity and *in vitro* ADME profiles of selected compounds described in this study

Cmpd	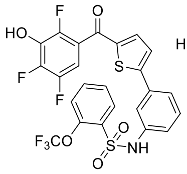 **II.15/III.A**	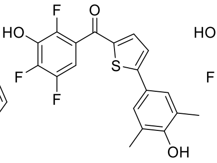 **III.2**	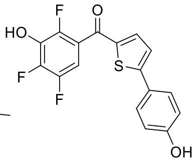 **III.15**	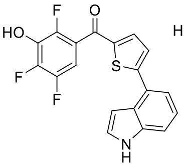 **III.33**	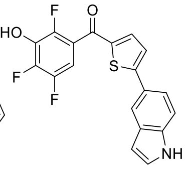 **III.34**
h17β-HSD2 IC_{50} [nM] (s.f.)	2 (3)	1.6 (0.25)	0.32 (22)	1.1 (1.4)	1.3 (4.5)
h17β-HSD1 IC_{50} [nM]	6	0.4	7	1.5	5.8
m17β-HSD2 IC_{50} [nM]	25	89	47% @50nM	34	34
aq. Solubility [µM]	50–100	>200	>200*	50–100	50–100
$t_{1/2}$ human liver S9 [min]	60	19	27*	51	>>60
$t_{1/2}$ mouse liver S9 [min]	46	70	79*	34	49

*These data are not included in the publication, but were obtained under the same conditions reported

The good metabolic stability profile and solubility of the new inhibitors is one of the highlights of this study (table 2). Remarkably, the *p*-hydroxy function is not a metabolite hotspot, since introduction of two *ortho*-substituents did not change the metabolic stability (**III.2** vs **III.12**, table 2), as seen for the hydroxyl on the benzoyl moiety in chapter II. The end game of this study consisted of an *in vivo* PK experiment using mice. As mentioned before, oral bioavailability is mandatory for osteoporosis drugs, as the therapy can last up to years, or even decades. We administered four compounds perorally via gavage, which resulted in highly increased area-under-the-curve (AUC) values compared to reference **II.15/III.A**. Compound **III.33** shows AUC values 13-times higher than the reference, with a maximum concentration of 1211 nM after 2h. The desired inhibitor concentration to be effective in an *in vivo* model is represented by the IC_{90}, which is roughly 10-times the IC_{50} of the compound; **III.33** is likely to maintain this concentration for 19h after a single administration. Furthermore, both indole derivatives **III.33** and **III.34** can still be detected in the blood after 24h (~ 50 nM), which enables an increase in blood concentrations after several days of once-a-day administration of the compounds.

Taken together the findings of the study, this simplified compound class has shown high potency and selectivity on both human and mouse 17β-HSD2. The reduction in molecular weight, together with the good metabolic stability and solubility profile, enabled this compound class to be promising drug-like molecules for osteoporosis therapy, with reasonable pharmacokinetic profiles. Especially compound **III.33** is a highly potent, non-toxic, 17β-HSD2 inhibitor, which shows the highest plasma concentrations in mice ever obtained for this compound class.

5. References

(1) Turanli, B.; Karagoz, K.; Gulfidan, G.; Sinha, R.; Mardinoglu, A.; Arga, K. Y. A Network-Based Cancer Drug Discovery: From Integrated Multi-Omics Approaches to Precision Medicine. *Curr. Pharm. Des.* **2019**, *24* (32), 3778–3790. https://doi.org/10.2174/1381612824666181106095959.

(2) Dugger, S. A.; Platt, A.; Goldstein, D. B. Drug Development in the Era of Precision Medicine. *Nat. Rev. Drug Discov.* **2018**, *17* (3), 183–196. https://doi.org/10.1038/nrd.2017.226.

(3) Gerber, D. E. Targeted Therapies: A New Generation of Cancer Treatments. *American Family Physician*. American Academy of Family Physicians February 1, 2008, pp 311–319.

(4) Srinivasarao, M.; Low, P. S. Ligand-Targeted Drug Delivery. *Chem. Rev.* **2017**, *117* (19), 12133–12164. https://doi.org/10.1021/acs.chemrev.7b00013.

(5) Klein, S. Signal Transduction Therapy of Cancer. *Mol. Aspects Med.* **2010**, *31* (4), 287–329. https://doi.org/10.1016/J.MAM.2010.04.001.

(6) Bhullar, K. S.; Lagarón, N. O.; McGowan, E. M.; Parmar, I.; Jha, A.; Hubbard, B. P.; Rupasinghe, H. P. V. Kinase-Targeted Cancer Therapies: Progress, Challenges and Future Directions. *Mol. Cancer* **2018**, *17* (1), 48. https://doi.org/10.1186/s12943-018-0804-2.

(7) Luo, J.; Solimini, N. L.; Elledge, S. J. Principles of Cancer Therapy: Oncogene and Non-Oncogene Addiction. *Cell* **2009**, *136* (5), 823–837. https://doi.org/10.1016/j.cell.2009.02.024.

(8) Yan, C.; Higgins, P. J. Drugging the Undruggable: Transcription Therapy for Cancer. *Biochim. Biophys. Acta* **2013**, *1835* (1), 76–85. https://doi.org/10.1016/j.bbcan.2012.11.002.

(9) Papavassiliou, A. G. Transcription-Factor-Modulating Agents: Precision and Selectivity in Drug Design. *Mol. Med. Today* **1998**, *4* (8), 358–366.

(10) Rodríguez-Paredes, M.; Esteller, M. Cancer Epigenetics Reaches Mainstream Oncology. *Nat. Med.* **2011**, *17* (3), 330–339. https://doi.org/10.1038/nm.2305.

(11) Lambert, M.; Jambon, S.; Depauw, S.; David-Cordonnier, M.-H.; Lambert, M.;

Jambon, S.; Depauw, S.; David-Cordonnier, M.-H. Targeting Transcription Factors for Cancer Treatment. *Molecules* **2018**, *23* (6), 1479. https://doi.org/10.3390/molecules23061479.

(12) Hassan, M.; Watari, H.; AbuAlmaaty, A.; Ohba, Y.; Sakuragi, N. Apoptosis and Molecular Targeting Therapy in Cancer. *Biomed Res. Int.* **2014**, *2014*, 150845. https://doi.org/10.1155/2014/150845.

(13) Breckenridge, D. G.; Xue, D. Regulation of Mitochondrial Membrane Permeabilization by BCL-2 Family Proteins and Caspases. *Curr. Opin. Cell Biol.* **2004**, *16* (6), 647–652. https://doi.org/10.1016/J.CEB.2004.09.009.

(14) Yip, K. W.; Reed, J. C. Bcl-2 Family Proteins and Cancer. *Oncogene* **2008**, *27* (50), 6398–6406. https://doi.org/10.1038/onc.2008.307.

(15) Debatin, K.-M.; Poncet, D.; Kroemer, G. Chemotherapy: Targeting the Mitochondrial Cell Death Pathway. *Oncogene* **2002**, *21* (57), 8786–8803. https://doi.org/10.1038/sj.onc.1206039.

(16) Borg, M. A.; Clemmons, A. Venetoclax: A Novel Treatment for Patients With Del(17p) Chronic Lymphocytic Leukemia. *J. Adv. Pract. Oncol.* **2017**, *8* (6), 647–652.

(17) Pfeffer, C. M.; Singh, A. T. K. Apoptosis: A Target for Anticancer Therapy. *Int. J. Mol. Sci.* **2018**, *19* (2). https://doi.org/10.3390/ijms19020448.

(18) Elmore, S. Apoptosis: A Review of Programmed Cell Death. *Toxicol. Pathol.* **2007**, *35* (4), 495–516. https://doi.org/10.1080/01926230701320337.

(19) Bagnoli, M.; Canevari, S.; Mezzanzanica, D. Cellular FLICE-Inhibitory Protein (c-FLIP) Signalling: A Key Regulator of Receptor-Mediated Apoptosis in Physiologic Context and in Cancer. *Int. J. Biochem. Cell Biol.* **2010**, *42* (2), 210–213. https://doi.org/10.1016/J.BIOCEL.2009.11.015.

(20) de Miguel, D.; Lemke, J.; Anel, A.; Walczak, H.; Martinez-Lostao, L. Onto Better TRAILs for Cancer Treatment. *Cell Death Differ.* **2016**, *23* (5), 733–747. https://doi.org/10.1038/cdd.2015.174.

(21) Stuckey, D. W.; Shah, K. TRAIL on Trial: Preclinical Advances in Cancer Therapy. *Trends Mol. Med.* **2013**, *19* (11), 685–694.

https://doi.org/10.1016/j.molmed.2013.08.007.

(22) Oiseth, S. J.; Aziz, M. S. Cancer Immunotherapy: A Brief Review of the History, Possibilities, and Challenges Ahead. *J. Cancer Metastasis Treat.* **2017**, *3* (10), 250. https://doi.org/10.20517/2394-4722.2017.41.

(23) Lee, A.; Djamgoz, M. B. A. Anti-Tumour Treatment Triple Negative Breast Cancer: Emerging Therapeutic Modalities and Novel Combination Therapies. **2018**. https://doi.org/10.1016/j.ctrv.2017.11.003.

(24) Sharma, P.; Hu-Lieskovan, S.; Wargo, J. A.; Ribas, A. Primary, Adaptive, and Acquired Resistance to Cancer Immunotherapy. *Cell* **2017**, *168* (4), 707–723. https://doi.org/10.1016/J.CELL.2017.01.017.

(25) Kitamura, T.; Qian, B.-Z.; Pollard, J. W. Immune Cell Promotion of Metastasis. *Nat. Rev. Immunol.* **2015**, *15* (2), 73–86. https://doi.org/10.1038/nri3789.

(26) Darvin, P.; Toor, S. M.; Sasidharan Nair, V.; Elkord, E. Immune Checkpoint Inhibitors: Recent Progress and Potential Biomarkers. *Exp. Mol. Med.* **2018**, *50* (12), 165. https://doi.org/10.1038/s12276-018-0191-1.

(27) Sherwood, L. M.; Parris, E. E.; Folkman, J. Tumor Angiogenesis: Therapeutic Implications. *N. Engl. J. Med.* **1971**, *285* (21), 1182–1186. https://doi.org/10.1056/NEJM197111182852108.

(28) De Palma, M.; Biziato, D.; Petrova, T. V. Microenvironmental Regulation of Tumour Angiogenesis. *Nat. Rev. Cancer* **2017**, *17* (8), 457–474. https://doi.org/10.1038/nrc.2017.51.

(29) Potente, M.; Gerhardt, H.; Carmeliet, P. Basic and Therapeutic Aspects of Angiogenesis. *Cell* **2011**, *146* (6), 873–887. https://doi.org/10.1016/j.cell.2011.08.039.

(30) Dallinga, M. G.; Boas, S. E.; Klaassen, I.; Merks, R. H.; van Noorden, C. J.; Schlingemann, R. O. Tip Cells in Angiogenesis. In *eLS*; John Wiley & Sons, Ltd: Chichester, UK, 2015; pp 1–10. https://doi.org/10.1002/9780470015902.a0025977.

(31) Bergers, G.; Benjamin, L. E. Tumorigenesis and the Angiogenic Switch. *Nature Reviews Cancer*. Nature Publishing Group June 1, 2003, pp 401–410.

https://doi.org/10.1038/nrc1093.

(32) Tonnesen, M. G.; Feng, X.; Clark, R. A. F. Angiogenesis in Wound Healing. *J. Investig. Dermatology Symp. Proc.* **2000**, *5* (1), 40–46. https://doi.org/10.1046/j.1087-0024.2000.00014.x.

(33) Weis, S. M.; Cheresh, D. A. Tumor Angiogenesis: Molecular Pathways and Therapeutic Targets. *Nat. Med.* **2011**, *17* (11), 1359–1370. https://doi.org/10.1038/nm.2537.

(34) Therapontos, C.; Erskine, L.; Gardner, E. R.; Figg, W. D.; Vargesson, N. Thalidomide Induces Limb Defects by Preventing Angiogenic Outgrowth during Early Limb Formation. *Proc. Natl. Acad. Sci. U. S. A.* **2009**, *106* (21), 8573–8578. https://doi.org/10.1073/pnas.0901505106.

(35) Zirlik, K.; Duyster, J. Anti-Angiogenics: Current Situation and Future Perspectives. *Oncol. Res. Treat.* **2018**, *41* (4), 166–171. https://doi.org/10.1159/000488087.

(36) Sullivan, L. A.; Brekken, R. A. The VEGF Family in Cancer and Antibody-Based Strategies for Their Inhibition. *MAbs* **2010**, *2* (2), 165–175.

(37) Gotink, K. J.; Henk, •; Verheul, M. W. Anti-Angiogenic Tyrosine Kinase Inhibitors: What Is Their Mechanism of Action? https://doi.org/10.1007/s10456-009-9160-6.

(38) Rundhaug, J. E. Matrix Metalloproteinases and Angiogenesis. *J. Cell. Mol. Med.* **2005**, *9* (2), 267–285. https://doi.org/10.1111/j.1582-4934.2005.tb00355.x.

(39) Piccard, H.; Van den Steen, P. E.; Opdenakker, G. Hemopexin Domains as Multifunctional Liganding Modules in Matrix Metalloproteinases and Other Proteins. *J. Leukoc. Biol.* **2007**, *81* (4), 870–892. https://doi.org/10.1189/jlb.1006629.

(40) Tam, E. M.; Moore, T. R. B.; Butler, G. S.; Overall, C. M. Characterization of the Distinct Collagen Binding, Helicase and Cleavage Mechanisms of Matrix Metalloproteinase 2 and 14 (Gelatinase A and MT1-MMP): The Differential Roles of the MMP Hemopexin C Domains and the MMP-2 Fibronectin Type II Modules in Collage. *J. Biol. Chem.* **2004**, *279* (41), 43336–43344.

https://doi.org/10.1074/jbc.M407186200.

(41) Zhou, Z.; Apte, S. S.; Soininen, R.; Cao, R.; Baaklini, G. Y.; Rauser, R. W.; Wang, J.; Cao, Y.; Tryggvason, K. Impaired Endochondral Ossification and Angiogenesis in Mice Deficient in Membrane-Type Matrix Metalloproteinase I. *Proc. Natl. Acad. Sci. U. S. A.* **2000**, *97* (8), 4052–4057. https://doi.org/10.1073/pnas.060037197.

(42) Pahwa, S.; Stawikowski, M. J.; Fields, G. B. Monitoring and Inhibiting MT1-MMP during Cancer Initiation and Progression. *Cancers (Basel).* **2014**, *6* (1), 416–435. https://doi.org/10.3390/cancers6010416.

(43) Itoh, Y. MT1-MMP: A Key Regulator of Cell Migration in Tissue. *IUBMB Life*. Informa Healthcare October 1, 2006, pp 589–596. https://doi.org/10.1080/15216540600962818.

(44) Koshikawa, N.; Giannelli, G.; Cirulli, V.; Miyazaki, K.; Quaranta, V. Role of Cell Surface Metalloprotease Mt1-Mmp in Epithelial Cell Migration over Laminin-5. *J. Cell Biol.* **2000**, *148* (3), 615–624. https://doi.org/10.1083/JCB.148.3.615.

(45) Endo, K.; Takino, T.; Miyamori, H.; Kinsen, H.; Yoshizaki, T.; Furukawa, M.; Sato, H. Cleavage of Syndecan-1 by Membrane Type Matrix Metalloproteinase-1 Stimulates Cell Migration. *J. Biol. Chem.* **2003**, *278* (42), 40764–40770. https://doi.org/10.1074/jbc.M306736200.

(46) Mori, H.; Tomari, T.; Koshikawa, N.; Kajita, M.; Itoh, Y.; Sato, H.; Tojo, H.; Yana, I.; Seiki, M. CD44 Directs Membrane-Type 1 Matrix Metalloproteinase to Lamellipodia by Associating with Its Hemopexin-like Domain. *EMBO J.* **2002**, *21* (15), 3949–3959. https://doi.org/10.1093/emboj/cdf411.

(47) Eisenach, P. A.; Roghi, C.; Fogarasi, M.; Murphy, G.; English, W. R. MT1-MMP Regulates VEGF-A Expression through a Complex with VEGFR-2 and Src. *J. Cell Sci.* **2010**, *123* (Pt 23), 4182–4193. https://doi.org/10.1242/jcs.062711.

(48) Rozanov, D. V; Ghebrehiwet, B.; Postnova, T. I.; Eichinger, A.; Deryugina, E. I.; Strongin, A. Y. The Hemopexin-like C-Terminal Domain of Membrane Type 1 Matrix Metalloproteinase Regulates Proteolysis of a Multifunctional Protein, GC1qR. *J. Biol. Chem.* **2002**, *277* (11), 9318–9325. https://doi.org/10.1074/jbc.M110711200.

(49) Van Wart, H. E.; Birkedal-Hansen, H. The Cysteine Switch: A Principle of Regulation of Metalloproteinase Activity with Potential Applicability to the Entire Matrix Metalloproteinase Gene Family. *Proc. Natl. Acad. Sci. U. S. A.* **1990**, *87* (14), 5578–5582.

(50) Brew, K.; Nagase, H. The Tissue Inhibitors of Metalloproteinases (TIMPs): An Ancient Family with Structural and Functional Diversity. *Biochim. Biophys. Acta* **2010**, *1803* (1), 55–71. https://doi.org/10.1016/j.bbamcr.2010.01.003.

(51) Cox, T. R.; Erler, J. T. Remodeling and Homeostasis of the Extracellular Matrix: Implications for Fibrotic Diseases and Cancer. *Dis. Model. Mech.* **2011**, *4* (2), 165–178. https://doi.org/10.1242/dmm.004077.

(52) Vihinen, P.; Kähäri, V.-M. Matrix Metalloproteinases in Cancer: Prognostic Markers and Therapeutic Targets. *Int. J. Cancer* **2002**, *99* (2), 157–166. https://doi.org/10.1002/ijc.10329.

(53) Egeblad, M.; Werb, Z. New Functions for the Matrix Metalloproteinases in Cancer Progression. *Nat. Rev. Cancer* **2002**, *2* (3), 161–174. https://doi.org/10.1038/nrc745.

(54) Fairchild, A.; Tirumani, S. H.; Rosenthal, M. H.; Howard, S. A.; Krajewski, K. M.; Nishino, M.; Shinagare, A. B.; Jagannathan, J. P.; Ramaiya, N. H. Hormonal Therapy in Oncology: A Primer for the Radiologist. *Am. J. Roentgenol.* **2015**, *204* (6), W620–W630. https://doi.org/10.2214/AJR.14.13604.

(55) Grimberg, A. Somatostatin and Cancer: Applying Endocrinology to Oncology. *Cancer Biol. Ther.* **2004**, *3* (8), 731–733.

(56) Gründker, C.; Emons, G. The Role of Gonadotropin-Releasing Hormone in Cancer Cell Proliferation and Metastasis. *Front. Endocrinol. (Lausanne).* **2017**, *8*, 187. https://doi.org/10.3389/fendo.2017.00187.

(57) Pufall, M. A. Glucocorticoids and Cancer. *Adv. Exp. Med. Biol.* **2015**, *872*, 315–333. https://doi.org/10.1007/978-1-4939-2895-8_14.

(58) Liu, D.; Ahmet, A.; Ward, L.; Krishnamoorthy, P.; Mandelcorn, E. D.; Leigh, R.; Brown, J. P.; Cohen, A.; Kim, H. A Practical Guide to the Monitoring and Management of the Complications of Systemic Corticosteroid Therapy. *Allergy*

Asthma. Clin. Immunol. **2013**, *9* (1), 30. https://doi.org/10.1186/1710-1492-9-30.

(59) Mohammed, H.; Russell, I. A.; Stark, R.; Rueda, O. M.; Hickey, T. E.; Tarulli, G. A.; Serandour, A. A.; Birrell, S. N.; Bruna, A.; Saadi, A.; et al. Progesterone Receptor Modulates ERα Action in Breast Cancer. *Nature* **2015**, *523* (7560), 313–317. https://doi.org/10.1038/nature14583.

(60) Karantanos, T.; Corn, P. G.; Thompson, T. C. Prostate Cancer Progression after Androgen Deprivation Therapy: Mechanisms of Castrate Resistance and Novel Therapeutic Approaches. *Oncogene* **2013**, *32* (49), 5501–5511. https://doi.org/10.1038/onc.2013.206.

(61) Li, Z.; Bishop, A. C.; Alyamani, M.; Garcia, J. A.; Dreicer, R.; Bunch, D.; Liu, J.; Upadhyay, S. K.; Auchus, R. J.; Sharifi, N. Conversion of Abiraterone to D4A Drives Anti-Tumour Activity in Prostate Cancer. *Nature* **2015**, *523* (7560), 347–351. https://doi.org/10.1038/nature14406.

(62) Yin, L.; Hu, Q. CYP17 Inhibitors - Abiraterone, C17,20-Lyase Inhibitors and Multi-Targeting Agents. *Nature Reviews Urology*. Nature Publishing Group January 26, 2014, pp 32–42. https://doi.org/10.1038/nrurol.2013.274.

(63) Yin, L.; Hu, Q.; Hartmann, R. W. Recent Progress in Pharmaceutical Therapies for Castration-Resistant Prostate Cancer. *Int. J. Mol. Sci.* **2013**, *14* (7), 13958–13978. https://doi.org/10.3390/ijms140713958.

(64) Dutertre, M.; Smith, C. L. Molecular Mechanisms of Selective Estrogen Receptor Modulator (SERM) Action. *J. Pharmacol. Exp. Ther.* **2000**, *295* (2).

(65) Riggs, B. L.; Hartmann, L. C. Selective Estrogen-Receptor Modulators — Mechanisms of Action and Application to Clinical Practice. *N. Engl. J. Med.* **2003**, *348* (7), 618–629. https://doi.org/10.1056/nejmra022219.

(66) Kim, E. H.; Larson, J. A.; Andriole, G. L. Management of Benign Prostatic Hyperplasia. *Annu. Rev. Med.* **2016**, *67* (1), 137–151. https://doi.org/10.1146/annurev-med-063014-123902.

(67) Montie, J. E.; Pienta, K. J. Review of the Role of Androgenic Hormones in the Epidemiology of Benign Prostatc Hyperplasia and Prostate Cancer. *Urology* **1994**, *43* (6), 892–899. https://doi.org/10.1016/0090-4295(94)90163-5.

(68) Ho, C. K. M.; Habib, F. K. Estrogen and Androgen Signaling in the Pathogenesis of BPH. *Nat. Rev. Urol.* **2011**, *8* (1), 29–41. https://doi.org/10.1038/nrurol.2010.207.

(69) Kim, E. H.; Brockman, J. A.; Andriole, G. L. The Use of 5-Alpha Reductase Inhibitors in the Treatment of Benign Prostatic Hyperplasia. *Asian J. Urol.* **2018**, *5* (1), 28–32. https://doi.org/10.1016/j.ajur.2017.11.005.

(70) Sountoulides, P.; Rountos, T. Adverse Effects of Androgen Deprivation Therapy for Prostate Cancer: Prevention and Management. *ISRN Urol.* **2013**, *2013*, 240108. https://doi.org/10.1155/2013/240108.

(71) Stulnig, T. M.; Waldhäusl, W. 11β-Hydroxysteroid Dehydrogenase Type 1 in Obesity and Type 2 Diabetes. *Diabetologia*. Springer-Verlag January 1, 2004, pp 1–11. https://doi.org/10.1007/s00125-003-1284-4.

(72) Hermanowski-Vosatka, A.; Balkovec, J. M.; Cheng, K.; Chen, H. Y.; Hernandez, M.; Koo, G. C.; Le Grand, C. B.; Li, Z.; Metzger, J. M.; Mundt, S. S.; et al. 11beta-HSD1 Inhibition Ameliorates Metabolic Syndrome and Prevents Progression of Atherosclerosis in Mice. *J. Exp. Med.* **2005**, *202* (4), 517–527. https://doi.org/10.1084/jem.20050119.

(73) Morgan, N. N.; Zebo, R.; Ponticiello, R. P.; O’Connor, S. P.; Ye, X.; Wu, S.; Harper, T. W.; Sheriff, S.; Wang, H.; Ramamurthy, V.; et al. Discovery of Clinical Candidate BMS-823778 as an Inhibitor of Human 11β-Hydroxysteroid Dehydrogenase Type 1 (11β-HSD-1). *ACS Med. Chem. Lett.* **2018**, *9* (12), 1170–1174. https://doi.org/10.1021/acsmedchemlett.8b00307.

(74) Consensus Development Conference: Diagnosis, Prophylaxis, and Treatment of Osteoporosis. *Am. J. Med.* **1993**, *94* (6), 646–650. https://doi.org/10.1016/0002-9343(93)90218-E.

(75) Raisz, L. G. Pathogenesis of Osteoporosis: Concepts, Conflicts, and Prospects. *J. Clin. Invest.* **2005**, *115* (12), 3318–3325. https://doi.org/10.1172/JCI27071.

(76) Chin, K.-Y.; Ima-Nirwana, S. Sex Steroids and Bone Health Status in Men. *Int. J. Endocrinol.* **2012**, *2012*, 208719. https://doi.org/10.1155/2012/208719.

(77) Lips, P. Vitamin D Deficiency and Secondary Hyperparathyroidism in the

Elderly: Consequences for Bone Loss and Fractures and Therapeutic Implications. *Endocr. Rev.* **2001**, *22* (4), 477–501. https://doi.org/10.1210/edrv.22.4.0437.

(78) Khosla, S.; Oursler, M. J.; Monroe, D. G. Estrogen and the Skeleton. *Trends Endocrinol. Metab.* **2012**, *23* (11), 576–581. https://doi.org/10.1016/j.tem.2012.03.008.

(79) van Beek, E. .; Cohen, L. .; Leroy, I. .; Ebetino, F. .; Löwik, C. W. G. .; Papapoulos, S. . Differentiating the Mechanisms of Antiresorptive Action of Nitrogen Containing Bisphosphonates. *Bone* **2003**, *33* (5), 805–811. https://doi.org/10.1016/J.BONE.2003.07.007.

(80) Frith, J. C.; Mönkkönen, J.; Blackburn, G. M.; Russell, R. G. G.; Rogers, M. J. Clodronate and Liposome-Encapsulated Clodronate Are Metabolized to a Toxic ATP Analog, Adenosine 5′-(β,γ-Dichloromethylene) Triphosphate, by Mammalian Cells In Vitro. *J. Bone Miner. Res.* **1997**, *12* (9), 1358–1367. https://doi.org/10.1359/jbmr.1997.12.9.1358.

(81) Reid, I. R. Bisphosphonates in the Treatment of Osteoporosis: A Review of Their Contribution and Controversies. *Skeletal Radiol.* **2011**, *40* (9), 1191–1196. https://doi.org/10.1007/s00256-011-1164-9.

(82) de Villiers, T. J. Selective Estrogen Receptor Modulators in the Treatment of Osteoporosis: A Review of the Clinical Evidence. *Clin. Investig. (Lond).* **2011**, *1* (5), 719–724. https://doi.org/10.4155/cli.11.46.

(83) Hsu, H.; Lacey, D. L.; Dunstan, C. R.; Solovyev, I.; Colombero, A.; Timms, E.; Tan, H. L.; Elliott, G.; Kelley, M. J.; Sarosi, I.; et al. Tumor Necrosis Factor Receptor Family Member RANK Mediates Osteoclast Differentiation and Activation Induced by Osteoprotegerin Ligand. *Proc. Natl. Acad. Sci. U. S. A.* **1999**, *96* (7), 3540–3545.

(84) Deeks, E. D. Denosumab: A Review in Postmenopausal Osteoporosis. *Drugs Aging* **2018**, *35* (2), 163–173. https://doi.org/10.1007/s40266-018-0525-7.

(85) Khosla, S. Increasing Options for the Treatment of Osteoporosis. *N. Engl. J. Med.* **2009**, *361* (8), 818–820. https://doi.org/10.1056/NEJMe0905480.

(86) Lane, N. E.; Kelman, A. A Review of Anabolic Therapies for Osteoporosis.

Arthritis Res. Ther. **2003**, *5* (5), 214–222. https://doi.org/10.1186/ar797.

(87) Russow, G.; Jahn, D.; Appelt, J.; Märdian, S.; Tsitsilonis, S.; Keller, J.; Russow, G.; Jahn, D.; Appelt, J.; Märdian, S.; et al. Anabolic Therapies in Osteoporosis and Bone Regeneration. *Int. J. Mol. Sci.* **2018**, *20* (1), 83. https://doi.org/10.3390/ijms20010083.

(88) Bhattacharyya, S.; Pal, S.; Chattopadhyay, N. Targeted Inhibition of Sclerostin for Post-Menopausal Osteoporosis Therapy: A Critical Assessment of the Mechanism of Action. *Eur. J. Pharmacol.* **2018**, *826*, 39–47. https://doi.org/10.1016/j.ejphar.2018.02.028.

(89) McClung, M. R. Sclerostin Antibodies in Osteoporosis: Latest Evidence and Therapeutic Potential. *Ther. Adv. Musculoskelet. Dis.* **2017**, *9* (10), 263–270. https://doi.org/10.1177/1759720X17726744.

(90) Li, X.; Zhang, Y.; Kang, H.; Liu, W.; Liu, P.; Zhang, J.; Harris, S. E.; Wu, D. Sclerostin Binds to LRP5/6 and Antagonizes Canonical Wnt Signaling. *J. Biol. Chem.* **2005**, *280* (20), 19883–19887. https://doi.org/10.1074/jbc.M413274200.

(91) Hak, D. J.; Fitzpatrick, D.; Bishop, J. A.; Marsh, J. L.; Tilp, S.; Schnettler, R.; Simpson, H.; Alt, V. Delayed Union and Nonunions: Epidemiology, Clinical Issues, and Financial Aspects. *Injury* **2014**, *45*, S3–S7. https://doi.org/10.1016/J.INJURY.2014.04.002.

(92) Jahagirdar, R.; Scammell, B. E. Principles of Fracture Healing and Disorders of Bone Union. *Surg.* **2009**, *27* (2), 63–69. https://doi.org/10.1016/J.MPSUR.2008.12.011.

(93) Calori, G. M.; Albisetti, W.; Agus, A.; Iori, S.; Tagliabue, L. Risk Factors Contributing to Fracture Non-Unions. *Injury* **2007**, *38*, S11–S18. https://doi.org/10.1016/S0020-1383(07)80004-0.

(94) Einhorn, T. A.; Gerstenfeld, L. C. Fracture Healing: Mechanisms and Interventions. *Nat. Rev. Rheumatol.* **2015**, *11* (1), 45–54. https://doi.org/10.1038/nrrheum.2014.164.

(95) Wojda, S. J.; Donahue, S. W. Parathyroid Hormone for Bone Regeneration. *J. Orthop. Res.* **2018**, *36* (10), 2586–2594. https://doi.org/10.1002/jor.24075.

(96) Shi, Z.; Zhou, H.; Pan, B.; Lu, L.; Liu, J.; Kang, Y.; Yao, X.; Feng, S. Effectiveness of Teriparatide on Fracture Healing: A Systematic Review and Meta-Analysis. *PLoS One* **2016**, *11* (12), e0168691. https://doi.org/10.1371/journal.pone.0168691.

(97) Canalis, E.; Economides, A. N.; Gazzerro, E. Bone Morphogenetic Proteins, Their Antagonists, and the Skeleton. *Endocr. Rev.* **2003**, *24* (2), 218–235. https://doi.org/10.1210/er.2002-0023.

(98) Sandhu, H. S.; Khan, S. N. Animal Models for Preclinical Assessment of Bone Morphogenetic Proteins in the Spine. *Spine (Phila. Pa. 1976).* **2002**, *27* (16 Suppl 1), S32-8.

(99) Krishnakumar, G. S.; Roffi, A.; Reale, D.; Kon, E.; Filardo, G. Clinical Application of Bone Morphogenetic Proteins for Bone Healing: A Systematic Review. *Int. Orthop.* **2017**, *41* (6), 1073–1083. https://doi.org/10.1007/s00264-017-3471-9.

(100) Tahami, M.; Haddad, B.; Abtahian, A.; Hashemi, A.; Aminian, A.; Konan, S. Potential Role of Local Estrogen in Enhancement of Fracture Healing: Preclinical Study in Rabbits. *Arch. bone Jt. Surg.* **2016**, *4* (4), 323–329.

(101) Beil, F. T.; Barvencik, F.; Gebauer, M.; Seitz, S.; Rueger, J. M.; Ignatius, A.; Pogoda, P.; Schinke, T.; Amling, M. Effects of Estrogen on Fracture Healing in Mice. *J. Trauma Inj. Infect. Crit. Care* **2010**, *69* (5), 1259–1265. https://doi.org/10.1097/TA.0b013e3181c4544d.

(102) Gesicki, M.; Tibba, J.; Nguyen, C. K.; Beil, F. T.; Rueger, J. M.; Haberland, M.; Amling, M. Testosterone Is a Potent Accelerator of Fracture Healing: Early Structural Reconstruction and Improved Biomechanical Stability. *Osteosynthesis Trauma Care* **2003**, *11* (S 1), 3–5. https://doi.org/10.1055/s-2003-42285.

(103) Compston, J. E. Sex Steroids and Bone. *Physiol. Rev.* **2001**, *81* (1), 419–447. https://doi.org/10.1152/physrev.2001.81.1.419.

(104) Sacco, S. M.; Ward, W. E. Revisiting Estrogen: Efficacy and Safety for Postmenopausal Bone Health. *J. Osteoporos.* **2010**, *2010*, 708931. https://doi.org/10.4061/2010/708931.

(105) de Villiers, T. J.; Pines, A.; Panay, N.; Gambacciani, M.; Archer, D. F.; Baber, R. J.; Davis, S. R.; Gompel, A. A.; Henderson, V. W.; Langer, R.; et al. Updated 2013 International Menopause Society Recommendations on Menopausal Hormone Therapy and Preventive Strategies for Midlife Health. *Climacteric* **2013**, *16* (3), 316–337. https://doi.org/10.3109/13697137.2013.795683.

(106) Moeller, G. Multifunctionality of Human 17β-Hydroxysteroid Dehydrogenases. *Mol. Cell. Endocrinol.* **2006**, *248* (1–2), 47–55. https://doi.org/10.1016/J.MCE.2005.11.031.

(107) Marchais-Oberwinkler, S.; Henn, C.; Möller, G.; Klein, T.; Negri, M.; Oster, A.; Spadaro, A.; Werth, R.; Wetzel, M.; Xu, K.; et al. 17β-Hydroxysteroid Dehydrogenases (17β-HSDs) as Therapeutic Targets: Protein Structures, Functions, and Recent Progress in Inhibitor Development. *J. Steroid Biochem. Mol. Biol.* **2011**, *125* (1–2), 66–82. https://doi.org/10.1016/j.jsbmb.2010.12.013.

(108) Tamaki, Y.; Shiba, E.; Miyoshi, Y.; Noguchi, S.; Taguchi, T.; Ando, A. Involvement of Up-Regulation of 17β-Hydroxysteroid Dehydrogenase Type 1 in Maintenance of Intratumoral High Estradiol Levels in Postmenopausal Breast Cancers. *Int. J. Cancer* **2002**, *94* (5), 685–689. https://doi.org/10.1002/ijc.1525.

(109) Verma, M. K.; Miki, Y.; Abe, K.; Suzuki, T.; Niikawa, H.; Suzuki, S.; Kondo, T.; Sasano, H. Intratumoral Localization and Activity of 17β-Hydroxysteroid Dehydrogenase Type 1 in Non-Small Cell Lung Cancer: A Potent Prognostic Factor. *J. Transl. Med.* **2013**, *11* (1), 167. https://doi.org/10.1186/1479-5876-11-167.

(110) Delvoux, B.; D'Hooghe, T.; Kyama, C.; Koskimies, P.; Hermans, R. J. J.; Dunselman, G. A.; Romano, A. Inhibition of Type 1 17β-Hydroxysteroid Dehydrogenase Impairs the Synthesis of 17β-Estradiol in Endometriosis Lesions. *J. Clin. Endocrinol. Metab.* **2014**, *99* (1), 276–284. https://doi.org/10.1210/jc.2013-2851.

(111) Stanbrough, M.; Bubley, G. J.; Ross, K.; Golub, T. R.; Rubin, M. A.; Penning, T. M.; Febbo, P. G.; Balk, S. P. Increased Expression of Genes Converting Adrenal Androgens to Testosterone in Androgen-Independent Prostate Cancer. *Cancer Res.* **2006**, *66* (5), 2815–2825. https://doi.org/10.1158/0008-5472.CAN-05-4000.

(112) Jansson, A. K.; Gunnarsson, C.; Cohen, M.; Sivik, T.; Stal, O. 17 -Hydroxysteroid Dehydrogenase 14 Affects Estradiol Levels in Breast Cancer Cells and Is a Prognostic Marker in Estrogen Receptor-Positive Breast Cancer. *Cancer Res.* **2006**, *66* (23), 11471–11477. https://doi.org/10.1158/0008-5472.CAN-06-1448.

(113) Martel, C.; Rhéaume, E.; Takahashi, M.; Trudel, C.; Couët, J.; Luu-The, V.; Simard, J.; Labrie, F. Distribution of 17ß-Hydroxysteroid Dehydrogenase Gene Expression and Activity in Rat and Human Tissues. *J. Steroid Biochem. Mol. Biol.* **1992**, *41* (3–8), 597–603. https://doi.org/10.1016/0960-0760(92)90390-5.

(114) Wu, L.; Einstein, M.; Geissler, W. M.; Chan, H. K.; Elliston, K. O.; Andersson, S. Expression Cloning and Characterization of Human 17 Beta-Hydroxysteroid Dehydrogenase Type 2, a Microsomal Enzyme Possessing 20 Alpha-Hydroxysteroid Dehydrogenase Activity. *J. Biol. Chem.* **1993**, *268* (17), 12964–12969.

(115) Tavani, A.; La Vecchia, C. The Adverse Effects of Hormone Replacement Therapy. *Drugs Aging* **1999**, *14* (5), 347–357. https://doi.org/10.2165/00002512-199914050-00003.

(116) Dong, Y.; Qiu, Q. Q.; Debear, J.; Lathrop, W. F.; Bertolini, D. R.; Tamburini, P. P. 17Beta-Hydroxysteroid Dehydrogenases in Human Bone Cells. *J. Bone Miner. Res.* **1998**, *13* (10), 1539–1546. https://doi.org/10.1359/jbmr.1998.13.10.1539.

(117) Verma, R. P.; Hansch, C. Matrix Metalloproteinases (MMPs): Chemical-Biological Functions and (Q)SARs. *Bioorganic and Medicinal Chemistry*. 2007, pp 2223–2268. https://doi.org/10.1016/j.bmc.2007.01.011.

(118) Uttamchandani, M.; Wang, J.; Li, J.; Hu, M.; Sun, H.; Chen, K. Y.-T.; Liu, K.; Yao, S. Q. Inhibitor Fingerprinting of Matrix Metalloproteases Using a Combinatorial Peptide Hydroxamate Library. *J. Am. Chem. Soc.* **2007**, *129* (25), 7848–7858. https://doi.org/10.1021/ja070870h.

(119) Arkadash, V.; Yosef, G.; Shirian, J.; Cohen, I.; Horev, Y.; Grossman, M.; Sagi, I.; Radisky, E. S.; Shifman, J. M.; Papo, N. Development of High-Affinity and High-Specificity Inhibitors of Matrix Metalloproteinase 14 through Computational Design and Directed Evolution. **2017**.

https://doi.org/10.1074/jbc.M116.756718.

(120) Kaimal, R.; Aljumaily, R.; Tressel, S. L.; Pradhan, R. V; Covic, L.; Kuliopulos, A.; Zarwan, C.; Kim, Y. B.; Sharifi, S.; Agarwal, A.; et al. Selective Blockade of Matrix Metalloprotease-14 with a Monoclonal Antibody Abrogates Invasion, Angiogenesis, and Tumor Growth in Ovarian Cancer. *Cancer Res.* **2013**, *73* (8), 2457–2467. https://doi.org/10.1158/0008-5472.CAN-12-1426.

(121) Coussens, L. M.; Fingleton, B.; Matrisian, L. M. Matrix Metalloproteinase Inhibitors and Cancer: Trials and Tribulations. *Science*. American Association for the Advancement of Science March 29, 2002, pp 2387–2392. https://doi.org/10.1126/science.1067100.

(122) Overall, C. M.; Kleifeld, O. Validating Matrix Metalloproteinases as Drug Targets and Anti-Targets for Cancer Therapy. *Nature Reviews Cancer*. Nature Publishing Group March 1, 2006, pp 227–239. https://doi.org/10.1038/nrc1821.

(123) Gomis-Rüth, F. X. Structural Aspects of the Metzincin Clan of Metalloendopeptidases. *Applied Biochemistry and Biotechnology - Part B Molecular Biotechnology*. Humana Press 2003, pp 157–202. https://doi.org/10.1385/MB:24:2:157.

(124) Overall, C. M.; Kleifeld, O. Towards Third Generation Matrix Metalloproteinase Inhibitors for Cancer Therapy. *Br. J. Cancer* **2006**, *94* (7), 941–946. https://doi.org/10.1038/sj.bjc.6603043.

(125) Remacle, A. G.; Golubkov, V. S.; Shiryaev, S. A.; Dahl, R.; Stebbins, J. L.; Chernov, A. V.; Cheltsov, A. V.; Pellecchia, M.; Strongin, A. Y. Novel MT1-MMP Small-Molecule Inhibitors Based on Insights into Hemopexin Domain Function in Tumor Growth. *Cancer Res.* **2012**, *72* (9), 2339–2349. https://doi.org/10.1158/0008-5472.CAN-11-4149.

(126) Poirier, D.; Bydal, P.; Tremblay, M. R.; Sam, K.-M.; Luu-The, V. Inhibitors of Type II 17β-Hydroxysteroid Dehydrogenase. *Mol. Cell. Endocrinol.* **2001**, *171* (1–2), 119–128. https://doi.org/10.1016/S0303-7207(00)00427-5.

(127) Gunn, D.; Akuche, C.; Baryza, J.; Blue, M.-L.; Brennan, C.; Campbell, A.-M.; Choi, S.; Cook, J.; Conrad, P.; Dixon, B.; et al. 4,5-Disubstituted Cis-Pyrrolidinones as Inhibitors of Type II 17beta-Hydroxysteroid Dehydrogenase.

Part 2. SAR. *Bioorg. Med. Chem. Lett.* **2005**, *15* (12), 3053–3057. https://doi.org/10.1016/j.bmcl.2005.04.025.

(128) Wood, J.; Bagi, C. M.; Akuche, C.; Bacchiocchi, A.; Baryza, J.; Blue, M. L.; Brennan, C.; Campbell, A. M.; Choi, S.; Cook, J. H.; et al. 4,5-Disubstituted Cis-Pyrrolidinones as Inhibitors of Type II 17β-Hydroxysteroid Dehydrogenase. Part 3. Identification of Lead Candidate. *Bioorganic Med. Chem. Lett.* **2006**, *16* (18), 4965–4968. https://doi.org/10.1016/j.bmcl.2006.06.041.

(129) Bagi, C. M.; Wood, J.; Wilkie, D.; Dixon, B. Effect of 17β-Hydroxysteroid Dehydrogenase Type 2 Inhibitor on Bone Strength in Ovariectomized Cynomolgus Monkeys. *J. Musculoskelet. Neuronal Interact.* **2008**, *8* (3), 267–280.

(130) Wetzel, M.; Marchais-Oberwinkler, S.; Perspicace, E.; Möller, G.; Adamski, J.; Hartmann, R. W. Introduction of an Electron Withdrawing Group on the Hydroxyphenylnaphthol Scaffold Improves the Potency of 17β-Hydroxysteroid Dehydrogenase Type 2 (17β-HSD2) Inhibitors. *J. Med. Chem.* **2011**, *54* (21), 7547–7557. https://doi.org/10.1021/jm2008453.

(131) Perspicace, E.; Giorgio, A.; Carotti, A.; Marchais-Oberwinkler, S.; Hartmann, R. W. Novel N-Methylsulfonamide and Retro-N-Methylsulfonamide Derivatives as 17β-Hydroxysteroid Dehydrogenase Type 2 (17β-HSD2) Inhibitors with Good ADME-Related Physicochemical Parameters. *Eur. J. Med. Chem.* **2013**, *69*, 201–215. https://doi.org/10.1016/j.ejmech.2013.08.026.

(132) Gargano, E. M.; Allegretta, G.; Perspicace, E.; Carotti, A.; Van Koppen, C.; Frotscher, M.; Marchais-Oberwinkler, S.; Hartmann, R. R. W. 17β-Hydroxysteroid Dehydrogenase Type 2 Inhibition: Discovery of Selective and Metabolically Stable Compounds Inhibiting Both the Human Enzyme and Its Murine Ortholog. *PLoS One* **2015**, *10* (7), 1–19. https://doi.org/10.1371/journal.pone.0134754.

(133) Oster, A.; Hinsberger, S.; Werth, R.; Marchais-Oberwinkler, S.; Frotscher, M.; Hartmann, R. W. Bicyclic Substituted Hydroxyphenylmethanones as Novel Inhibitors of 17β-Hydroxysteroid Dehydrogenase Type 1 (17β-HSD1) for the Treatment of Estrogen-Dependent Diseases. *J. Med. Chem.* **2010**, *53*, 8176–8186. https://doi.org/10.1021/jm101073q.

(134) Abdelsamie, A. S.; Bey, E.; Gargano, E. M.; van Koppen, C. J.; Empting, M.; Frotscher, M. Towards the Evaluation in an Animal Disease Model: Fluorinated 17β-HSD1 Inhibitors Showing Strong Activity towards Both the Human and the Rat Enzyme. *Eur. J. Med. Chem.* **2015**, *103*, 56–68. https://doi.org/10.1016/j.ejmech.2015.08.030.

(135) Rajabi, M.; Mousa, S. A. The Role of Angiogenesis in Cancer Treatment. *Biomedicines* **2017**, *5* (2). https://doi.org/10.3390/biomedicines5020034.

(136) Abdalla, A. M. E.; Xiao, L.; Ullah, M. W.; Yu, M.; Ouyang, C.; Yang, G. Current Challenges of Cancer Anti-Angiogenic Therapy and the Promise of Nanotherapeutics. *Theranostics* **2018**, *8* (2), 533–548. https://doi.org/10.7150/thno.21674.

(137) Sela-Passwell, N.; Rosenblum, G.; Shoham, T.; Sagi, I. Structural and Functional Bases for Allosteric Control of MMP Activities: Can It Pave the Path for Selective Inhibition? *Biochimica et Biophysica Acta - Molecular Cell Research*. Elsevier January 1, 2010, pp 29–38. https://doi.org/10.1016/j.bbamcr.2009.04.010.

(138) Evensen, N. A.; Li, J.; Yang, J.; Yu, X.; Sampson, N. S.; Zucker, S.; Cao, J.; Hanahan, D.; Weinberg, R.; Normanno, N.; et al. Development of a High-Throughput Three-Dimensional Invasion Assay for Anti-Cancer Drug Discovery. *PLoS One* **2013**, *8* (12), e82811. https://doi.org/10.1371/journal.pone.0082811.

(139) Itoh, Y.; Takamura, A.; Ito, N.; Maru, Y.; Sato, H.; Suenaga, N.; Aoki, T.; Seiki, M. Homophilic Complex Formation of MT1-MMP Facilitates ProMMP-2 Activation on the Cell Surface and Promotes Tumor Cell Invasion. *EMBO J.* **2001**, *20* (17), 4782–4793. https://doi.org/10.1093/emboj/20.17.4782.

(140) Pearson, J. R. D.; Regad, T. Targeting Cellular Pathways in Glioblastoma Multiforme. *Signal Transduct. Target. Ther.* **2017**, *2*, 17040. https://doi.org/10.1038/sigtrans.2017.40.

(141) Rivera, S.; Khrestchatisky, M.; Kaczmarek, L.; Rosenberg, G. A.; Jaworski, D. M. Metzincin Proteases and Their Inhibitors: Foes or Friends in Nervous System Physiology? *J. Neurosci.* **2010**, *30* (46), 15337–15357. https://doi.org/10.1523/JNEUROSCI.3467-10.2010.

(142) Levin, M.; Udi, Y.; Solomonov, I.; Sagi, I. Next Generation Matrix Metalloproteinase Inhibitors — Novel Strategies Bring New Prospects. *Biochimica et Biophysica Acta - Molecular Cell Research*. Elsevier November 1, 2017, pp 1927–1939. https://doi.org/10.1016/j.bbamcr.2017.06.009.

(143) Moore, B. A.; Aznavoorian, S.; Engler, J. A.; Windsor, L. J. Induction of Collagenase-3 (MMP-13) in Rheumatoid Arthritis Synovial Fibroblasts. *Biochim. Biophys. Acta - Mol. Basis Dis.* **2000**, *1502* (2), 307–318. https://doi.org/10.1016/S0925-4439(00)00056-9.

(144) Wang, M.; Sampson, E. R.; Jin, H.; Li, J.; Ke, Q. H.; Im, H.-J.; Chen, D. MMP13 Is a Critical Target Gene during the Progression of Osteoarthritis. *Arthritis Res. Ther.* **2013**, *15* (1), R5. https://doi.org/10.1186/AR4133.

(145) Ghayee, H. K.; Auchus, R. J. Basic Concepts and Recent Developments in Human Steroid Hormone Biosynthesis. *Rev. Endocr. Metab. Disord.* **2007**, *8* (4), 289–300. https://doi.org/10.1007/s11154-007-9052-2.

(146) Broersen, L. H. A.; Pereira, A. M.; Jørgensen, J. O. L.; Dekkers, O. M. Adrenal Insufficiency in Corticosteroids Use: Systematic Review and Meta-Analysis. *J. Clin. Endocrinol. Metab.* **2015**, *100* (6), 2171–2180. https://doi.org/10.1210/jc.2015-1218.

(147) Chen, C.-L.; Weiss, N. S.; Newcomb, P.; Barlow, W.; White, E. Hormone Replacement Therapy in Relation to Breast Cancer. *JAMA* **2002**, *287* (6), 734–741.

(148) Lu, M.-L.; Huang, Y.-W.; Lin, S.-X. Purification, Reconstitution, and Steady-State Kinetics of the Trans-Membrane 17β-Hydroxysteroid Dehydrogenase 2. *J. Biol. Chem.* **2002**, *277* (25), 22123–22130. https://doi.org/10.1074/JBC.M111726200.

(149) Abdelsamie, A.S. van Koppen, C.J. Bey, E.; Salah, M.; Börger, C.; Siebenbürger, L.; Laschke, M. W.; Menger, M. D.; Frotscher, M. Treatment of Estrogen-Dependent Diseases: Design, Synthesis and Profiling of a Selective 17β-HSD1 Inhibitor with Sub-Nanomolar IC50 for a Proof-of-Principle Study. *Eur. J. Med. Chem.* **2017**, *127*, 944–957. https://doi.org/10.1016/j.ejmech.2016.11.004.

(150) Miettinen, M. M.; Mustonen, M. V. J.; Poutanen, M. H.; Isomaa, V. V; Vihko, R. K. Human 17β-Hydroxysteroid Dehydrogenase Type 1 and Type 2 Isoenzymes Have Opposite Activities in Cultured Cells and Characteristic Cell-and Tissue-Specific Expression. *Biochem. J* **1996**, *314* (3), 839–845. https://doi.org/10.1042/bj3140839.

(151) Oster, A.; Klein, T.; Henn, C.; Werth, R.; Marchais-Oberwinkler, S.; Frotscher, M.; Hartmann, R. W. Bicyclic Substituted Hydroxyphenylmethanone Type Inhibitors of 17β-Hydroxysteroid Dehydrogenase Type1 (17β-HSD1): The Role of the Bicyclic Moiety. *ChemMedChem* **2011**, *6*, 476–487. https://doi.org/10.1002/cmdc.201000457.

(152) Histing, T.; Andonyan, A.; Klein, M.; Scheuer, C.; Stenger, D.; Holstein, J. H.; Veith, N. T.; Pohlemann, T.; Menger, M. D. Obesity Does Not Affect the Healing of Femur Fractures in Mice. *Injury* **2016**, *47* (7), 1435–1444. https://doi.org/10.1016/j.injury.2016.04.030.

(153) Histing, T.; Garcia, P.; Holstein, J. H.; Klein, M.; Matthys, R.; Nuetzi, R.; Steck, R.; Laschke, M. W.; Wehner, T.; Bindl, R.; et al. Small Animal Bone Healing Models: Standards, Tips, and Pitfalls Results of a Consensus Meeting. *Bone* **2011**, *49* (4), 591–599. https://doi.org/10.1016/j.bone.2011.07.007.

(154) Wada, T.; Nakashima, T.; Hiroshi, N.; Penninger, J. M. RANKL-RANK Signaling in Osteoclastogenesis and Bone Disease. *Trends Mol. Med.* **2006**, *12* (1), 17–25. https://doi.org/10.1016/j.molmed.2005.11.007.

(155) Jackson, A. C.; Tenniswood, M.; Bird, C. E.; Clark, A. F. Effects of Androgen and Estradiol Administration on the Weight of the Ventral Prostate, Seminal Vesicles, and Testes of Immature Rats. *Invest. Urol.* **1977**, *14* (5), 351–355.

(156) Riggs, B. L.; Khosla, S.; Melton, L. J. A Unitary Model for Involutional Osteoporosis: Estrogen Deficiency Causes Both Type I and Type II Osteoporosis in Postmenopausal Women and Contributes to Bone Loss in Aging Men. *J. Bone Miner. Res.* **1998**, *13* (5), 763–773. https://doi.org/10.1359/jbmr.1998.13.5.763.

6. Supporting Information

6.1. Supporting Information for Publication I (Chapter II)

Supporting Information (SI)

Targeted Endocrine Therapy: Design, Synthesis and *Proof-of-Principle* of 17ß-Hydroxysteroid Dehydrogenase Type 2 Inhibitors in Bone Fracture Healing

Ahmed S. Abdelsamie, Steven Herath, Yannik Biskupek, Carsten Börger, Lorenz Siebenbürger, Mohamed Salah, Claudia Scheuer, Sandrine Marchais-Oberwinkler, Martin Frotscher, Tim Pohlemann, Michael D. Menger, Rolf W. Hartmann, Matthias W. Laschke, Chris J. van Koppen

Table of contents

Page

1. Synthesis of intermediates 2b, 4b-8b and 2a-8a S2

2. NMR spectra, HRMS, LC.MS of compounds 1-16, 8a and 8b S6

3. Experimental biological results S67

1. Synthesis of intermediates 2b, 4b-8b and 2a-8a

(5-Bromothiophen-2-yl)(2-fluoro-3-methoxyphenyl)methanone (2b). The title compound was prepared by reaction of 2-bromothiophene (650 mg, 3.97 mmol), 2-fluoro-3-methoxybenzoyl chloride (500 mg, 2.65 mmol) and aluminum chloride (353 mg, 2.65 mmol) according to method A. The crude product was used directly in the subsequent reaction without further purification [700 mg; MS (ESI): *m/z* 314.9 $(M+H)^+$, $C_{12}H_9BrFO_2S^+$ Calcd 314.9].

[5-(3-Aminophenyl)thiophen-2-yl](2-fluoro-3-methoxyphenyl)methanone (2a). The title compound was prepared by reaction of (5-bromothiophen-2-yl)(2-fluoro-3-methoxyphenyl)methanone **(2b)** (700 mg, 2.35 mmol) and 3-aminophenylboronic acid (387 mg, 2.82 mmol), cesium carbonate (3063 mg, 9.40 mmol) and tetrakis(triphenylphosphine) palladium (136 mg, 118 μmol) according to method B. The product was purified by CC (petroleum ether/ethyl acetate 2:1); yield: 88% (640 mg). ^{1}H NMR (500 MHz, acetone-d_6) δ 7.53 (dd, *J* = 4.0, 1.6 Hz, 1H), 7.46 (d, *J* = 4.0 Hz, 1H), 7.36 (td, *J* = 8.2, 1.6 Hz, 1H), 7.29 (td, *J* = 8.0, 1.2 Hz, 1H), 7.19 – 7.11 (m, 2H), 7.09 (t, *J* = 2.0 Hz, 1H), 7.01 (ddd, *J* = 7.6, 1.7, 0.9 Hz, 1H), 6.74 (ddd, *J* = 8.0, 2.2, 0.8 Hz, 1H), 4.91 (s, 2H), 3.96 (s, 3H). MS (ESI): *m/z* 328.1 $(M+H)^+$, $C_{18}H_{15}FNO_2S^+$ Calcd 328.0.

(5-Bromothiophen-2-yl)(2-chloro-3-methoxyphenyl)methanone (3b). 2-Chloro-3-methoxy-benzoic acid (400 mg, 2.14 mmol, 1 equiv.) was dissolved in thionyl chloride (4320 mg, 36.4 mmol, 17 equiv.) and stirred under reflux for 1 h. The solution was concentrated in vacuum and the crude product was reacted with 2-bromothiophene (523 mg, 3.21 mmol) and aluminium chloride (285 mg, 2.14 mmol) according to method A. In slight variation, the mixture was stirred at room temperature overnight. The crude product was used directly in the subsequent reaction without further purification [500 mg; MS (ESI): *m/z* 330.96 $(M+H)^+$, $C_{12}H_9BrClO_2S^+$ Calcd 330.9].

(5-Bromothiophen-2-yl)(4-chloro-3-methoxyphenyl)methanone (4b). 4-Chloro-3-methoxy-benzoic acid (600 mg, 3.21 mmol, 1 equiv.) was dissolved in thionyl chloride (6500 mg, 54.6 mmol, 17 equiv.) and stirred under reflux for 1 h. The solution was concentrated under reduced pressure and the crude product was reacted with 2-bromothiophene (785 mg, 4.81 mmol) and aluminum chloride (428 mg, 3.21 mmol) according to method A. In slight variation, the mixture was stirred at room temperature overnight. The crude product was used directly in the subsequent reaction without further purification [500 mg; MS (ESI): *m/z* 330.9 $(M+H)^+$, $C_{12}H_9BrClO_2S^+$ Calcd 330.9].

[5-(3-Aminophenyl)thiophen-2-yl](4-chloro-3-methoxyphenyl)methanone (4a). The title compound was prepared by reaction of (5-bromothiophen-2-yl)(4-chloro-3-methoxyphenyl)methanone **(4b)** (500 mg, 1.50 mmol) and 3-aminophenylboronic acid (248 mg, 1.80 mmol), cesium carbonate (1955 mg, 6.00 mmol) and tetrakis(triphenylphosphine) palladium (87 mg, 75 µmol) according to method B. The product was purified by CC (petroleum ether/ethyl acetate 3:1); yield: 89% (450 mg). ^{1}H NMR (500 MHz, acetone-d_6) δ 7.74 (d, J = 4.0 Hz, 1H), 7.59 (d, J = 8.1 Hz, 1H), 7.53 (d, J = 1.8 Hz, 1H), 7.48 (td, J = 2.9, 2.0 Hz, 2H), 7.16 (t, J = 7.8 Hz, 1H), 7.10 (t, J = 2.0 Hz, 1H), 7.02 (ddd, J = 7.6, 1.6, 0.9 Hz, 1H), 6.74 (ddd, J = 8.0, 2.2, 0.7 Hz, 1H), 4.91 (s, 2H), 4.02 (s, 3H). MS (ESI): *m/z* 344.1 $(M+H)^+$, $C_{18}H_{15}ClNO_2S^+$ Calcd 344.0.

(5-Bromothiophene-2-yl)-(3-methoxy-2,6-difluorophenyl)methanone (5b). The title compound was prepared by reaction of 2-bromothiophene (333 mg, 2.04 mmol), 2,6-difluoro-4-methoxybenzoyl chloride (280 mg, 1.36 mmol) and aluminum chloride (180 mg, 1.36 mmol) according to method A. The crude product was used directly in the subsequent reaction without further purification [430 mg; MS (ESI): *m/z* 332.9 $(M+H)^+$, $C_{12}H_8BrF_2O_2S^+$ Calcd 332.9].

[5-(3-Aminophenyl)thiophene-2-yl](3-methoxy-2,6-difluorophenyl)methanone (5a). The title compound was prepared by reaction of (5-bromothiophene-2-yl)(3-methoxy-2,6-difluorophenyl)methanone **(5b)** (430 mg, 1.30 mmol) and 3-aminophenylboronic acid (213 mg, 1.55 mmol), cesium carbonate (1689 mg, 5.18 mmol) and tetrakis(triphenylphosphine) palladium (75 mg, 65 µmol) according to method B. The product was purified by CC (petroleum ether/ethyl acetate 2:1); yield: 89% (390 mg). ^{1}H NMR (500 MHz, acetone-d_6) δ 7.58 (d, J = 4.0 Hz, 1H), 7.48 (d, J = 4.1 Hz, 1H), 7.36 (td, J = 9.4, 5.2 Hz, 1H), 7.19 – 7.11 (m, 2H), 7.10 (t, J = 2.0 Hz, 1H), 7.02 (d, J = 7.6 Hz, 1H), 6.76 (dd, J = 8.0, 1.7 Hz, 1H), 4.93 (s, 2H), 3.95 (s, 3H). MS (ESI): *m/z* 346.1 $(M+H)^+$, $C_{18}H_{14}F_2NO_2S^+$ Calcd 346.0.

(5-Bromothiophen-2-yl)(6-chloro-2-fluoro-3-methoxyphenyl)methanone (6b). The title compound was prepared by reaction of 2-bromothiophene (450 mg, 2.76 mmol), 6-chloro-2-fluoro-3-methoxybenzoyl chloride (412 mg, 1.84 mmol) and aluminum chloride (246 mg, 1.84 mmol) according to method A. The crude product was used directly in the subsequent reaction without further purification [500 mg; MS (ESI): *m/z* 348.9 $(M+H)^+$, $C_{12}H_8BrClFO_2S^+$ Calcd 348.9].

[5-(3-Aminophenyl)thiophen-2-yl](6-chloro-2-fluoro-3-methoxyphenyl)methanone (6a). The title compound was prepared by reaction of (5-bromothiophen-2-yl)(6-chloro-2-fluoro-3-methoxyphenyl)methanone **(6b)** (500 mg, 1.43 mmol) and 3-aminophenylboronic acid (235 mg, 1.71 mmol), cesium carbonate (1864 mg, 5.72 mmol) and tetrakis(triphenylphosphine) palladium (83 mg, 72 μmol) according to method B. The product was purified by CC (petroleum ether/ethyl acetate 1:1); yield: 73% (380 g). ^1H NMR (500 MHz, acetone-d_6) δ 7.51 (d, *J* = 4.0 Hz, 1H), 7.47 (d, *J* = 4.1 Hz, 1H), 7.38 – 7.30 (m, 2H), 7.16 (t, *J* = 7.8 Hz, 1H), 7.09 (t, *J* = 2.0 Hz, 1H), 7.02 (ddd, *J* = 7.6, 1.6, 0.9 Hz, 1H), 6.75 (ddd, *J* = 8.1, 2.2, 0.8 Hz, 1H), 4.92 (s, 2H), 3.97 (s, 3H). MS (ESI): *m/z* 362.1 $(M+H)^+$, $C_{18}H_{14}ClFNO_2S^+$ Calcd 362.0.

(5-Bromothiophen-2-yl)(2-chloro-6-fluoro-3-methoxyphenyl)methanone (7b). The title compound was prepared by reaction of 2-bromothiophene (450 mg, 2.76 mmol), 2-chloro-6-fluoro-3-methoxybenzoyl chloride (412 mg, 1.84 mmol) and aluminum chloride (246 mg, 1.84 mmol) according to method A. The crude product was used directly in the subsequent reaction without further purification [500 mg; MS (ESI): *m/z* 348.9 $(M+H)^+$, $C_{12}H_8BrClFO_2S^+$ Calcd 348.9].

[5-(3-aminophenyl)thiophen-2-yl](2-chloro-6-fluoro-3-methoxyphenyl)methanone (7a). The title compound was prepared by reaction of (5-bromothiophen-2-yl)(2-chloro-6-fluoro-3-methoxyphenyl)methanone **(7b)** (500 mg, 1.43 mmol) and 3-aminophenylboronic acid (235 mg, 1.71 mmol), cesium carbonate (1864 mg, 5.72 mmol) and tetrakis(triphenylphosphine) palladium (83 mg, 72 μmol) according to method B. The product was purified by CC (petroleum ether/ethyl acetate 1:1); yield: 86% (450 g). ^1H NMR (500 MHz, acetone-d_6) δ 7.49 (d, *J* = 4.1 Hz, 1H), 7.46 (d, *J* = 4.1 Hz, 1H), 7.32 – 7.28 (m, 2H), 7.16 (t, *J* = 7.8 Hz, 1H), 7.09 (t, *J* = 2.0 Hz, 1H), 7.01 (ddd, *J* = 7.6, 1.7, 0.9 Hz, 1H), 6.75 (ddd, *J* = 8.0, 2.2, 0.9 Hz, 1H), 3.97 (s, 3H). MS (ESI): *m/z* 362.0 $(M+H)^+$, $C_{18}H_{14}ClFNO_2S^+$ Calcd 362.0.

(5-Bromo-thiophen-2-yl)-(2,4,5-trifluoro-3-methoxy-phenyl)-methanone (8b). The title compound was prepared by reaction of 2-bromothiophene (3000 mg, 18.4 mmol), 2,4,5-trifluoro-3-methoxy-benzoyl chloride (4132 mg, 18.4 mmol) and aluminium chloride (2453 mg, 18.4 mmol) according to method A. The product was purified by CC (petroleum ether/ethyl acetate 97:3), yield 75% (5845 mg). ^1H NMR (500 MHz, acetone-d_6) δ 7.54 (dd, *J*

= 4.1, 1.9 Hz, 1H), 7.39 – 7.32 (m, 2H), 4.11 (t, *J* = 1.2 Hz, 3H). ^{13}C NMR (125 MHz, acetone-*d6*) δ 181.8, 151.3 – 149.2 (m), 148.1 (ddd, *J* = 246.2, 11.6, 3.3 Hz), 147.0 (ddd, *J* = 253.4, 15.0, 5.5 Hz), 145.5, 139.2 (ddd, *J* = 15.5, 11.1, 2.3 Hz), 137.8 (d, *J* = 2.4 Hz), 133.3, 124.9, 122.9 (ddd, *J* = 15.9, 6.4, 4.0 Hz), 62.7 (t, *J* = 3.5 Hz). ^{19}F NMR (470 MHz, acetone-d_6) δ -76.5 ($CF_{3,\ \mathrm{TFA}}$), -131.2 – -135.3 (m), -139.9 – -142.0 (m), -147.7 (dt, *J* = 20.3, 9.0 Hz). MS (ESI): *m/z* 350.9 (M+H)$^+$, $C_{12}H_7BrF_3O_2S^+$ Calcd 350.9.

[5-(3-Aminophenyl)-thiophen-2-yl](2,4,5-trifluoro-3-methoxyphenyl)methanone (8a). The title compound was prepared by reaction of (5-bromothiophen-2-yl) (2,4,5-trifluoro-3-methoxyphenyl)methanone **(8b)** (1000 mg, 2.85 mmol) and 3-aminophenylboronic acid (468 mg, 3.42 mmol), cesium carbonate (3712 mg, 11.39 mmol) and tetrakis(triphenylphosphine) palladium (165 mg, 143 µmol) according to method B. The product was purified by CC (petroleum ether/ethyl acetate 7:3); yield: 90% (930 mg). ^{1}H NMR (500 MHz, acetone-d_6) δ 7.64 (dd, *J* = 4.0, 1.8 Hz, 1H), 7.47 (d, *J* = 4.1 Hz, 1H), 7.36 (ddd, *J* = 9.9, 8.3, 5.7 Hz, 1H), 7.16 (t, *J* = 7.8 Hz, 1H), 7.10 (t, *J* = 2.0 Hz, 1H), 7.02 (ddd, *J* = 7.6, 1.7, 0.9 Hz, 1H), 6.75 (ddd, *J* = 8.1, 2.2, 0.8 Hz, 1H), 4.92 (s, 2H), 4.11 (t, *J* = 1.0 Hz, 3H). ^{13}C NMR (126 MHz, acetone-d_6) δ 149.3, 149.2 (ddd, *J* = 248.5, 7.4, 3.9 Hz), 147.1 (ddd, *J* = 245.9, 11.5, 3.1 Hz), 145.8 (ddd, *J* = 252.7, 15.2, 5.5 Hz), 138.2 (ddd, *J* = 16.0, 11.3, 2.2 Hz), 137.5 (d, *J* = 2.5 Hz), 133.5, 129.9, 124.9, 124.2, 122.9 (ddd, *J* = 16.4, 6.3, 4.2 Hz), 120.7 (d, *J* = 1.3 Hz), 116.9, 115.6, 114.6, 111.5, 110.1 (dt, *J* = 20.7, 3.4 Hz), 61.8 (t, *J* = 3.5 Hz). ^{19}F NMR (470 MHz, acetone-*d6*) δ -76.5 ($CF_{3,\ \mathrm{TFA}}$), -133.3 – -135.8 (m), -140.9 – -141.0 (m), -147.9 – -148.1 (m). MS (ESI): *m/z* 364.1 (M+H)$^+$, $C_{18}H_{13}F_3NO_2S^+$ Calcd 364.0.

2. NMR spectra, HRMS, LC.MS of compounds 1-16, 8a and 8b

^{1}H, ^{13}C spectra, HRMS, and LC.MS of Compound 1.

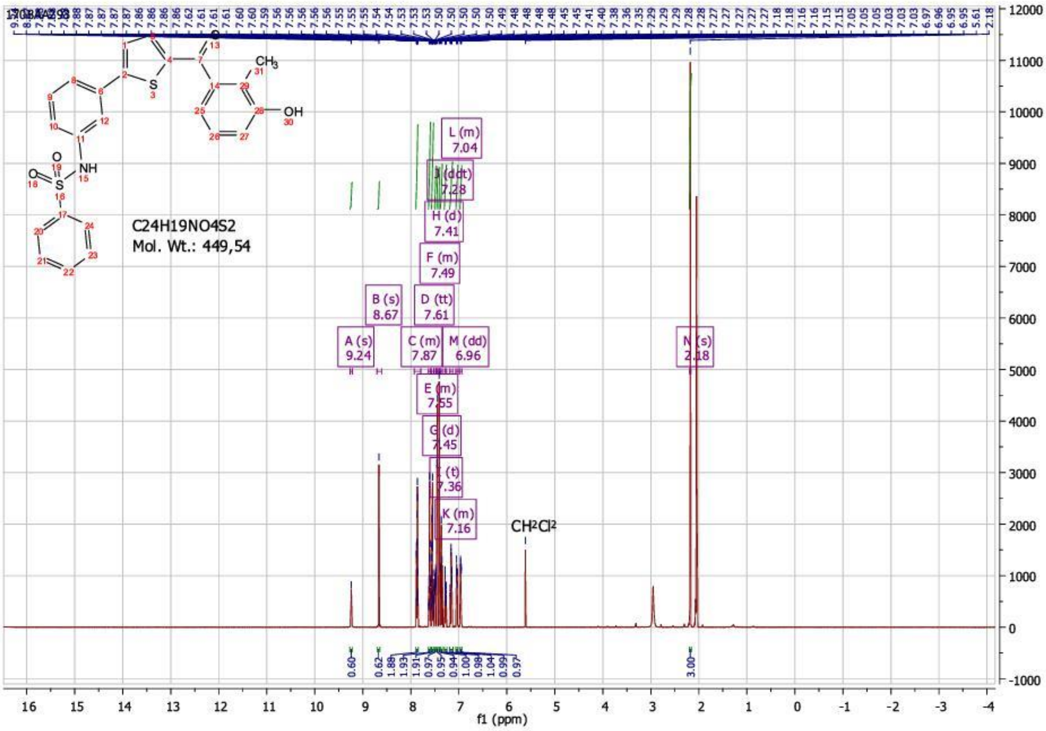

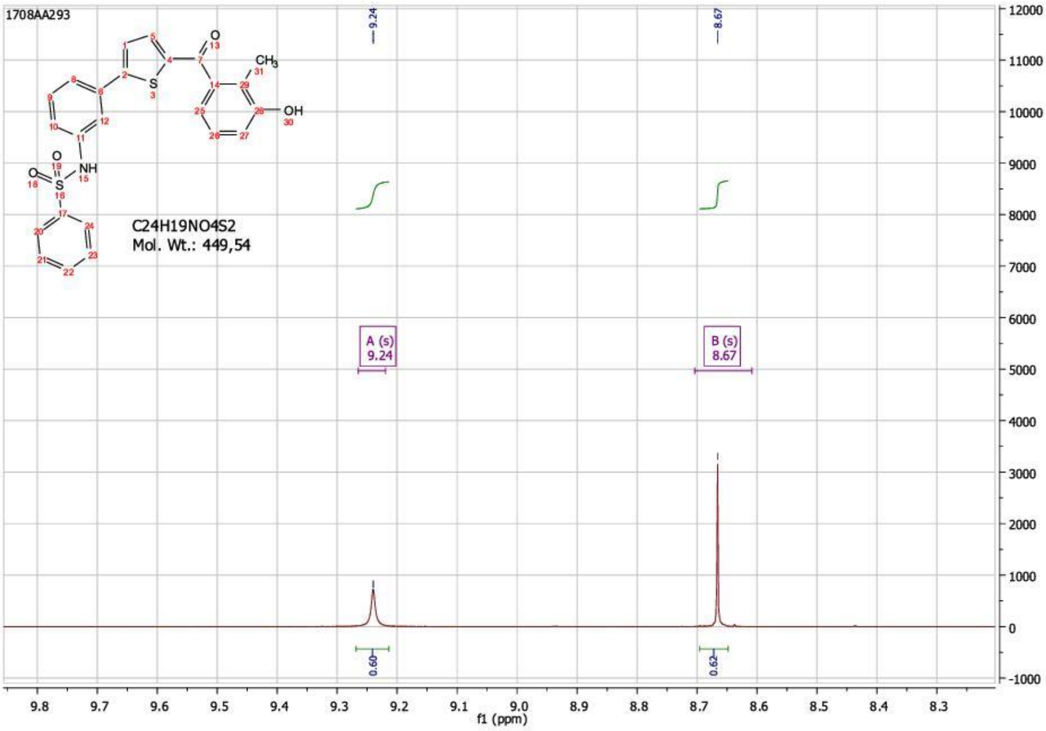

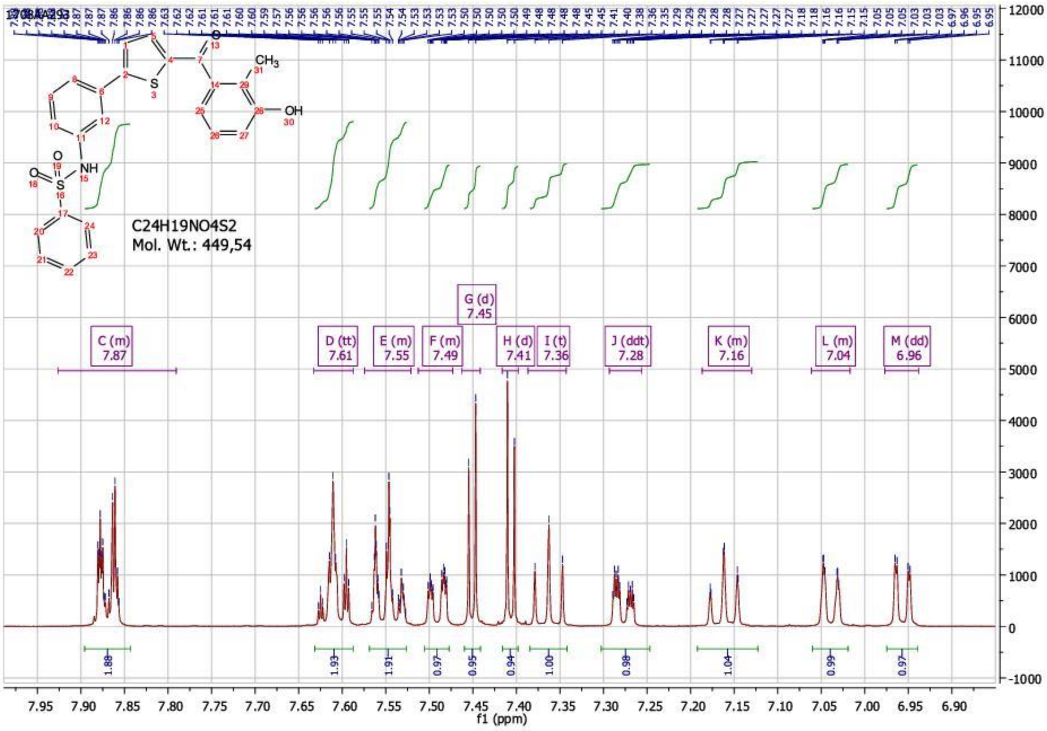
1708AA293
7.87
7.87
7.87
7.86
7.86
7.86
7.86
7.63
7.62
7.62
7.61
7.61
7.61
7.60
7.60
7.59
7.57
7.56
7.56
7.56
7.56
7.56
7.55
7.55
7.55
7.54
7.54
7.53
7.53
7.53
7.53
7.50
7.50
7.50
7.50
7.50
7.49
7.48
7.48
7.48
7.48
7.45
7.45
7.41
7.40
7.38
7.36
7.35
7.29
7.29
7.29
7.28
7.28
7.27
7.27
7.27
7.27
7.27
7.18
7.18
7.16
7.16
7.15
7.15
7.05
7.05
7.05
7.03
7.03
7.03
6.97
6.96
6.95
6.95
O
13
CH3
31
OH
30
S
3
1
2
4
5
7
6
8
9
10
11
12
14
25
26
27
28
29
O
19
NH
15
O
18
S
16
17
20
21
22
23
24
C24H19NO4S2
Mol. Wt.: 449,54
C (m)
7.87
D (tt)
7.61
E (m)
7.55
F (m)
7.49
G (d)
7.45
H (d)
7.41
I (t)
7.36
J (ddt)
7.28
K (m)
7.16
L (m)
7.04
M (dd)
6.96
1.88
1.93
1.91
0.97
0.95
0.94
1.00
0.98
1.04
0.99
0.97
12000
11000
10000
9000
8000
7000
6000
5000
4000
3000
2000
1000
0
-1000
7.95
7.90
7.85
7.80
7.75
7.70
7.65
7.60
7.55
7.50
7.45
7.40
7.35
7.30
7.25
7.20
7.15
7.10
7.05
7.00
6.95
6.90
f1 (ppm)

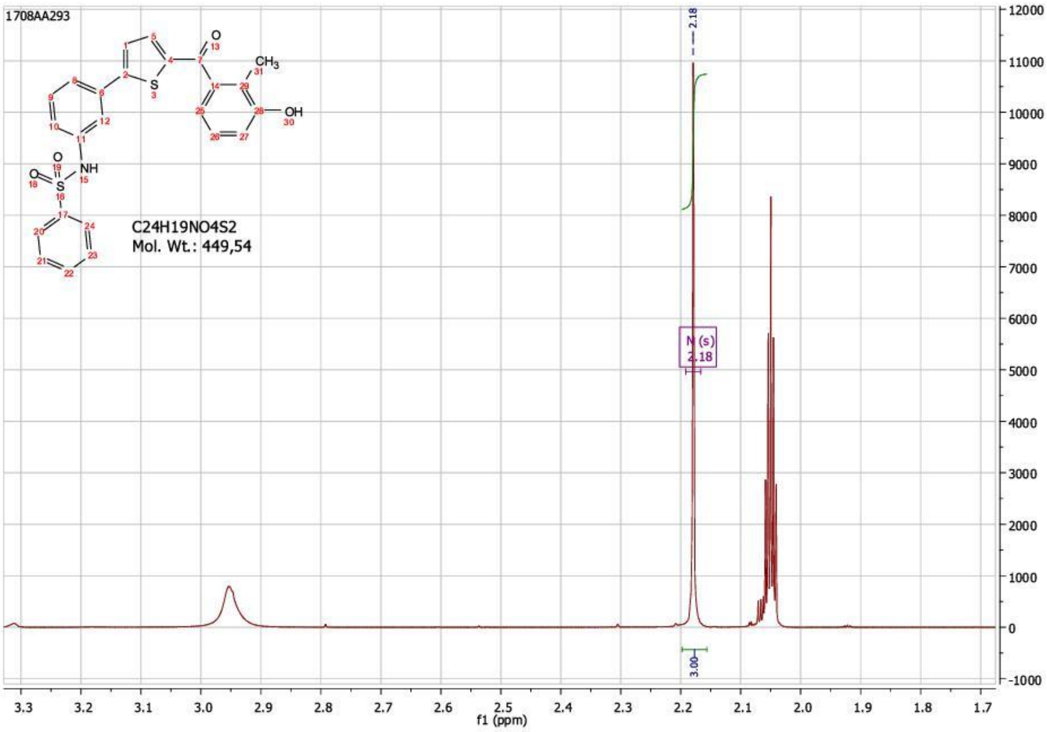
1708AA293
2.18
O
13
CH3
31
OH
30
S
3
1
2
4
5
7
6
8
9
10
11
12
14
25
26
27
28
29
O
19
NH
15
O
18
S
16
17
20
21
22
23
24
C24H19NO4S2
Mol. Wt.: 449,54
N (s)
2.18
3.00
12000
11000
10000
9000
8000
7000
6000
5000
4000
3000
2000
1000
0
-1000
3.3
3.2
3.1
3.0
2.9
2.8
2.7
2.6
2.5
2.4
2.3
2.2
2.1
2.0
1.9
1.8
1.7
f1 (ppm)

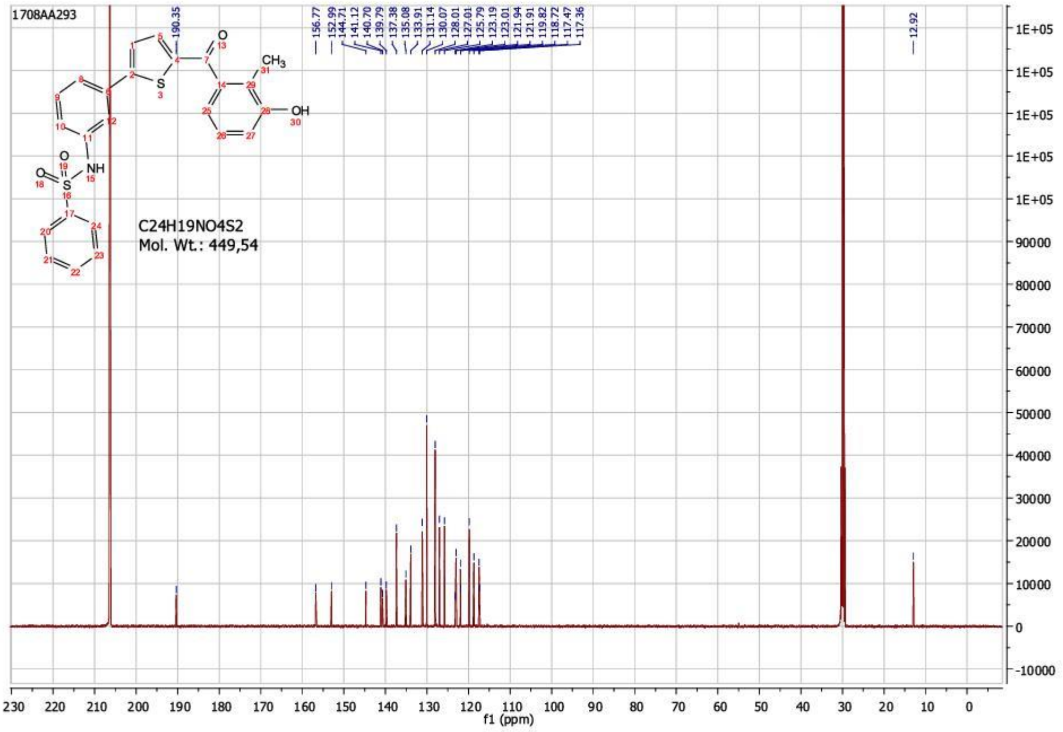
1708AA293
190.35
156.77
152.99
144.71
141.12
140.70
139.79
137.38
135.08
133.91
131.14
130.07
128.01
127.01
125.79
123.19
123.01
121.94
121.91
119.82
118.72
117.47
117.36
12.92
O
CH3
OH
S
NH
O
O
S
1
2
3
4
5
6
7
8
9
10
11
12
13
14
15
16
17
18
19
20
21
22
23
24
25
26
27
28
29
30
31
C24H19NO4S2
Mol. Wt.: 449,54
1E+05
1E+05
1E+05
1E+05
1E+05
90000
80000
70000
60000
50000
40000
30000
20000
10000
0
-10000
230 220 210 200 190 180 170 160 150 140 130 120 110 100 90 80 70 60 50 40 30 20 10 0
f1 (ppm)

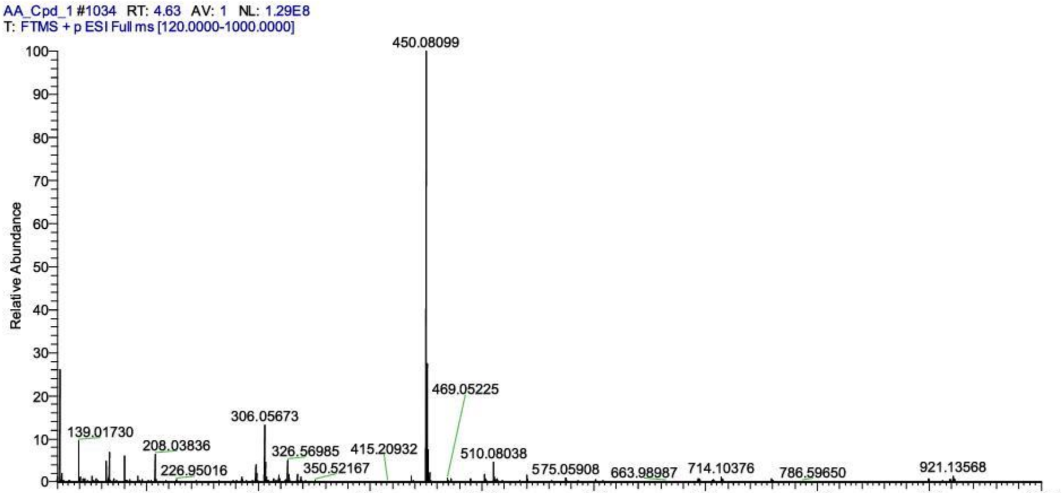
AA_Cpd_1 #1034 RT: 4.63 AV: 1 NL: 1.29E8
T: FTMS + p ESI Full ms [120.0000-1000.0000]
450.08099
469.05225
306.05673
139.01730
208.03836
326.56985
415.20932
510.08038
226.95016
350.52167
575.05908
663.98987
714.10376
786.59650
921.13568
Relative Abundance
100
90
80
70
60
50
40
30
20
10
0
200
300
400
500
600
700
800
900
1000
m/z

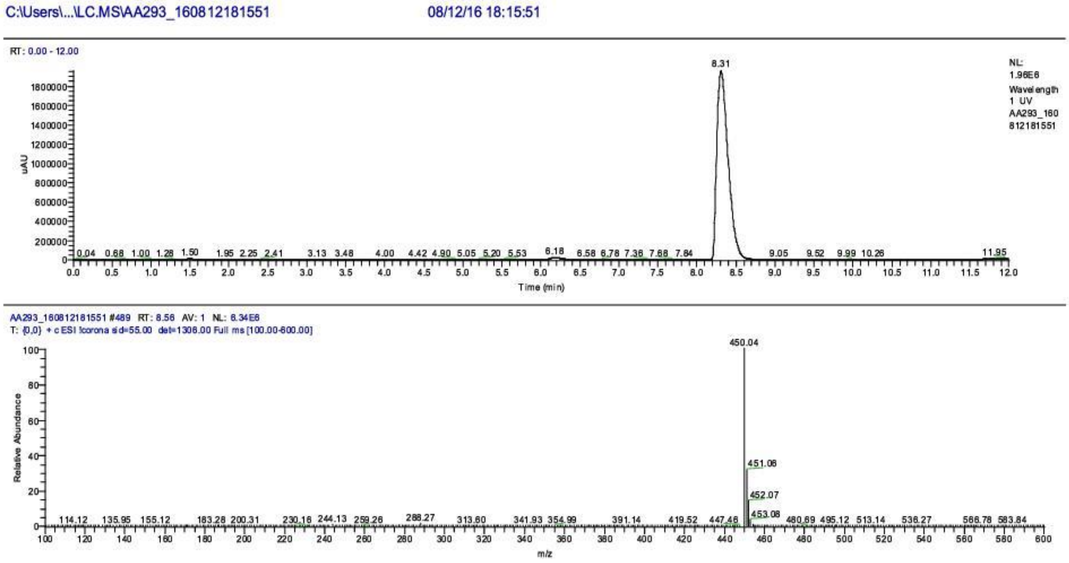

^{1}H, ^{13}C spectra, HRMS, and LC.MS of Compound 2.

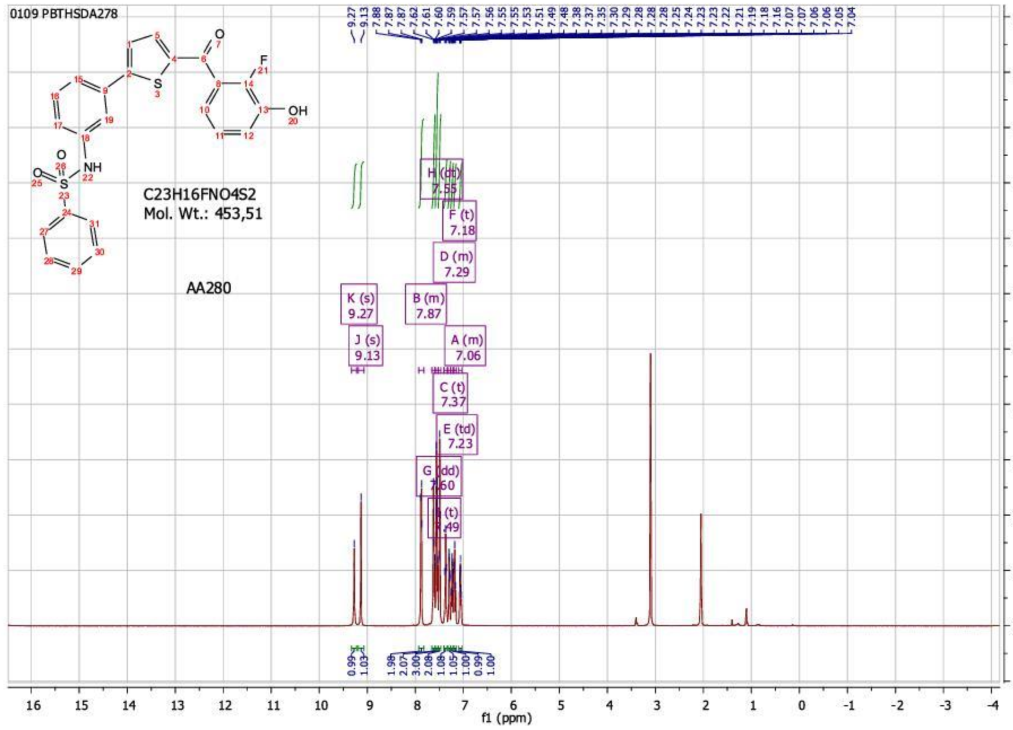

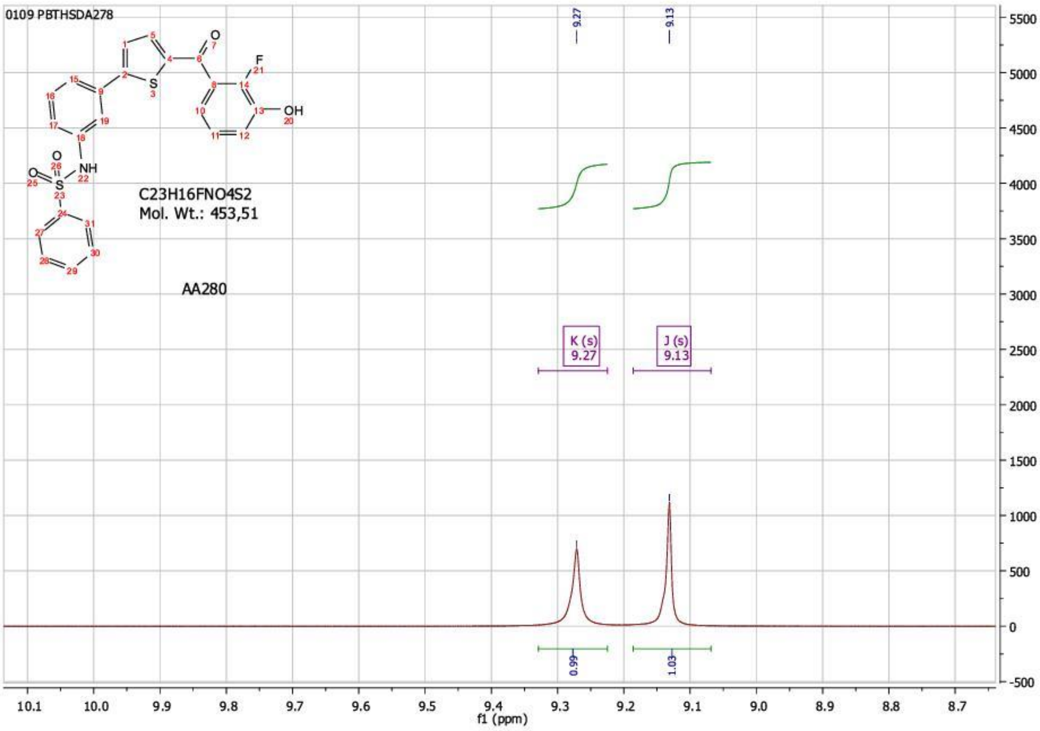
0109 PBTHSDA278
C23H16FNO4S2
Mol. Wt.: 453,51
AA280
9.27
9.13
K (s)
9.27
J (s)
9.13
0.99
1.03
f1 (ppm)
10.1
10.0
9.9
9.8
9.7
9.6
9.5
9.4
9.3
9.2
9.1
9.0
8.9
8.8
8.7
5500
5000
4500
4000
3500
3000
2500
2000
1500
1000
500
0
-500

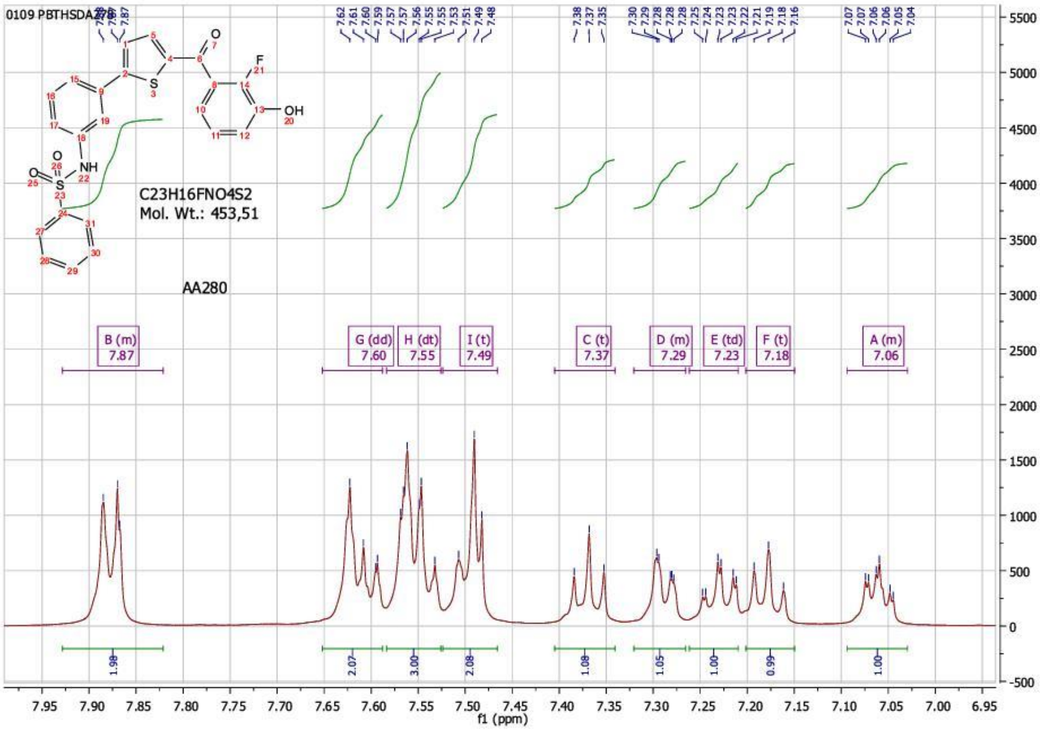
0109 PBTHSDA278
7.88
7.86
7.87
7.62
7.61
7.60
7.59
7.57
7.57
7.56
7.55
7.55
7.53
7.51
7.49
7.48
7.38
7.37
7.35
7.30
7.29
7.28
7.28
7.28
7.25
7.24
7.23
7.23
7.22
7.21
7.19
7.18
7.16
7.07
7.07
7.06
7.06
7.05
7.04
C23H16FNO4S2
Mol. Wt.: 453,51
AA280
B (m)
7.87
G (dd)
7.60
H (dt)
7.55
I (t)
7.49
C (t)
7.37
D (m)
7.29
E (td)
7.23
F (t)
7.18
A (m)
7.06
1.98
2.07
3.00
2.08
1.08
1.05
1.00
0.99
1.00
f1 (ppm)
7.95
7.90
7.85
7.80
7.75
7.70
7.65
7.60
7.55
7.50
7.45
7.40
7.35
7.30
7.25
7.20
7.15
7.10
7.05
7.00
6.95
5500
5000
4500
4000
3500
3000
2500
2000
1500
1000
500
0
-500

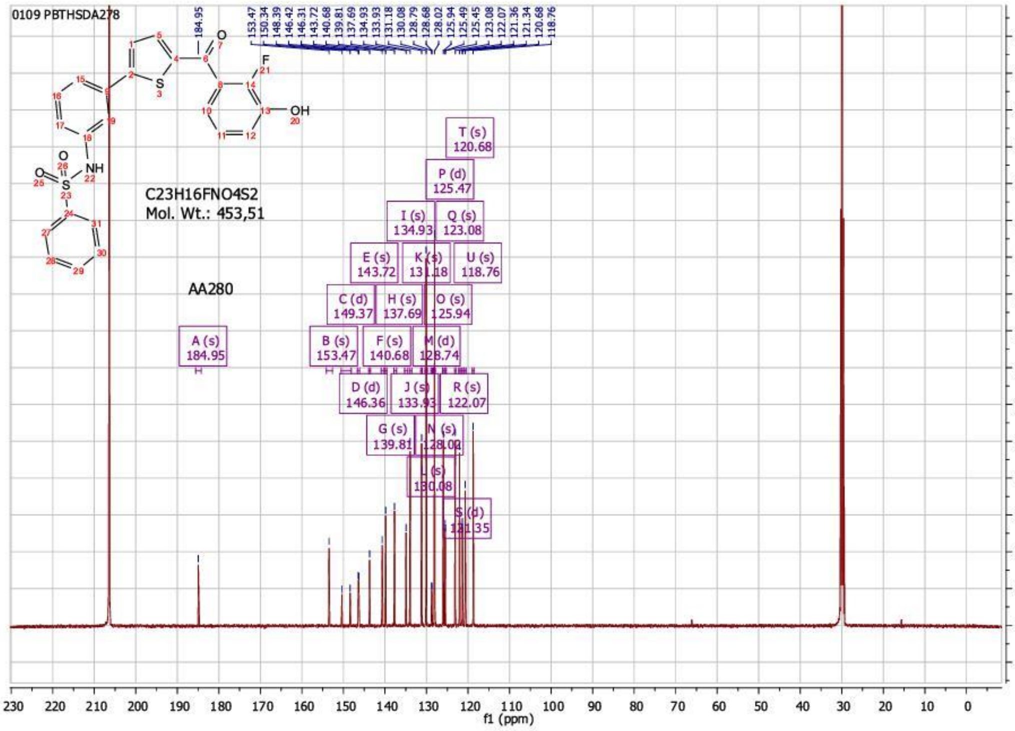
0109 PBTHSDA278
C23H16FNO4S2
Mol. Wt.: 453,51
AA280
184.95
153.47
150.34
148.39
146.42
146.31
143.72
140.68
139.81
137.69
134.93
133.93
131.18
130.08
128.79
128.68
128.02
125.94
125.49
125.45
123.08
122.07
121.36
121.34
120.68
118.76
A (s) 184.95
B (s) 153.47
C (d) 149.37
D (d) 146.36
E (s) 143.72
F (s) 140.68
G (s) 139.81
H (s) 137.69
I (s) 134.93
J (s) 133.93
K (s) 131.18
L (s) 130.08
M (d) 128.74
N (s) 128.02
O (s) 125.94
P (d) 125.47
Q (s) 123.08
R (s) 122.07
S (d) 121.35
T (s) 120.68
U (s) 118.76
f1 (ppm)

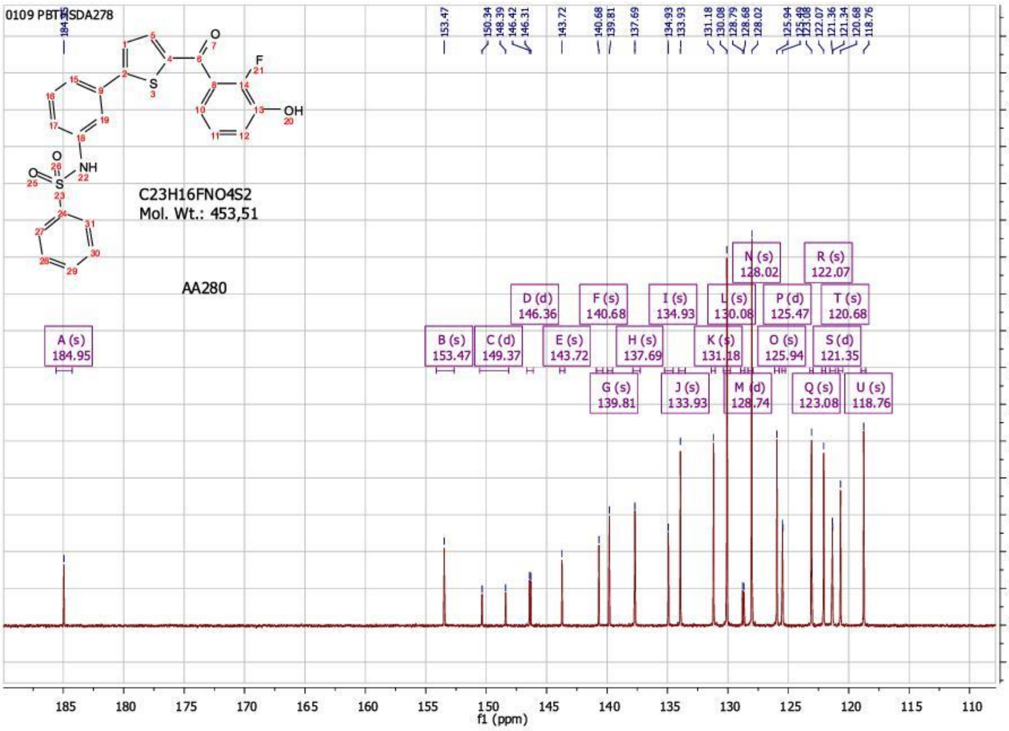
0109 PBTHSDA278
C23H16FNO4S2
Mol. Wt.: 453,51
AA280
184.95
153.47
150.34
148.39
146.42
146.31
143.72
140.68
139.81
137.69
134.93
133.93
131.18
130.08
128.79
128.68
128.02
125.94
125.49
125.45
123.08
122.07
121.36
121.34
120.68
118.76
A (s) 184.95
B (s) 153.47
C (d) 149.37
D (d) 146.36
E (s) 143.72
F (s) 140.68
G (s) 139.81
H (s) 137.69
I (s) 134.93
J (s) 133.93
K (s) 131.18
L (s) 130.08
M (d) 128.74
N (s) 128.02
O (s) 125.94
P (d) 125.47
Q (s) 123.08
R (s) 122.07
S (d) 121.35
T (s) 120.68
U (s) 118.76
f1 (ppm)

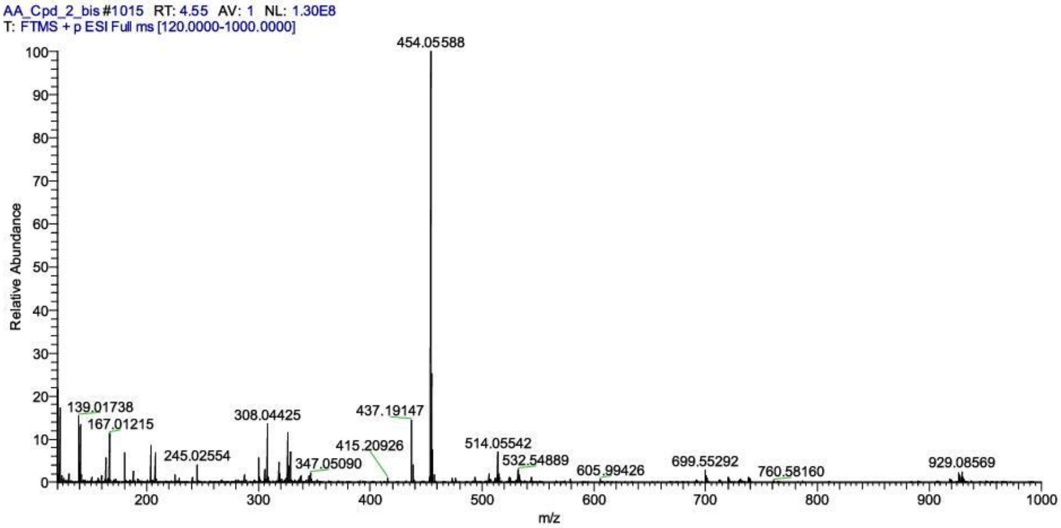

C:\Users\...\LC.MS_Final\AA280-b 11/30/17 13:53:21

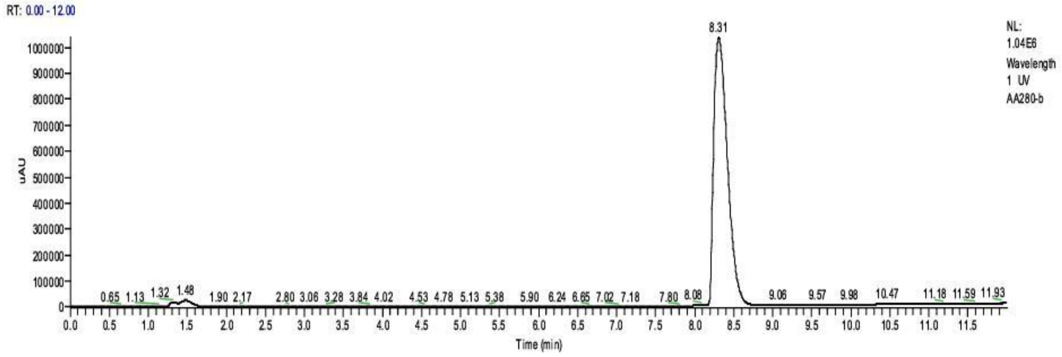

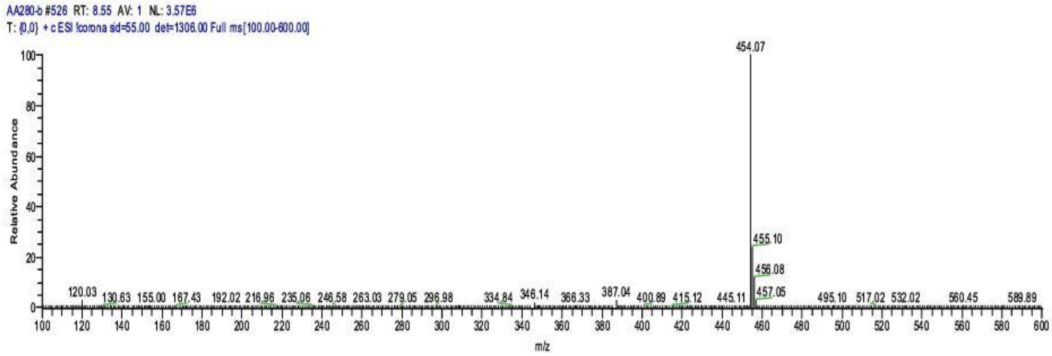

^{1}H, ^{13}C spectra, HRMS, and LC.MS of Compound 3.

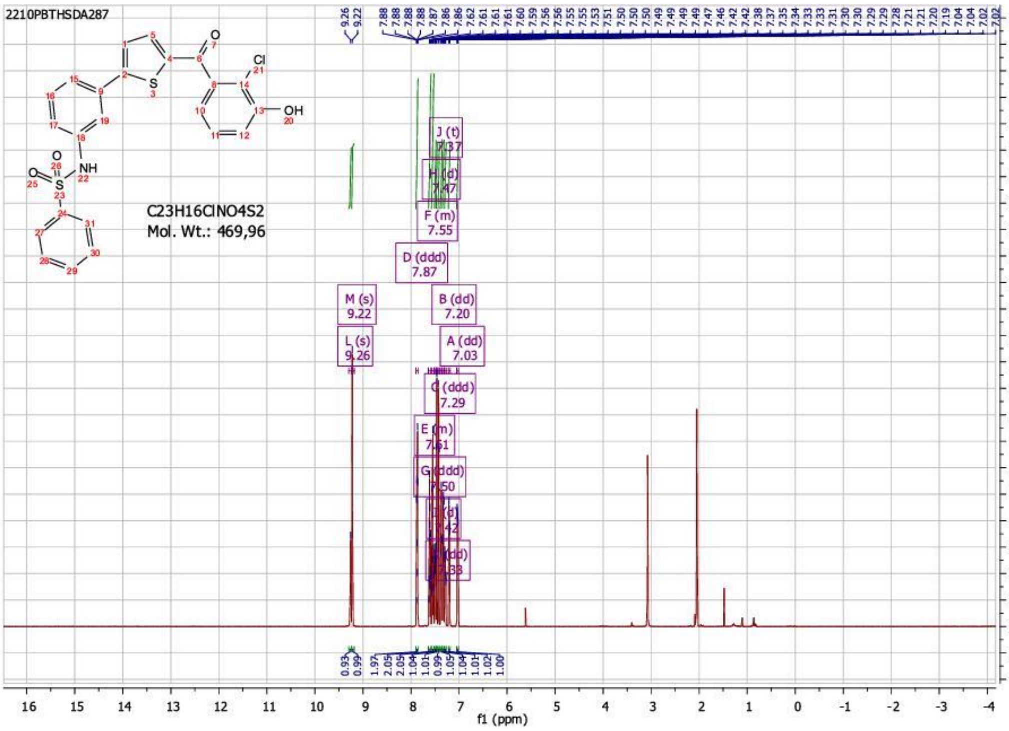

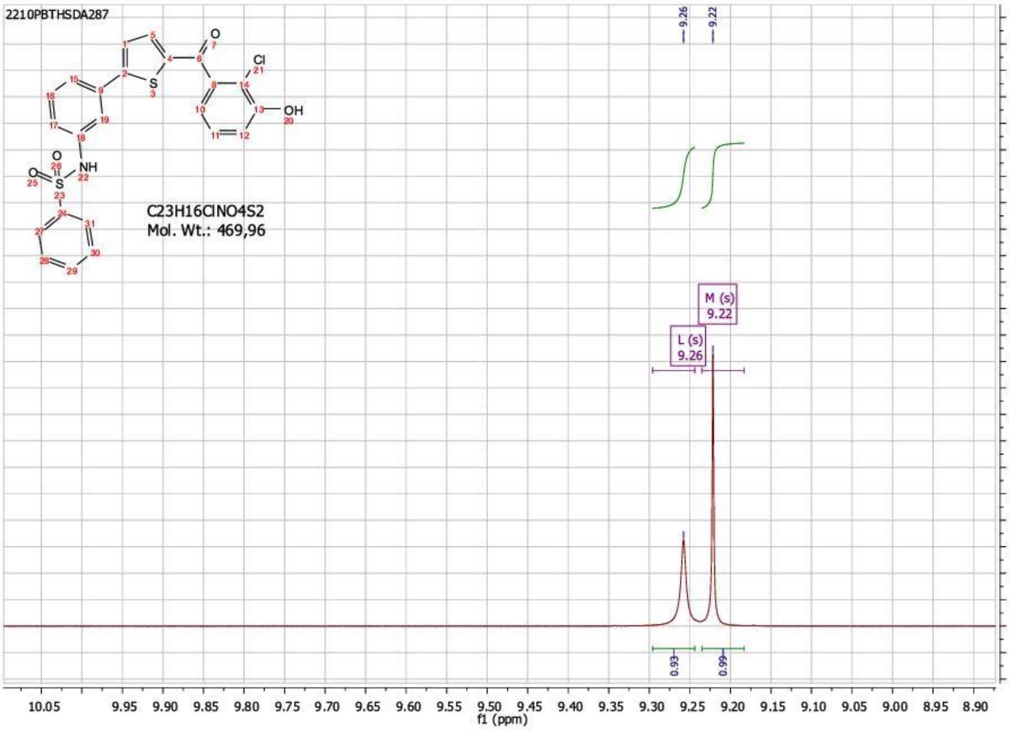

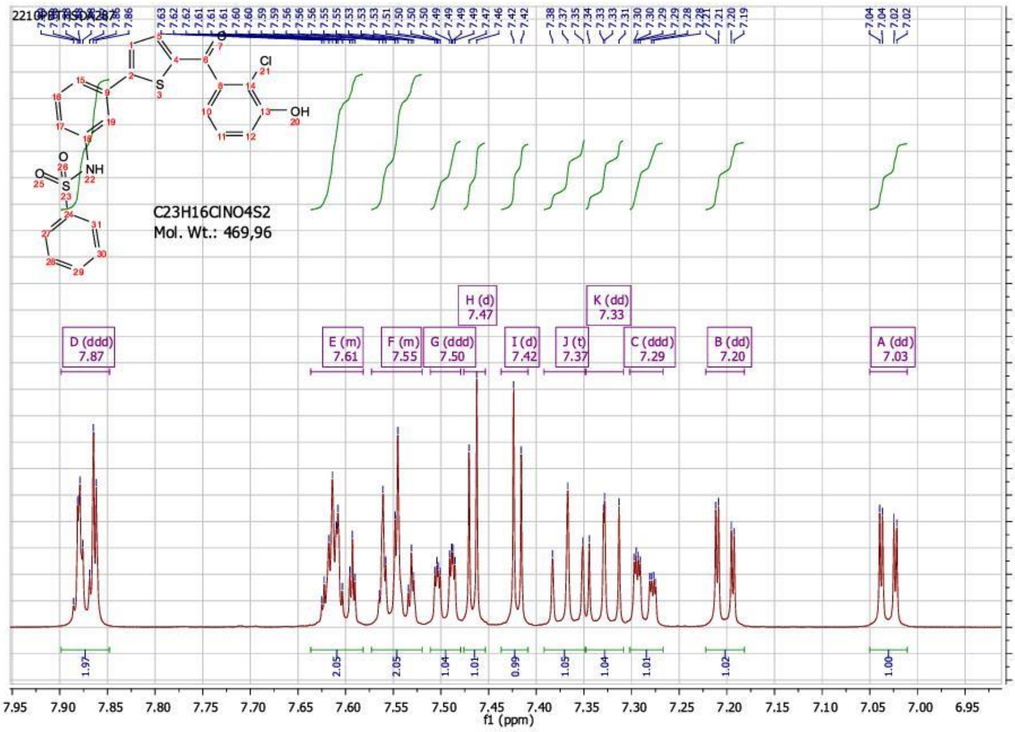
2210PBTHSDA287
7.63 7.62 7.62 7.61 7.61 7.61 7.60 7.60 7.59 7.59 7.56 7.56 7.56 7.55 7.55 7.53 7.53 7.53 7.51 7.50 7.50 7.50 7.49 7.49 7.49 7.49 7.47 7.46 7.42 7.42
7.38 7.37 7.35 7.34 7.33 7.33 7.31 7.30 7.30 7.29 7.29 7.28 7.28 7.21 7.21 7.20 7.19
7.04 7.04 7.02 7.02
Cl
OH
O
NH
S
C23H16ClNO4S2
Mol. Wt.: 469,96
D (ddd) 7.87
E (m) 7.61
F (m) 7.55
G (ddd) 7.50
H (d) 7.47
I (d) 7.42
J (t) 7.37
K (dd) 7.33
C (ddd) 7.29
B (dd) 7.20
A (dd) 7.03
1.97
2.05
2.05
1.04
1.01
0.99
1.05
1.04
1.01
1.02
1.00
f1 (ppm)

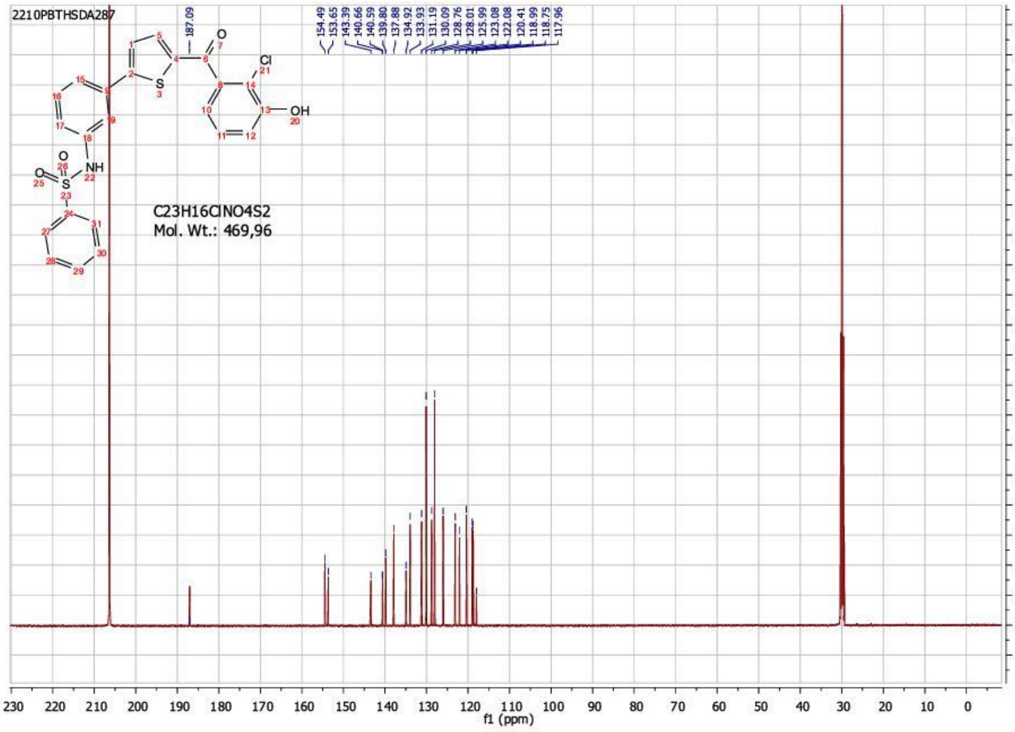
2210PBTHSDA287
187.09
154.49 153.65 143.39 140.66 140.59 139.80 137.88 134.92 133.93 131.19 130.09 128.76 128.01 125.99 123.08 122.08 120.41 118.99 118.75 117.96
Cl
OH
O
NH
S
C23H16ClNO4S2
Mol. Wt.: 469,96
f1 (ppm)

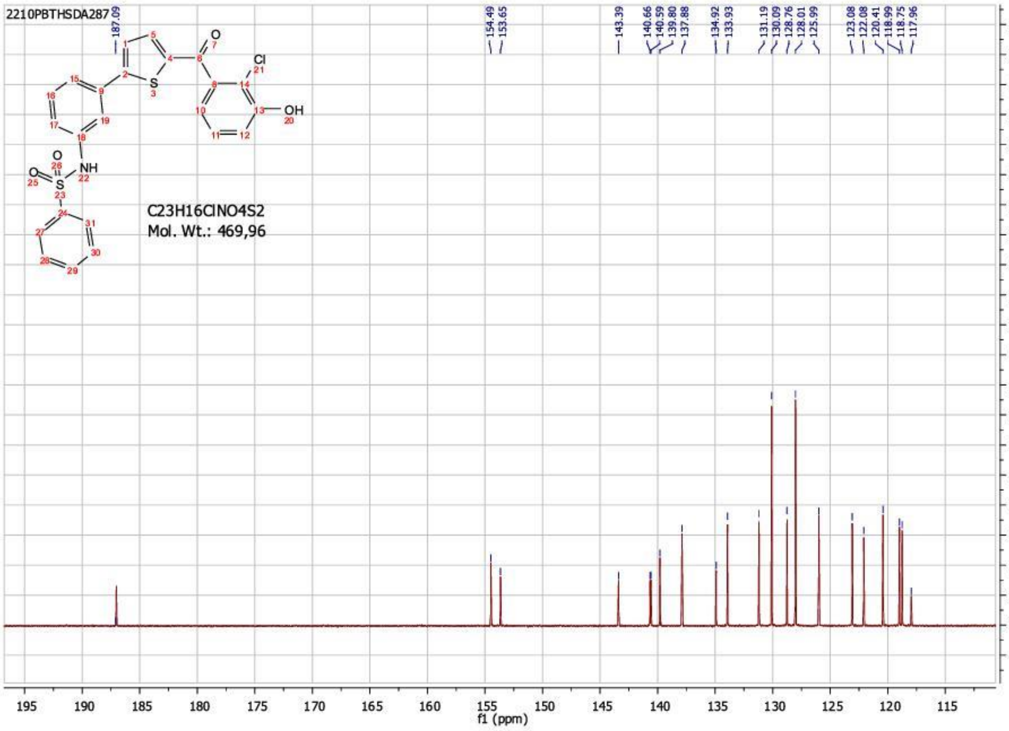
2210PBTHSDA287
187.09
154.49
153.65
143.39
140.66
140.59
139.80
137.88
134.92
133.93
131.19
130.09
128.76
128.01
125.99
123.08
122.08
120.41
118.99
118.75
117.96
O
Cl
OH
NH
S
C23H16ClNO4S2
Mol. Wt.: 469,96
f1 (ppm)
195
190
185
180
175
170
165
160
155
150
145
140
135
130
125
120
115
2E+05
1E+05
90000
80000
70000
60000
50000
40000
30000
20000
10000
0
-10000

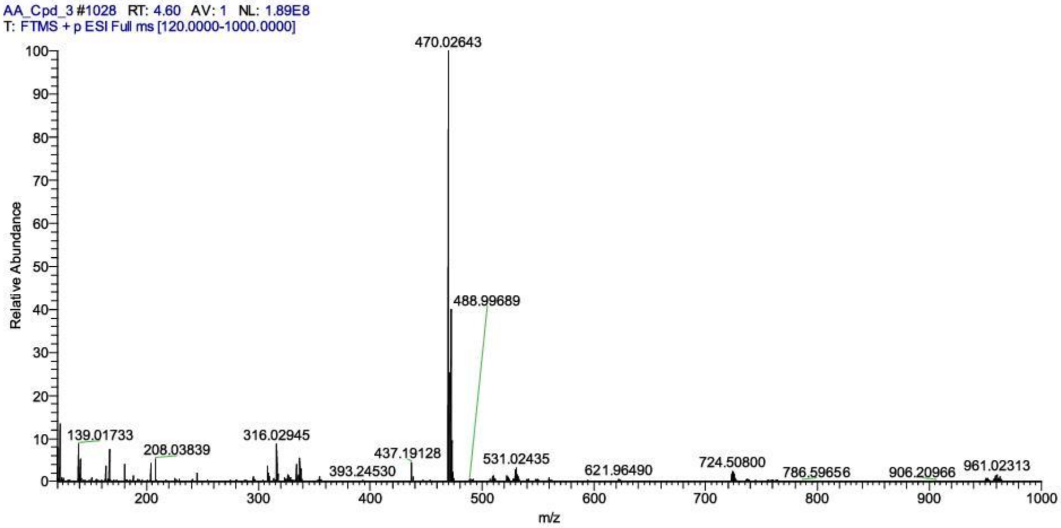
AA_Cpd_3 #1028 RT: 4.60 AV: 1 NL: 1.89E8
T: FTMS + p ESI Full ms [120.0000-1000.0000]
Relative Abundance
m/z
470.02643
488.99689
139.01733
208.03839
316.02945
393.24530
437.19128
531.02435
621.96490
724.50800
786.59656
906.20966
961.02313
100
90
80
70
60
50
40
30
20
10
0
200
300
400
500
600
700
800
900
1000

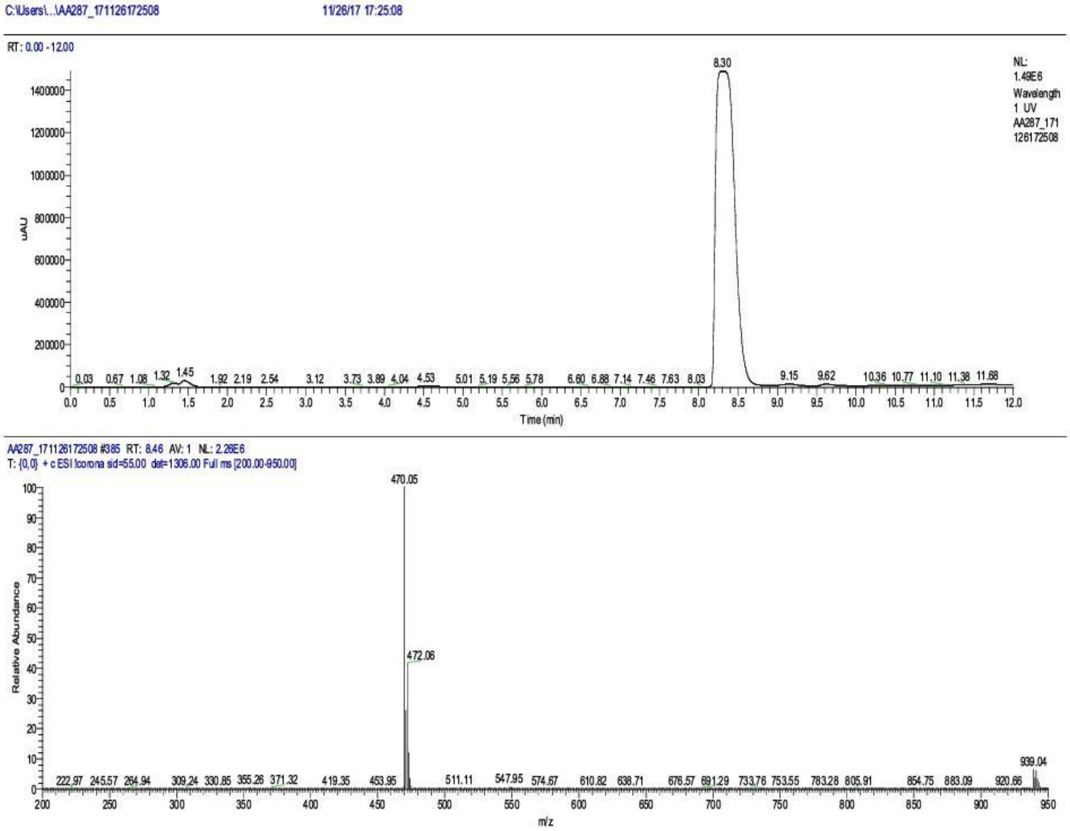

^{1}H, ^{13}C spectra, HRMS, and LC.MS of Compound 4.

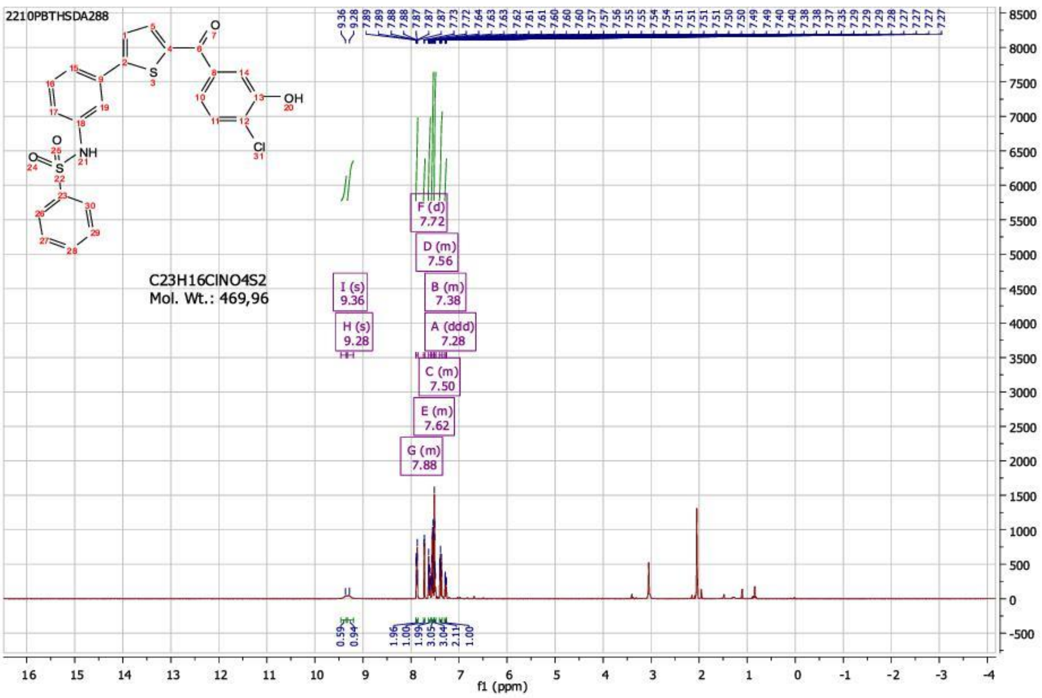

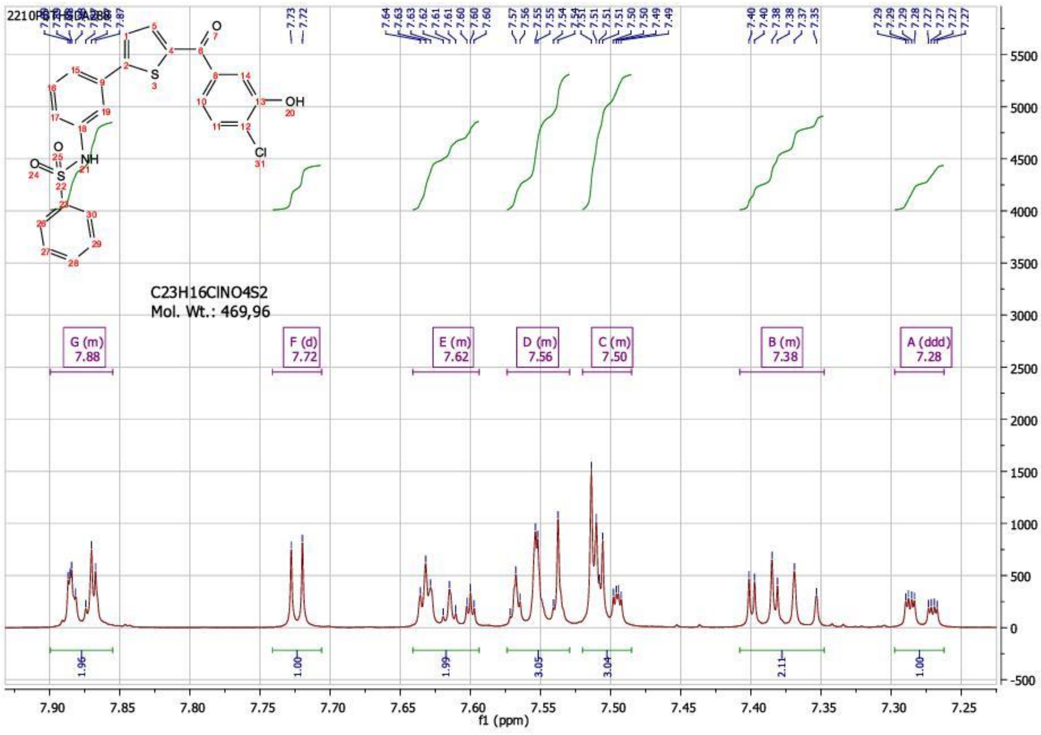
2210PBTHSDA288
C23H16ClNO4S2
Mol. Wt.: 469,96
OH
Cl
NH
S
O
7.87
7.73
7.72
7.64
7.63
7.63
7.62
7.61
7.61
7.60
7.60
7.60
7.57
7.56
7.55
7.55
7.54
7.54
7.51
7.51
7.51
7.50
7.50
7.49
7.49
7.40
7.40
7.38
7.38
7.37
7.35
7.29
7.29
7.29
7.28
7.27
7.27
7.27
7.27
G (m) 7.88
F (d) 7.72
E (m) 7.62
D (m) 7.56
C (m) 7.50
B (m) 7.38
A (ddd) 7.28
1.96
1.00
1.99
3.05
3.04
2.11
1.00
f1 (ppm)

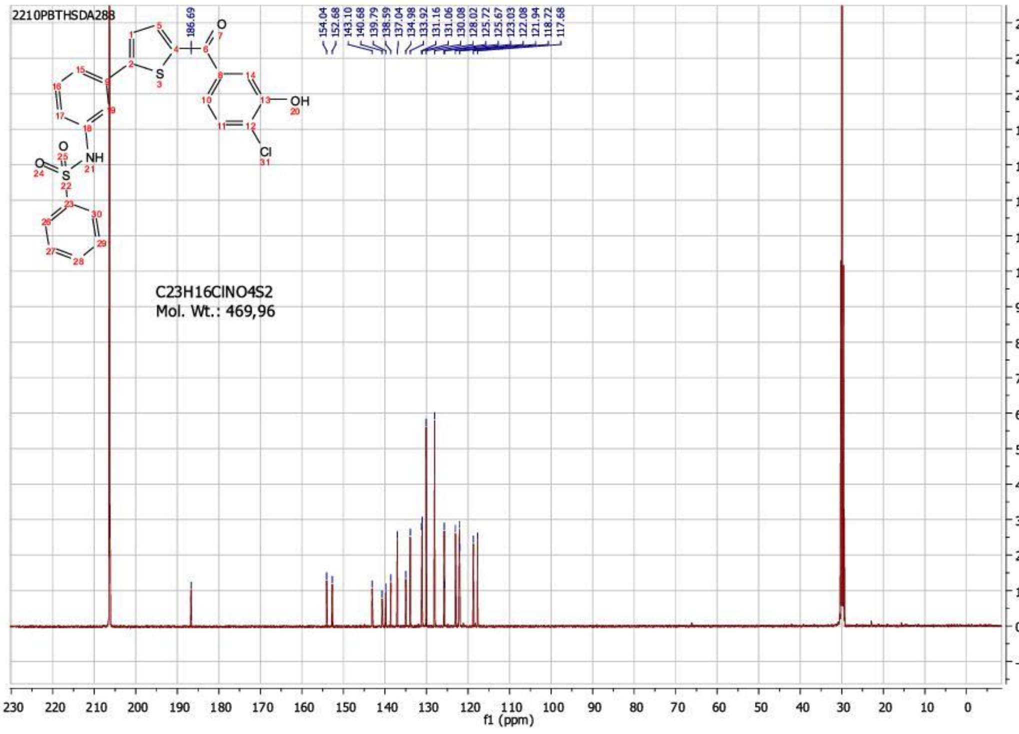
2210PBTHSDA288
C23H16ClNO4S2
Mol. Wt.: 469,96
OH
Cl
NH
S
O
186.69
154.04
152.68
143.10
140.68
139.79
138.59
137.04
134.98
133.92
131.16
131.06
130.08
128.02
125.72
125.67
123.03
122.08
121.94
118.22
117.68
f1 (ppm)

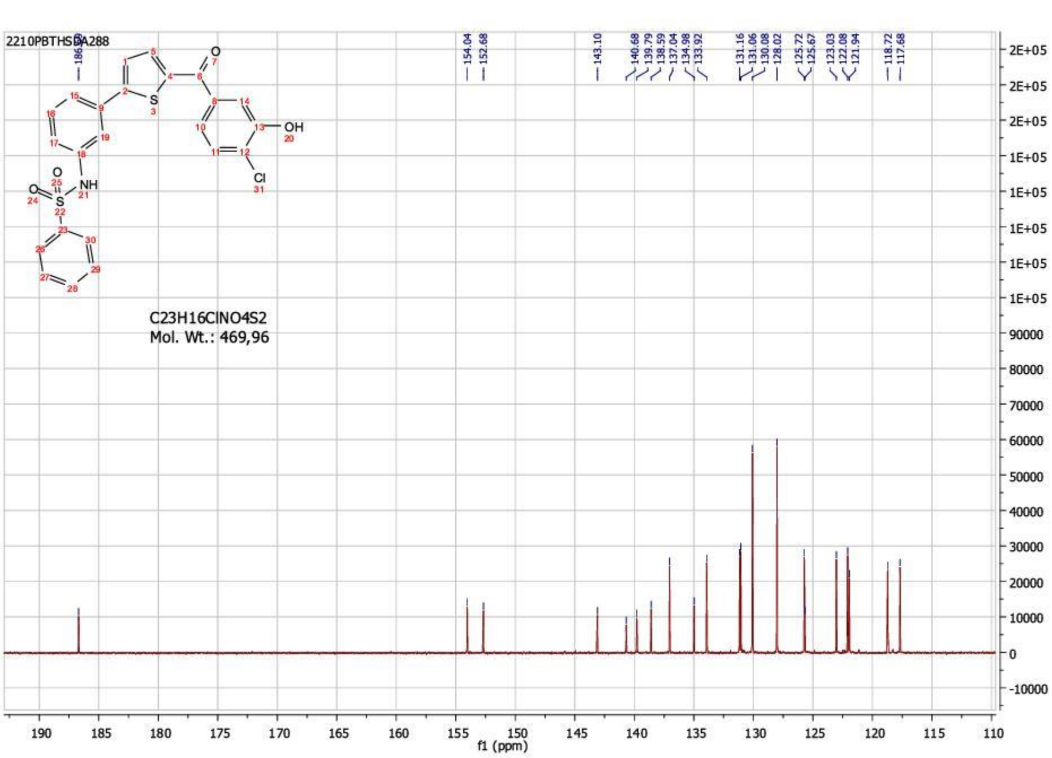
2210PBTHSDA288
186
154.04
152.68
143.10
140.68
139.79
138.59
137.04
134.98
133.92
131.16
131.06
130.08
128.02
125.72
125.67
123.03
122.08
121.94
118.72
117.68
O
S
OH
NH
Cl
C23H16ClNO4S2
Mol. Wt.: 469,96
2E+05
1E+05
90000
80000
70000
60000
50000
40000
30000
20000
10000
0
-10000
190
185
180
175
170
165
160
155
150
145
140
135
130
125
120
115
110
f1 (ppm)

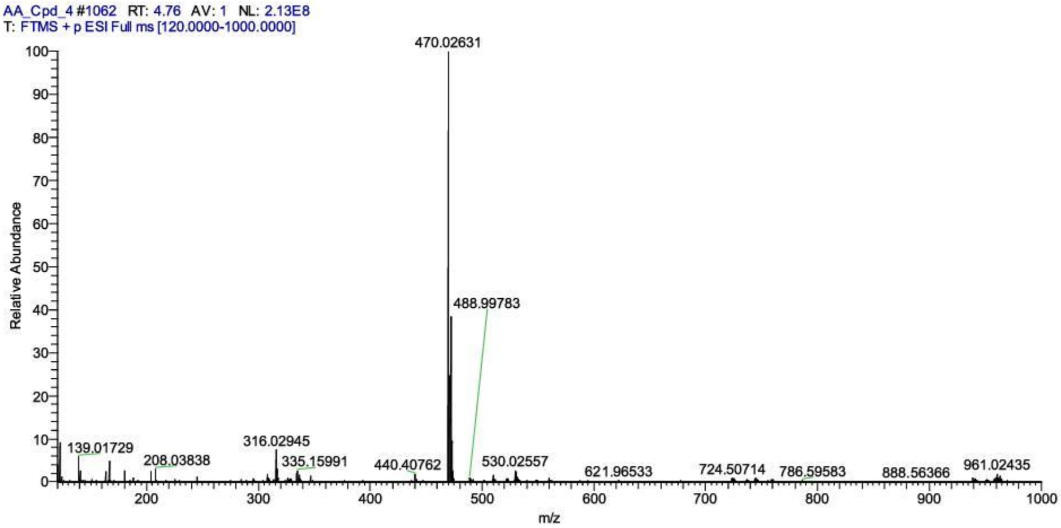
AA_Cpd_4 #1062 RT: 4.76 AV: 1 NL: 2.13E8
T: FTMS + p ESI Full ms [120.0000-1000.0000]
470.02631
488.99783
139.01729
208.03838
316.02945
335.15991
440.40762
530.02557
621.96533
724.50714
786.59583
888.56366
961.02435
Relative Abundance
0
10
20
30
40
50
60
70
80
90
100
200
300
400
500
600
700
800
900
1000
m/z

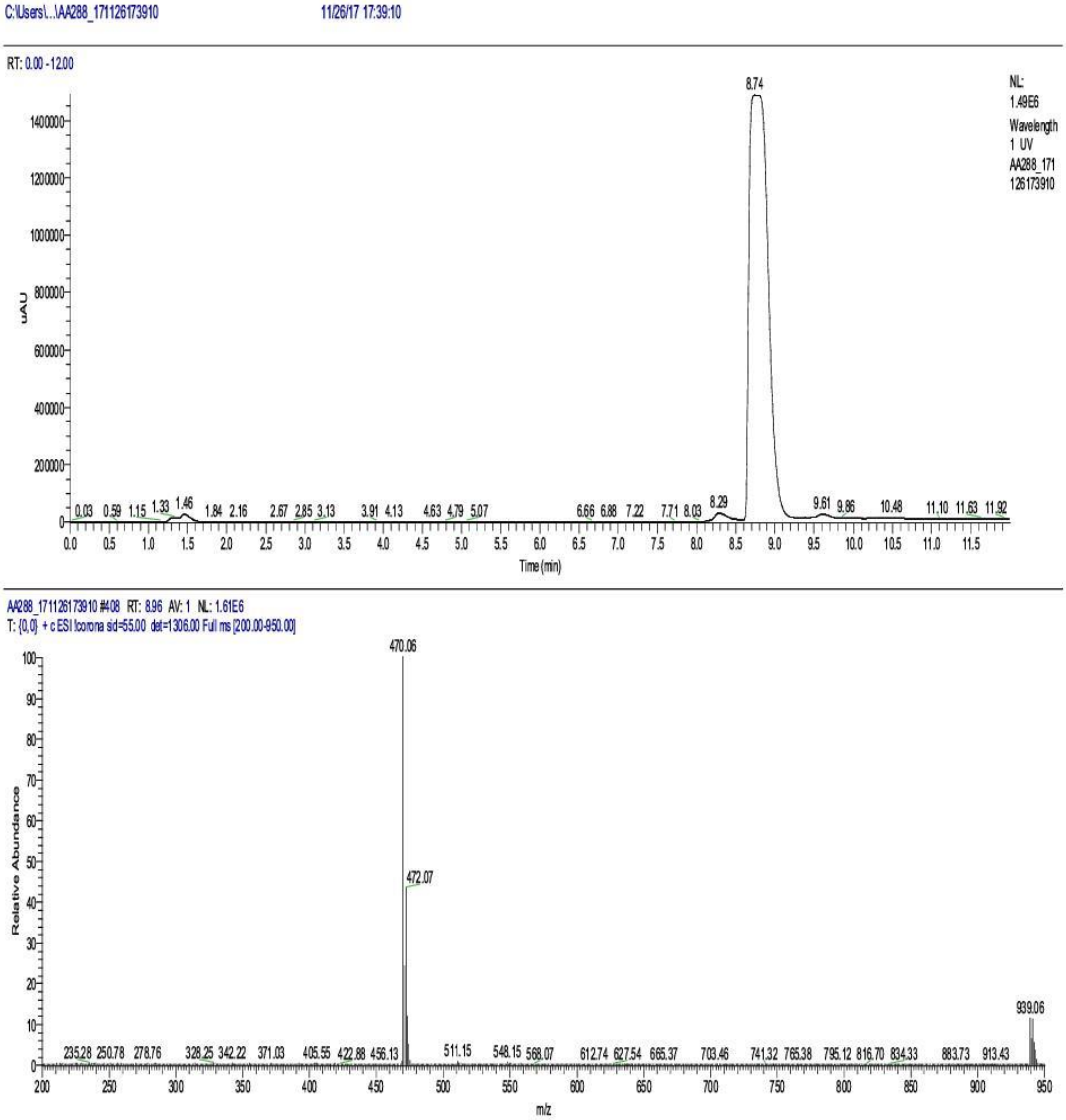
C:\Users\...\AA288_171126173910
11/26/17 17:39:10
RT: 0.00 - 12.00
NL:
1.49E6
Wavelength
1 UV
AA288_171
126173910
8.74
0.03 0.59 1.15 1.33 1.46 1.84 2.16 2.67 2.85 3.13 3.91 4.13 4.63 4.79 5.07 6.66 6.88 7.22 7.71 8.03 8.29 9.61 9.86 10.48 11.10 11.63 11.92
uAU
1400000
1200000
1000000
800000
600000
400000
200000
0
0.0 0.5 1.0 1.5 2.0 2.5 3.0 3.5 4.0 4.5 5.0 5.5 6.0 6.5 7.0 7.5 8.0 8.5 9.0 9.5 10.0 10.5 11.0 11.5
Time (min)
AA288_171126173910 #408 RT: 8.96 AV: 1 NL: 1.61E6
T: {0,0} + c ESI !corona sid=55.00 det=1306.00 Full ms [200.00-950.00]
470.06
472.07
939.06
235.28 250.78 278.76 328.25 342.22 371.03 405.55 422.88 456.13 511.15 548.15 568.07 612.74 627.54 665.37 703.46 741.32 765.38 795.12 816.70 834.33 883.73 913.43
Relative Abundance
100
90
80
70
60
50
40
30
20
10
0
200 250 300 350 400 450 500 550 600 650 700 750 800 850 900 950
m/z

^{1}H, ^{13}C spectra, HRMS, and LC.MS of Compound 5.

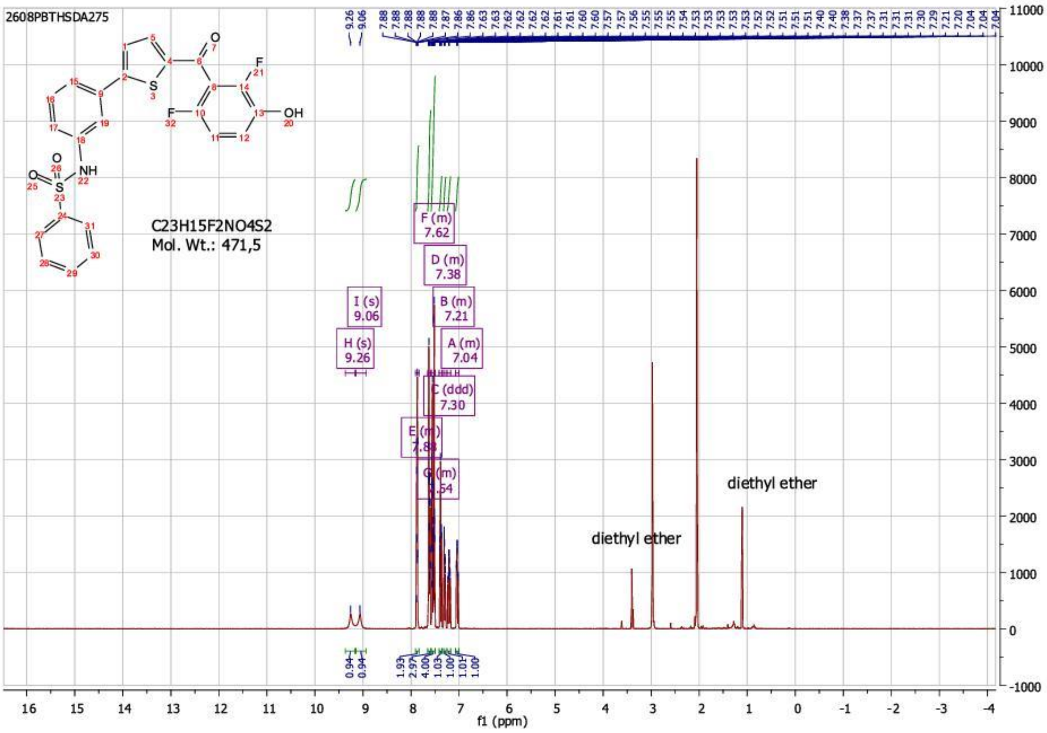

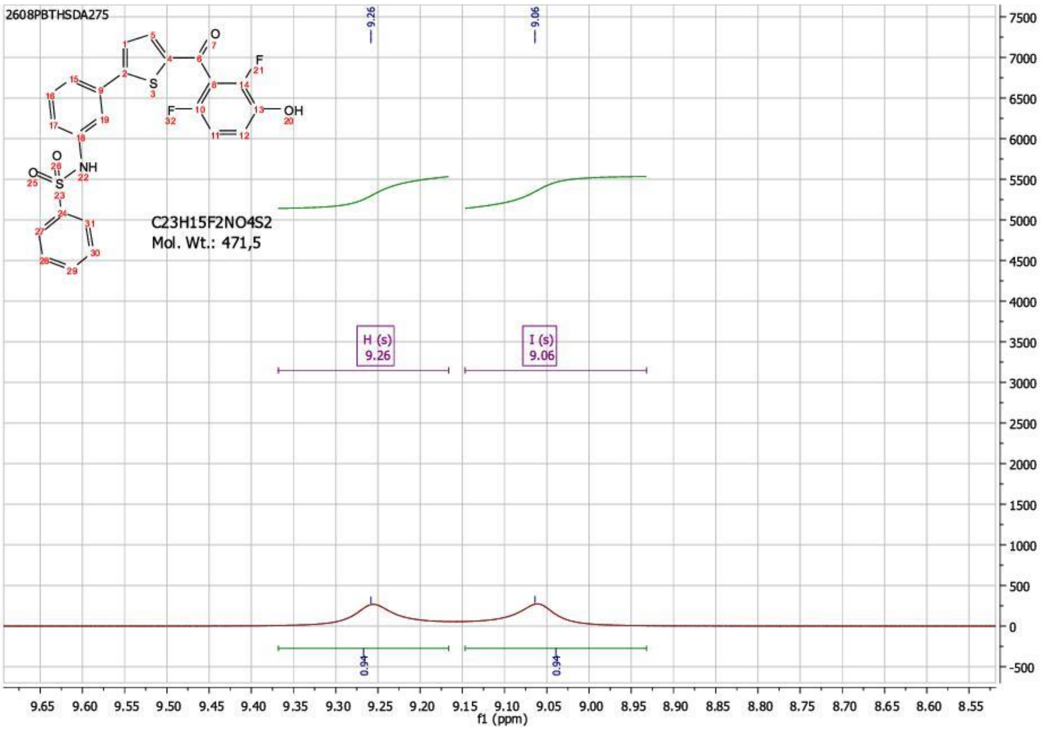

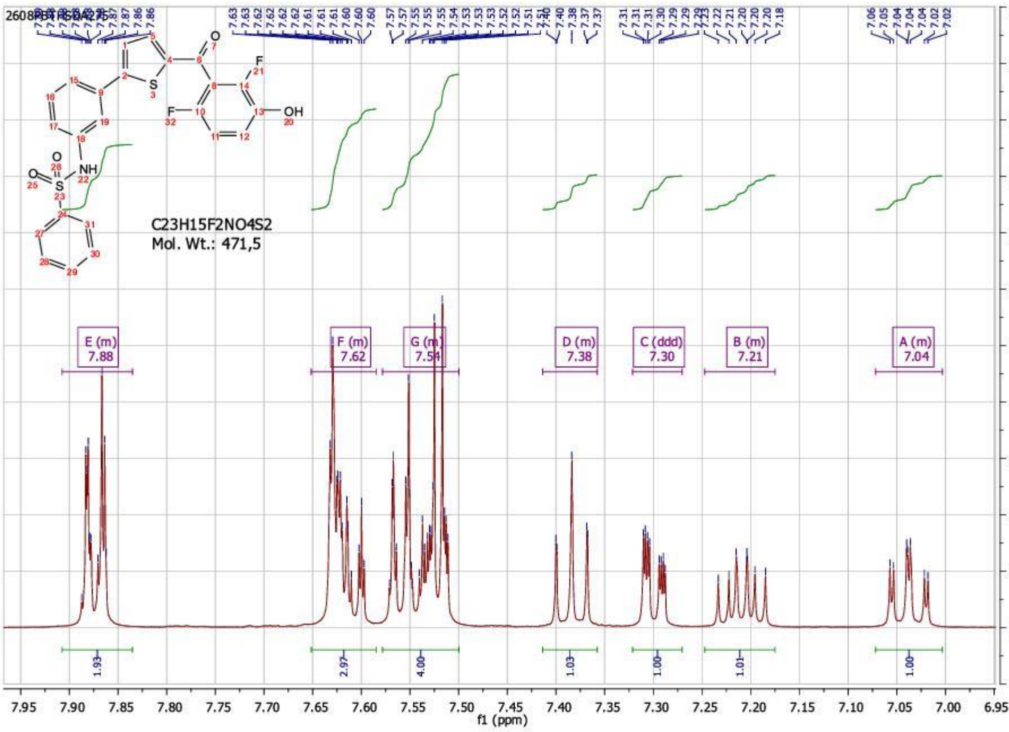
2608PBTHSDA275
C23H15F2NO4S2
Mol. Wt.: 471,5
E (m) 7.88
F (m) 7.62
G (m) 7.54
D (m) 7.38
C (ddd) 7.30
B (m) 7.21
A (m) 7.04
1.93
2.97
4.00
1.03
1.00
1.01
1.00
f1 (ppm)

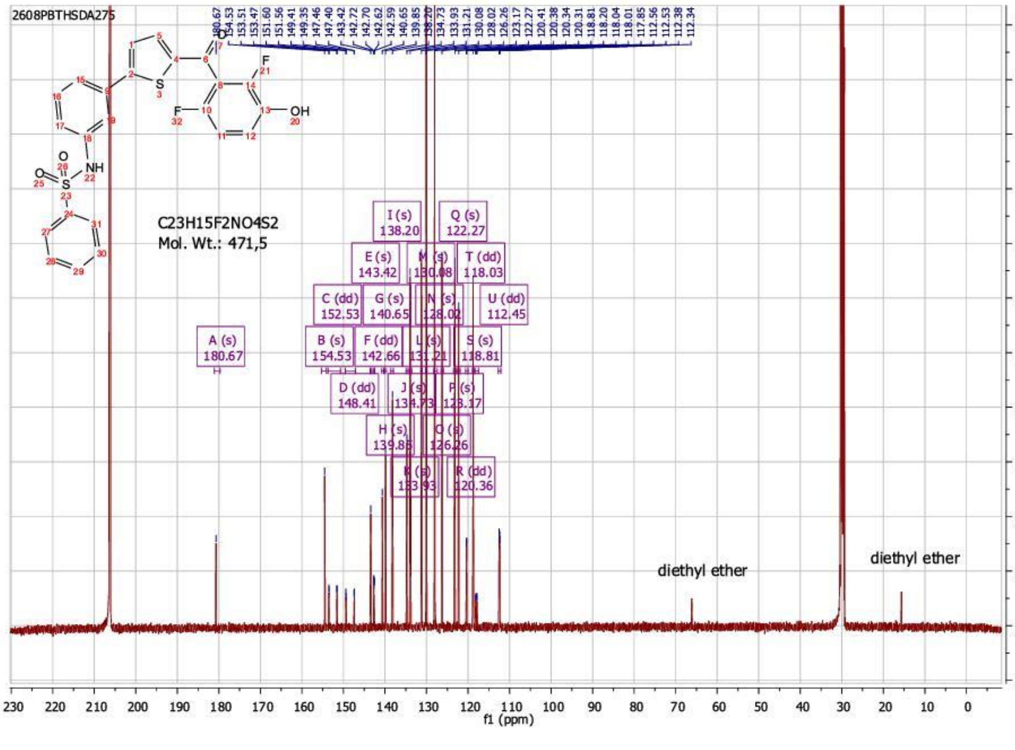
2608PBTHSDA275
C23H15F2NO4S2
Mol. Wt.: 471,5
A (s) 180.67
B (s) 154.53
C (dd) 152.53
D (dd) 148.41
E (s) 143.42
F (dd) 142.66
G (s) 140.65
H (s) 139.85
I (s) 138.20
J (s) 134.73
K (s) 133.93
L (s) 131.21
M (s) 130.08
N (s) 128.02
O (s) 126.26
P (s) 123.17
Q (s) 122.27
R (dd) 120.36
S (s) 118.81
T (dd) 118.03
U (dd) 112.45
diethyl ether
diethyl ether
f1 (ppm)

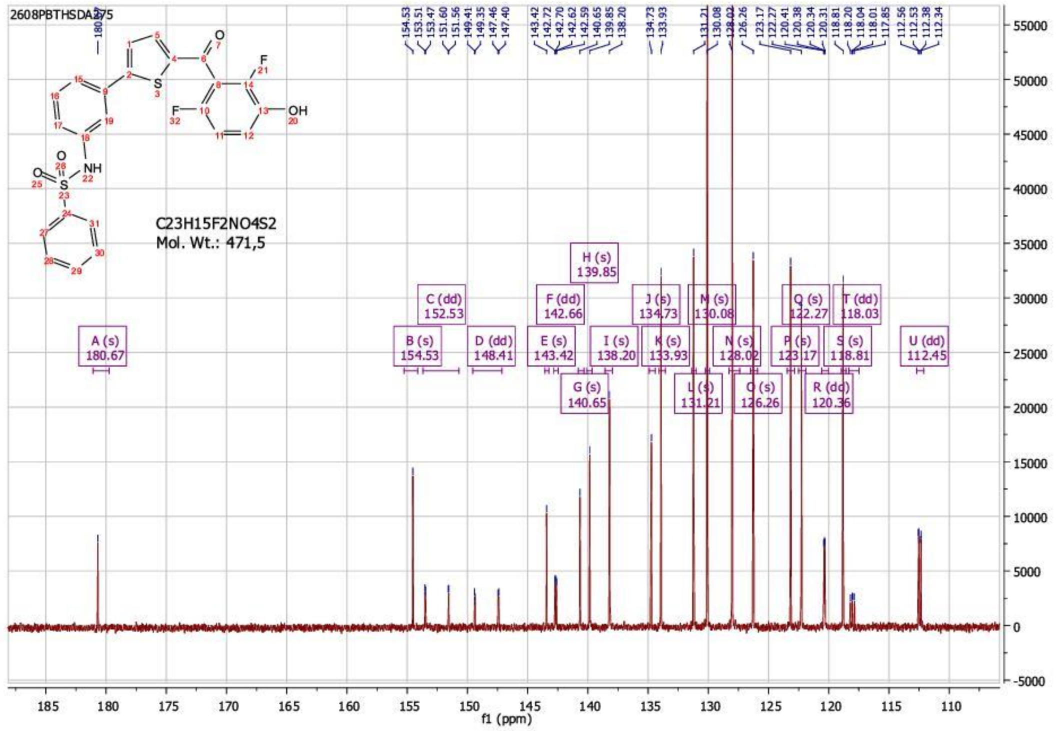
2608PBTHSDA275
C23H15F2NO4S2
Mol. Wt.: 471,5
180.67
154.53 153.51 153.47 151.60 151.56 149.41 149.35 147.46 147.40
143.42 142.72 142.70 142.62 142.59 140.65 139.85 138.20
134.73 133.93
131.21 130.08 128.02 126.26
123.17 122.27 120.41 120.38 120.34 120.31
118.81 118.20 118.04 118.01 117.85
112.56 112.53 112.38 112.34
A (s) 180.67
B (s) 154.53
C (dd) 152.53
D (dd) 148.41
E (s) 143.42
F (dd) 142.66
G (s) 140.65
H (s) 139.85
I (s) 138.20
J (s) 134.73
K (s) 133.93
L (s) 131.21
M (s) 130.08
N (s) 128.02
O (s) 126.26
P (s) 123.17
Q (s) 122.27
R (dd) 120.36
S (s) 118.81
T (dd) 118.03
U (dd) 112.45
f1 (ppm)
185 180 175 170 165 160 155 150 145 140 135 130 125 120 115 110
55000 50000 45000 40000 35000 30000 25000 20000 15000 10000 5000 0 -5000

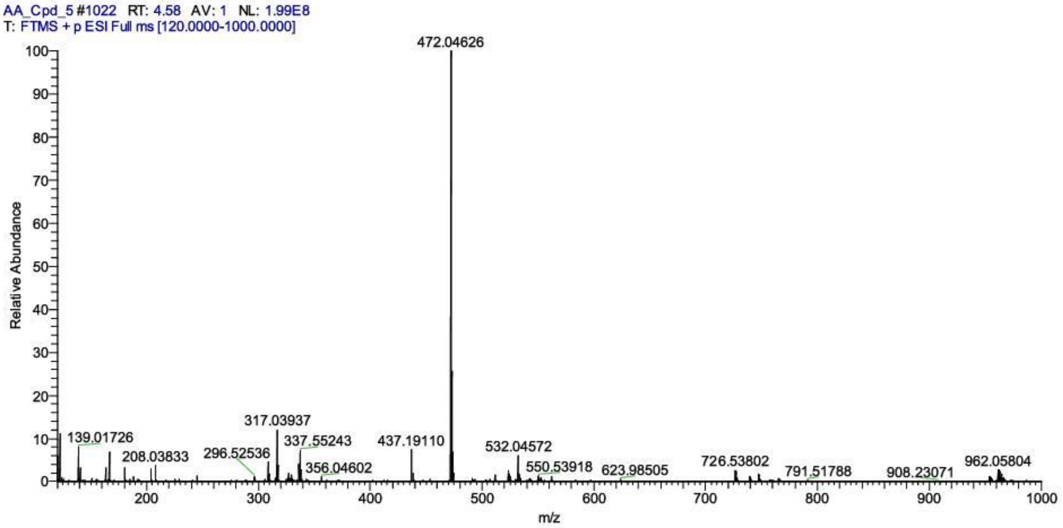
AA_Cpd_5 #1022 RT: 4.58 AV: 1 NL: 1.99E8
T: FTMS + p ESI Full ms [120.0000-1000.0000]
472.04626
139.01726
208.03833
296.52536
317.03937
337.55243
356.04602
437.19110
532.04572
550.53918
623.98505
726.53802
791.51788
908.23071
962.05804
Relative Abundance
m/z
0 10 20 30 40 50 60 70 80 90 100
200 300 400 500 600 700 800 900 1000

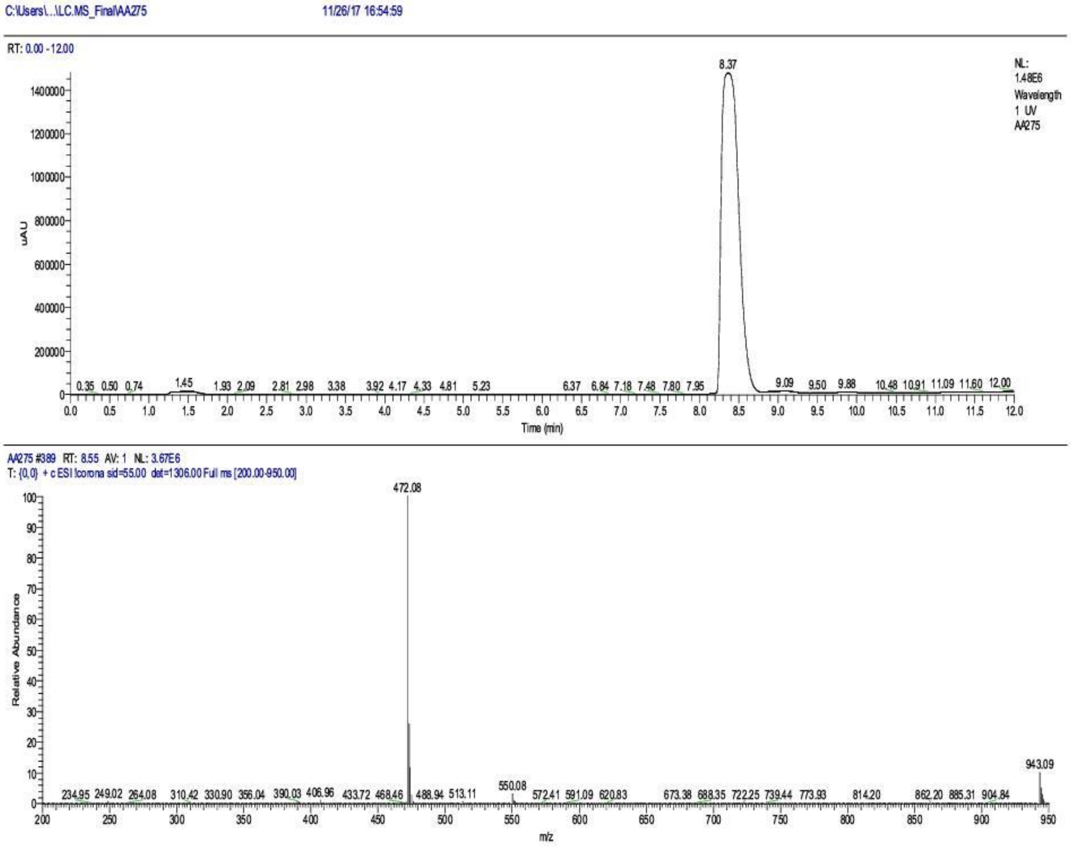

^{1}H, ^{13}C spectra, HRMS, and LC.MS of Compound 6.

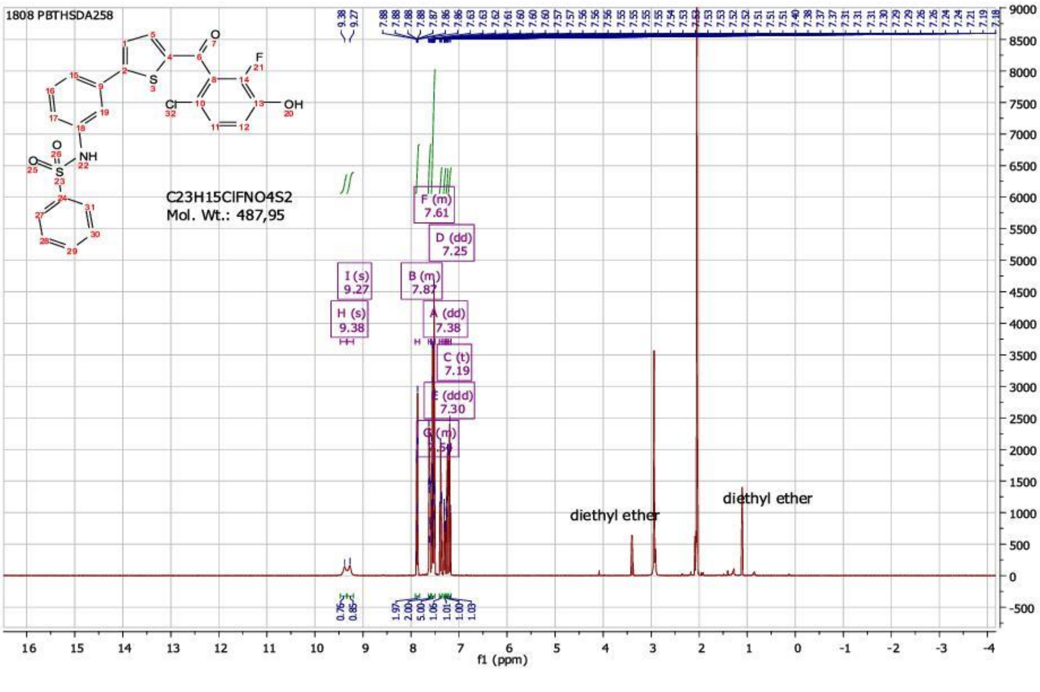

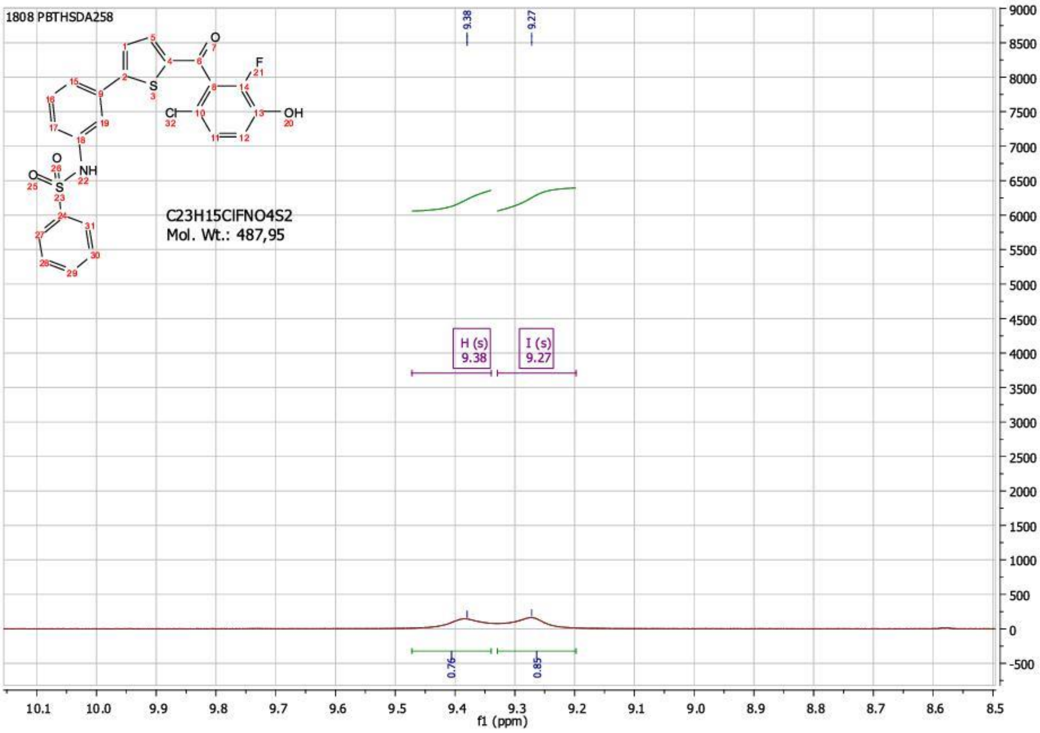
1808 PBTHSDA258
9.38
9.27
O
F
OH
Cl
S
NH
C23H15ClFNO4S2
Mol. Wt.: 487,95
H (s)
9.38
I (s)
9.27
0.76
0.85
10.1
10.0
9.9
9.8
9.7
9.6
9.5
9.4
9.3
9.2
9.1
9.0
8.9
8.8
8.7
8.6
8.5
f1 (ppm)
9000
8500
8000
7500
7000
6500
6000
5500
5000
4500
4000
3500
3000
2500
2000
1500
1000
500
0
-500

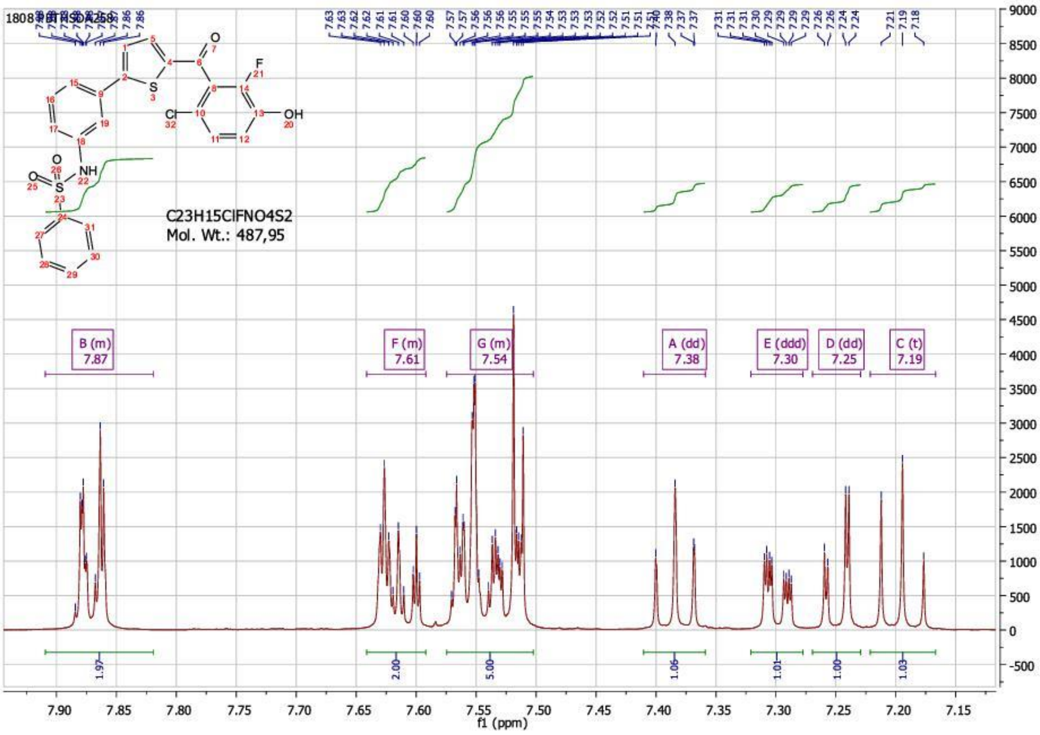
1808 PBTHSDA258
O
F
OH
Cl
S
NH
C23H15ClFNO4S2
Mol. Wt.: 487,95
B (m)
7.87
F (m)
7.61
G (m)
7.54
A (dd)
7.38
E (ddd)
7.30
D (dd)
7.25
C (t)
7.19
1.97
2.00
5.00
1.06
1.01
1.00
1.03
7.90
7.85
7.80
7.75
7.70
7.65
7.60
7.55
7.50
7.45
7.40
7.35
7.30
7.25
7.20
7.15
f1 (ppm)
9000
8500
8000
7500
7000
6500
6000
5500
5000
4500
4000
3500
3000
2500
2000
1500
1000
500
0
-500

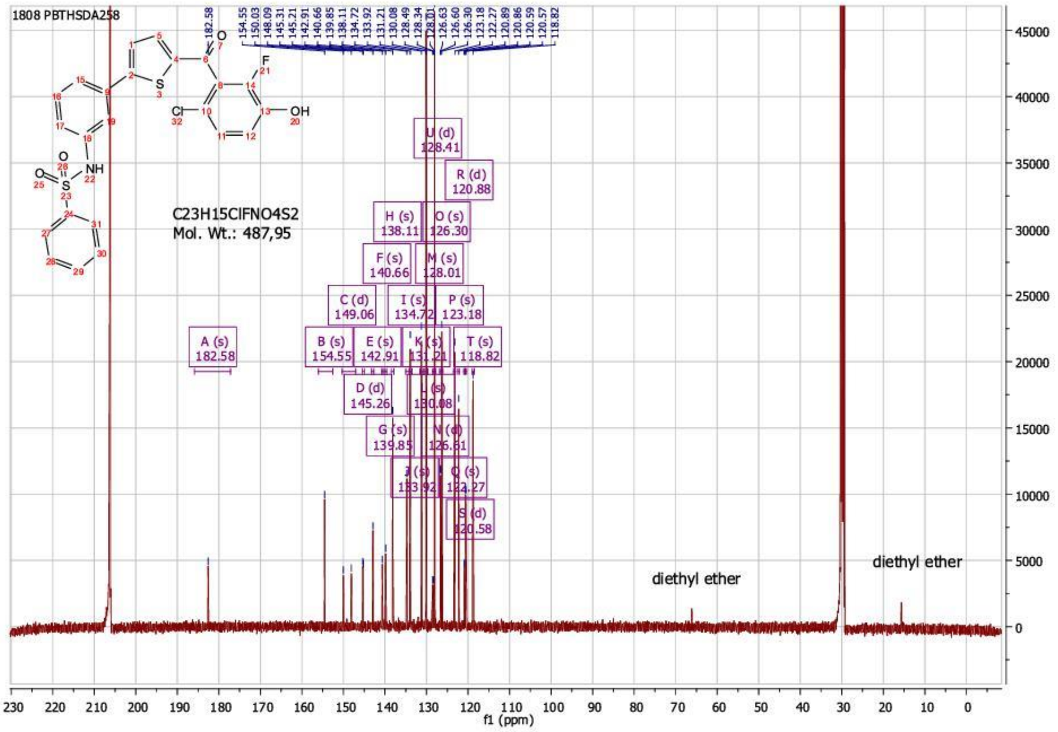
1808 PBTHSDA258
C23H15ClFNO4S2
Mol. Wt.: 487,95
182.58
154.55 150.03 148.09 145.31 145.21 142.91 140.66 139.85 138.11 134.72 133.92 131.21 130.08 128.49 128.34 128.01 126.63 126.60 126.30 123.18 122.27 120.89 120.86 120.59 120.57 118.82
A (s) 182.58
B (s) 154.55
C (d) 149.06
D (d) 145.26
E (s) 142.91
F (s) 140.66
G (s) 139.85
H (s) 138.11
I (s) 134.72
J (s) 133.92
K (s) 131.21
L (s) 130.08
M (s) 128.01
N (d) 126.61
O (s) 126.30
P (s) 123.18
Q (s) 122.27
R (d) 120.88
S (d) 120.58
T (s) 118.82
U (d) 128.41
diethyl ether
diethyl ether
f1 (ppm)

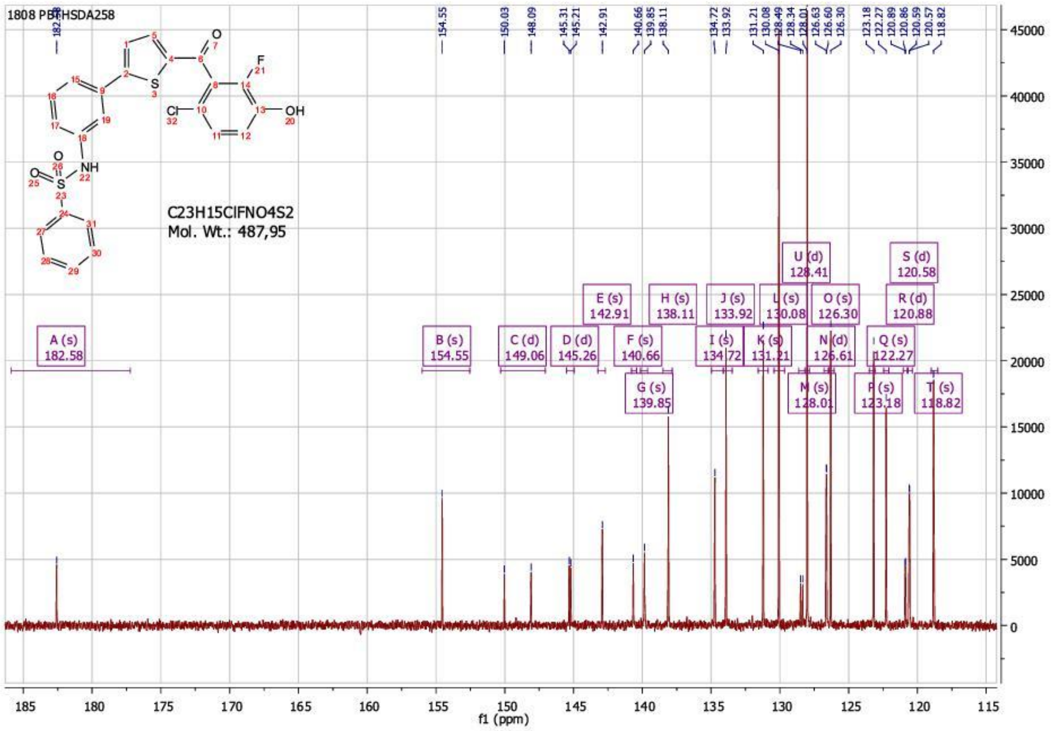
1808 PBTHSDA258
C23H15ClFNO4S2
Mol. Wt.: 487,95
182.58
154.55 150.03 148.09 145.31 145.21 142.91 140.66 139.85 138.11 134.72 133.92 131.21 130.08 128.49 128.34 128.01 126.63 126.60 126.30 123.18 122.27 120.89 120.86 120.59 120.57 118.82
A (s) 182.58
B (s) 154.55
C (d) 149.06
D (d) 145.26
E (s) 142.91
F (s) 140.66
G (s) 139.85
H (s) 138.11
I (s) 134.72
J (s) 133.92
K (s) 131.21
L (s) 130.08
M (s) 128.01
N (d) 126.61
O (s) 126.30
P (s) 123.18
Q (s) 122.27
R (d) 120.88
S (d) 120.58
T (s) 118.82
U (d) 128.41
f1 (ppm)

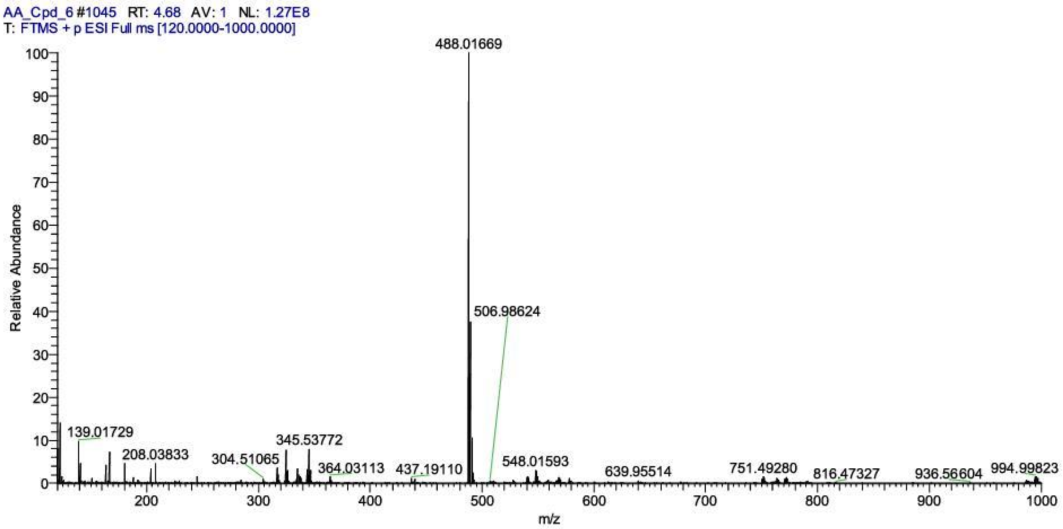

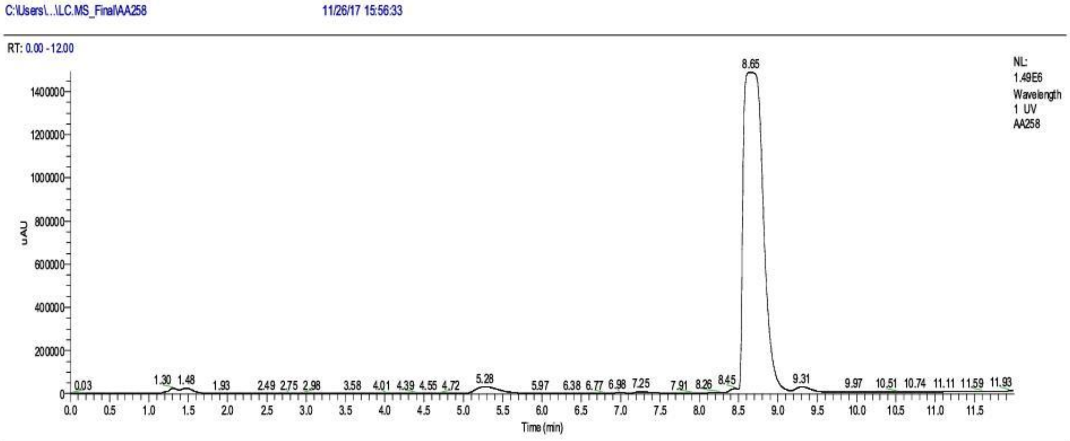

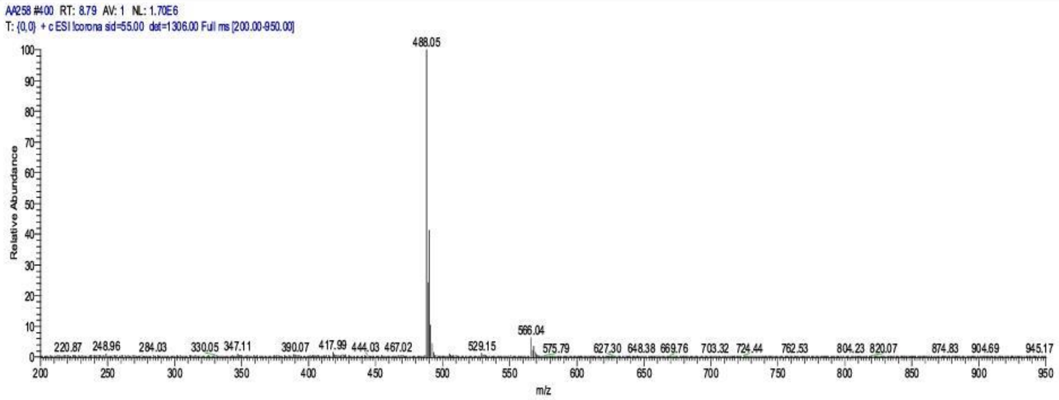

^{1}H, ^{13}C spectra, HRMS, and LC.MS of Compound 7.

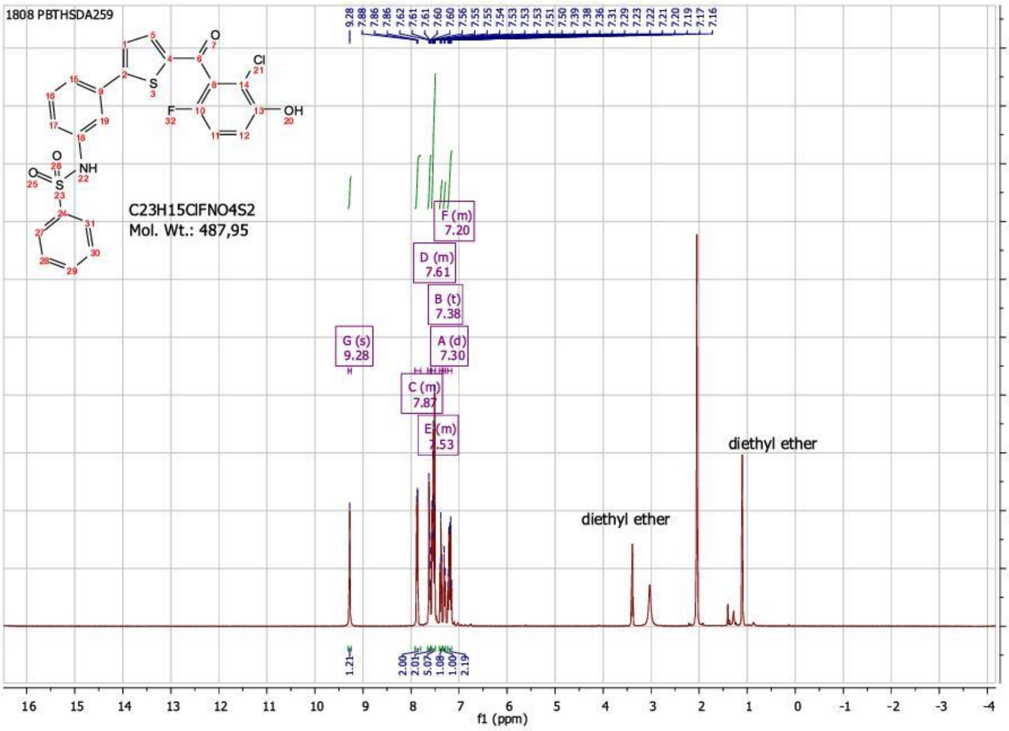
1808 PBTHSDA259
C23H15ClFNO4S2
Mol. Wt.: 487,95
G (s) 9.28
C (m) 7.87
D (m) 7.61
E (m) 7.53
B (t) 7.38
A (d) 7.30
F (m) 7.20
diethyl ether
diethyl ether
1.21
2.00
2.01
5.07
1.08
1.00
2.19
f1 (ppm)

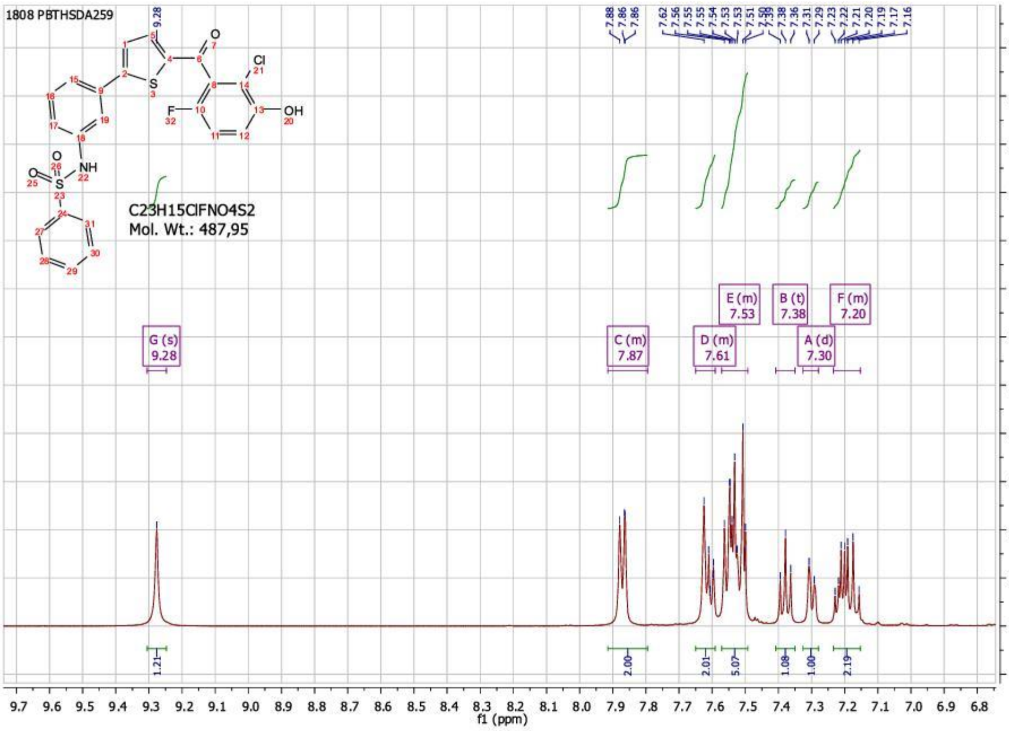
1808 PBTHSDA259
C23H15ClFNO4S2
Mol. Wt.: 487,95
G (s) 9.28
C (m) 7.87
D (m) 7.61
E (m) 7.53
B (t) 7.38
A (d) 7.30
F (m) 7.20
1.21
2.00
2.01
5.07
1.08
1.00
2.19
f1 (ppm)

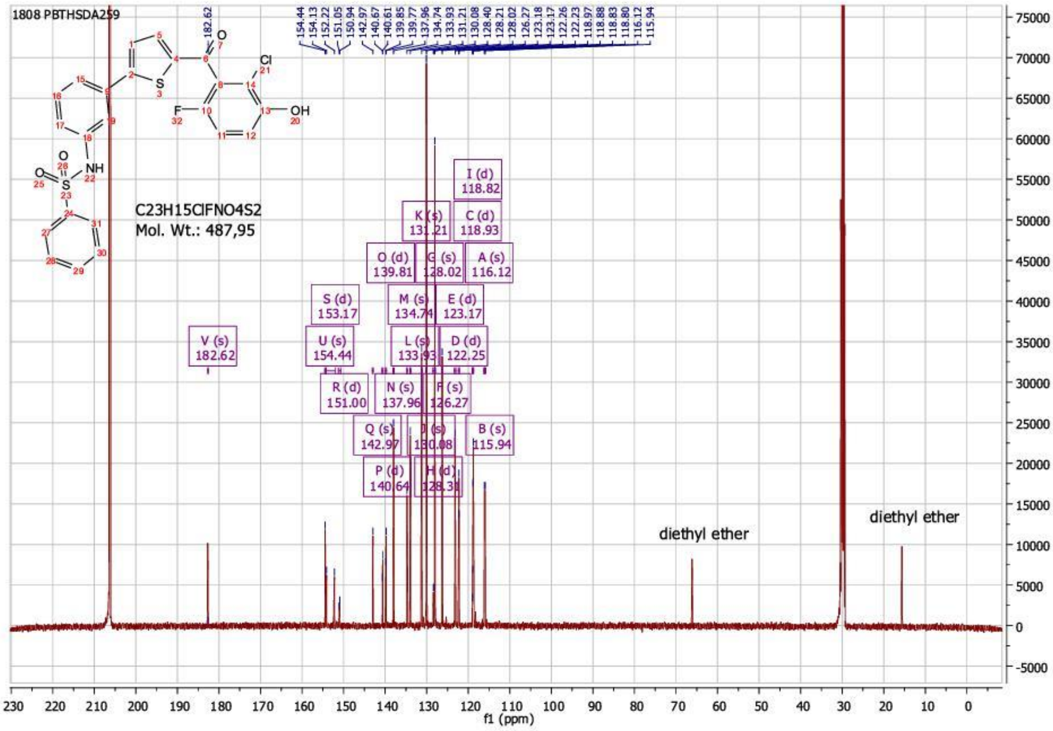
1808 PBTHSDA259
C23H15ClFNO4S2
Mol. Wt.: 487,95
Cl
OH
F
NH
O
S
182.62
154.44
154.13
152.22
151.05
150.94
142.97
140.67
140.61
139.85
139.77
137.96
134.74
133.93
131.21
130.08
128.40
128.21
128.02
126.27
123.18
123.17
122.26
122.23
118.97
118.88
118.83
118.80
116.12
115.94
V (s) 182.62
U (s) 154.44
S (d) 153.17
R (d) 151.00
Q (s) 142.97
P (d) 140.64
O (d) 139.81
N (s) 137.96
M (s) 134.74
L (s) 133.93
K (s) 131.21
J (s) 130.08
H (d) 128.31
G (s) 128.02
F (s) 126.27
E (d) 123.17
D (d) 122.25
C (d) 118.93
I (d) 118.82
B (s) 115.94
A (s) 116.12
diethyl ether
diethyl ether
f1 (ppm)

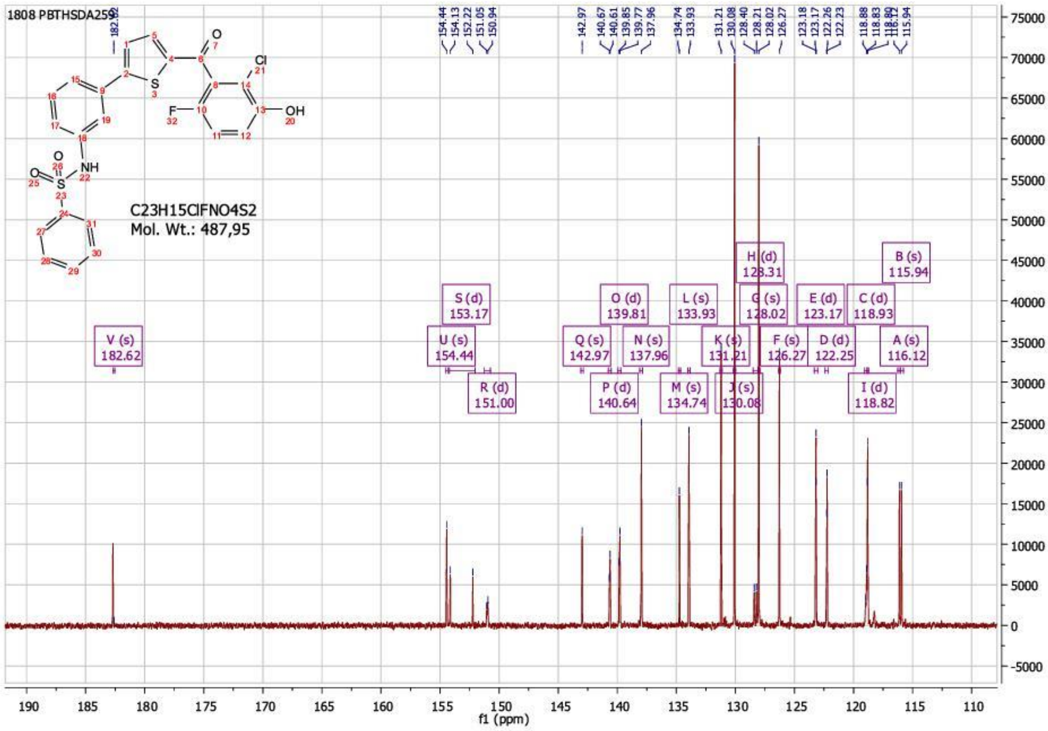
1808 PBTHSDA259
C23H15ClFNO4S2
Mol. Wt.: 487,95
Cl
OH
F
NH
O
S
182.62
154.44
154.13
152.22
151.05
150.94
142.97
140.67
140.61
139.85
139.77
137.96
134.74
133.93
131.21
130.08
128.40
128.21
128.02
126.27
123.18
123.17
122.26
122.23
118.88
118.83
116.12
115.94
V (s) 182.62
U (s) 154.44
S (d) 153.17
R (d) 151.00
Q (s) 142.97
P (d) 140.64
O (d) 139.81
N (s) 137.96
M (s) 134.74
L (s) 133.93
K (s) 131.21
J (s) 130.08
H (d) 128.31
G (s) 128.02
F (s) 126.27
E (d) 123.17
D (d) 122.25
C (d) 118.93
I (d) 118.82
B (s) 115.94
A (s) 116.12
f1 (ppm)

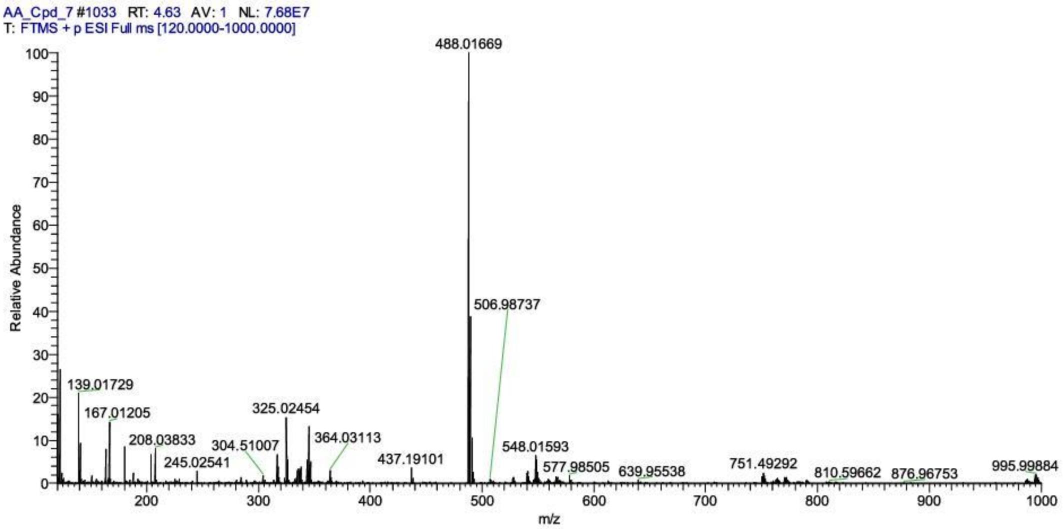

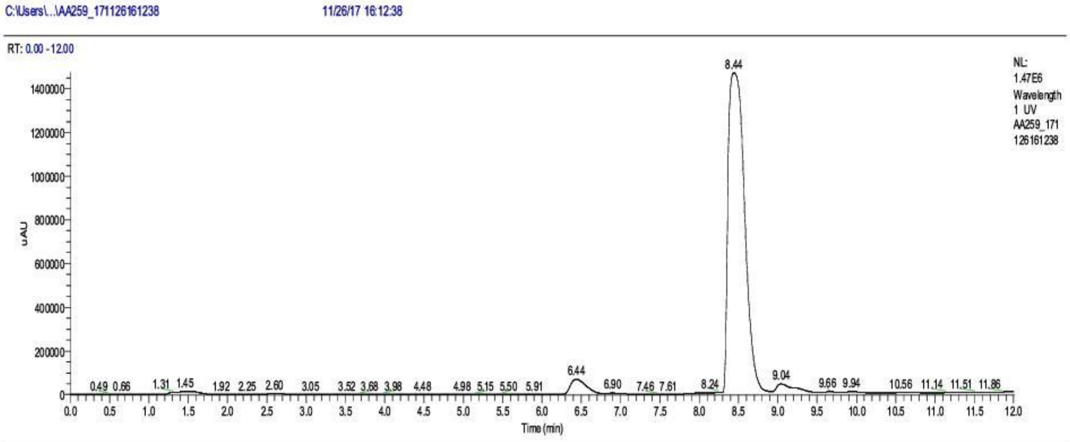

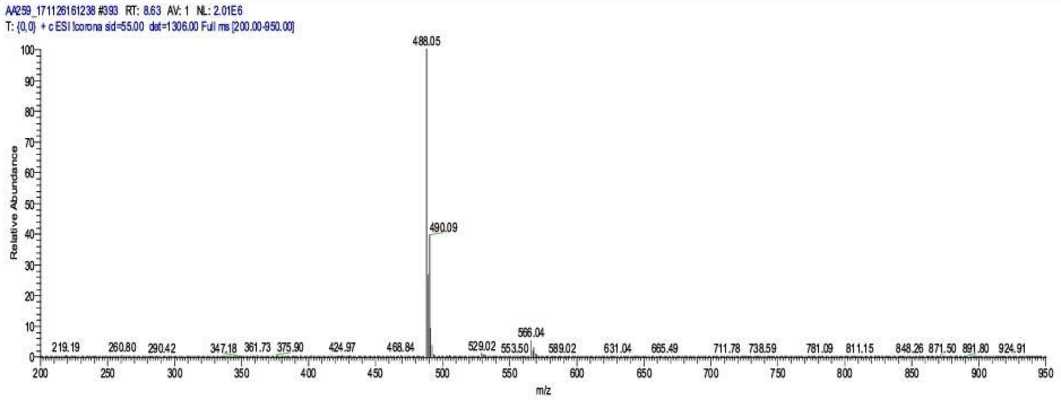

^{1}H, ^{13}C spectra, HRMS, and LC.MS of Compound 8.

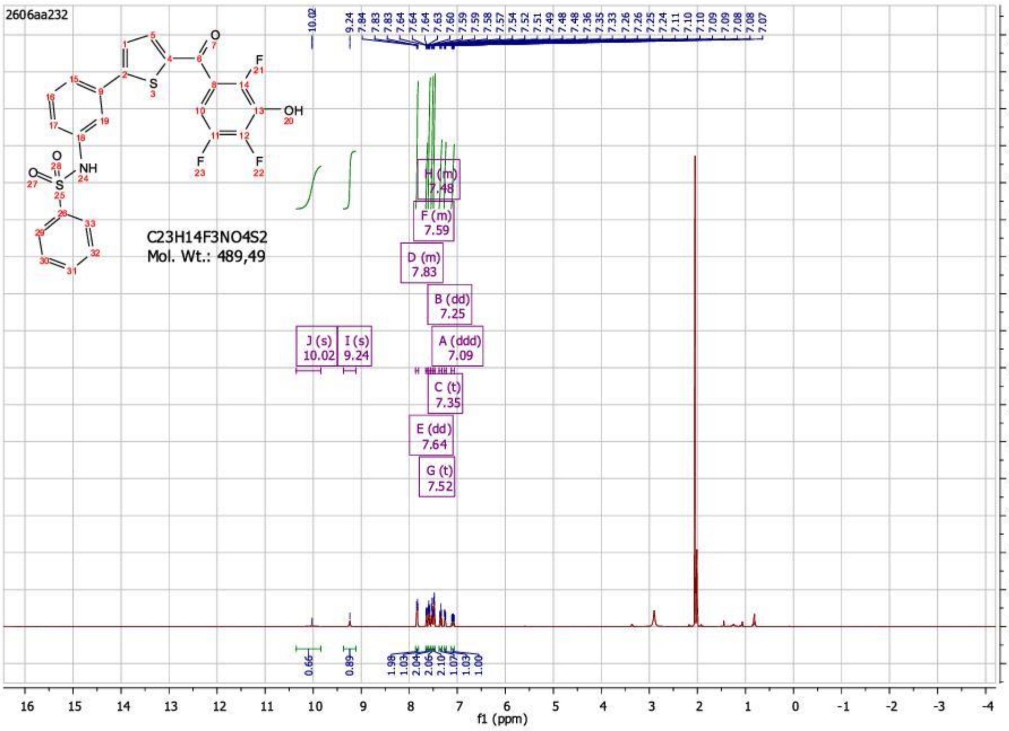
2606aa232
C23H14F3NO4S2
Mol. Wt.: 489,49
OH
F
NH
O
S
10.02
9.24
7.84
7.83
7.83
7.64
7.64
7.63
7.60
7.59
7.59
7.58
7.57
7.54
7.52
7.51
7.49
7.48
7.48
7.36
7.35
7.33
7.26
7.26
7.25
7.24
7.11
7.10
7.09
7.09
7.08
7.08
7.07
H (m) 7.48
F (m) 7.59
D (m) 7.83
B (dd) 7.25
J (s) 10.02
I (s) 9.24
A (ddd) 7.09
C (t) 7.35
E (dd) 7.64
G (t) 7.52
0.66
0.89
1.98
1.03
2.04
2.06
2.10
1.07
1.03
1.00
f1 (ppm)

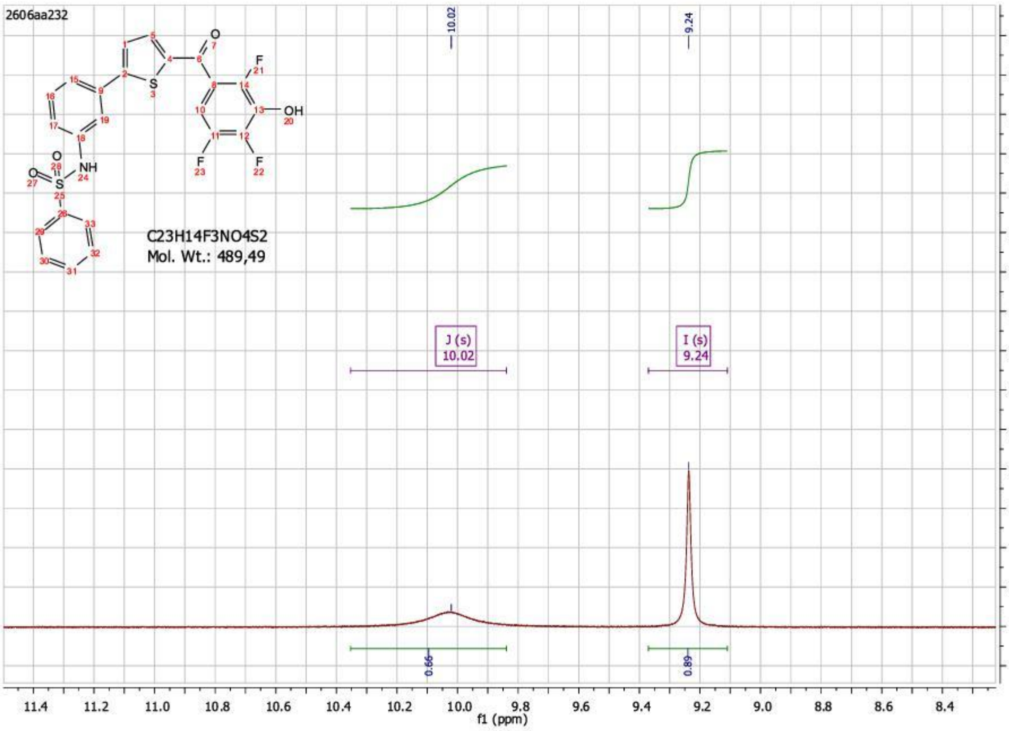
2606aa232
C23H14F3NO4S2
Mol. Wt.: 489,49
OH
F
NH
O
S
10.02
9.24
J (s) 10.02
I (s) 9.24
0.66
0.89
f1 (ppm)

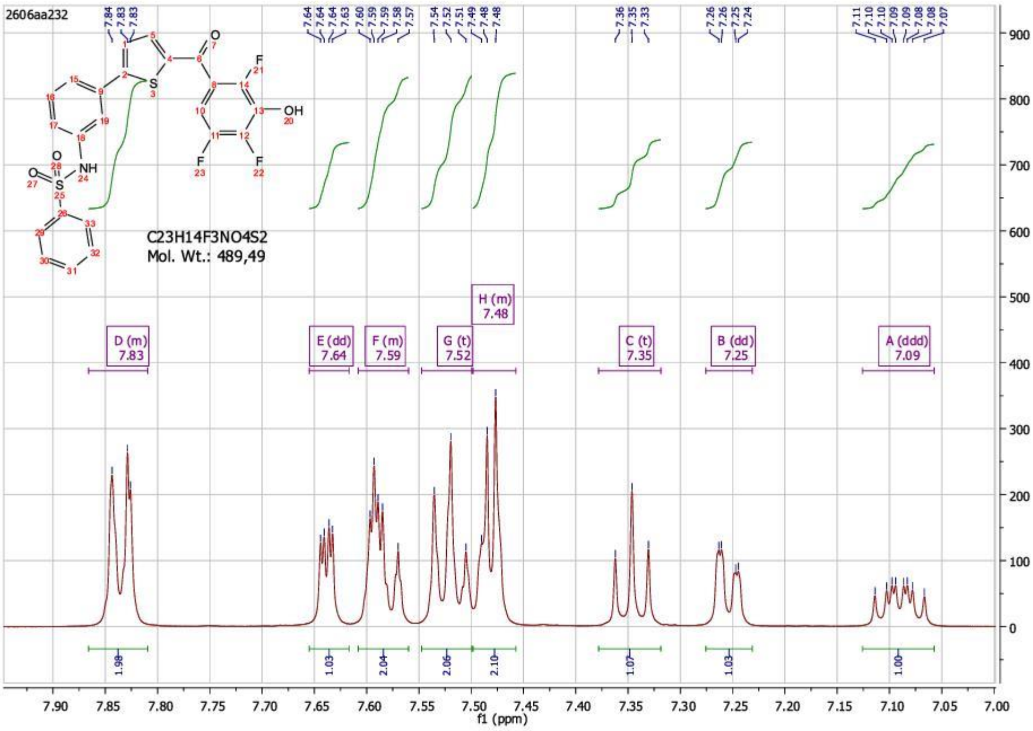
2606aa232
C23H14F3NO4S2
Mol. Wt.: 489,49
OH
NH
F
S
O
D (m) 7.83
E (dd) 7.64
F (m) 7.59
G (t) 7.52
H (m) 7.48
C (t) 7.35
B (dd) 7.25
A (ddd) 7.09
1.98
1.03
2.04
2.06
2.10
1.07
1.03
1.00
f1 (ppm)

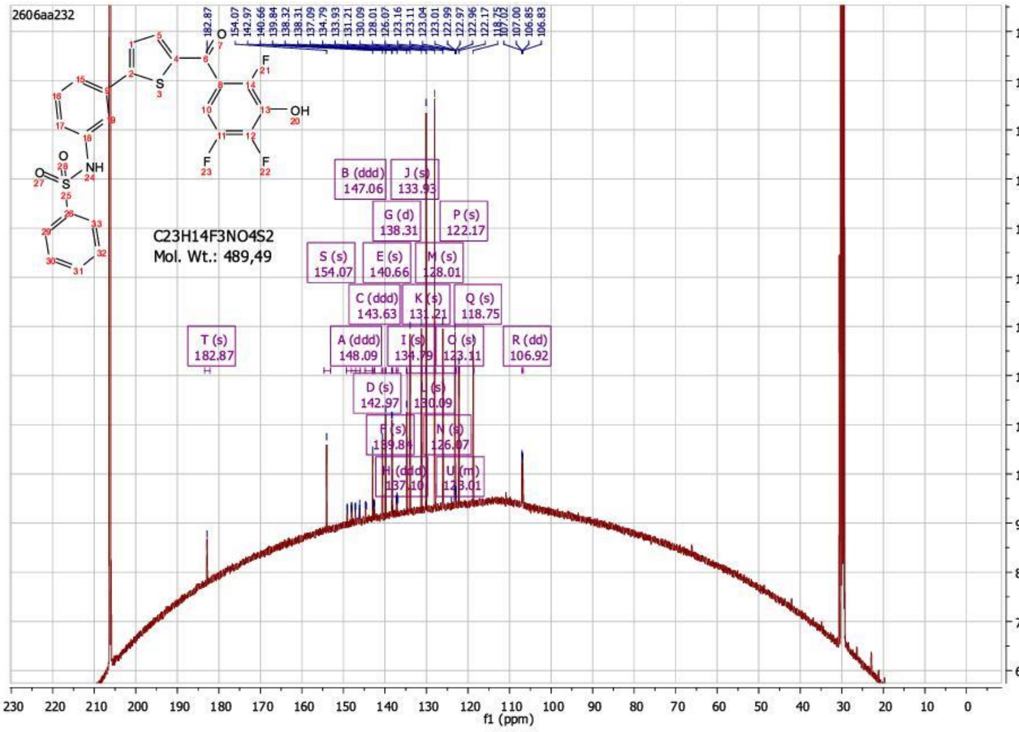
2606aa232
C23H14F3NO4S2
Mol. Wt.: 489,49
T (s) 182.87
S (s) 154.07
A (ddd) 148.09
B (ddd) 147.06
C (ddd) 143.63
D (s) 142.97
E (s) 140.66
F (s) 139.84
G (d) 138.31
H (ddd) 137.10
I (s) 134.79
J (s) 133.93
K (s) 131.21
L (s) 130.09
M (s) 128.01
N (s) 126.07
O (s) 123.11
U (m) 123.01
P (s) 122.17
Q (s) 118.75
R (dd) 106.92
f1 (ppm)

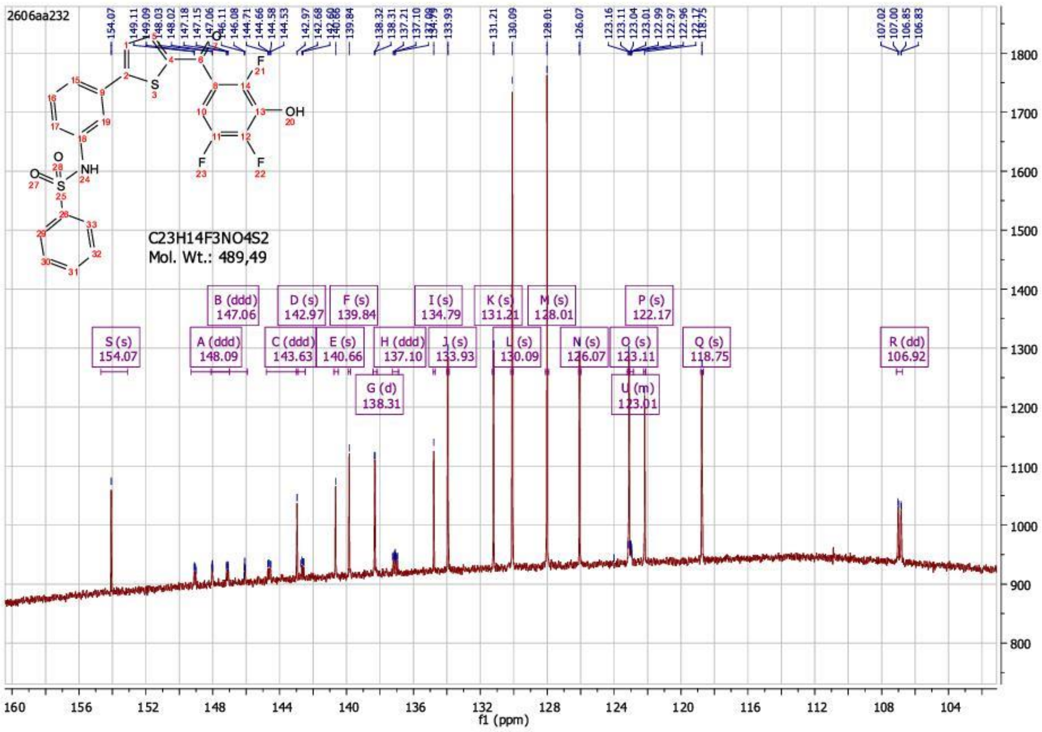
2606aa232
154.07
149.11
149.09
148.03
148.02
147.18
147.15
147.06
146.11
146.08
144.71
144.66
144.58
144.53
142.97
142.68
139.84
138.32
138.31
137.21
137.10
133.93
131.21
130.09
128.01
126.07
123.16
123.11
123.04
123.01
122.99
122.97
122.96
122.17
118.75
107.02
107.00
106.85
106.83
O
S
F
OH
F
F
NH
O
S
O
C23H14F3NO4S2
Mol. Wt.: 489,49
S (s) 154.07
A (ddd) 148.09
B (ddd) 147.06
C (ddd) 143.63
D (s) 142.97
E (s) 140.66
F (s) 139.84
G (d) 138.31
H (ddd) 137.10
I (s) 134.79
J (s) 133.93
K (s) 131.21
L (s) 130.09
M (s) 128.01
N (s) 126.07
O (s) 123.11
U (m) 123.01
P (s) 122.17
Q (s) 118.75
R (dd) 106.92
1800
1700
1600
1500
1400
1300
1200
1100
1000
900
800
160
156
152
148
144
140
136
132
128
124
120
116
112
108
104
f1 (ppm)

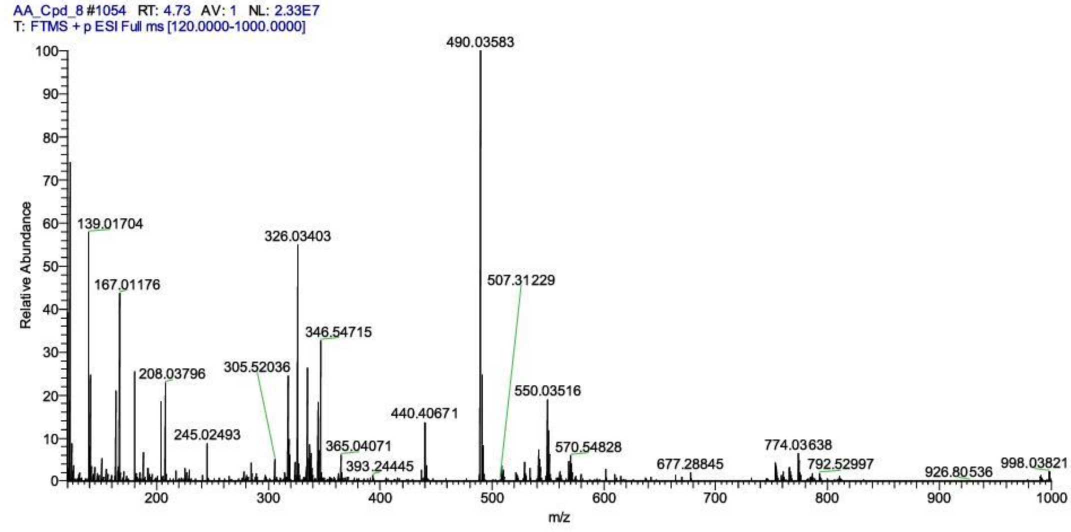
AA_Cpd_8 #1054 RT: 4.73 AV: 1 NL: 2.33E7
T: FTMS + p ESI Full ms [120.0000-1000.0000]
Relative Abundance
100
90
80
70
60
50
40
30
20
10
0
490.03583
139.01704
326.03403
167.01176
507.31229
346.54715
208.03796
305.52036
550.03516
440.40671
245.02493
365.04071
570.54828
393.24445
774.03638
677.28845
792.52997
926.80536
998.03821
200
300
400
500
600
700
800
900
1000
m/z

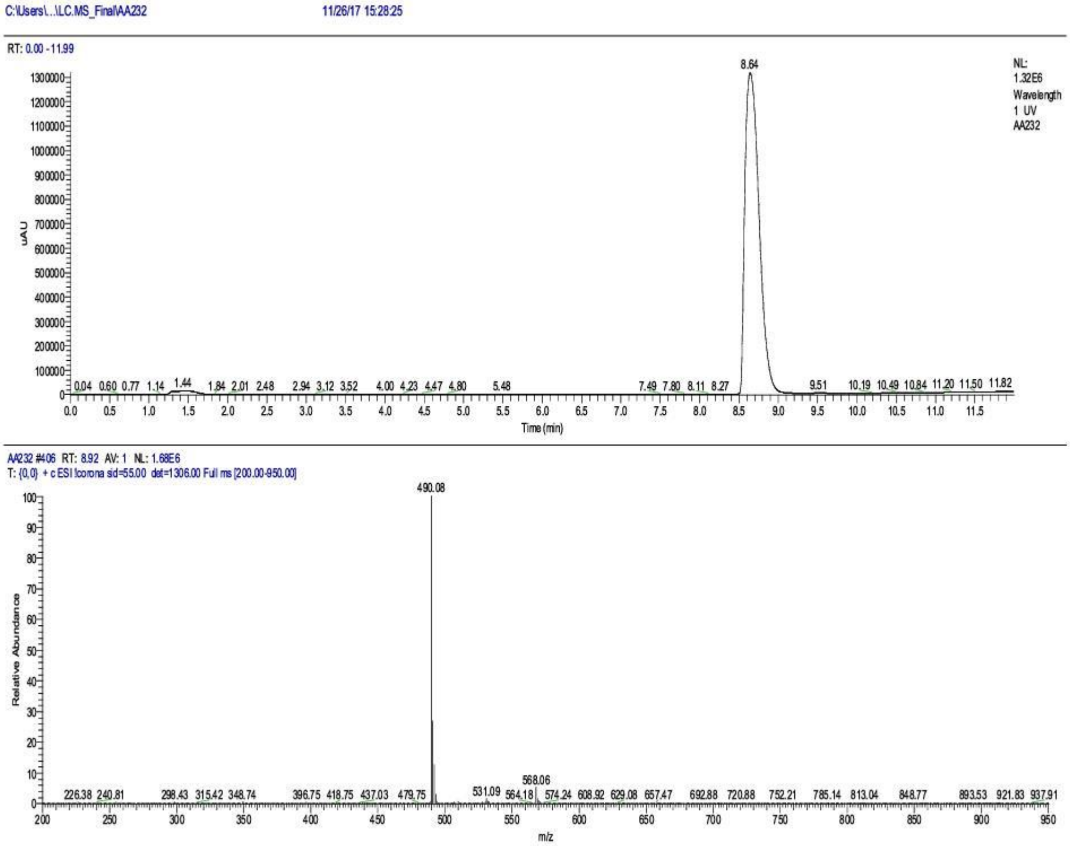

^{1}H, ^{13}C spectra, HRMS, and LC.MS of Compound 9.

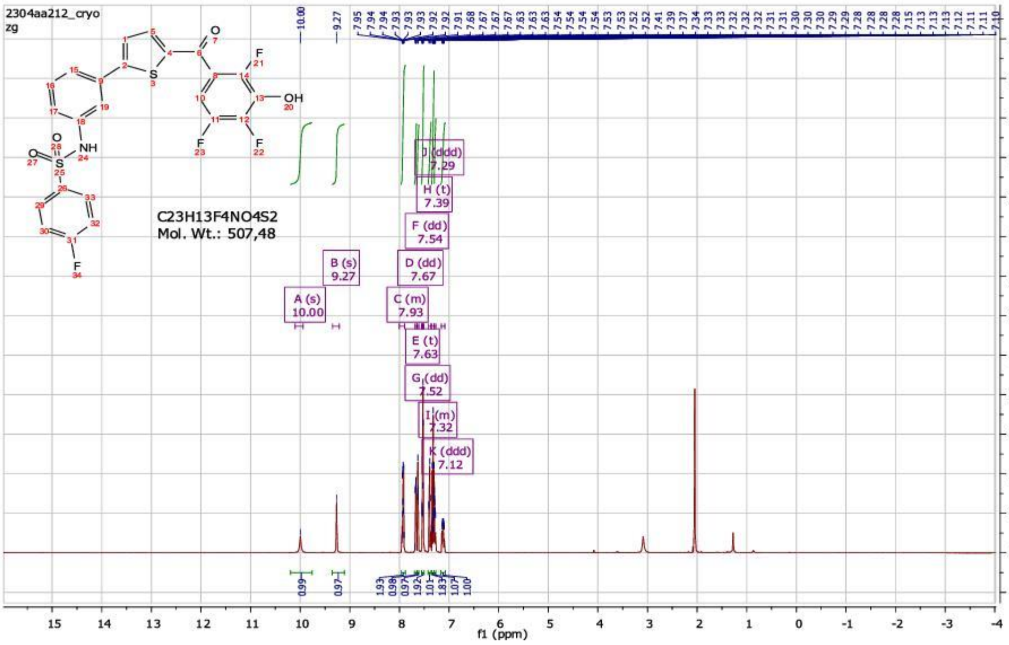

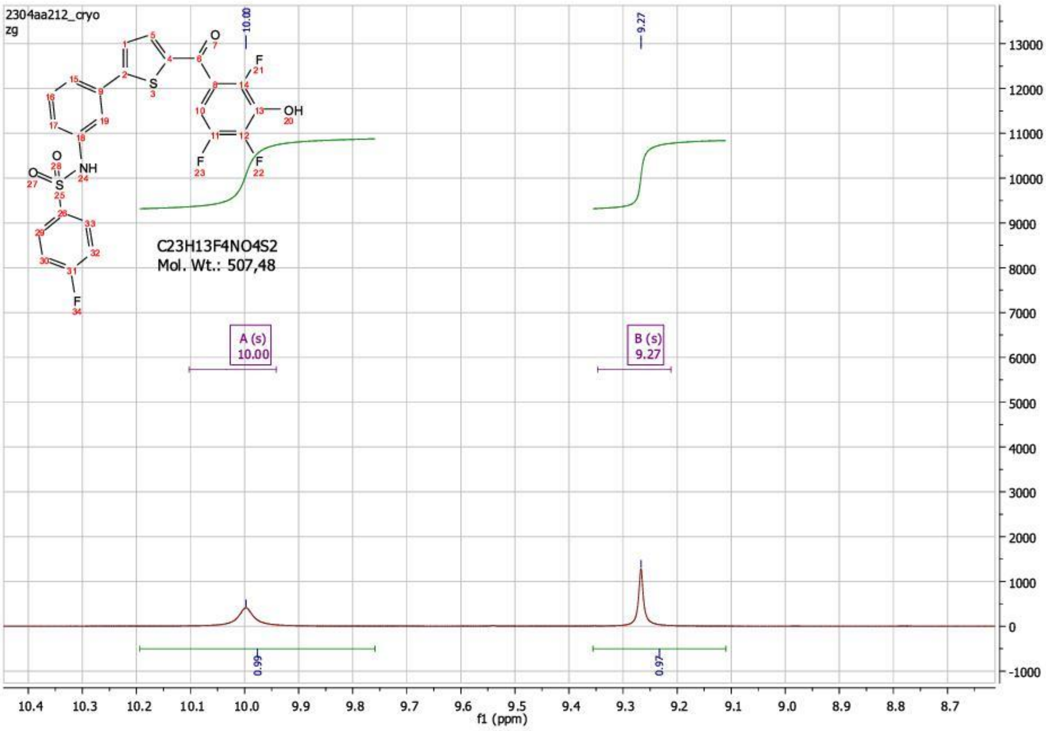
2304aa212_cryo
zg
C23H13F4NO4S2
Mol. Wt.: 507,48
OH
F
NH
A (s)
10.00
B (s)
9.27
0.99
0.97
f1 (ppm)

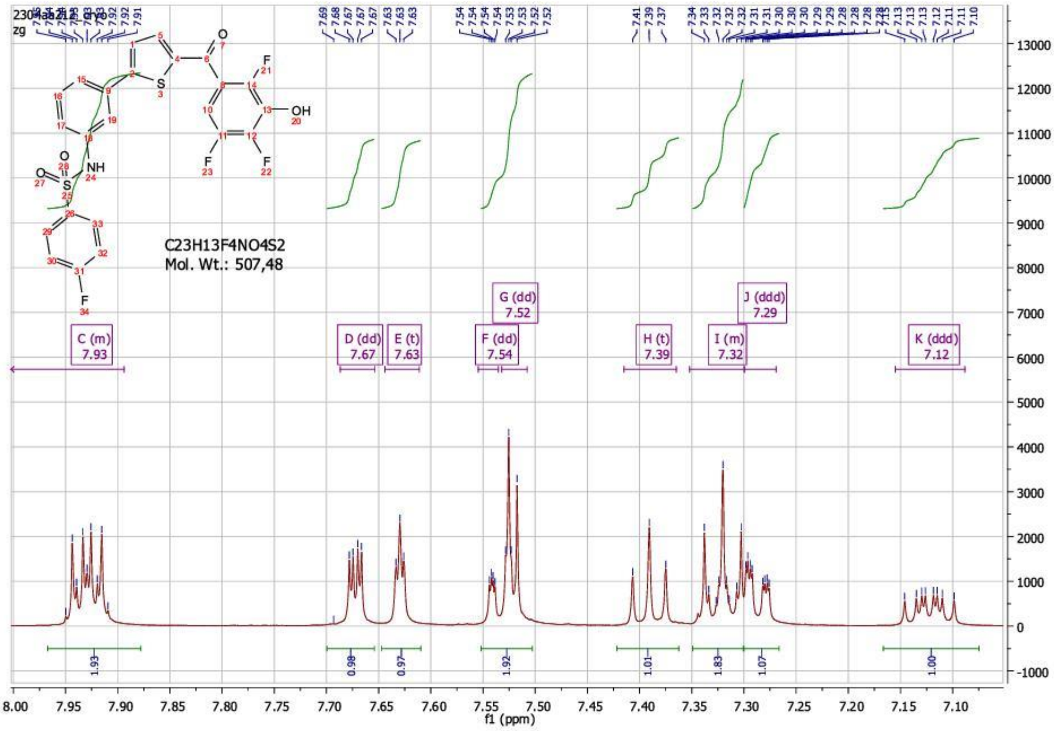
2304aa212_cryo
zg
C23H13F4NO4S2
Mol. Wt.: 507,48
C (m)
7.93
D (dd)
7.67
E (t)
7.63
F (dd)
7.54
G (dd)
7.52
H (t)
7.39
I (m)
7.32
J (ddd)
7.29
K (ddd)
7.12
1.93
0.98
0.97
1.92
1.01
1.83
1.07
1.00
f1 (ppm)

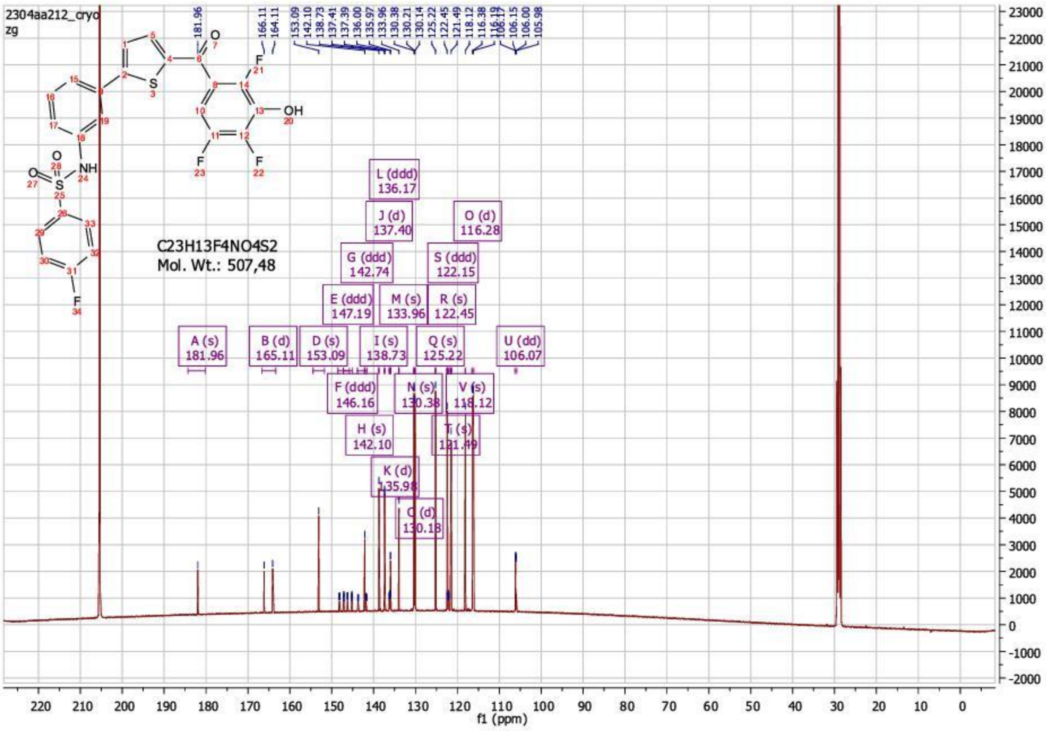
2304aa212_cryo
zg
C23H13F4NO4S2
Mol. Wt.: 507,48
OH
NH
A (s) 181.96
B (d) 165.11
D (s) 153.09
E (ddd) 147.19
F (ddd) 146.16
G (ddd) 142.74
H (s) 142.10
I (s) 138.73
J (d) 137.40
K (d) 135.98
L (ddd) 136.17
M (s) 133.96
N (s) 130.38
C (d) 130.18
Q (s) 125.22
R (s) 122.45
S (ddd) 122.15
T (s) 121.49
V (s) 118.12
O (d) 116.28
U (dd) 106.07
f1 (ppm)

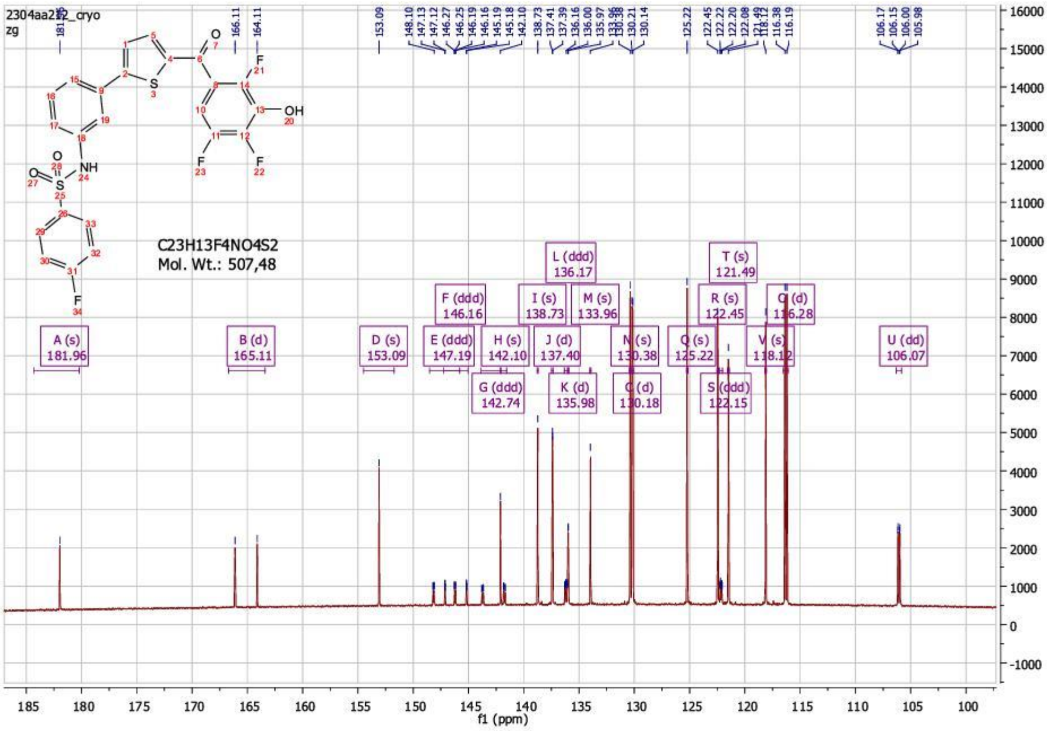
2304aa212_cryo
zg
C23H13F4NO4S2
Mol. Wt.: 507,48
OH
NH
A (s) 181.96
B (d) 165.11
D (s) 153.09
E (ddd) 147.19
F (ddd) 146.16
G (ddd) 142.74
H (s) 142.10
I (s) 138.73
J (d) 137.40
K (d) 135.98
L (ddd) 136.17
M (s) 133.96
N (s) 130.38
C (d) 130.18
Q (s) 125.22
R (s) 122.45
S (ddd) 122.15
T (s) 121.49
V (s) 118.12
O (d) 116.28
U (dd) 106.07
f1 (ppm)

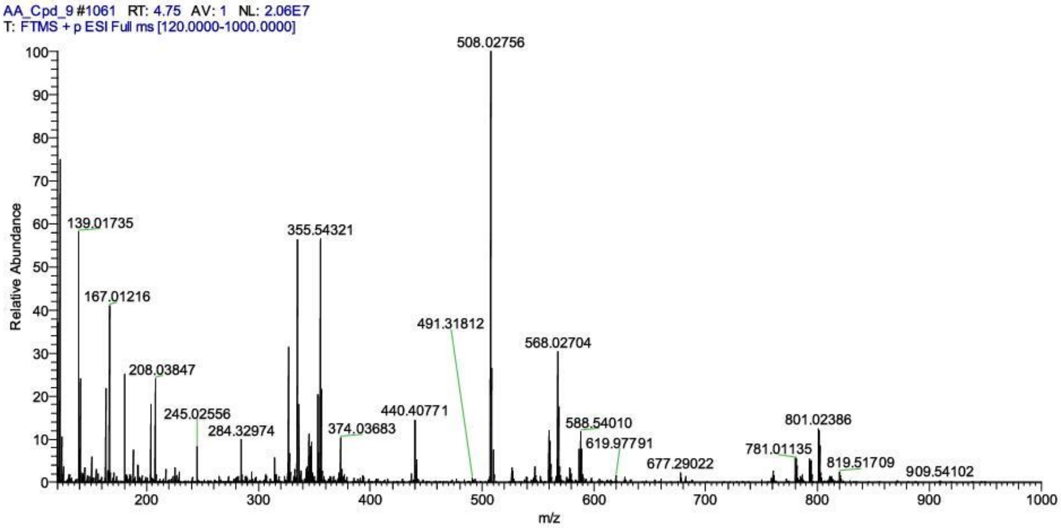

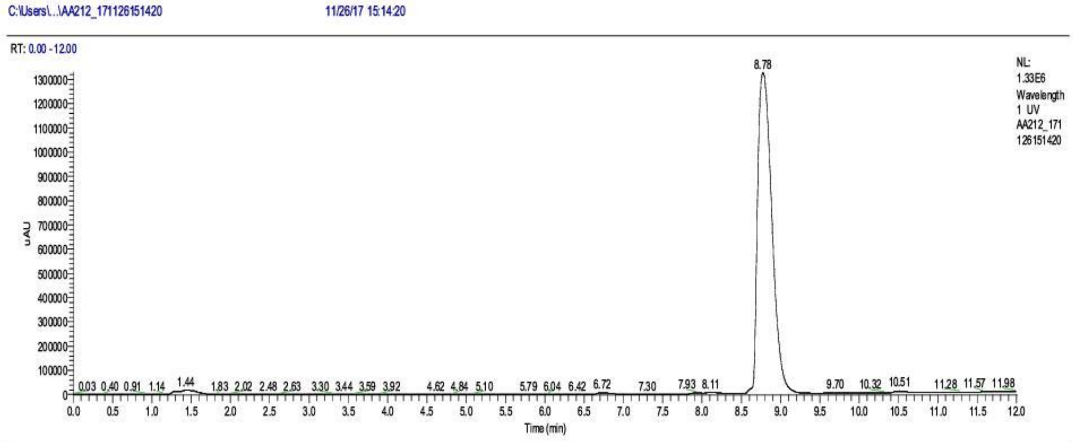

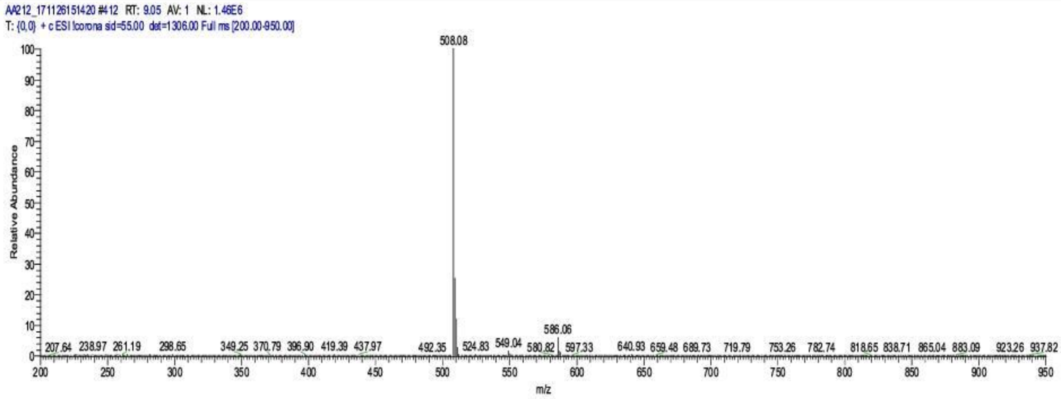

^{1}H, ^{13}C spectra, HRMS, and LC.MS of Compound 10.

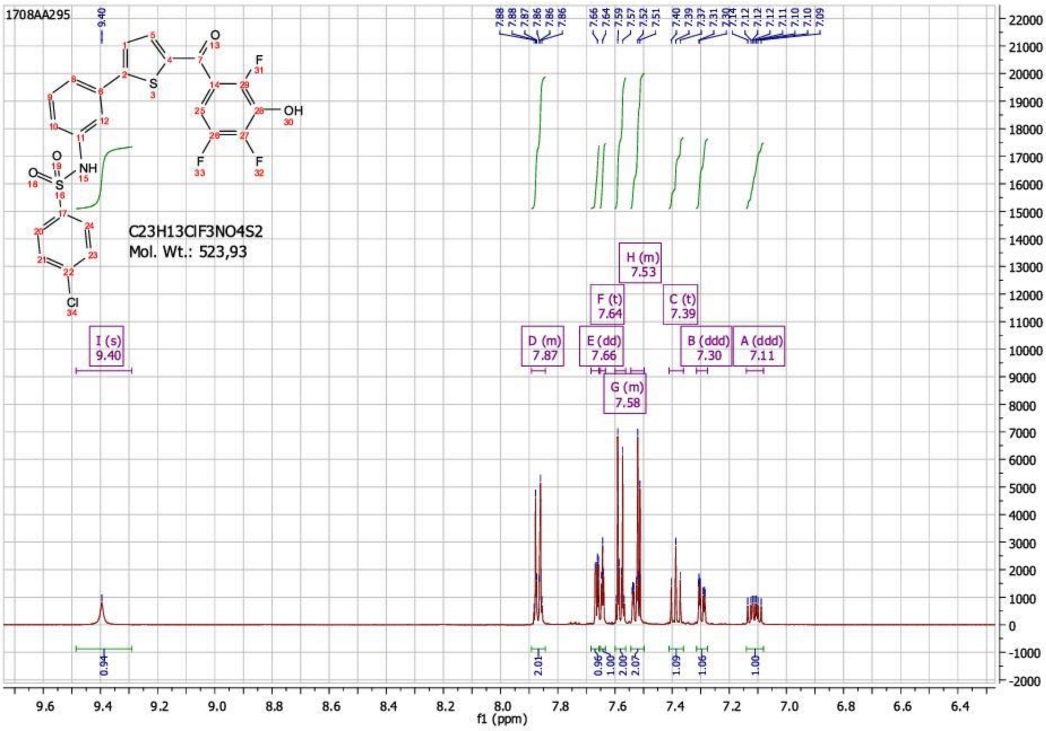
1708AA295
C23H13ClF3NO4S2
Mol. Wt.: 523,93
I (s) 9.40
D (m) 7.87
E (dd) 7.66
F (t) 7.64
G (m) 7.58
H (m) 7.53
C (t) 7.39
B (ddd) 7.30
A (ddd) 7.11
0.94
2.01
0.96
1.00
2.00
2.07
1.09
1.06
1.00
f1 (ppm)

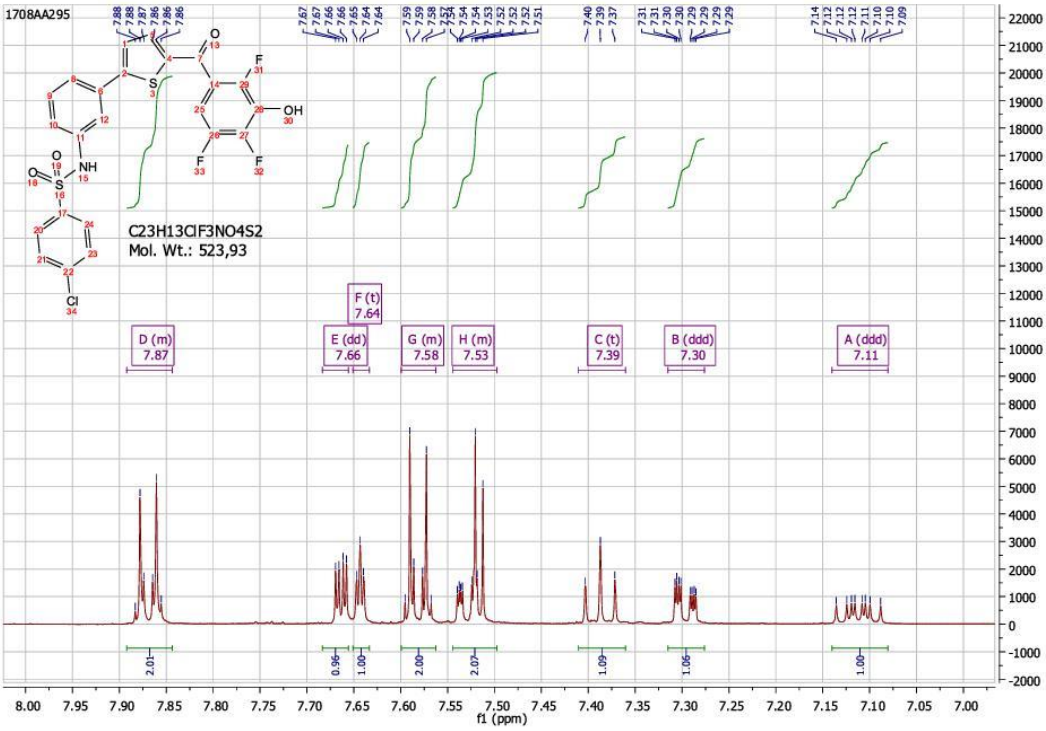
1708AA295
C23H13ClF3NO4S2
Mol. Wt.: 523,93
D (m) 7.87
E (dd) 7.66
F (t) 7.64
G (m) 7.58
H (m) 7.53
C (t) 7.39
B (ddd) 7.30
A (ddd) 7.11
2.01
0.96
1.00
2.00
2.07
1.09
1.06
1.00
f1 (ppm)

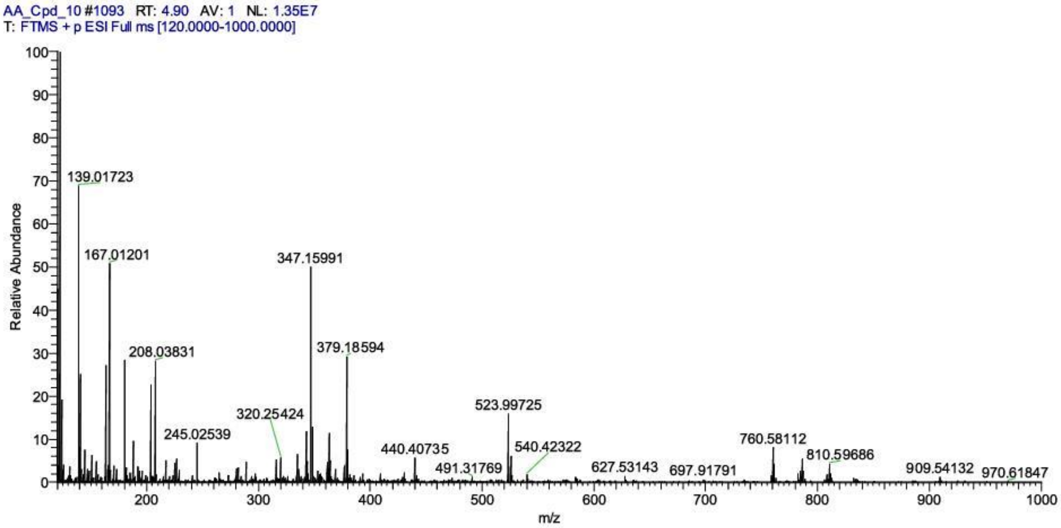

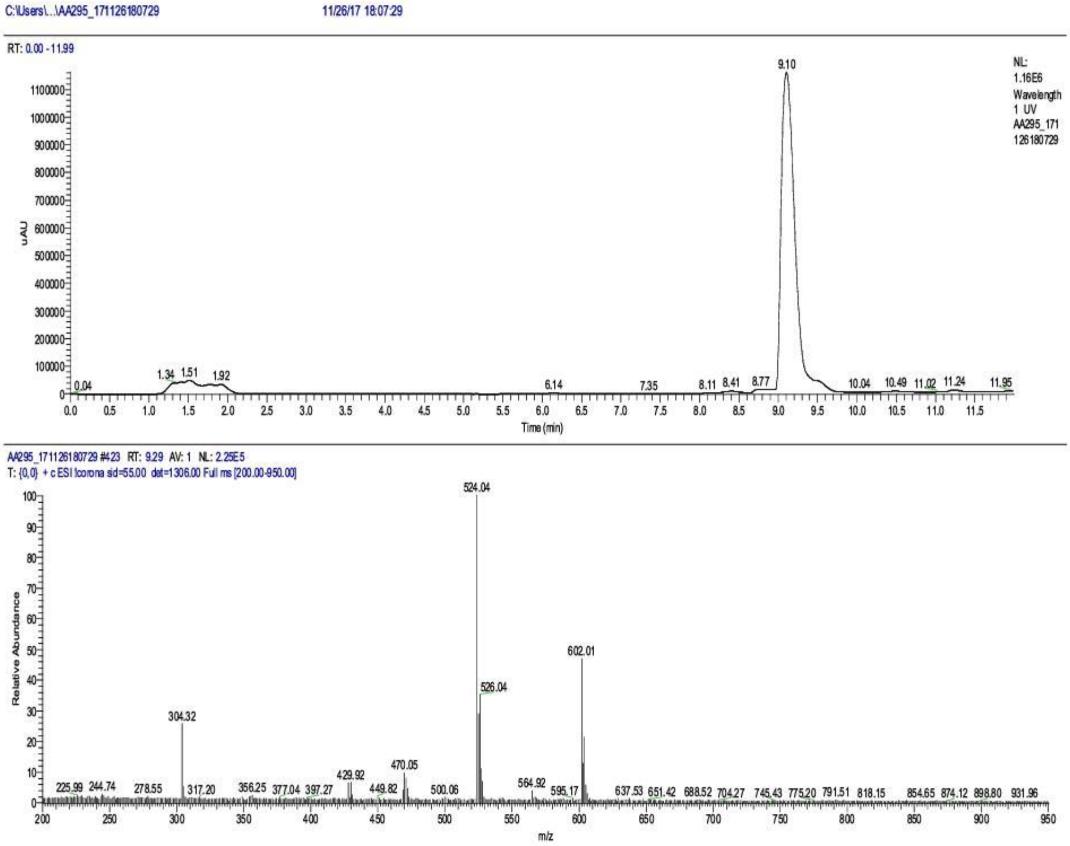

^{1}H, ^{13}C spectra, HRMS, and LC.MS of Compound 11.

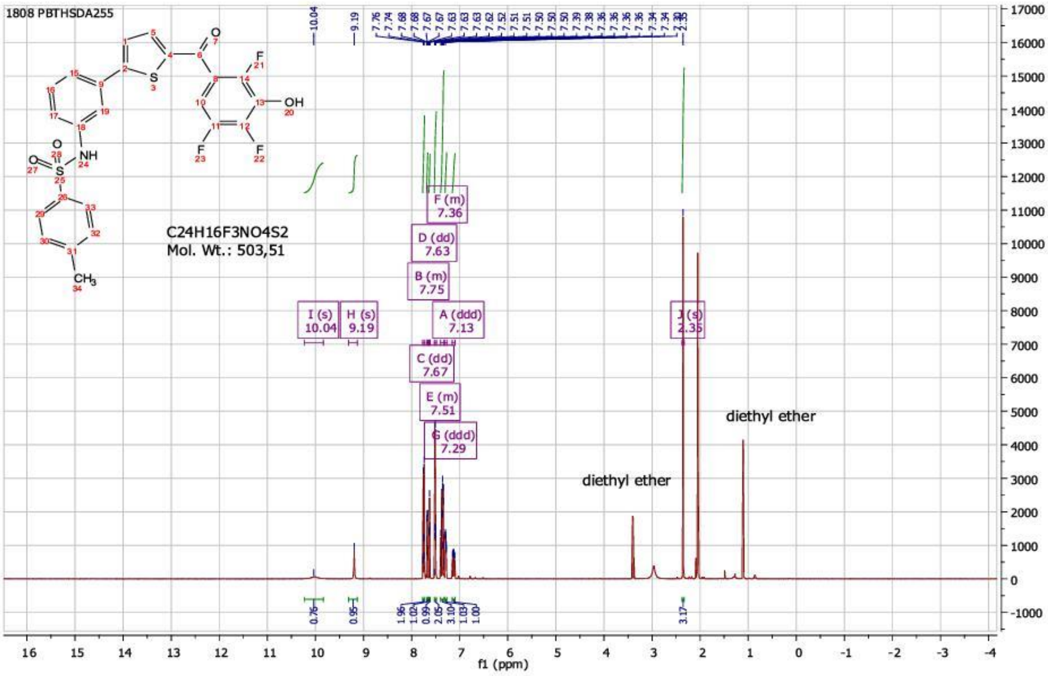
1808 PBTHSDA255
C24H16F3NO4S2
Mol. Wt.: 503,51
10.04
9.19
7.76 7.74 7.68 7.68 7.67 7.67 7.63 7.63 7.63 7.62 7.52 7.51 7.51 7.50 7.50 7.50 7.39 7.38 7.36 7.36 7.36 7.36 7.34 7.34 7.30 2.35
F (m) 7.36
D (dd) 7.63
B (m) 7.75
I (s) 10.04
H (s) 9.19
A (ddd) 7.13
J (s) 2.35
C (dd) 7.67
E (m) 7.51
G (ddd) 7.29
diethyl ether
diethyl ether
0.76
0.95
1.96 1.02 0.99 2.05 3.10 1.03 1.00
3.17
f1 (ppm)

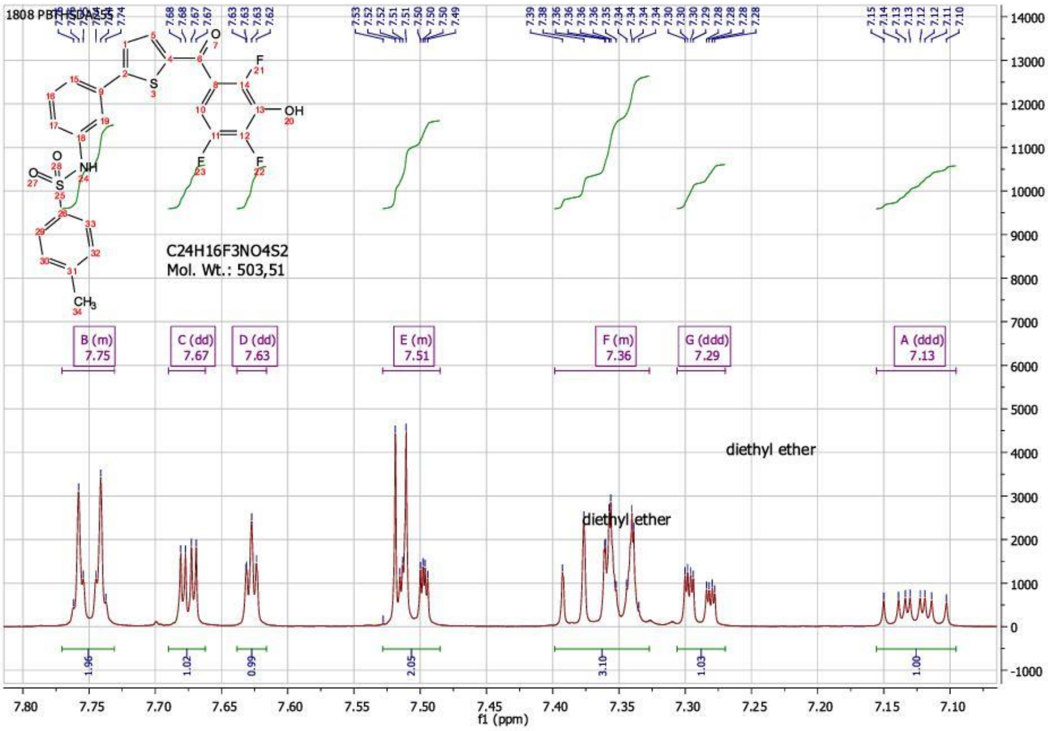
1808 PBTHSDA255
7.76 7.75 7.74
7.68 7.68 7.67 7.67
7.63 7.63 7.63 7.62
7.53 7.52 7.52 7.51 7.50 7.50 7.50 7.49
7.39 7.38 7.36 7.36 7.36 7.35 7.34 7.34 7.34 7.30 7.30 7.29 7.28 7.28 7.28 7.28
7.15 7.14 7.13 7.13 7.12 7.12 7.11 7.10
C24H16F3NO4S2
Mol. Wt.: 503,51
B (m) 7.75
C (dd) 7.67
D (dd) 7.63
E (m) 7.51
F (m) 7.36
G (ddd) 7.29
A (ddd) 7.13
diethyl ether
diethyl ether
1.96
1.02
0.99
2.05
3.10
1.03
1.00
f1 (ppm)

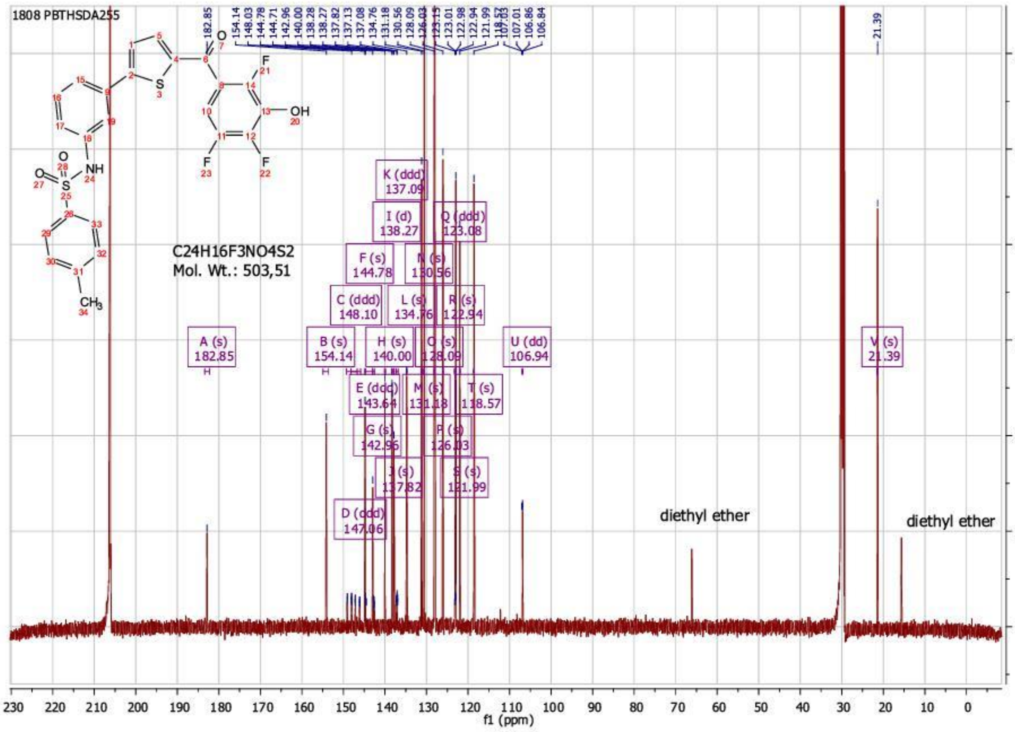
1808 PBTHSDA255
C24H16F3NO4S2
Mol. Wt.: 503,51
A (s) 182.85
B (s) 154.14
C (ddd) 148.10
D (ddd) 147.06
E (ddd) 143.64
F (s) 144.78
G (s) 142.96
H (s) 140.00
I (d) 138.27
J (s) 137.82
K (ddd) 137.09
L (s) 134.76
M (s) 131.18
N (s) 130.56
O (s) 128.09
P (s) 126.03
Q (ddd) 123.08
R (s) 122.94
S (s) 121.99
T (s) 118.57
U (dd) 106.94
V (s) 21.39
diethyl ether
diethyl ether
f1 (ppm)

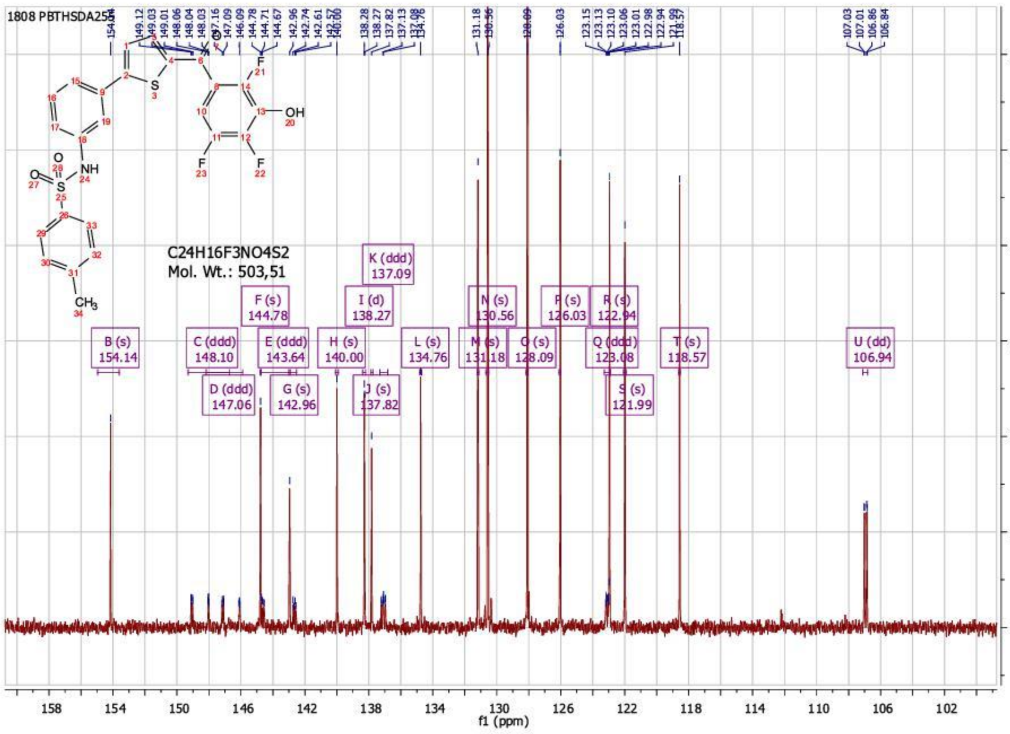
1808 PBTHSDA255
C24H16F3NO4S2
Mol. Wt.: 503,51
B (s) 154.14
C (ddd) 148.10
D (ddd) 147.06
E (ddd) 143.64
F (s) 144.78
G (s) 142.96
H (s) 140.00
I (d) 138.27
J (s) 137.82
K (ddd) 137.09
L (s) 134.76
M (s) 131.18
N (s) 130.56
O (s) 128.09
P (s) 126.03
Q (ddd) 123.08
R (s) 122.94
S (s) 121.99
T (s) 118.57
U (dd) 106.94
f1 (ppm)

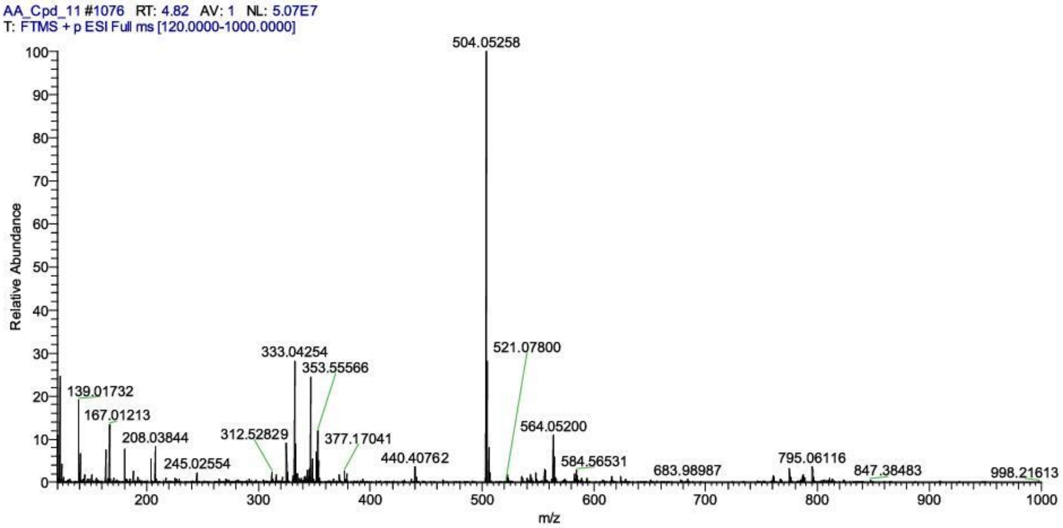

C:\Users\...\LC.MS_Final\AA255 11/26/17 15:42:29

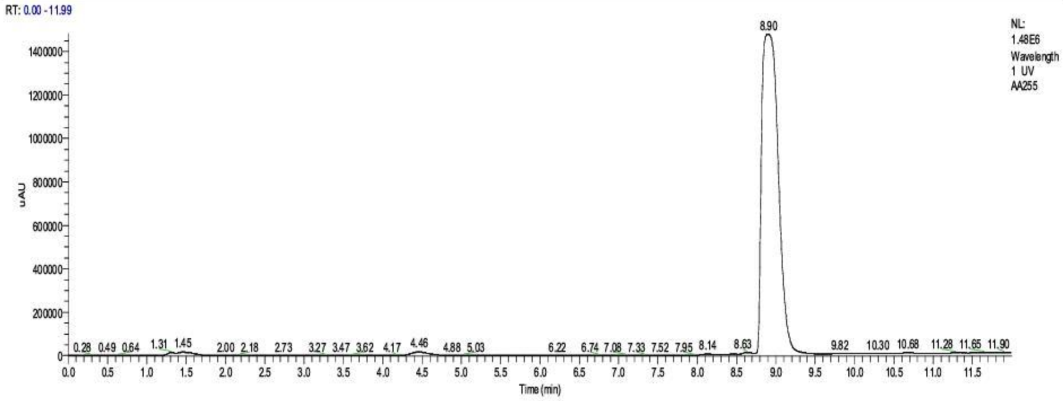

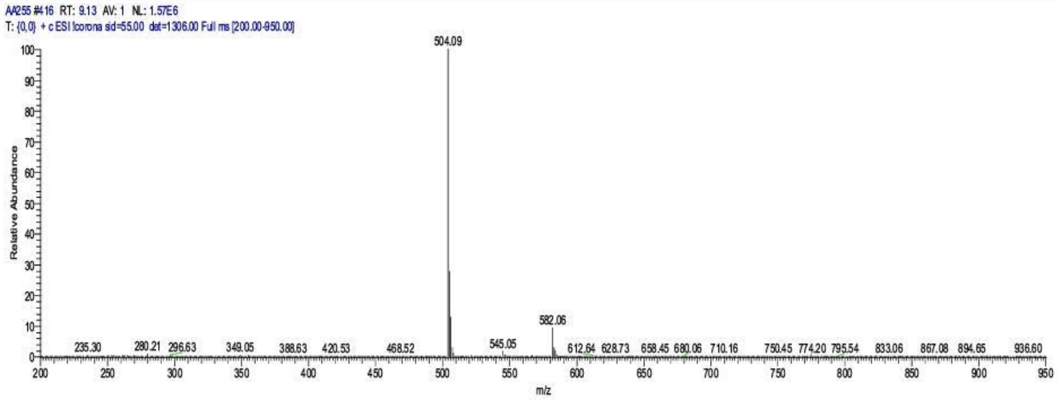

^{1}H, ^{13}C spectra, HRMS, and LC.MS of Compound 12.

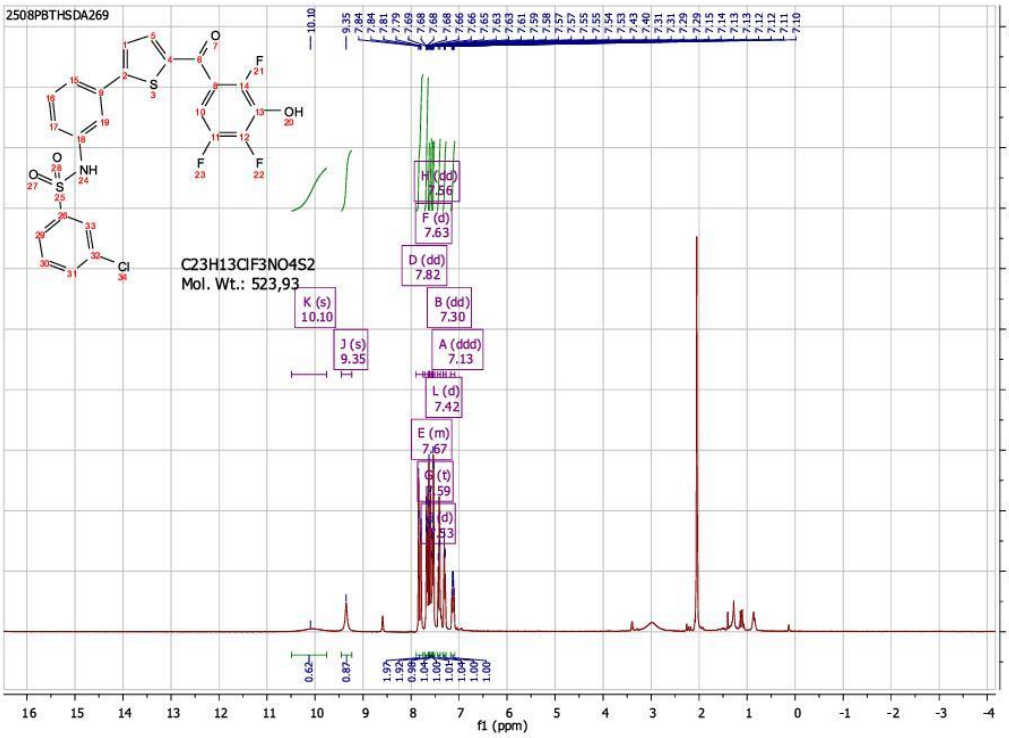
2508PBTHSDA269
C23H13ClF3NO4S2
Mol. Wt.: 523,93
10.10
9.35
7.84 7.84 7.81 7.79 7.69 7.68 7.68 7.68 7.66 7.65 7.63 7.63 7.61 7.59 7.58 7.57 7.57 7.55 7.55 7.54 7.53 7.43 7.40 7.31 7.31 7.29 7.29 7.15 7.14 7.13 7.13 7.12 7.12 7.11 7.10
K (s) 10.10
J (s) 9.35
H (dd) 7.56
F (d) 7.63
D (dd) 7.82
B (dd) 7.30
A (ddd) 7.13
L (d) 7.42
E (m) 7.67
G (t) 7.59
I (d) 7.53
0.62
0.87
1.97
1.92
0.98
1.04
1.00
1.01
1.04
1.00
1.00
16 15 14 13 12 11 10 9 8 7 6 5 4 3 2 1 0 -1 -2 -3 -4
f1 (ppm)
5000 4500 4000 3500 3000 2500 2000 1500 1000 500 0

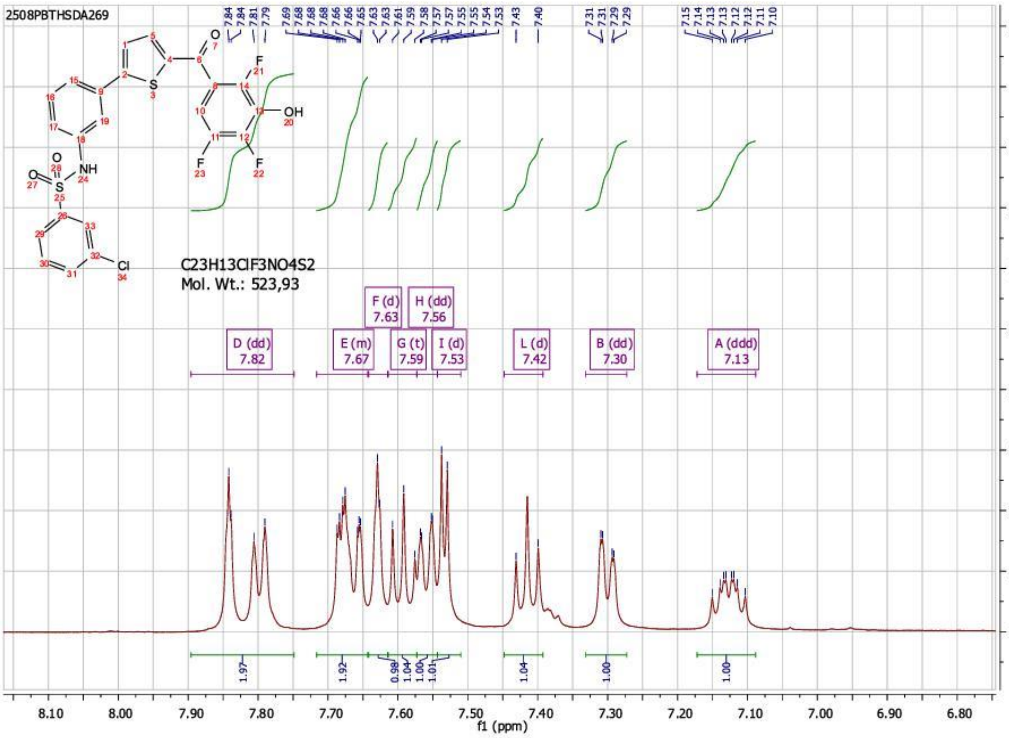
2508PBTHSDA269
C23H13ClF3NO4S2
Mol. Wt.: 523,93
7.84 7.84 7.81 7.79
7.69 7.68 7.68 7.68 7.66 7.65 7.63 7.63 7.61 7.59 7.58 7.57 7.57 7.55 7.55 7.54 7.53
7.43
7.40
7.31 7.31 7.29 7.29
7.15 7.14 7.13 7.13 7.12 7.12 7.11 7.10
F (d) 7.63
H (dd) 7.56
D (dd) 7.82
E (m) 7.67
G (t) 7.59
I (d) 7.53
L (d) 7.42
B (dd) 7.30
A (ddd) 7.13
1.97
1.92
0.98
1.04
1.00
1.01
1.04
1.00
1.00
8.10 8.00 7.90 7.80 7.70 7.60 7.50 7.40 7.30 7.20 7.10 7.00 6.90 6.80
f1 (ppm)
5000 4500 4000 3500 3000 2500 2000 1500 1000 500 0

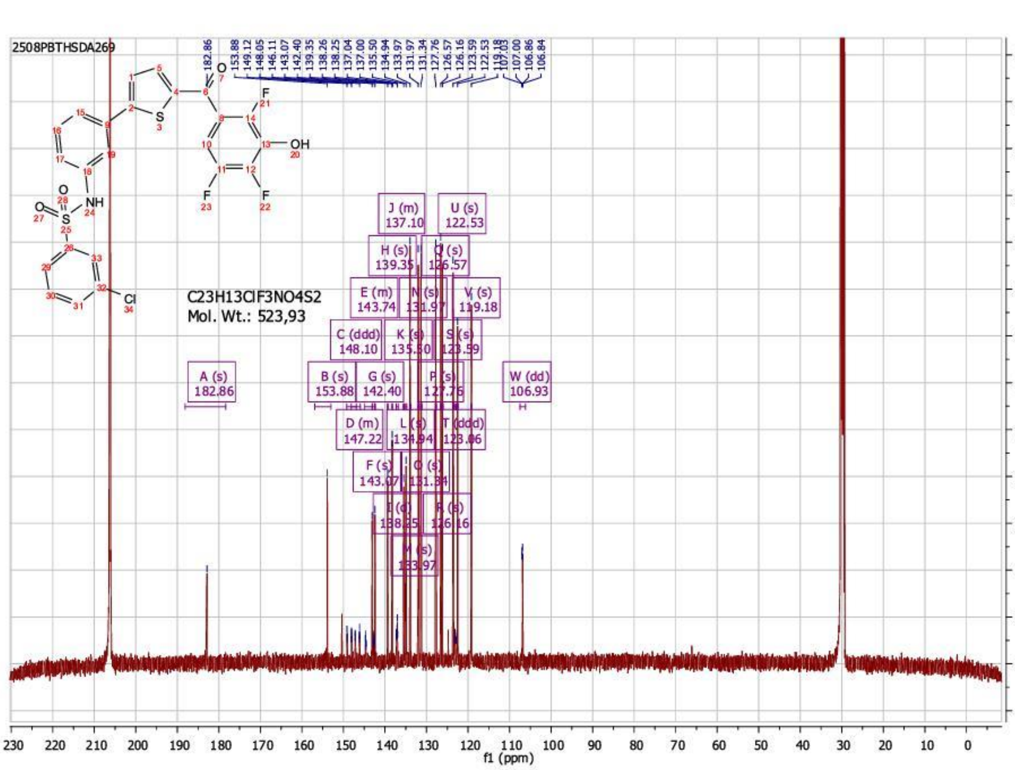
2508PBTHSDA269
C23H13ClF3NO4S2
Mol. Wt.: 523,93
A (s) 182.86
B (s) 153.88
C (ddd) 148.10
D (m) 147.22
E (m) 143.74
F (s) 143.07
G (s) 142.40
H (s) 139.35
I (d) 138.25
J (m) 137.10
K (s) 135.50
L (s) 134.94
M (s) 133.97
N (s) 131.97
O (s) 131.34
P (s) 127.76
Q (s) 126.57
R (s) 126.16
S (s) 123.59
T (ddd) 123.06
U (s) 122.53
V (s) 119.18
W (dd) 106.93
f1 (ppm)

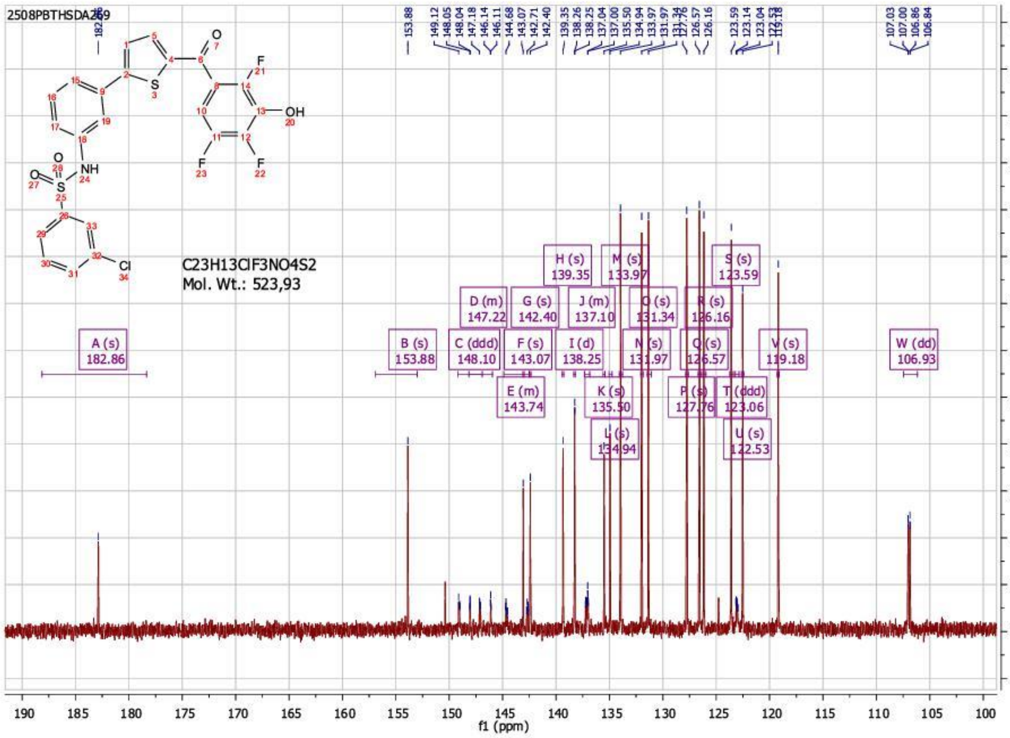
2508PBTHSDA269
C23H13ClF3NO4S2
Mol. Wt.: 523,93
A (s) 182.86
B (s) 153.88
C (ddd) 148.10
D (m) 147.22
E (m) 143.74
F (s) 143.07
G (s) 142.40
H (s) 139.35
I (d) 138.25
J (m) 137.10
K (s) 135.50
L (s) 134.94
M (s) 133.97
N (s) 131.97
O (s) 131.34
P (s) 127.76
Q (s) 126.57
R (s) 126.16
S (s) 123.59
T (ddd) 123.06
U (s) 122.53
V (s) 119.18
W (dd) 106.93
f1 (ppm)

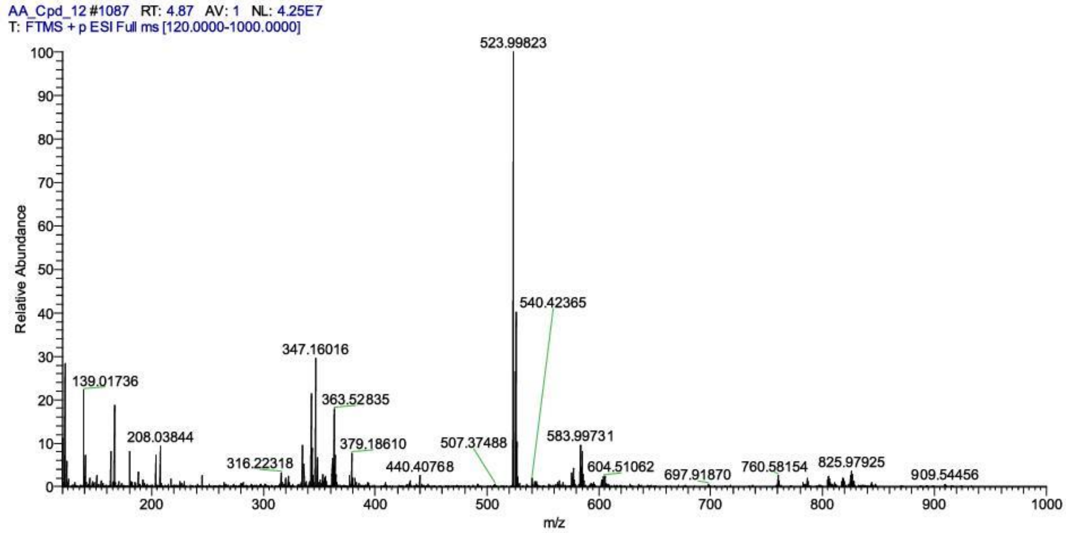

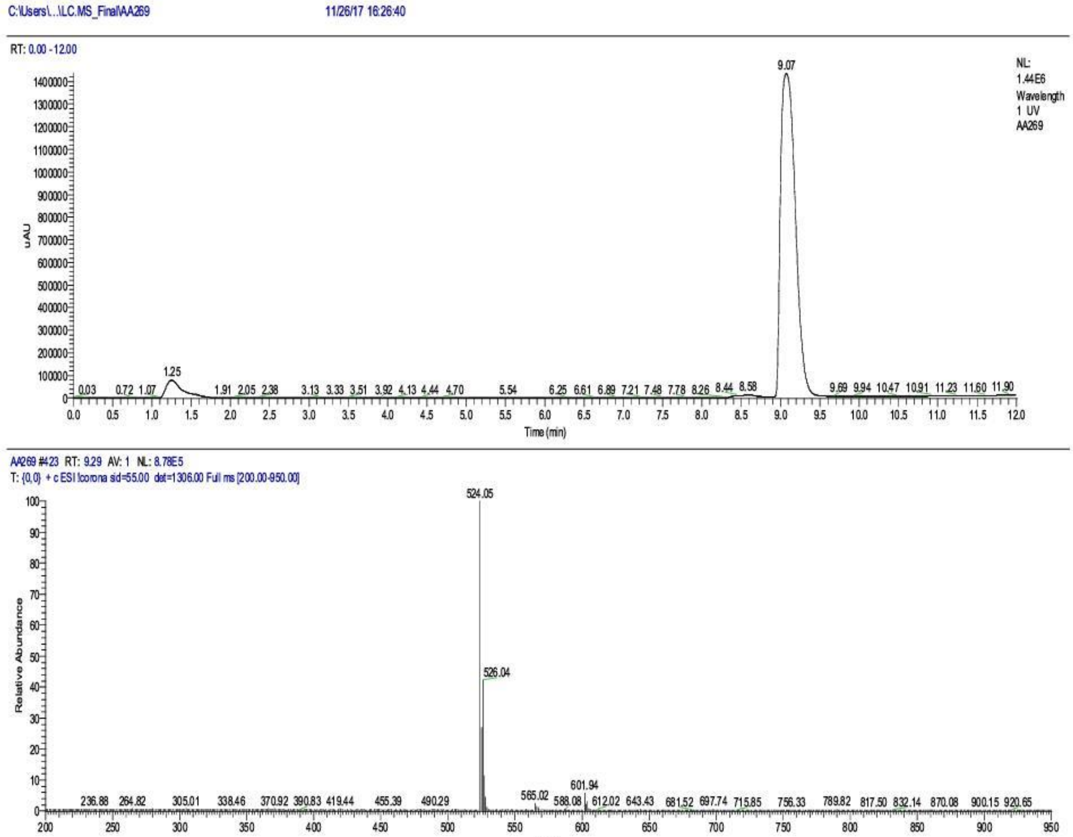

^{1}H, ^{13}C spectra, HRMS, and LC.MS of Compound 13.

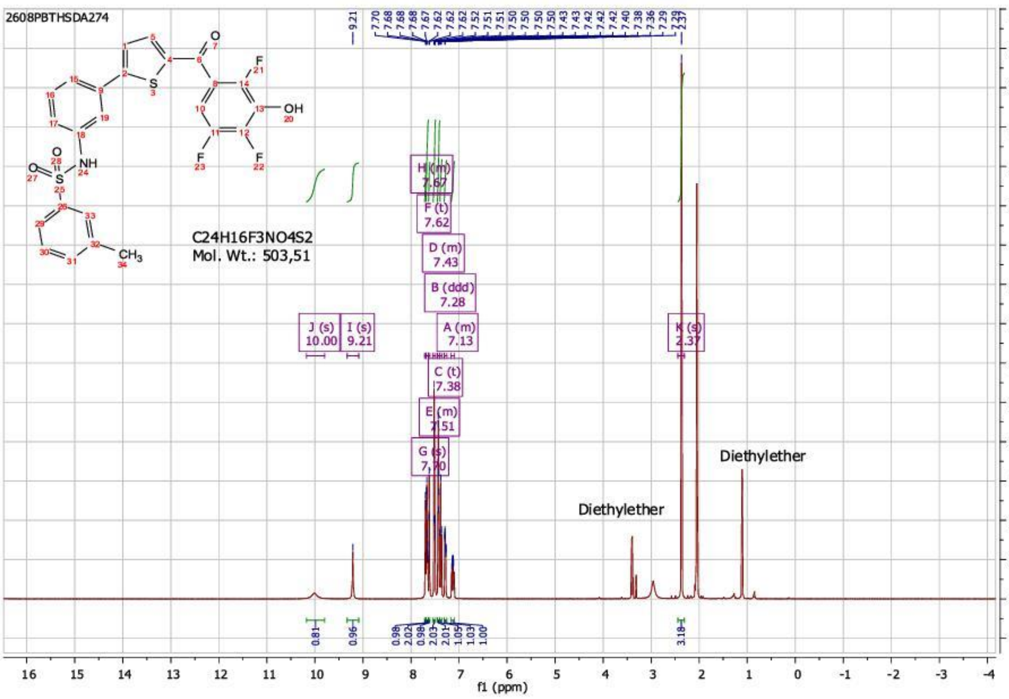
2608PBTHSDA274
9.21
7.70
7.68
7.68
7.68
7.67
7.62
7.62
7.62
7.52
7.51
7.51
7.50
7.50
7.50
7.50
7.43
7.43
7.42
7.42
7.42
7.40
7.38
7.36
7.29
7.29
2.37
O
F
OH
S
NH
CH3
F
F
C24H16F3NO4S2
Mol. Wt.: 503,51
J (s) 10.00
I (s) 9.21
H (m) 7.67
F (t) 7.62
D (m) 7.43
B (ddd) 7.28
A (m) 7.13
C (t) 7.38
E (m) 7.51
G (s) 7.70
K (s) 2.37
Diethylether
Diethylether
0.81
0.96
0.98
2.02
0.98
2.03
2.01
1.05
1.03
1.00
3.18
16 15 14 13 12 11 10 9 8 7 6 5 4 3 2 1 0 -1 -2 -3 -4
f1 (ppm)
7500 7000 6500 6000 5500 5000 4500 4000 3500 3000 2500 2000 1500 1000 500 0 -500

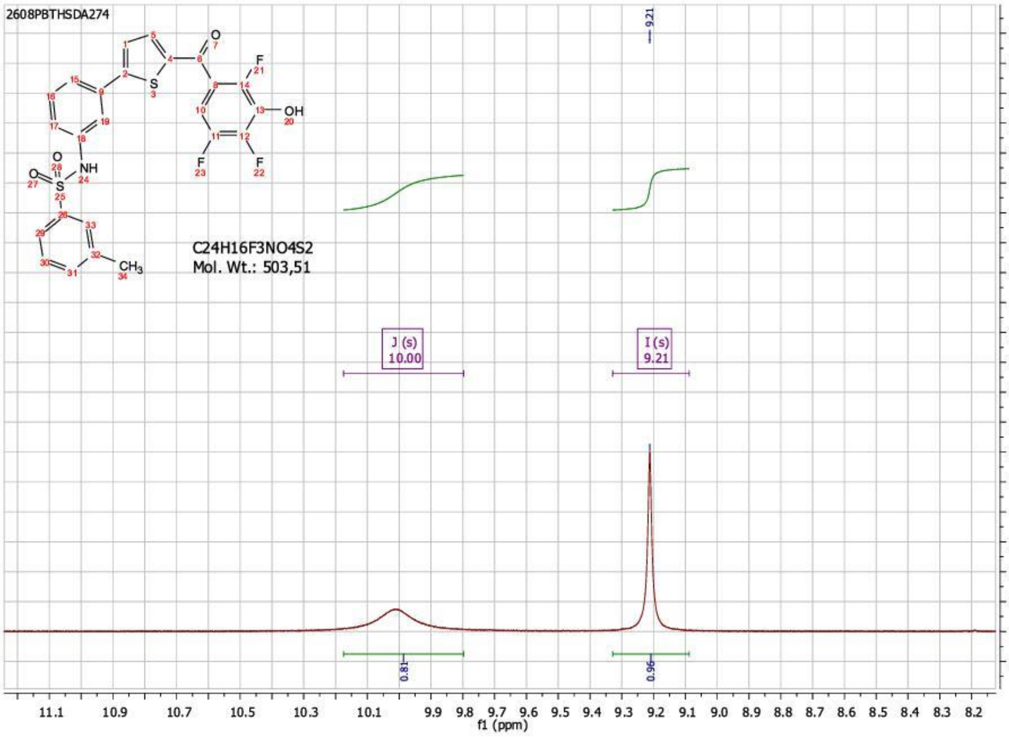
2608PBTHSDA274
9.21
O
F
OH
S
NH
CH3
F
F
C24H16F3NO4S2
Mol. Wt.: 503,51
J (s) 10.00
I (s) 9.21
0.81
0.96
11.1 10.9 10.7 10.5 10.3 10.1 9.9 9.8 9.7 9.6 9.5 9.4 9.3 9.2 9.1 9.0 8.9 8.8 8.7 8.6 8.5 8.4 8.3 8.2
f1 (ppm)
2000 1900 1800 1700 1600 1500 1400 1300 1200 1100 1000 900 800 700 600 500 400 300 200 100 0 -100

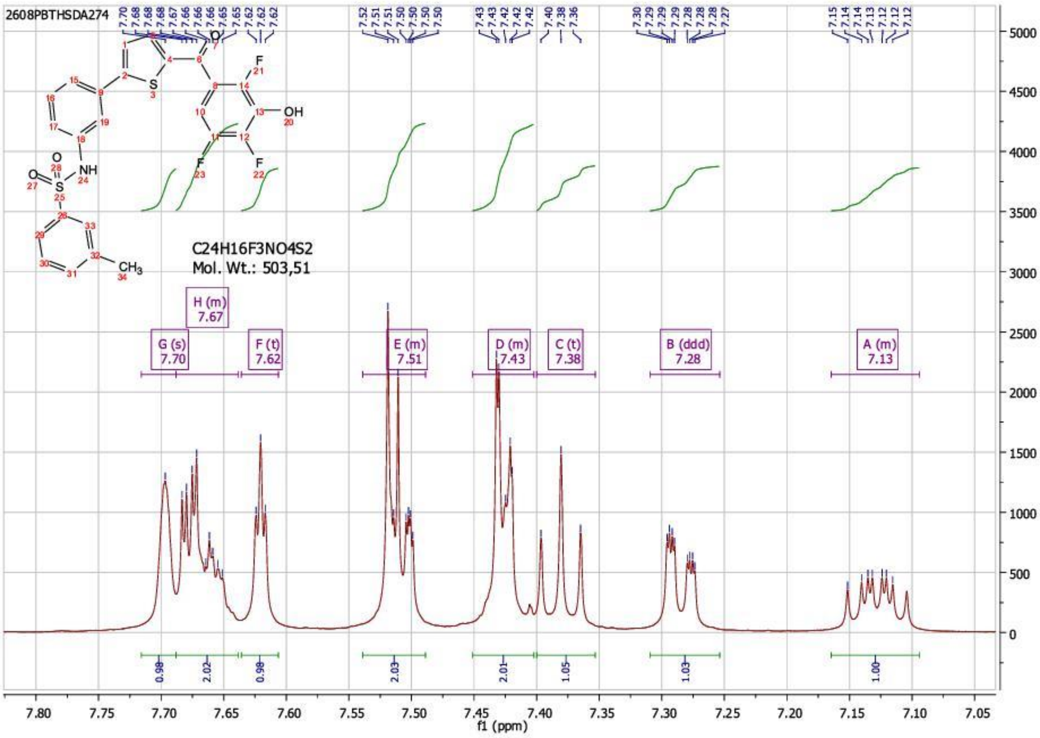
2608PBTHSDA274
7.70 7.68 7.68 7.67 7.67 7.66 7.66 7.65 7.62 7.62 7.62
7.52 7.51 7.51 7.50 7.50 7.50 7.50
7.43 7.43 7.42 7.42 7.42 7.40 7.38 7.36
7.30 7.29 7.29 7.29 7.28 7.28 7.28 7.27
7.15 7.14 7.14 7.13 7.12 7.12 7.12
C24H16F3NO4S2
Mol. Wt.: 503,51
H (m) 7.67
G (s) 7.70
F (t) 7.62
E (m) 7.51
D (m) 7.43
C (t) 7.38
B (ddd) 7.28
A (m) 7.13
0.98
2.02
0.98
2.03
2.01
1.05
1.03
1.00
f1 (ppm)

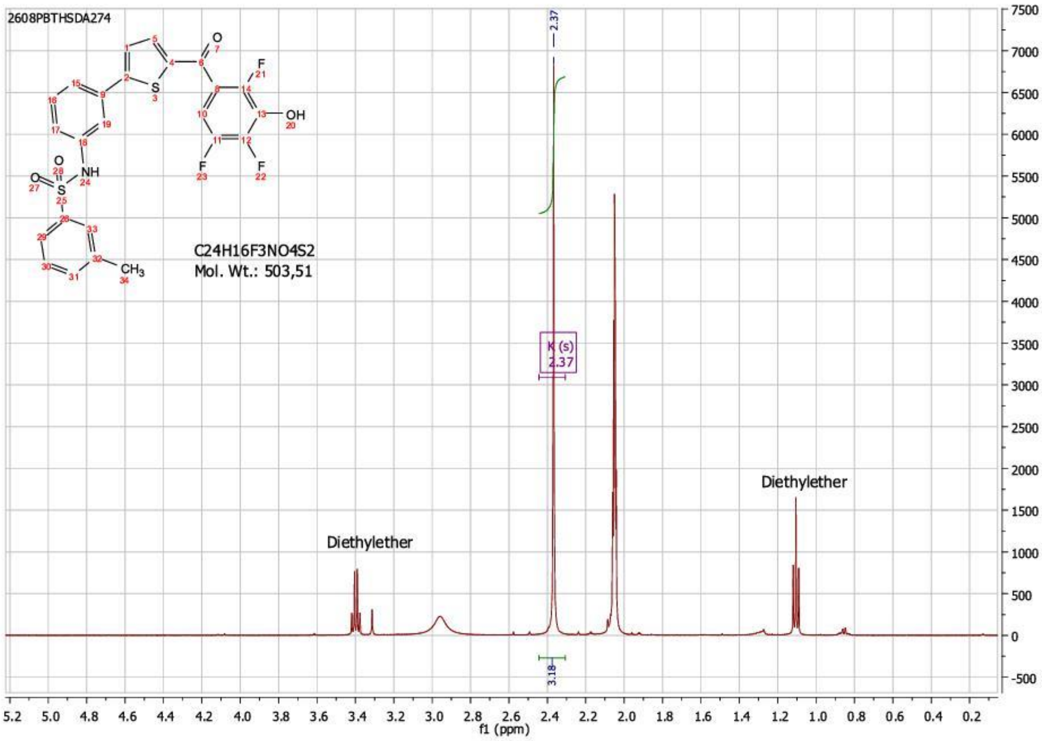
2608PBTHSDA274
2.37
C24H16F3NO4S2
Mol. Wt.: 503,51
K (s) 2.37
3.18
Diethylether
Diethylether
f1 (ppm)

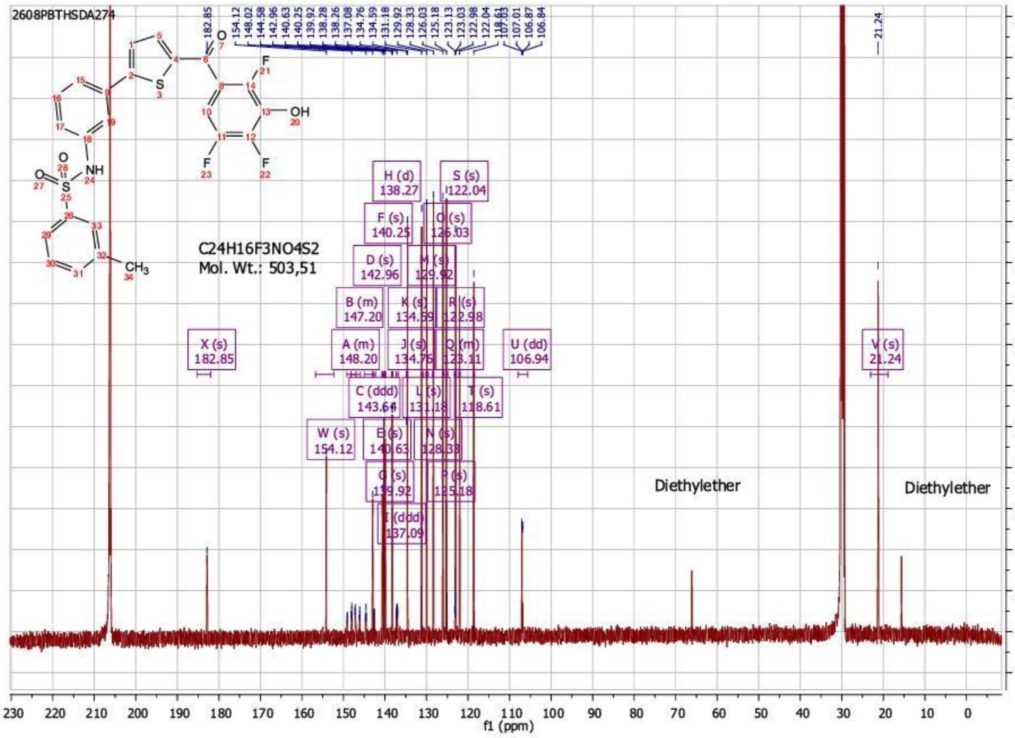
2608PBTHSDA274
C24H16F3NO4S2
Mol. Wt.: 503,51
O
S
F
OH
NH
CH3
182.85
154.12 148.02 144.58 142.96 140.63 140.25 139.92 138.28 138.26 137.08 134.76 134.59 131.18 129.92 128.33 126.03 125.18 123.13 123.03 122.98 122.04 118.61 107.03 107.01 106.87 106.84
21.24
X (s) 182.85
W (s) 154.12
A (m) 148.20
B (m) 147.20
C (ddd) 143.64
D (s) 142.96
E (s) 140.63
F (s) 140.25
G (s) 139.92
H (d) 138.27
I (ddd) 137.09
J (s) 134.76
K (s) 134.59
L (s) 131.18
M (s) 129.92
N (s) 128.33
O (s) 126.03
P (s) 125.18
Q (m) 123.11
R (s) 122.98
S (s) 122.04
T (s) 118.61
U (dd) 106.94
V (s) 21.24
Diethylether
Diethylether
30000 28000 26000 24000 22000 20000 18000 16000 14000 12000 10000 8000 6000 4000 2000 0 -2000
230 220 210 200 190 180 170 160 150 140 130 120 110 100 90 80 70 60 50 40 30 20 10 0
f1 (ppm)

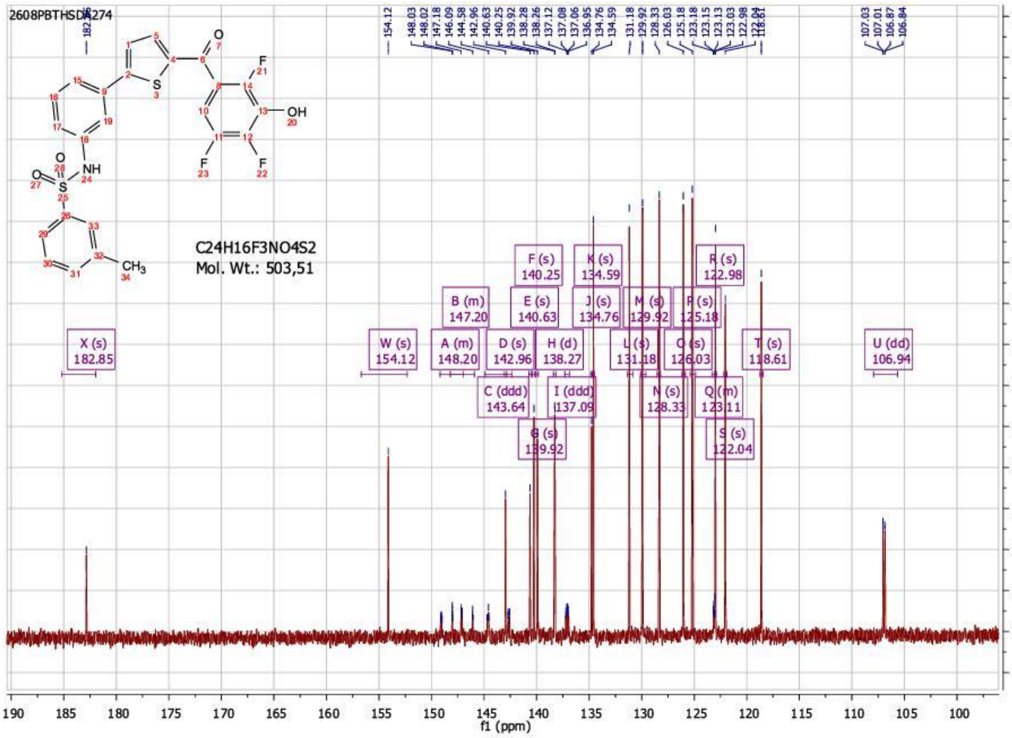
2608PBTHSDA274
C24H16F3NO4S2
Mol. Wt.: 503,51
O
S
F
OH
NH
CH3
182.85
154.12
148.03 148.02 147.18 146.09 144.58 142.96 140.63 140.25 139.92 138.28 138.26 137.12 137.08 137.06 136.95 134.76 134.59
131.18 129.92 128.33 126.03 125.18 123.15 123.13 123.03 122.98 122.04 118.61
107.03 107.01 106.87 106.84
X (s) 182.85
W (s) 154.12
A (m) 148.20
B (m) 147.20
C (ddd) 143.64
D (s) 142.96
E (s) 140.63
F (s) 140.25
G (s) 139.92
H (d) 138.27
I (ddd) 137.09
J (s) 134.76
K (s) 134.59
L (s) 131.18
M (s) 129.92
N (s) 128.33
O (s) 126.03
P (s) 125.18
Q (m) 123.11
R (s) 122.98
S (s) 122.04
T (s) 118.61
U (dd) 106.94
30000 28000 26000 24000 22000 20000 18000 16000 14000 12000 10000 8000 6000 4000 2000 0 -2000
190 185 180 175 170 165 160 155 150 145 140 135 130 125 120 115 110 105 100
f1 (ppm)

AA_Cpd_13 #1072 RT: 4.80 AV: 1 NL: 2.12E8
T: FTMS + p ESI Full ms [120.0000-1000.0000]

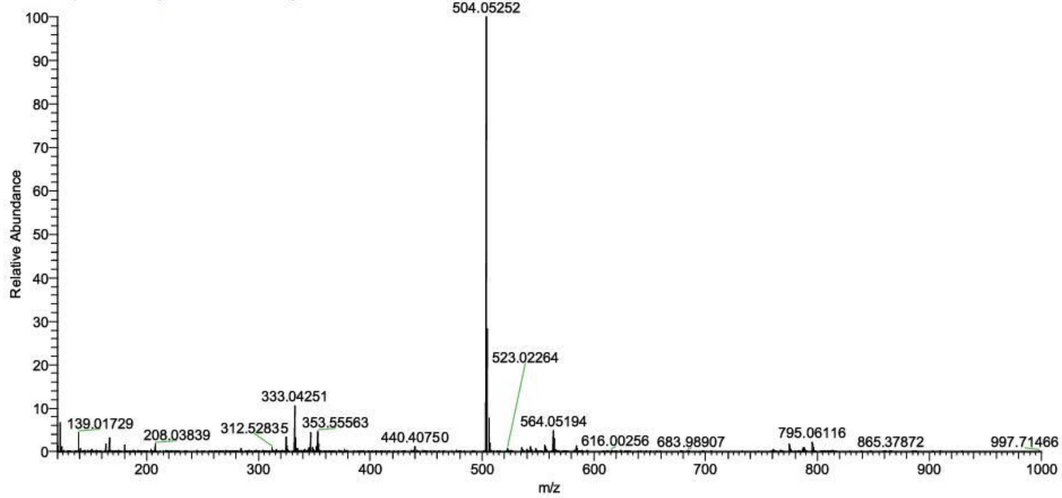

C:\Users\...\LC.MS_Final\AA274 11/26/17 16:40:45

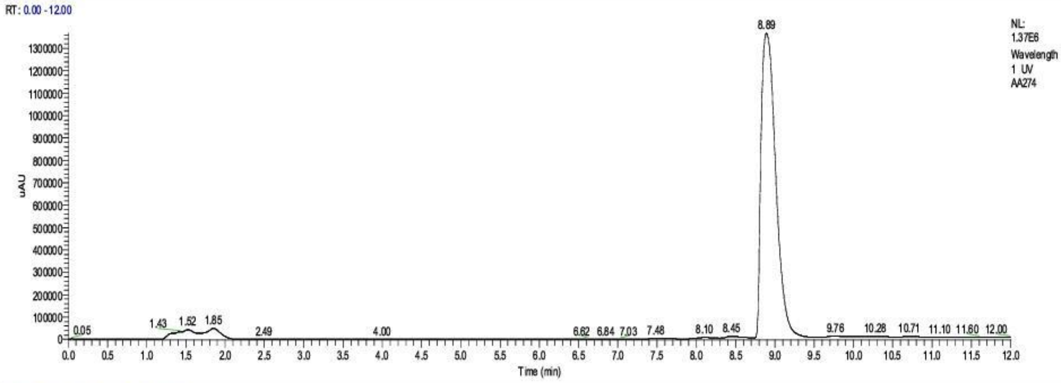

AA274 #417 RT: 9.16 AV: 1 NL: 9.53E5
T: {0,0} + c ESI !corona sid=55.00 det=1306.00 Full ms [200.00-950.00]

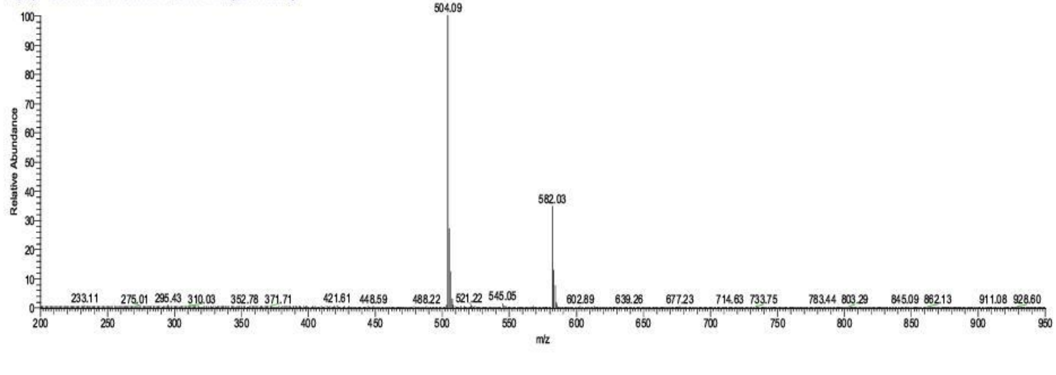

^{1}H, ^{13}C spectra, HRMS, and LC.MS of Compound 14.

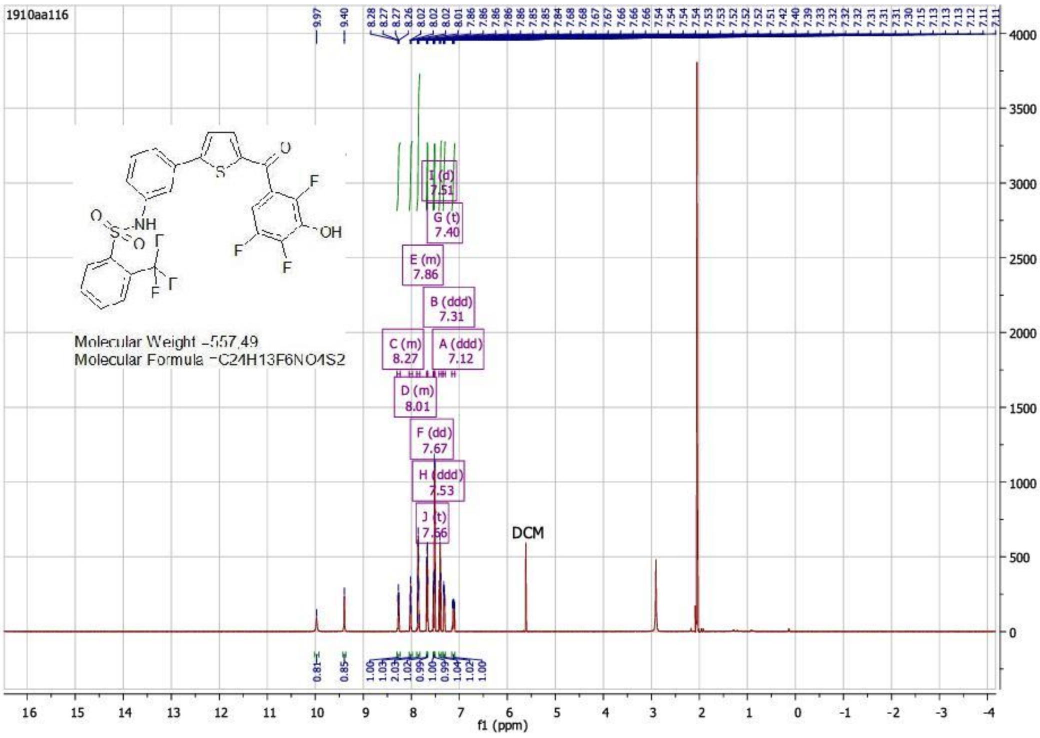

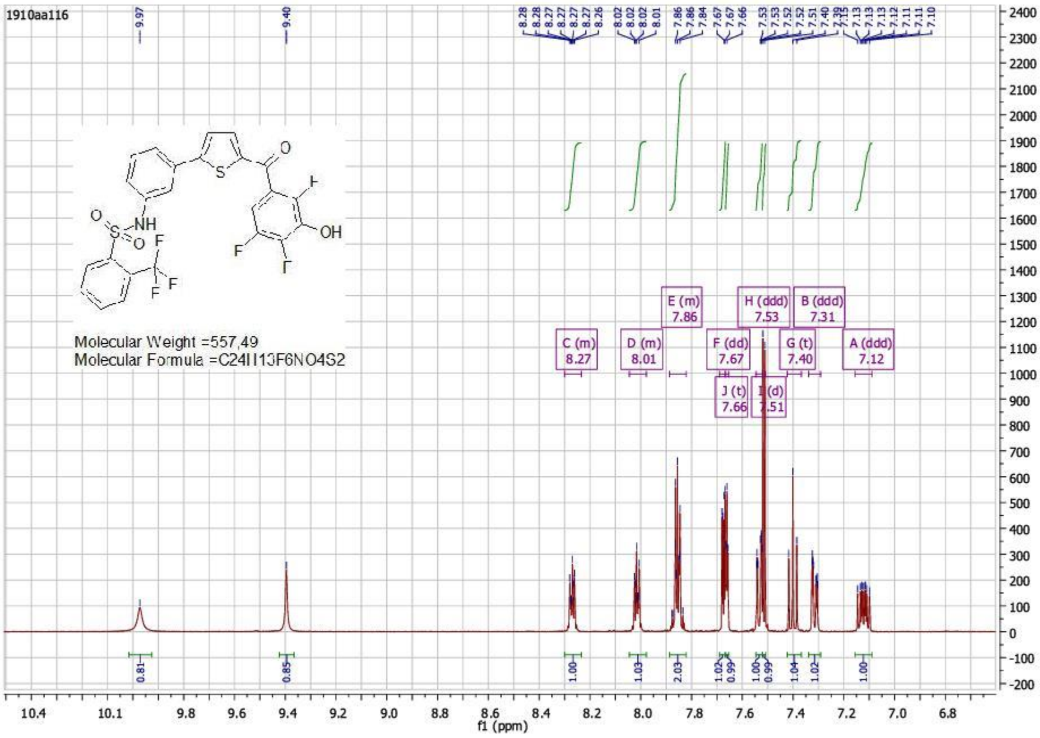

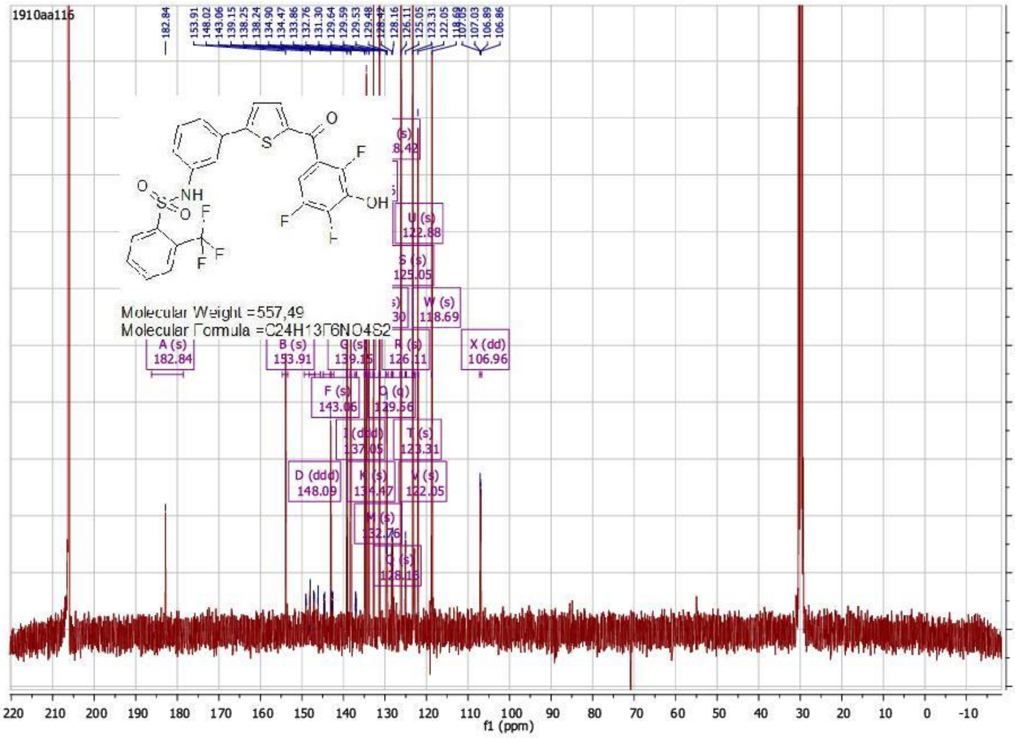
1910aa116
Molecular Weight =557,49
Molecular Formula =C24H13F6NO4S2
A (s) 182.84
B (s) 153.91
D (ddd) 148.09
F (s) 143.06
G (s) 139.15
I (ddd) 137.05
K (s) 134.47
M (s) 132.76
O (q) 129.56
Q (s) 128.16
R (s) 126.11
S (s) 125.05
T (s) 123.31
U (s) 122.88
V (s) 122.05
W (s) 118.69
X (dd) 106.96
f1 (ppm)

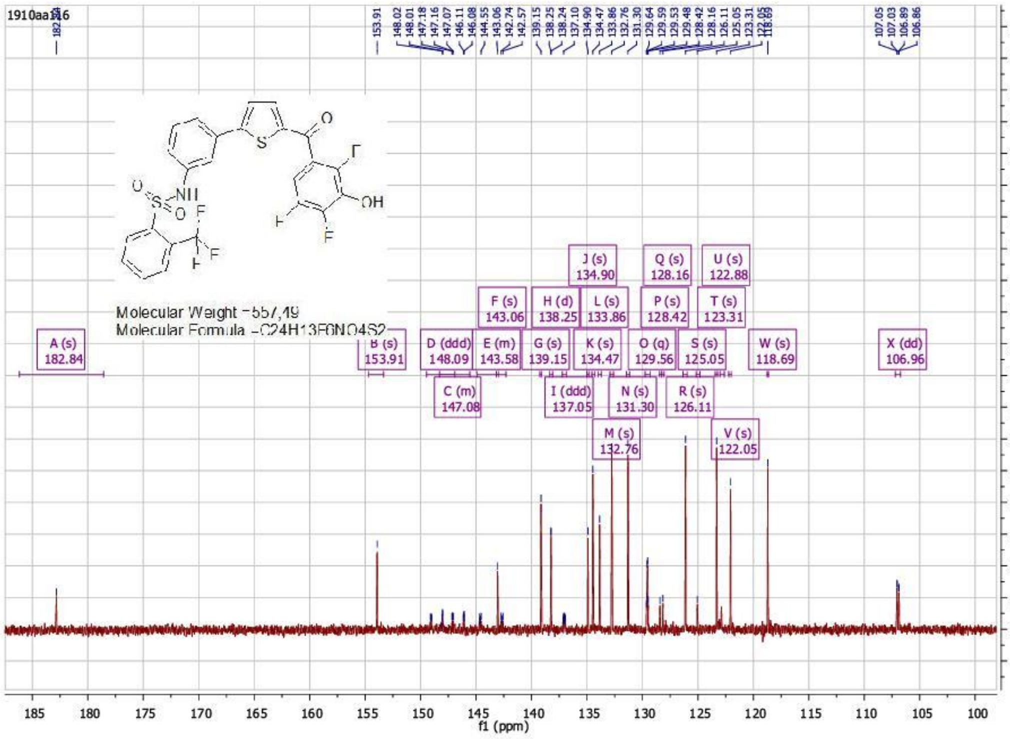
1910aa116
Molecular Weight =557,49
Molecular Formula =C24H13F6NO4S2
A (s) 182.84
B (s) 153.91
C (m) 147.08
D (ddd) 148.09
E (m) 143.58
F (s) 143.06
G (s) 139.15
H (d) 138.25
I (ddd) 137.05
J (s) 134.90
K (s) 134.47
L (s) 133.86
M (s) 132.76
N (s) 131.30
O (q) 129.56
P (s) 128.42
Q (s) 128.16
R (s) 126.11
S (s) 125.05
T (s) 123.31
U (s) 122.88
V (s) 122.05
W (s) 118.69
X (dd) 106.96
f1 (ppm)

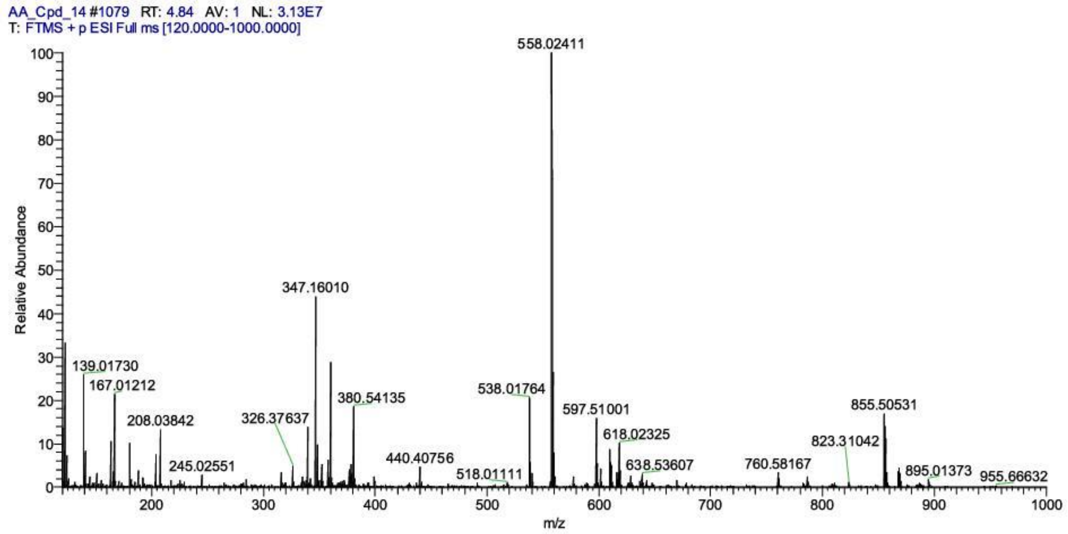

C:\Users\...\LC.MS_Final\AA116 11/26/17 15:00:14

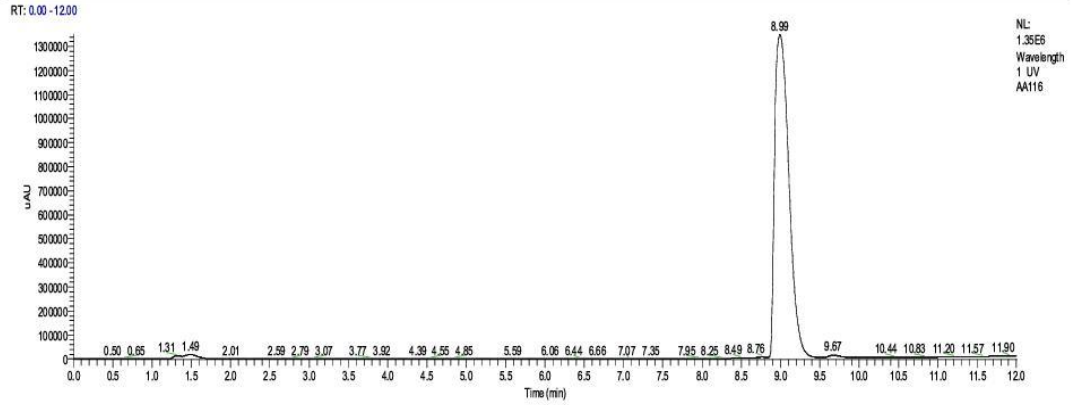

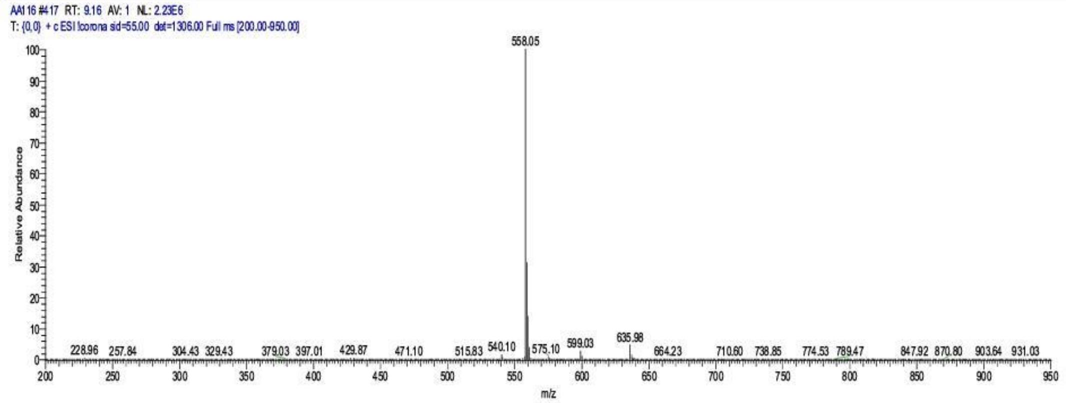

^{1}H, ^{13}C, ^{19}F spectra, HRMS, and LC.MS of Compound 15.

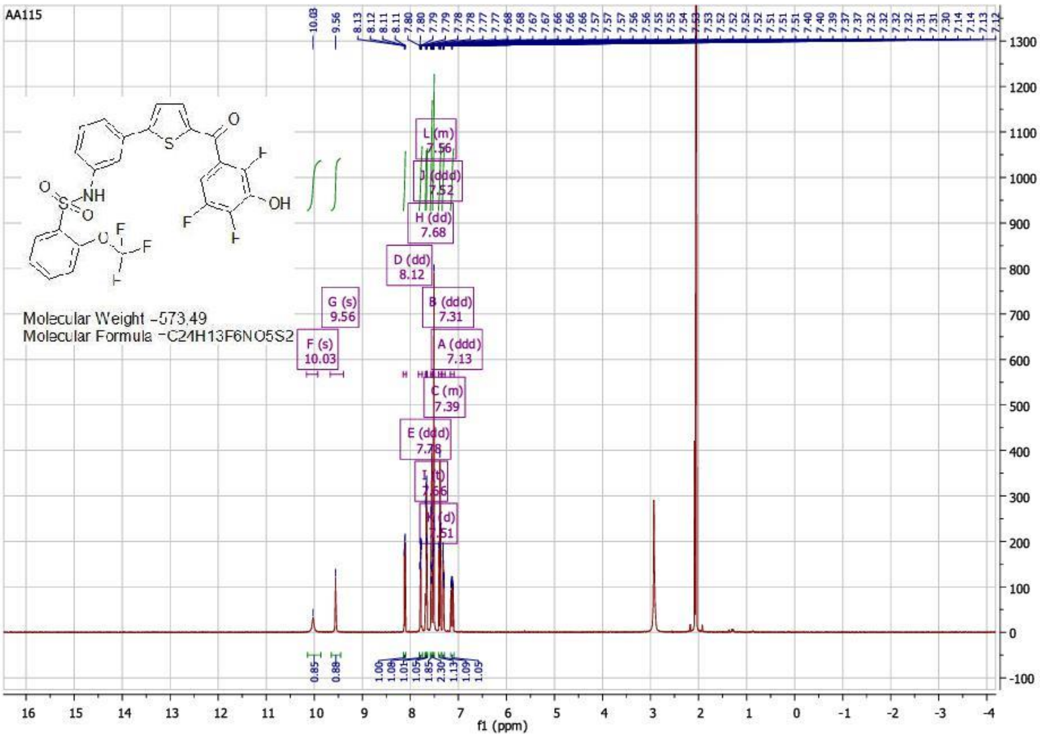

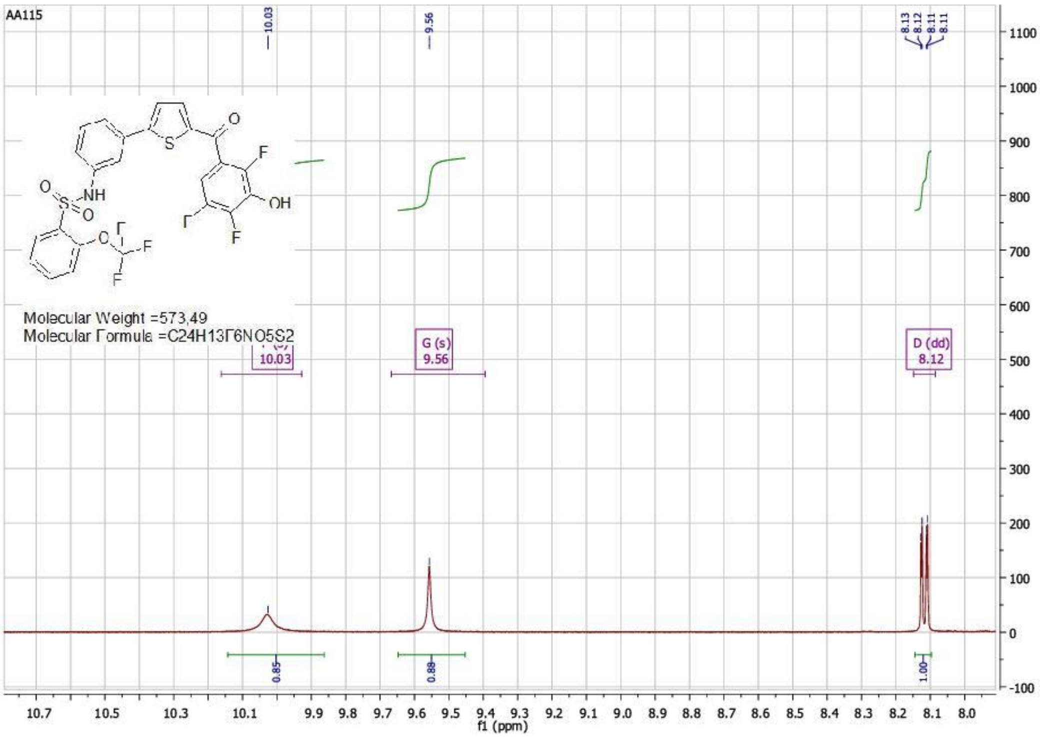

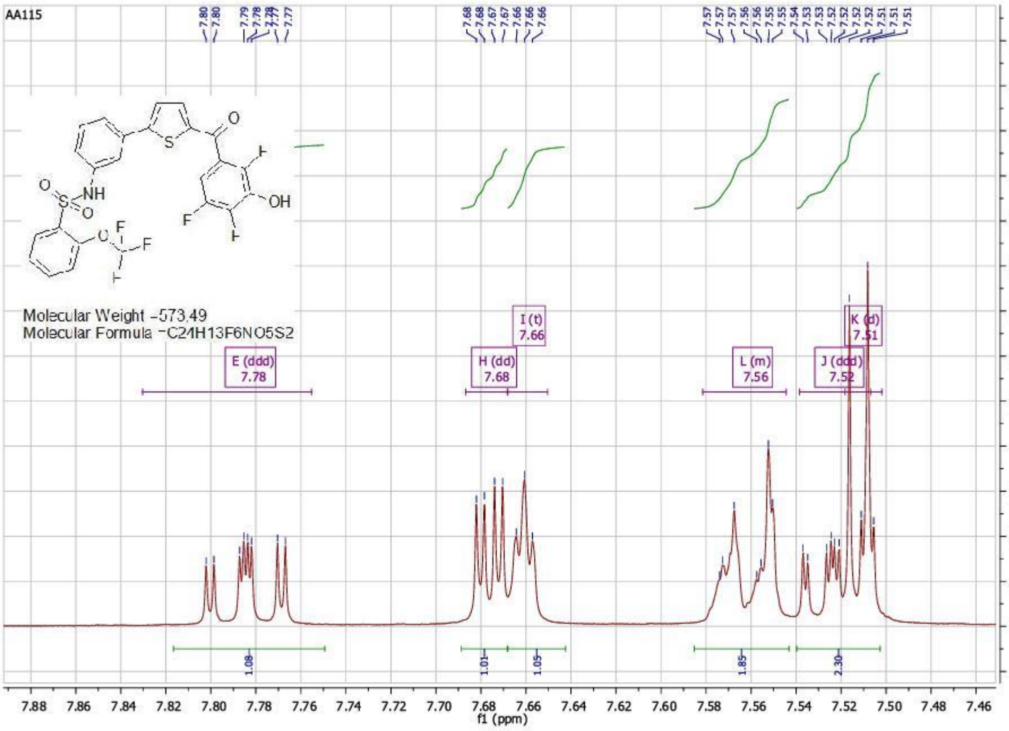
AA115
Molecular Weight =573.49
Molecular Formula =C24H13F6NO5S2
E (ddd) 7.78
H (dd) 7.68
I (t) 7.66
L (m) 7.56
J (ddd) 7.52
K (d) 7.51
1.08
1.01
1.05
1.85
2.30
f1 (ppm)

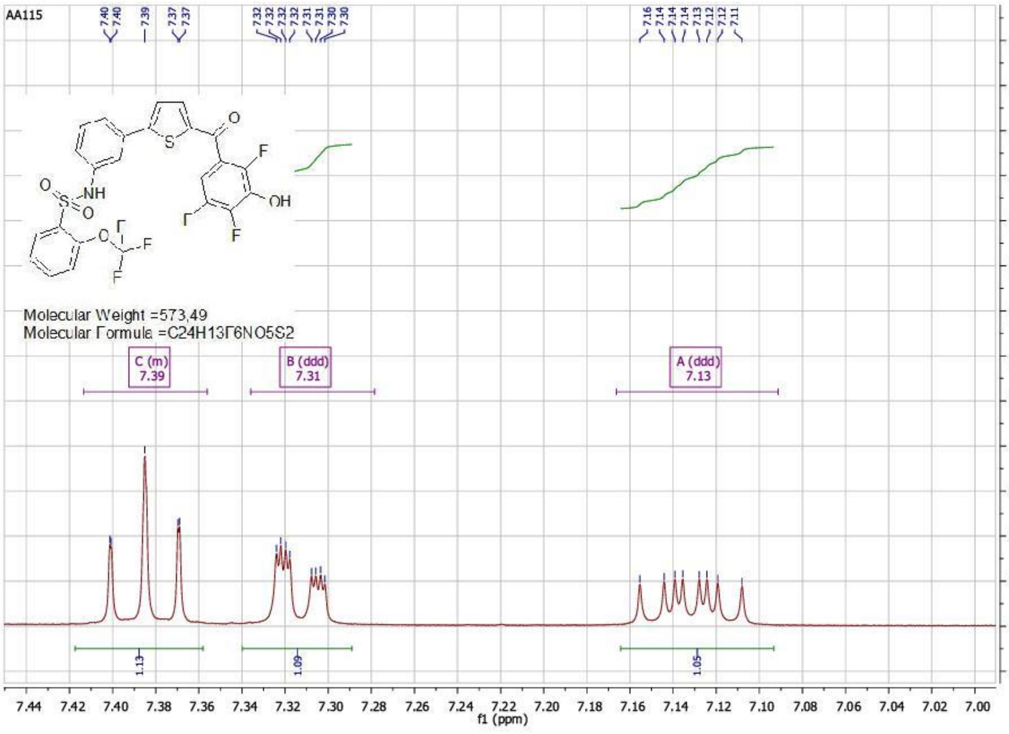
AA115
Molecular Weight =573.49
Molecular Formula =C24H13F6NO5S2
C (m) 7.39
B (ddd) 7.31
A (ddd) 7.13
1.13
1.09
1.05
f1 (ppm)

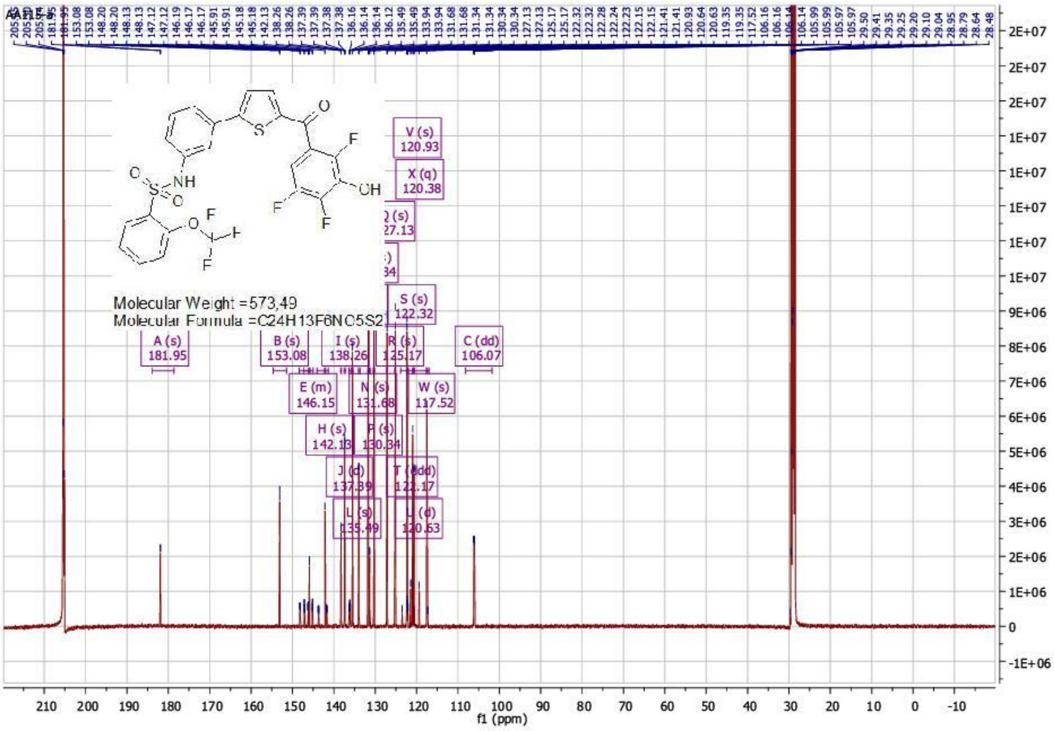
AA115
Molecular Weight =573,49
Molecular Formula =C24H13F6NO5S2
A (s) 181.95
B (s) 153.08
C (dd) 106.07
E (m) 146.15
H (s) 142.13
I (s) 138.26
J (d) 137.39
L (s) 135.49
N (s) 131.68
P (s) 130.34
R (s) 125.17
S (s) 122.32
T (ddd) 122.17
U (d) 120.63
V (s) 120.93
W (s) 117.52
X (q) 120.38
f1 (ppm)

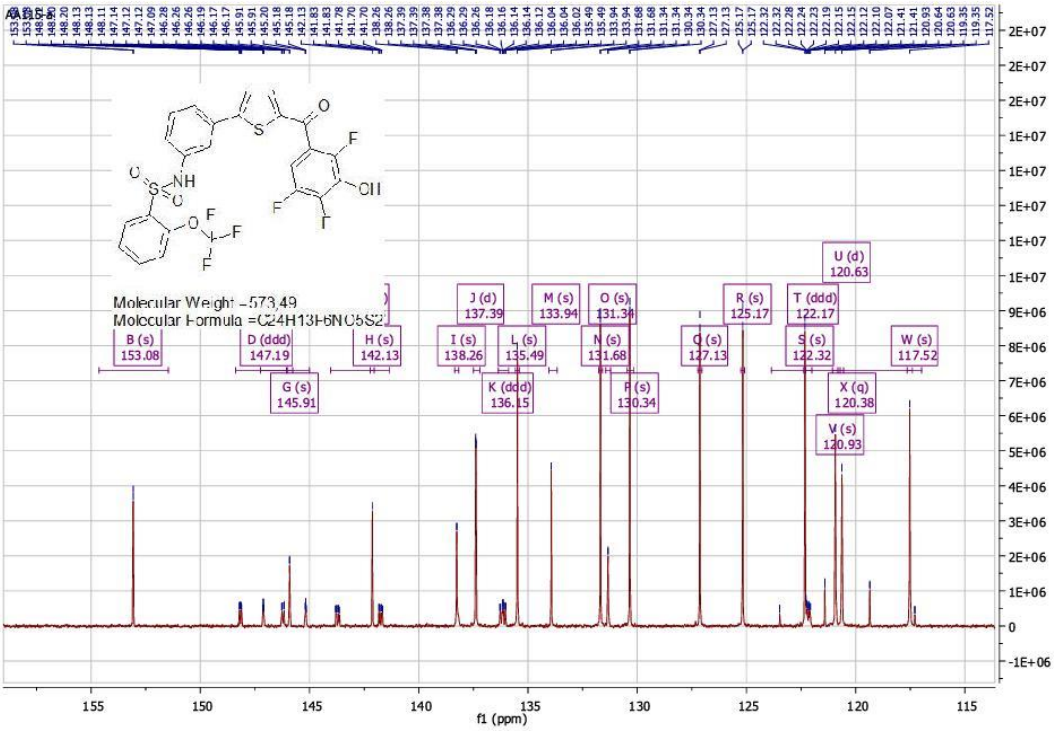
AA115
Molecular Weight =573,49
Molecular Formula =C24H13F6NO5S2
B (s) 153.08
D (ddd) 147.19
G (s) 145.91
H (s) 142.13
I (s) 138.26
J (d) 137.39
K (ddd) 136.15
L (s) 135.49
M (s) 133.94
N (s) 131.68
O (s) 131.34
P (s) 130.34
Q (s) 127.13
R (s) 125.17
S (s) 122.32
T (ddd) 122.17
U (d) 120.63
V (s) 120.93
W (s) 117.52
X (q) 120.38
f1 (ppm)

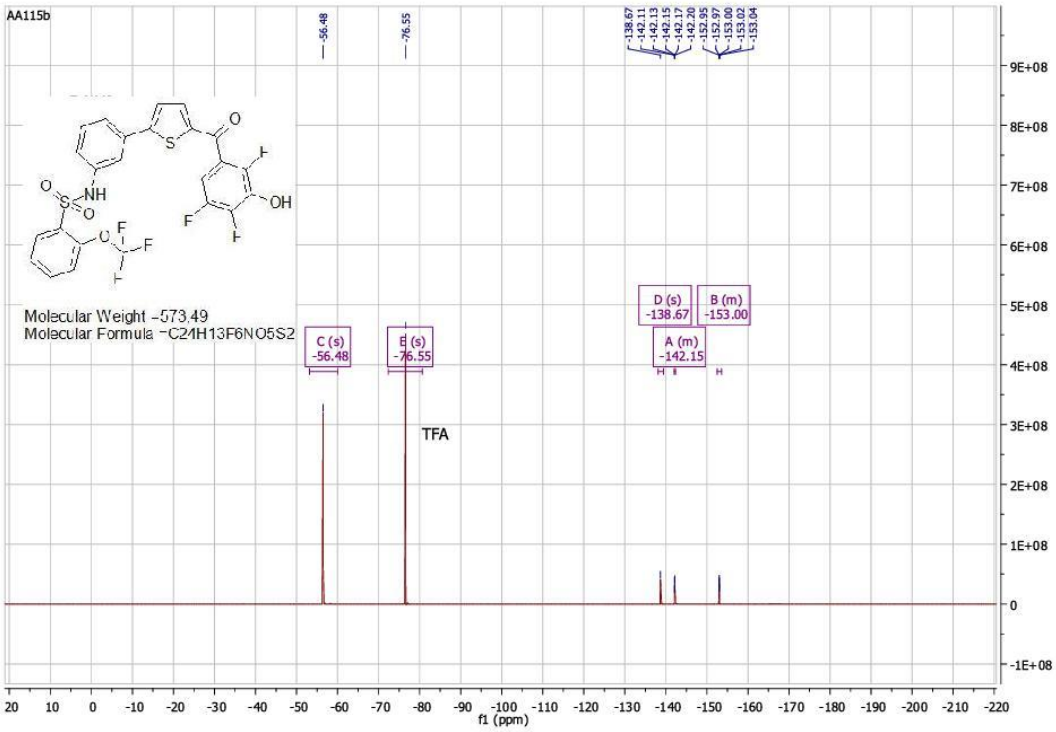
AA115b
-56.48
-76.55
-138.67
-142.11
-142.13
-142.15
-142.17
-142.20
-152.95
-152.97
-153.00
-153.02
-153.04
Molecular Weight =573.49
Molecular Formula =C24H13F6NO5S2
C (s) -56.48
E (s) -76.55
D (s) -138.67
B (m) -153.00
A (m) -142.15
TFA
9E+08
8E+08
7E+08
6E+08
5E+08
4E+08
3E+08
2E+08
1E+08
0
-1E+08
20 10 0 -10 -20 -30 -40 -50 -60 -70 -80 -90 -100 -110 -120 -130 -140 -150 -160 -170 -180 -190 -200 -210 -220
f1 (ppm)

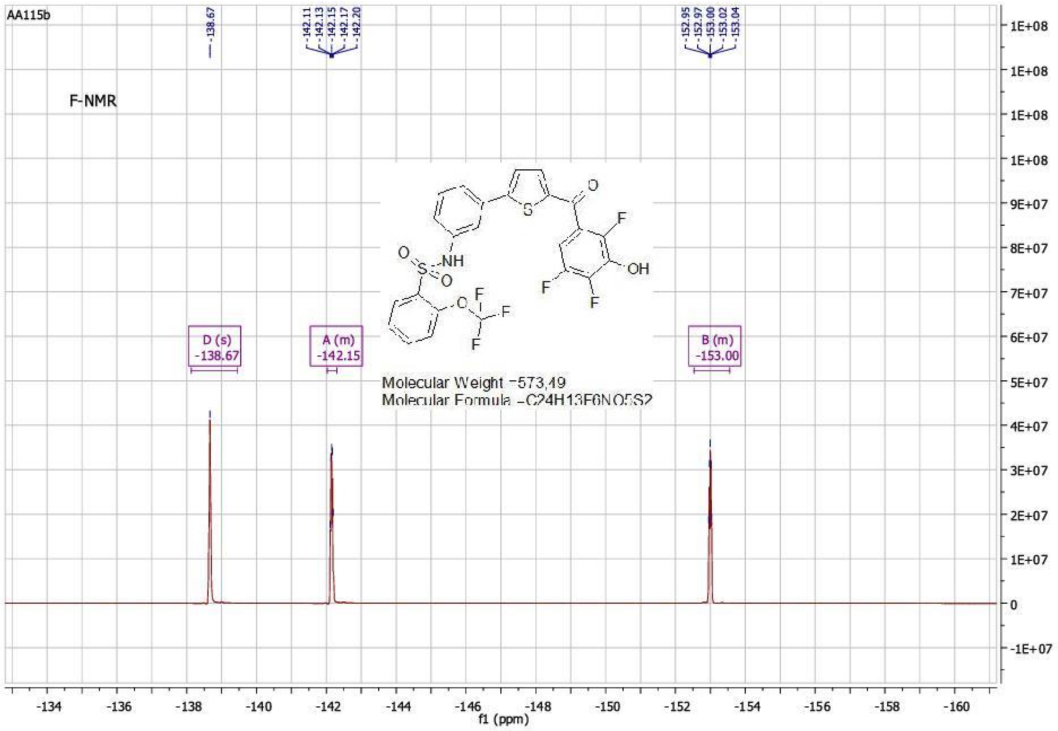
AA115b
-138.67
-142.11
-142.13
-142.15
-142.17
-142.20
-152.95
-152.97
-153.00
-153.02
-153.04
F-NMR
Molecular Weight =573.49
Molecular Formula =C24H13F6NO5S2
D (s) -138.67
A (m) -142.15
B (m) -153.00
1E+08
1E+08
1E+08
1E+08
9E+07
8E+07
7E+07
6E+07
5E+07
4E+07
3E+07
2E+07
1E+07
0
-1E+07
-134 -136 -138 -140 -142 -144 -146 -148 -150 -152 -154 -156 -158 -160
f1 (ppm)

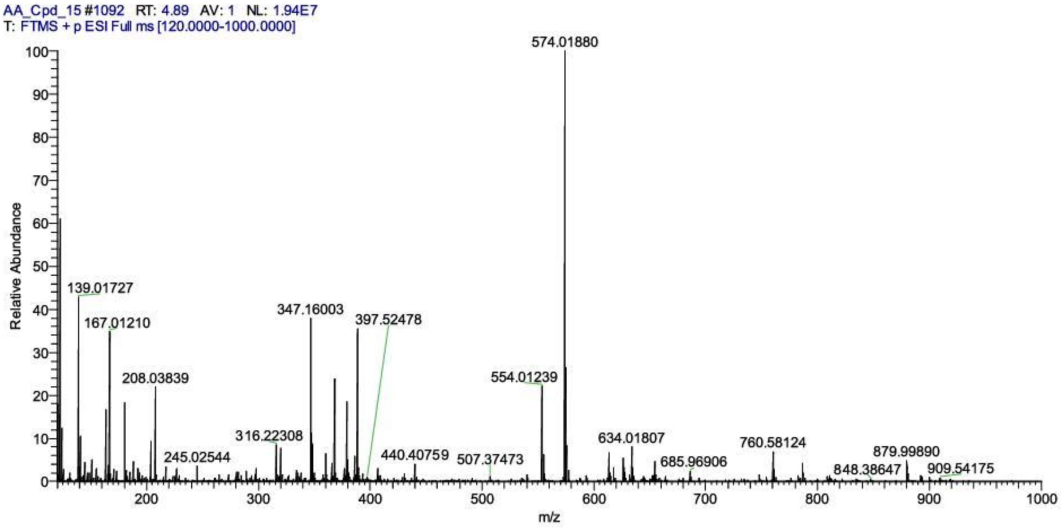

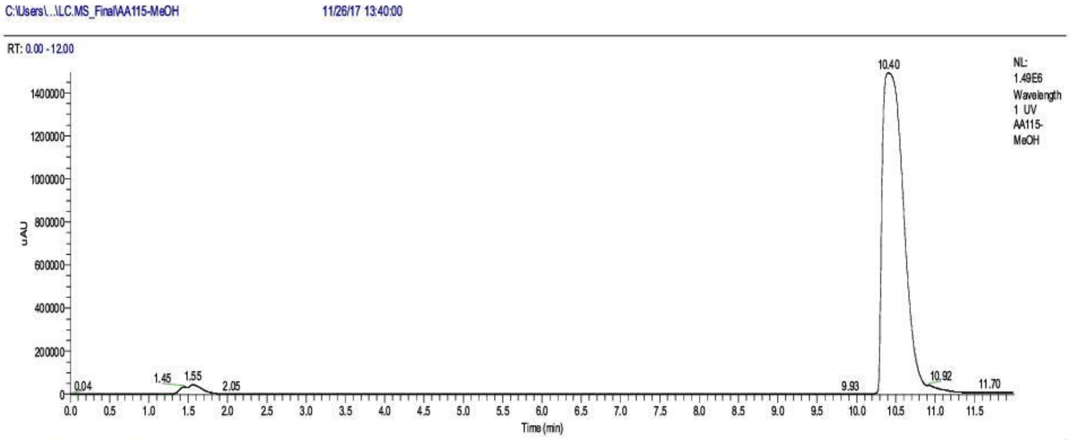

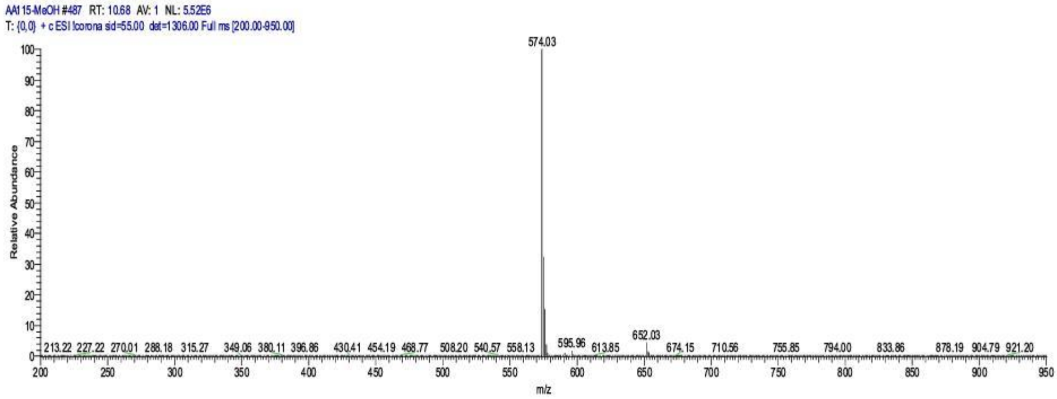

^{1}H, ^{13}C spectra, HRMS, and LC.MS of Compound 16.

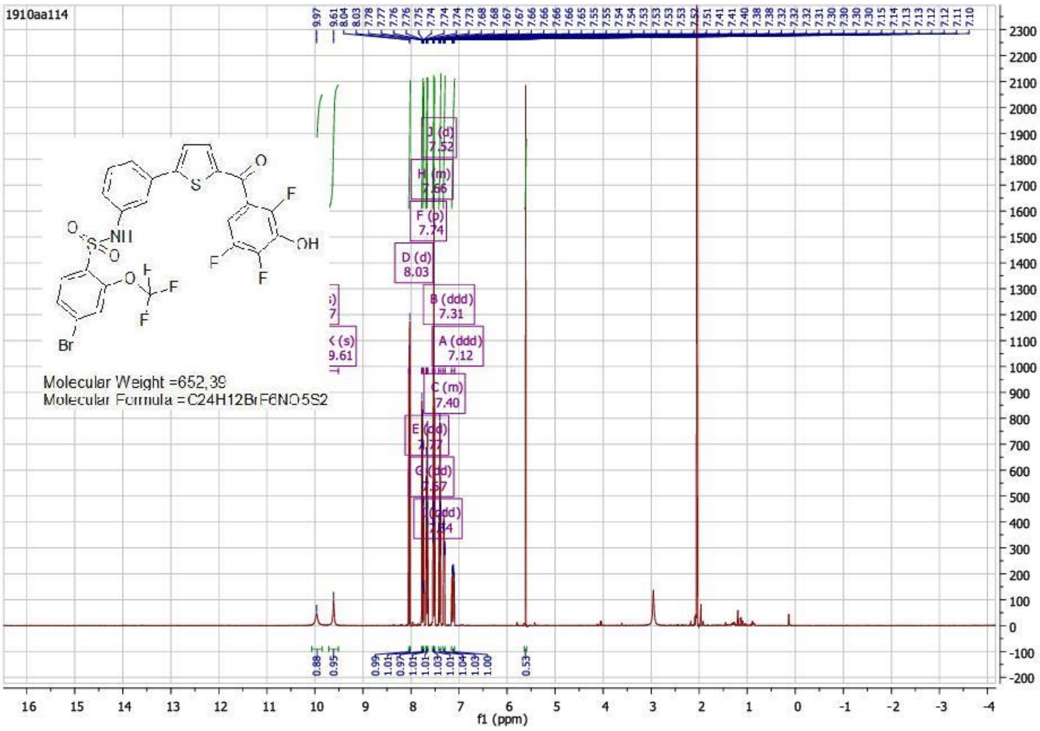
1910aa114
9.97
9.61
8.04
8.03
7.78
7.77
7.76
7.76
7.75
7.74
7.74
7.74
7.73
7.68
7.68
7.67
7.67
7.66
7.66
7.66
7.65
7.55
7.55
7.54
7.54
7.53
7.53
7.53
7.53
7.52
7.51
7.41
7.40
7.38
7.38
7.32
7.32
7.31
7.30
7.30
7.30
7.15
7.14
7.13
7.13
7.12
7.11
7.10
J (d) 7.52
H (m) 7.66
F (p) 7.74
D (d) 8.03
K (s) 9.61
B (ddd) 7.31
A (ddd) 7.12
C (m) 7.40
E (dd) 7.77
G (dd) 7.67
I (ddd) 7.54
O
S
F
NH
OH
F
F
O
F
F
Br
Molecular Weight =652,39
Molecular Formula =C24H12BrF6NO5S2
0.88
0.95
0.99
1.01
0.97
1.01
1.01
1.03
1.01
1.04
1.03
1.00
0.53
16
15
14
13
12
11
10
9
8
7
6
5
4
3
2
1
0
-1
-2
-3
-4
f1 (ppm)
2300
2200
2100
2000
1900
1800
1700
1600
1500
1400
1300
1200
1100
1000
900
800
700
600
500
400
300
200
100
0
-100
-200

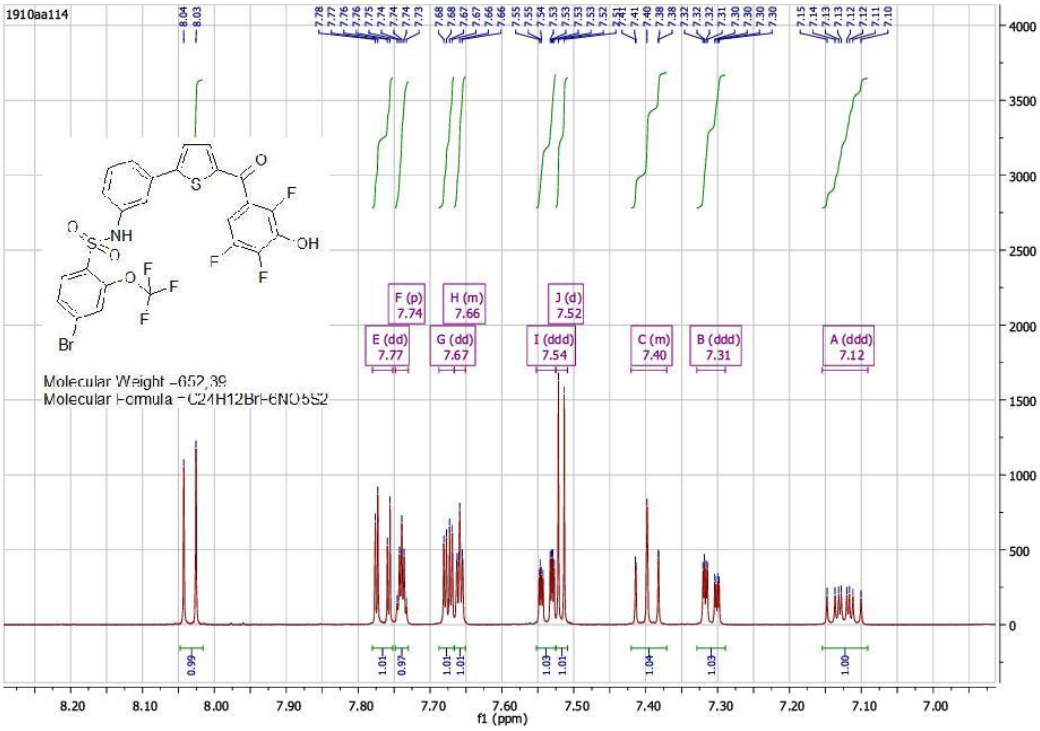
1910aa114
8.04
8.03
7.78
7.77
7.76
7.75
7.74
7.74
7.73
7.68
7.68
7.67
7.66
7.66
7.55
7.54
7.53
7.53
7.53
7.52
7.41
7.40
7.38
7.32
7.32
7.31
7.30
7.30
7.30
7.15
7.14
7.13
7.13
7.12
7.11
7.10
F (p) 7.74
H (m) 7.66
J (d) 7.52
E (dd) 7.77
G (dd) 7.67
I (ddd) 7.54
C (m) 7.40
B (ddd) 7.31
A (ddd) 7.12
Molecular Weight =652,39
Molecular Formula =C24H12BrF6NO5S2
0.99
1.01
0.97
1.01
1.01
1.03
1.01
1.04
1.03
1.00
8.20
8.10
8.00
7.90
7.80
7.70
7.60
7.50
7.40
7.30
7.20
7.10
7.00
f1 (ppm)
4000
3500
3000
2500
2000
1500
1000
500
0

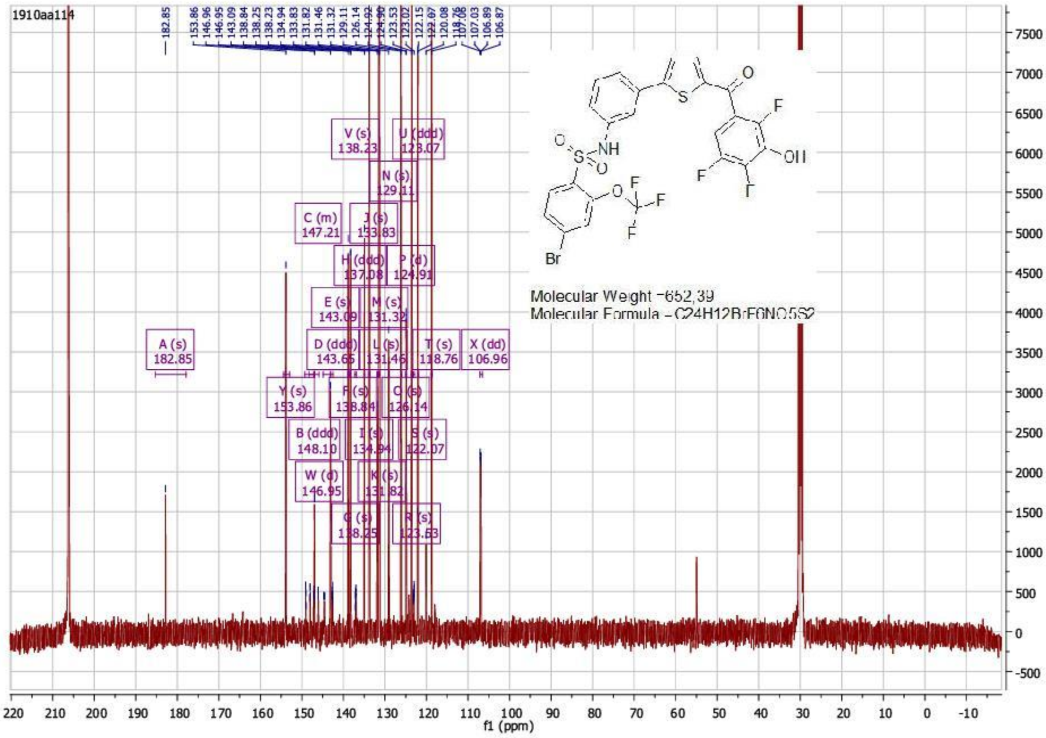
1910aa114
182.85
153.86
146.96
146.95
143.09
138.84
138.25
138.23
134.94
133.83
131.82
131.46
131.32
129.11
126.14
124.92
124.90
123.53
123.02
122.15
122.07
120.08
118.76
107.06
107.03
106.89
106.87
A (s) 182.85
Y (s) 153.86
B (ddd) 148.10
C (m) 147.21
W (d) 146.95
D (ddd) 143.65
E (s) 143.09
F (s) 138.84
Q (s) 138.25
V (s) 138.23
H (ddd) 137.08
I (s) 134.94
J (s) 133.83
K (s) 131.82
L (s) 131.46
M (s) 131.32
N (s) 129.11
O (s) 126.14
P (d) 124.91
R (s) 123.53
U (ddd) 123.07
S (s) 122.07
T (s) 118.76
X (dd) 106.96
Molecular Weight =652,39
Molecular Formula =C24H12BrF6NO5S2
f1 (ppm)
220 210 200 190 180 170 160 150 140 130 120 110 100 90 80 70 60 50 40 30 20 10 0 -10
7500 7000 6500 6000 5500 5000 4500 4000 3500 3000 2500 2000 1500 1000 500 0 -500

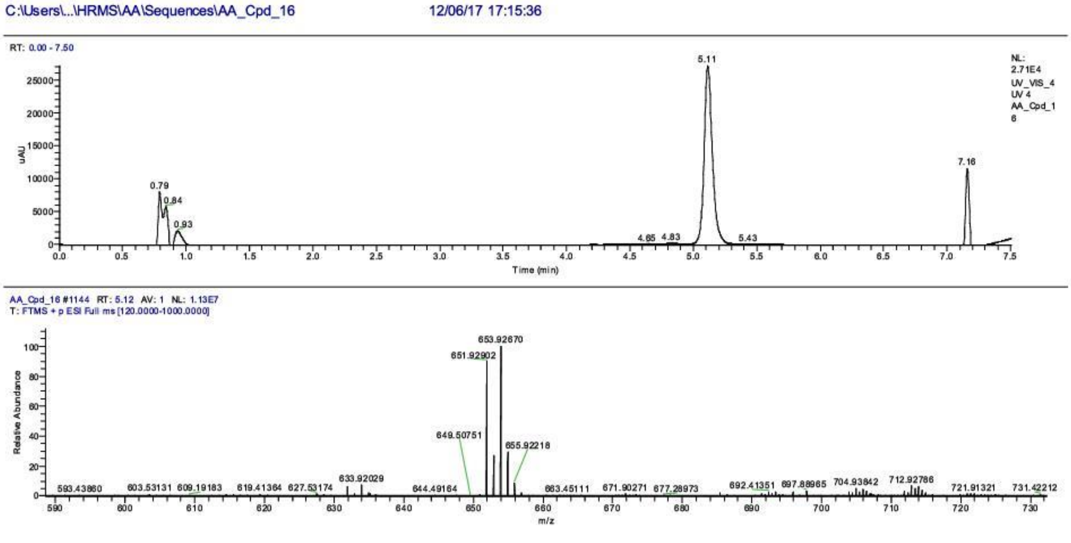
C:\Users\...\HRMS\AA\Sequences\AA_Cpd_16
12/06/17 17:15:36
RT: 0.00 - 7.50
NL: 2.71E4 UV_VIS_4 UV 4 AA_Cpd_16
uAU
25000 20000 15000 10000 5000 0
0.79
0.84
0.93
4.65
4.83
5.11
5.43
7.16
Time (min)
0.0 0.5 1.0 1.5 2.0 2.5 3.0 3.5 4.0 4.5 5.0 5.5 6.0 6.5 7.0 7.5
AA_Cpd_16 #1144 RT: 5.12 AV: 1 NL: 1.13E7
T: FTMS + p ESI Full ms [120.0000-1000.0000]
Relative Abundance
100 80 60 40 20 0
593.43860
603.53131
609.19183
619.41364
627.53174
633.92029
644.49164
649.50751
651.92902
653.92670
655.92218
663.45111
671.90271
677.28973
692.41351
697.88965
704.93842
712.92786
721.91321
731.42212
m/z
590 600 610 620 630 640 650 660 670 680 690 700 710 720 730

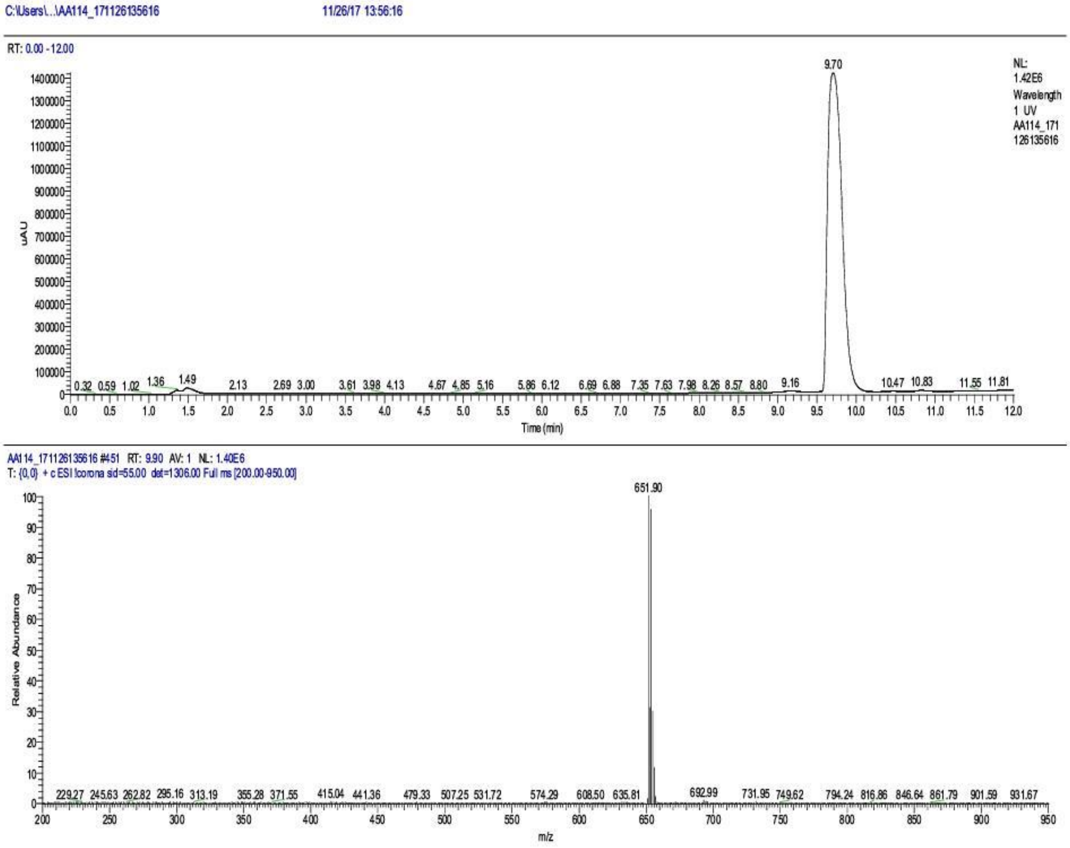
C:\Users\...\AA114_171126135616
11/26/17 13:56:16
RT: 0.00 - 12.00
NL:
1.42E6
Wavelength
1 UV
AA114_171
126135616
uAU
1400000
1300000
1200000
1100000
1000000
900000
800000
700000
600000
500000
400000
300000
200000
100000
0
9.70
0.32 0.59 1.02 1.36 1.49 2.13 2.69 3.00 3.61 3.98 4.13 4.67 4.85 5.16 5.86 6.12 6.69 6.88 7.35 7.63 7.98 8.26 8.57 8.80 9.16 10.47 10.83 11.55 11.81
0.0 0.5 1.0 1.5 2.0 2.5 3.0 3.5 4.0 4.5 5.0 5.5 6.0 6.5 7.0 7.5 8.0 8.5 9.0 9.5 10.0 10.5 11.0 11.5 12.0
Time (min)
AA114_171126135616 #451 RT: 9.90 AV: 1 NL: 1.40E6
T: {0,0} + c ESI !corona sid=55.00 det=1306.00 Full ms [200.00-950.00]
Relative Abundance
100
90
80
70
60
50
40
30
20
10
0
651.90
229.27 245.63 262.82 295.16 313.19 355.28 371.55 415.04 441.36 479.33 507.25 531.72 574.29 608.50 635.81 692.99 731.95 749.62 794.24 816.86 846.64 861.79 901.59 931.67
200 250 300 350 400 450 500 550 600 650 700 750 800 850 900 950
m/z

^{1}H, ^{13}C, ^{19}F spectra, and LC.MS of Compound 8a.

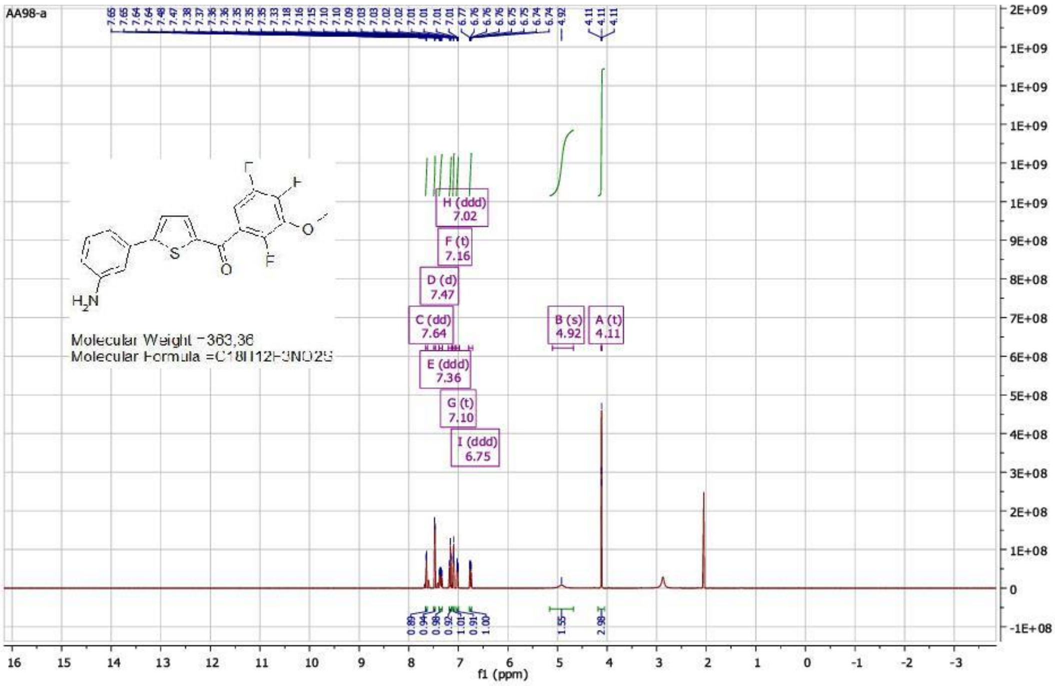

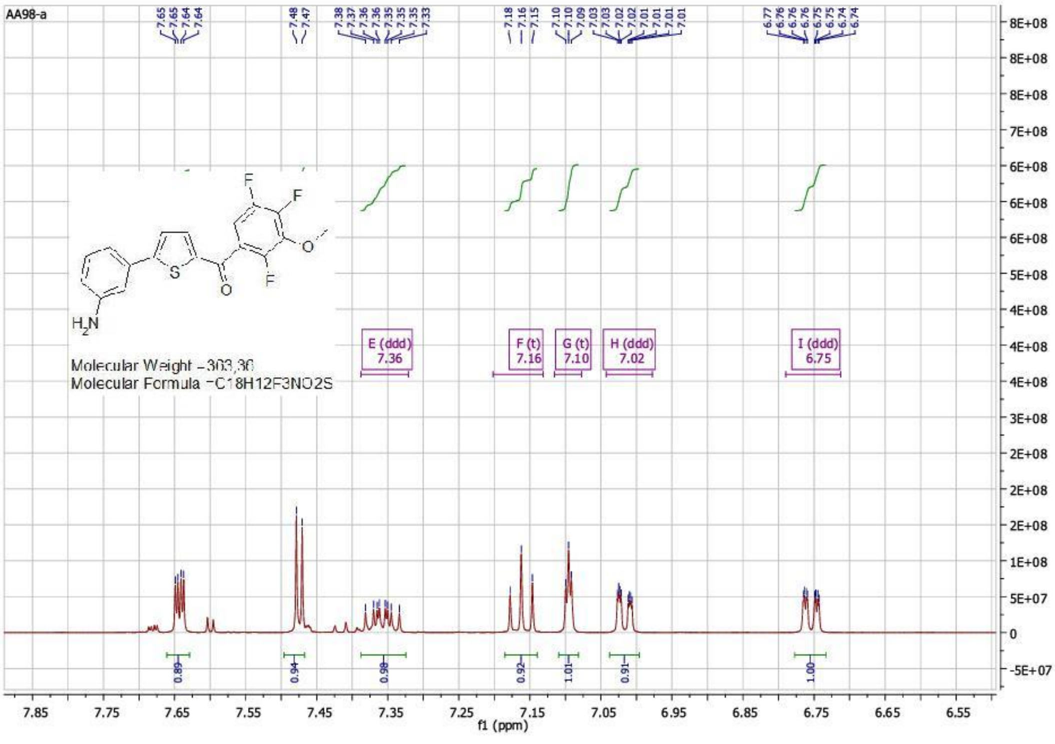

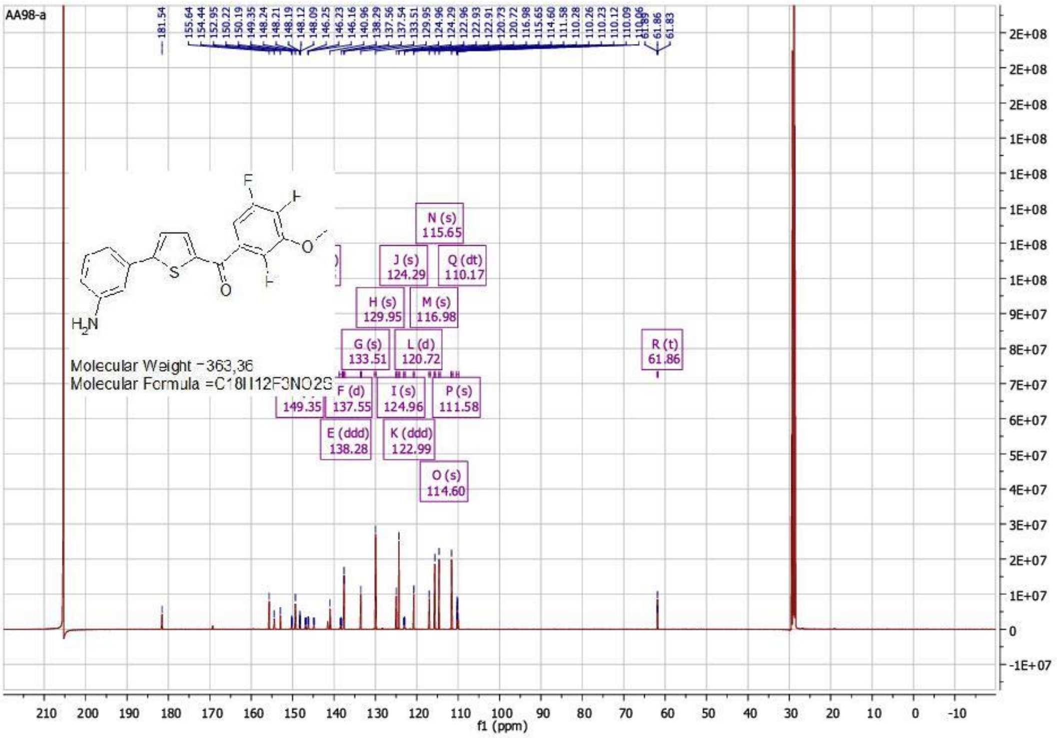
AA98-a
Molecular Weight =363,36
Molecular Formula =C18H12F3NO2S
H2N
S
O
F
F
F
O
N (s) 115.65
J (s) 124.29
Q (dt) 110.17
H (s) 129.95
M (s) 116.98
G (s) 133.51
L (d) 120.72
R (t) 61.86
149.35
F (d) 137.55
I (s) 124.96
P (s) 111.58
E (ddd) 138.28
K (ddd) 122.99
O (s) 114.60
f1 (ppm)

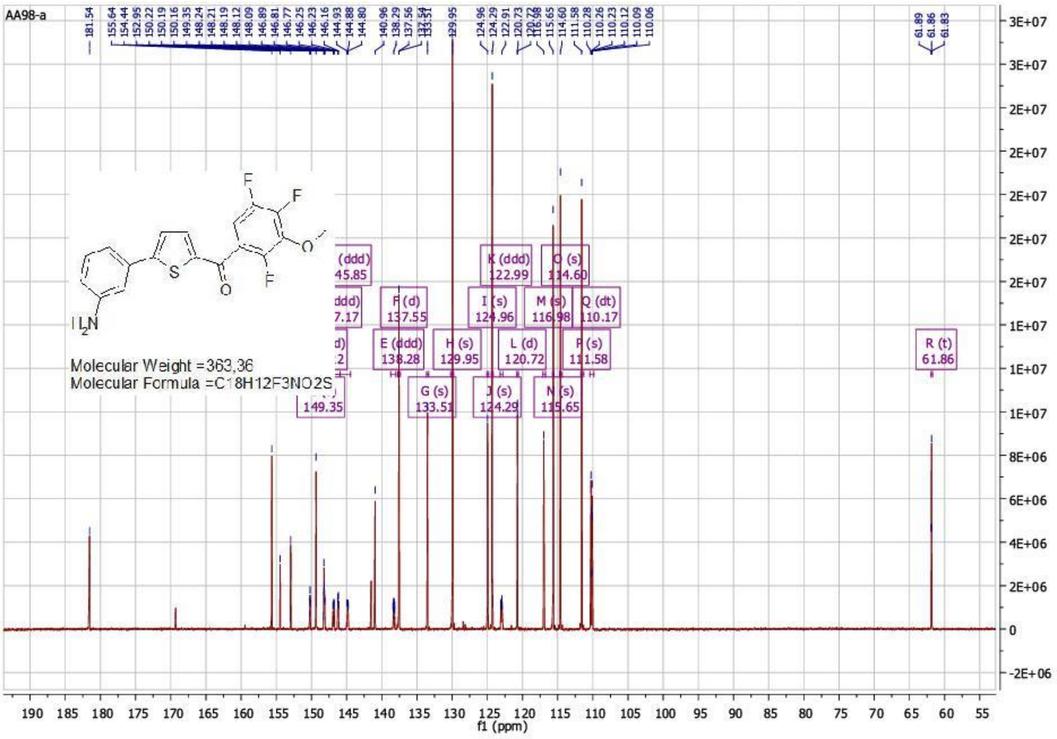
AA98-a
Molecular Weight =363,36
Molecular Formula =C18H12F3NO2S
H2N
S
O
F
F
F
O
(ddd) 145.85
K (ddd) 122.99
O (s) 114.60
(ddd) 7.17
F (d) 137.55
I (s) 124.96
M (s) 116.98
Q (dt) 110.17
E (ddd) 138.28
H (s) 129.95
L (d) 120.72
P (s) 111.58
R (t) 61.86
149.35
G (s) 133.51
J (s) 124.29
N (s) 115.65
f1 (ppm)

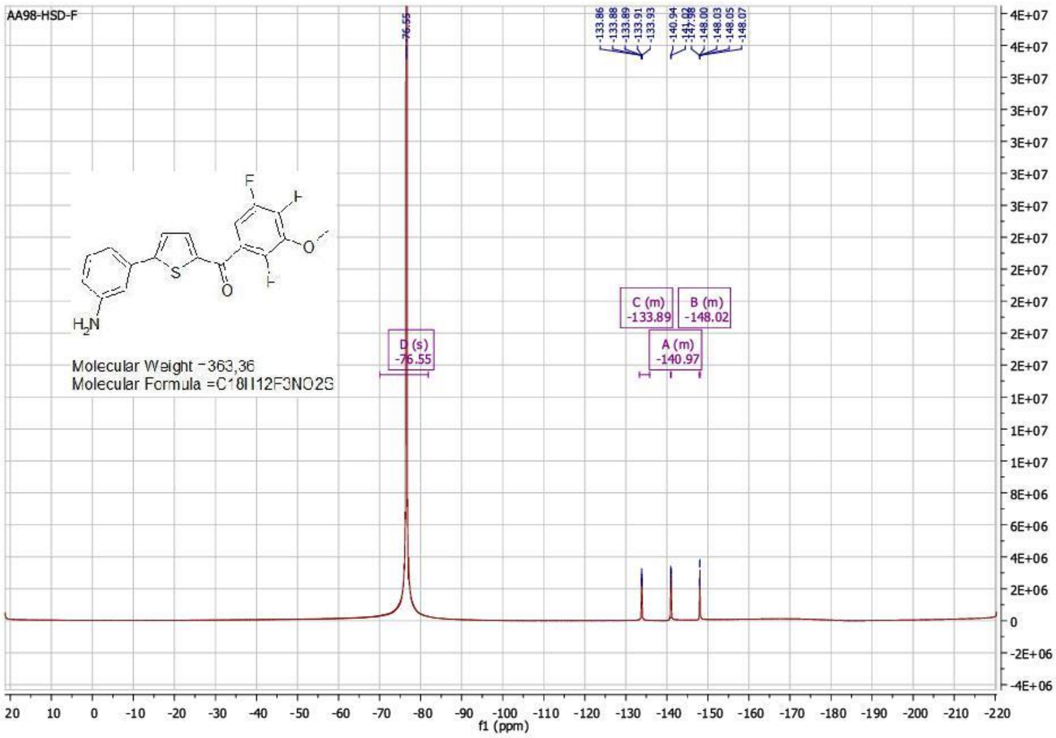
AA98-HSD-F
-76.55
-133.86
-133.88
-133.89
-133.91
-133.93
-140.94
-148.00
-148.03
-148.05
-148.07
C (m)
-133.89
B (m)
-148.02
A (m)
-140.97
D (s)
-76.55
F
F
O
F
S
O
H2N
Molecular Weight =363,36
Molecular Formula =C18H12F3NO2S
f1 (ppm)

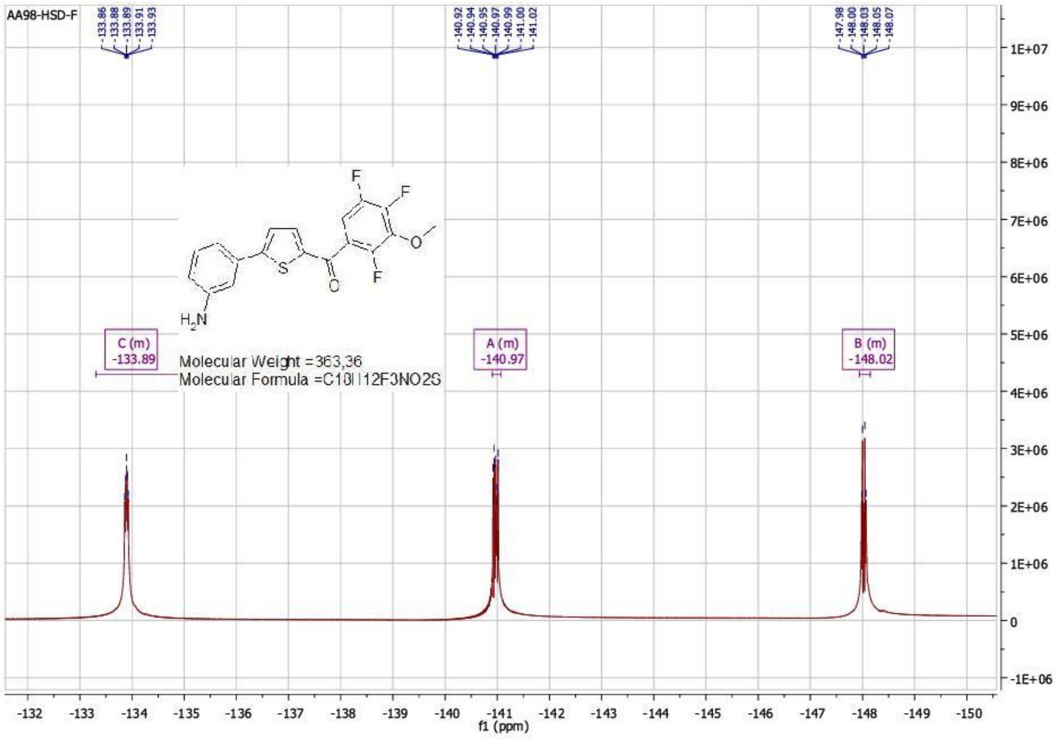
AA98-HSD-F
-133.86
-133.88
-133.89
-133.91
-133.93
-140.92
-140.94
-140.95
-140.97
-140.99
-141.00
-141.02
-147.98
-148.00
-148.03
-148.05
-148.07
C (m)
-133.89
A (m)
-140.97
B (m)
-148.02
F
F
O
F
S
O
H2N
Molecular Weight =363,36
Molecular Formula =C18H12F3NO2S
f1 (ppm)

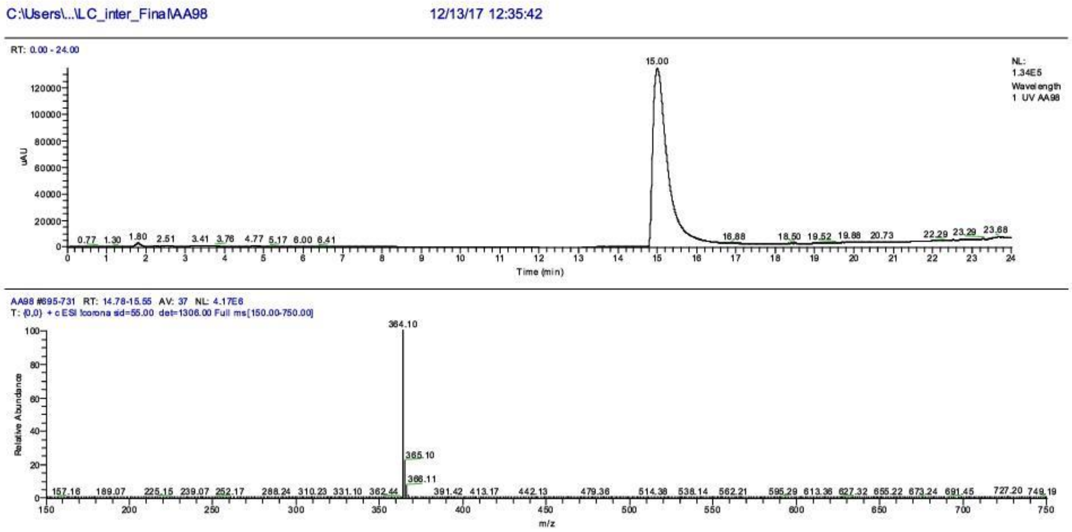

^{1}H, ^{13}C, ^{19}F spectra, and LC.MS of Compound 8b.

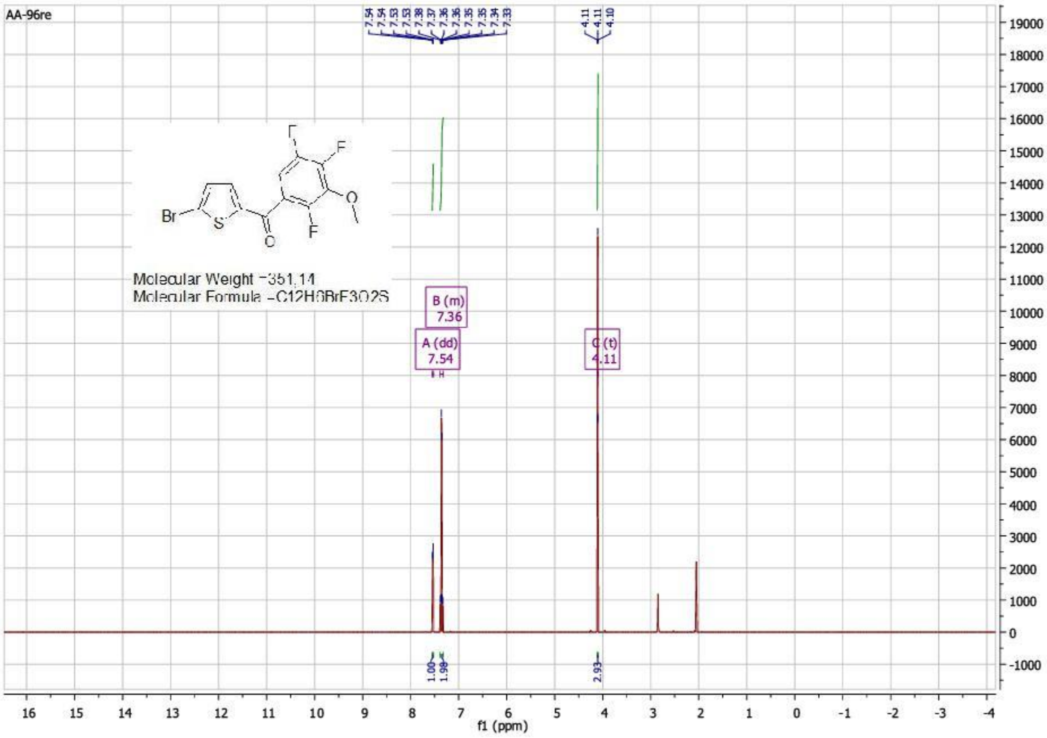

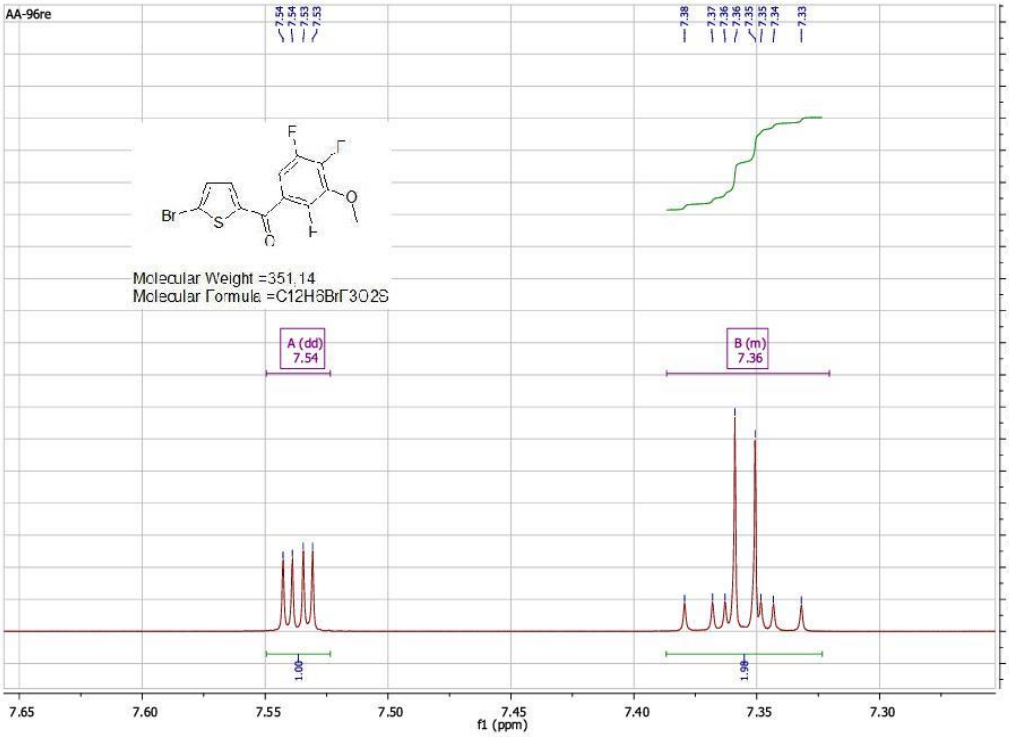
AA-96re
7.54
7.54
7.53
7.53
7.38
7.37
7.36
7.36
7.35
7.35
7.34
7.33
Br
S
O
F
F
F
O
Molecular Weight =351,14
Molecular Formula =C12H6BrF3O2S
A (dd)
7.54
B (m)
7.36
1.00
1.98
19000
18000
17000
16000
15000
14000
13000
12000
11000
10000
9000
8000
7000
6000
5000
4000
3000
2000
1000
0
-1000
7.65
7.60
7.55
7.50
7.45
7.40
7.35
7.30
f1 (ppm)

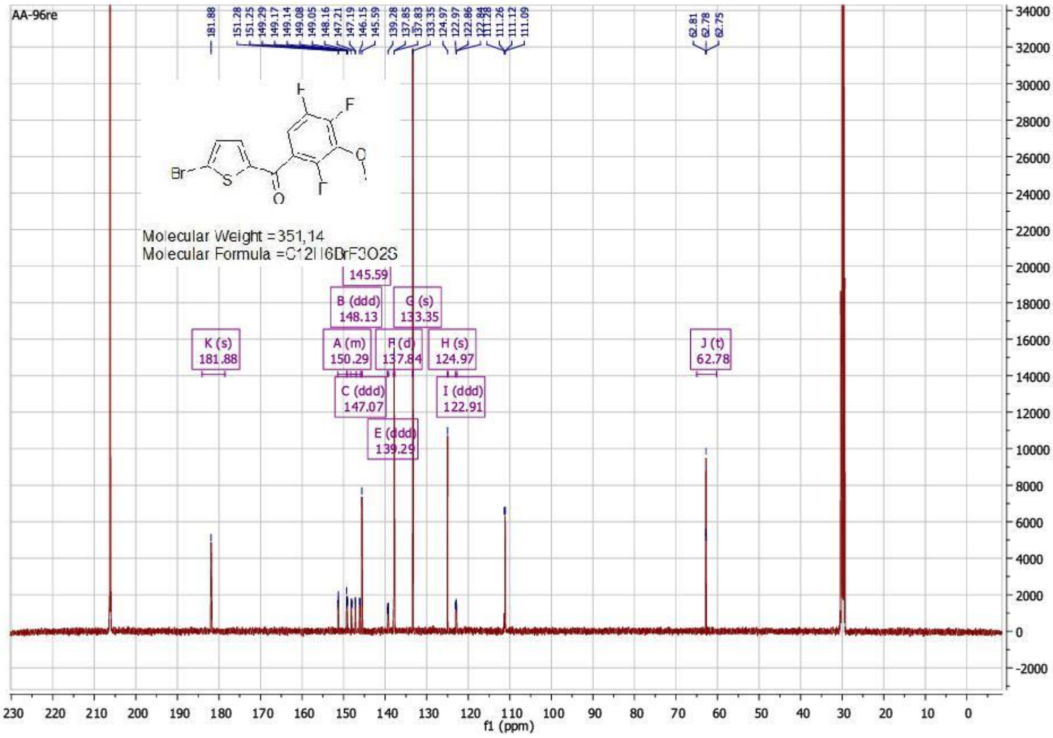
AA-96re
181.88
151.28
151.25
149.29
149.17
149.14
149.08
149.05
148.16
147.21
147.19
146.15
145.59
139.28
137.85
137.83
133.35
124.97
122.97
122.86
122.84
111.28
111.26
111.12
111.09
62.81
62.78
62.75
Br
S
O
F
F
F
O
Molecular Weight =351,14
Molecular Formula =C12H6BrF3O2S
145.59
B (ddd)
148.13
G (s)
133.35
K (s)
181.88
A (m)
150.29
F (d)
137.84
H (s)
124.97
J (t)
62.78
C (ddd)
147.07
I (ddd)
122.91
E (ddd)
139.29
34000
32000
30000
28000
26000
24000
22000
20000
18000
16000
14000
12000
10000
8000
6000
4000
2000
0
-2000
230
220
210
200
190
180
170
160
150
140
130
120
110
100
90
80
70
60
50
40
30
20
10
0
f1 (ppm)

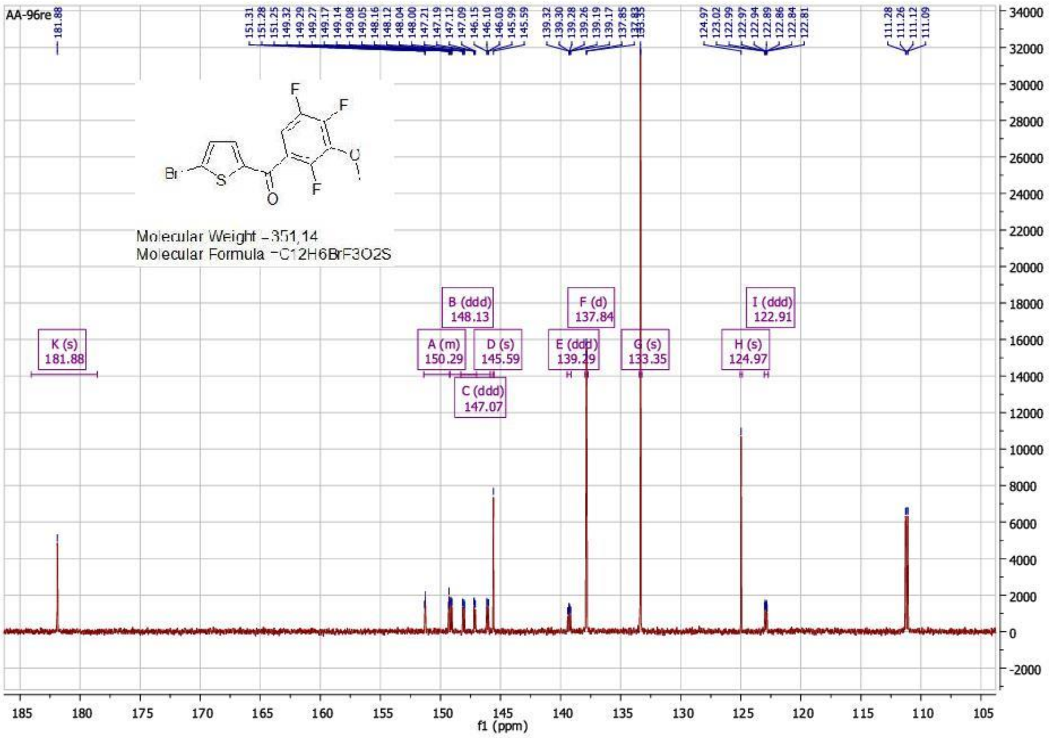
AA-96re
181.88
151.31 151.28 151.25 149.32 149.29 149.27 149.17 149.14 149.08 149.05 148.16 148.12 148.04 148.00 147.21 147.19 147.12 147.09 146.15 146.10 146.03 145.99 145.59
139.32 139.30 139.28 139.26 139.19 139.17 137.85 137.83 133.35
124.97 123.02 122.99 122.97 122.94 122.89 122.86 122.84 122.81
111.28 111.26 111.12 111.09
Br
S
O
F
F
F
O
Molecular Weight =351,14
Molecular Formula =C12H6BrF3O2S
K (s) 181.88
A (m) 150.29
B (ddd) 148.13
C (ddd) 147.07
D (s) 145.59
E (ddd) 139.29
F (d) 137.84
G (s) 133.35
H (s) 124.97
I (ddd) 122.91
34000 32000 30000 28000 26000 24000 22000 20000 18000 16000 14000 12000 10000 8000 6000 4000 2000 0 -2000
185 180 175 170 165 160 155 150 145 140 135 130 125 120 115 110 105
f1 (ppm)

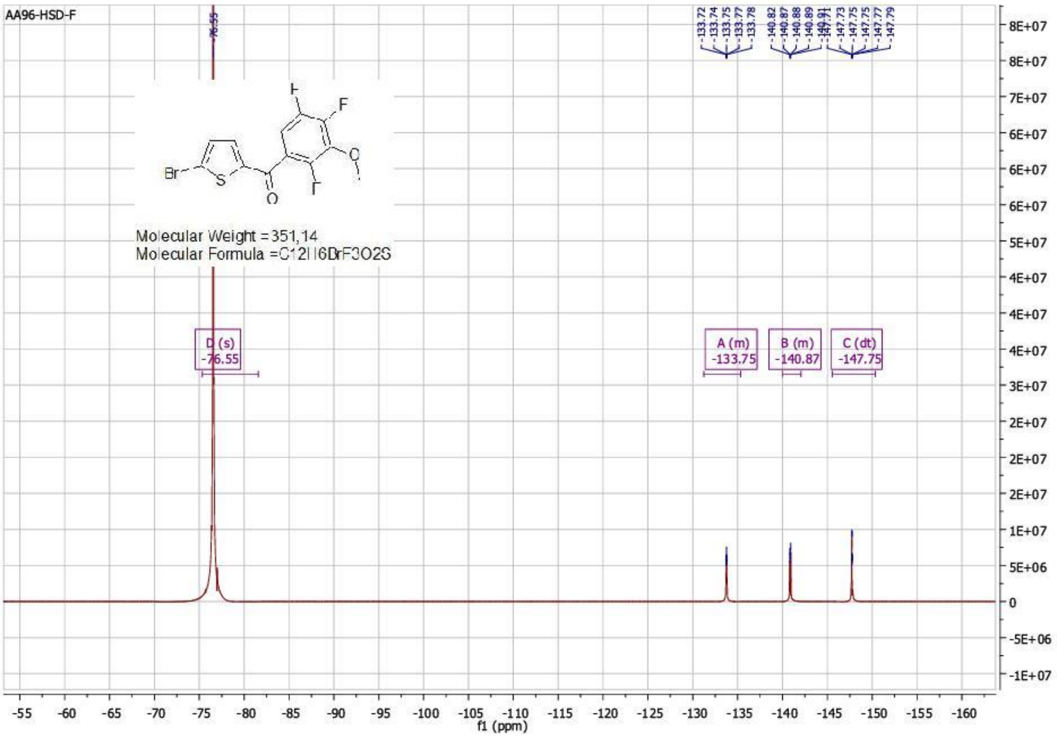
AA96-HSD-F
-76.55
-133.72 -133.74 -133.75 -133.77 -133.78
-140.82 -140.87 -140.88 -140.89 -140.91 -140.91
-147.71 -147.73 -147.75 -147.75 -147.77 -147.79
Br
S
O
F
F
F
O
Molecular Weight =351,14
Molecular Formula =C12H6BrF3O2S
D (s) -76.55
A (m) -133.75
B (m) -140.87
C (dt) -147.75
8E+07 8E+07 7E+07 6E+07 6E+07 6E+07 5E+07 4E+07 4E+07 4E+07 3E+07 2E+07 2E+07 2E+07 1E+07 5E+06 0 -5E+06 -1E+07
-55 -60 -65 -70 -75 -80 -85 -90 -95 -100 -105 -110 -115 -120 -125 -130 -135 -140 -145 -150 -155 -160
f1 (ppm)

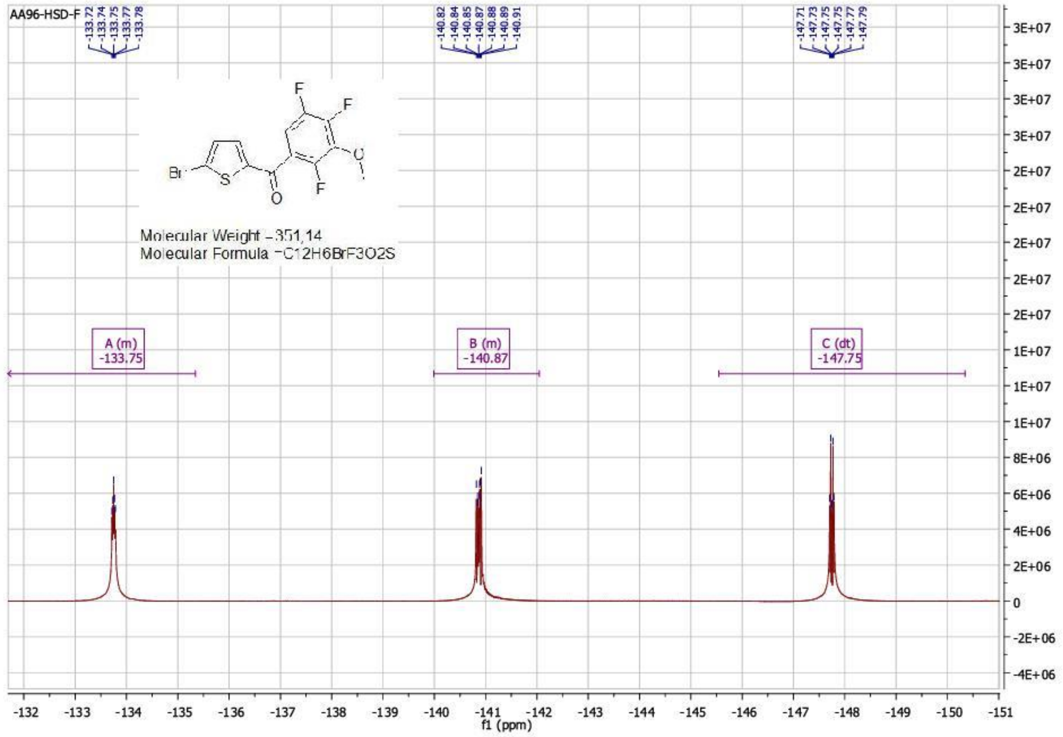

C:\Users\...\AA96_171127110129 11/27/17 11:01:29

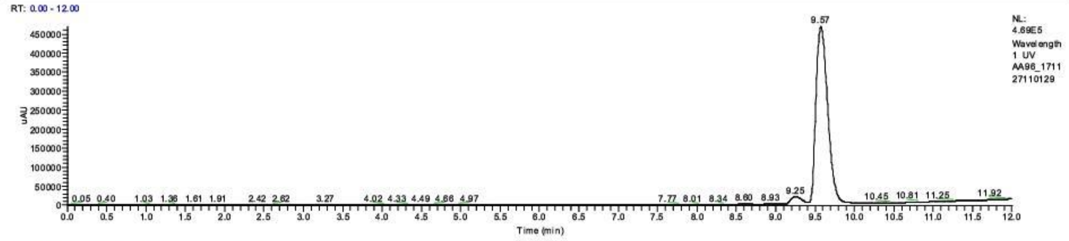

AA96_171127110129 #446 RT: 9.79 AV: 1 NL: 2.59E5
T: {0,0} + c ESI !corona sid=55.00 det=1306.00 Full ms [200.00-950.00]

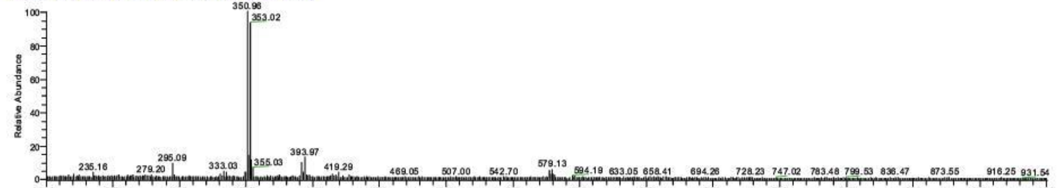

3. Experimental biological results

Fig. S1. Immunofluorescence microscopy of 17β-HSD2 expression in mouse cortical bone.

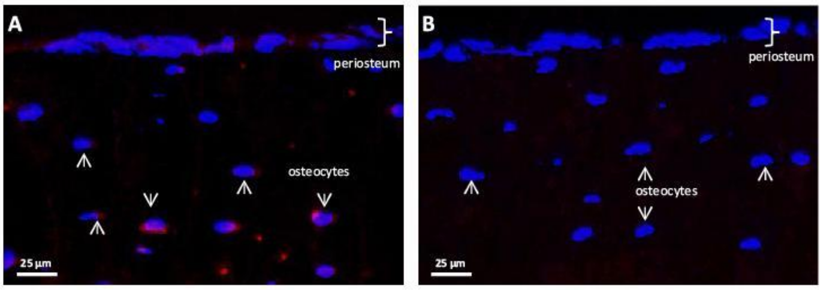

Longitudinal mouse femur cryosections of 6 µm were incubated with rabbit anti-mouse 17β-HSD2 antibody as primary antibody and an Alexa 555-conjugated goat anti-rabbit IgG as secondary antibody (A) or with secondary antibody only (B). Photographs show periosteum (accolade) and cortical bone below the periosteum. Cell nuclei are stained blue with DAPI. Osteocytes within the cortical bone are indicated by exemplary arrows. Expression of 17ß-HSD2 (red staining) is demonstrated in osteocytes. Weak17ß-HSD2 immunofluorescence is observed in the periosteum.

Table S1. Effect of compound **15** on bending stiffness and periosteal area of the callus after 14 and 28 days of treatment.

14 days	**Vehicle (N=8)**	**Compound 15 (N=8)**	
Bending stiffness (% of intact femur)	27.56 ± 6.62	22.47 ± 5.7	P=0.57
Periosteal Area (mm^2)	5.16 ± 0.58	5.09 ± 0.56	P=0.93
28 days	**Vehicle (N=8)**	**Compound 15 (N=8)**	
Bending stiffness (% of intact femur)	40.87 ± 5.39	70.85 ± 7.34	P=0.005
Periosteal Area (mm^2)	2.94 ± 0.30	4.72 ± 0.65	P=0.026

Data are given as mean ± SEM. Comparison between the groups was performed using the Student's t-test. P-values were calculated using GraphPad Prism QuickCalcs. *N* indicates the number of animals per group.

Table S2. Effect of compound **15** on bone, cartilage and fibrous tissue areas in the periosteal callus of fractured femur after 14 and 28 days of treatment.

14 days	**Vehicle (N=8)**	**Compound 15 (N=8)**	
Bone area (mm^2)	4.21 ± 0.48	3.96 ± 0.44	P=0.71
Cartilage area (mm^2)	0.91 ± 0.22	1.02 ± 0.25	P=0.75
Fibrous tissue area (mm^2)	0.04 ± 0.02	0.11 ± 0.08	P=0.41

28 days	**Vehicle (N=8)**	**Compound 15 (N=8)**	
Bone area (mm^2)	2.89 ± 0.29	4.68 ± 0.65	P=0.025
Cartilage area (mm^2)	0.05 ± 0.05	0.04 ± 0.04	P=0.88
Fibrous tissue area (mm^2)	0 ± 0	0 ± 0	

Data are given as mean ± SEM. Comparison between the groups was performed using the Student's t-test. P-values were calculated using GraphPad Prism QuickCalcs. *N* indicates the number of animals per group.

Table S3. Effect of compound **15** on high density bone volume (as percentage of total volume) in callus of fractured femurs after 14 and 28 days of treatment

14 days	**Vehicle (N=8)**	**Compound 15 (N=8)**	
High-density bone (% of total callus volume)	7.4 ± 2.0	6.2 ± 1.1	P=0.61

28 days	**Vehicle (N=8)**	**Compound 15 (N=8)**	
High-density bone (% of total callus volume)	18.9 ± 1.4	17.3 ± 2.1	P=0.52

Data are given as mean ± SEM. Comparison between the groups was performed using the Student's t-test. P-values were calculated using GraphPad Prism QuickCalcs. *N* indicates the number of animals per group.

Table S4. Lack of effect of compound **15** on bone mineral density, trabecular number, trabecular thickness and trabecular separation in fractured femurs after 14 and 28 days of treatment

14 days	**Vehicle (N=8)**	**Compound 15 (N=8)**	
Bone Mineral Density (g/cm^3)	0.248 ± 0.035	0.227 ± 0.016	P=0.60
Trabecular number (mm^{-1})	5.656 ± 0.831	4.404 ± 0.547	P=0.23
Trabecular thickness (mm)	0.033 ± 0.001	0.035 ± 0.002	P=0.39
Trabecular separation (mm)	0.152 ± 0.032	0.165 ± 0.029	P=0.77

28 days	**Vehicle (N=8)**	**Compound 15 (N=8)**	
Bone Mineral Density (g/cm^3)	0.339 ± 0.016	0.308 ± 0.019	P=0.23
Trabecular number (mm^{-1})	4.135 ± 0.166	4.294 ± 0.258	P=0.61
Trabecular thickness (mm)	0.071 ± 0.002	0.065 ± 0.004	P=0.20
Trabecular separation (mm)	0.197 ± 0.007	0.196 ± 0.009	P=0.93

Data are given as mean ± SEM. Comparison between the groups was performed using the Student's t-test. P-values were calculated using GraphPad Prism QuickCalcs. *N* indicates the number of animals per group.

Table S5. Lack of effect of compound **15** on bone mineral density, trabecular number, thickness and separation in non-fractured (intact) femurs after 28 days of treatment

28 days	**Vehicle (N=8)**	**Compound 15 (N=8)**	
Bone Mineral Density (g/cm^3)	0.111 ± 0.009	0.101 ± 0.010	P=0.47
Trabecular number (mm^{-1})	1.743 ± 0.193	1.593 ± 0.248	P=0.64
Trabecular thickness (mm)	0.036 ± 0.001	0.039 ± 0.002	P=0.20
Trabecular separation (mm)	0.242 ± 0.010	0.254 ± 0.016	P=0.54

Data are given as mean ± SEM. Comparison between the groups was performed using the Student's t-test. P-values were calculated using GraphPad Prism QuickCalcs. *N* indicates the number of animals per group.

Table S6. Lack of effect of compound **15** on the diameter of fractured femurs *distant* of the fracture after 14 and 28 days of treatment

14 days	**Vehicle (N=8)**	**Compound 15 (N=8)**	
Femur diameter (mm)	1.54 ± 0.04	1.48 ± 0.04	P=0.30

28 days	**Vehicle (N=8)**	**Compound 15 (N=8)**	
Femur diameter (mm)	1.41 ± 0.06	1.33 ± 0.12	P=0.57

Data are given as mean ± SEM. Comparison between the groups was performed using the Student's t-test. P-values were calculated using GraphPad Prism QuickCalcs. *N* indicates the number of animals per group.

Table S7. Lack of effect of compound **15** on plasma levels of testosterone and estradiol after 28 days of treatment

28 days	**Vehicle (N=4)**	**Compound 15 (N=4)**	
Testosterone (ng/mL)	0.63 ± 0.15	0.47 ± 0.30	P=0.65
Estradiol (pg/mL)	30.56 ± 3.83	35.65 ± 5.18	P=0.46

Data are given as mean ± SEM. Comparison between the groups was performed using the Student's t-test. P-values were calculated using GraphPad Prism QuickCalcs. *N* indicates the number of animals per group.

Table S8. Lack of effect of compound **15** on seminal vesicles weight after 14 and 28 days of treatment

14 days	**Vehicle (N=4)**	**Compound 15 (N=4)**	
Seminal vesicles weight (mg)	249.5 ± 12.5	259.8 ± 19.9	P=0.68
Body weight (g)	25.5 ± 0.7	24.8 ± 0.5	P=0.45
Seminal vesicles weight / Body weight (%)	0.98 ± 0.06	1.05 ± 0.09	P=0.54

28 days	**Vehicle (N=4)**	**Compound 15 (N=4)**	
Seminal vesicles weight (mg)	371.0 ± 73.6	372.0 ± 74.4	P=0.99
Body weight (g)	27.0 ± 1.1	26.0 ± 0.4	P=0.43
Seminal vesicles weight / Body weight (%)	1.39 ± 0.29	1.43 ± 0.27	P=0.92

Data are given as mean ± SEM. Comparison between the groups was performed using the Student's t-test. P-values were calculated using GraphPad Prism QuickCalcs. *N* indicates the number of animals per group.

Table S9. Lack of effect of compound **15** on body weight, liver and testicles weight after 14 and 28 days of treatment

14 days	**Vehicle (N=8)**	**Compound 15 (N=8)**	
Body weight (g)	28.6 ± 2.3	28.8 ± 2.0	P=0.86
Liver weight (g)	1.321 ± 0.229	1.387 ± 0.089	P=0.46
Liver weight / Body weight (%)	4.59 ± 0.50	4.84 ± 0.41	P=0.29
Testicles weight (mg)	187.0 ± 18.9	198.0 ± 37.6	P=0.47
Testicles weight / Body weight (%)	0.65 ± 0.04	0.69 ± 0.16	P=0.50

28 days	**Vehicle (N=8)**	**Compound 15 (N=8)**	
Body weight (g)	26.1 ± 3.0	27.6 ± 4.7	P=0.46
Liver weight (g)	1.381 ± 0.195	1.445 ± 0.243	P=0.57
Liver weight / Body weight (%)	5.29 ± 0.49	5.27 ± 0.62	P=0.94
Testicles weight (mg)	165.1 ± 27.9	176.5 ± 12.2	P=0.31
Testicles weight / Body weight (%)	0.64 ± 0.13	0.66 ± 0.12	P=0.75

Data are given as mean ± SD. Comparison between the groups was perfomed using the Student's t-test. P-values were calculated using GraphPad Prism QuickCalcs. *N* indicates the number of animals per group.

6.2. Supporting Information for Publication II (Chapter III)

Supporting Information

Highly potent 17β-HSD2 inhibitors with a promising pharmacokinetic profile for targeted osteoporosis therapy

Lorenz Siebenbuerger,[†] *Victor Hernandez-Olmos,*[‡] *Ahmed S. Abdelsamie,*[⊥,‖] *Martin Frotscher,*[‖] *Chris J. van Koppen,*[∇] *Sandrine Marchais-Oberwinkler,*[◦] *Claudia Scheuer,*[‖‖] *Matthias W. Laschke,*[‖‖] *Michael D. Menger,*[‖‖] *Carsten Boerger,*[†] *Rolf W. Hartmann*[‖,§,*]

[†] PharmBioTec GmbH, Science Park 1, 66123 Saarbrücken, Germany

[‡] Fraunhofer Institute for Molecular Biology and Applied Ecology IME, Branch for Translational Medicine and Pharmacology TMP, Theodor-Stern-Kai 7, 60596 Frankfurt am Main

[⊥]Chemistry of Natural and Microbial Products Department, National Research Centre, Dokki, 12622 Cairo, Egypt

[‖]Department of Pharmacy, Saarland University, Campus C2.3, 66123 Saarbrücken, Germany

[∇]Elexopharm GmbH, Campus A1, 66123 Saarbrücken, Germany

[°]Institute for Pharmaceutical Chemistry, Philipps University Marburg, 35032, Marburg, Germany

[‖]Institute for Clinical and Experimental Surgery, Saarland University, 66421 Homburg/Saar, Germany

[§]Department of Drug Design and Optimization, Helmholtz Institute for Pharmaceutical Research Saarland (HIPS), Campus E8.1, 66123 Saarbrücken, Germany

[*]To whom correspondence should be addressed. Professor Dr. Rolf W. Hartmann. Phone: +(49) 681 98806 2000. E-Mail: rolf.hartmann@helmholtz-hzi.de.

Contents

1. Synthetic procedures and characterization of intermediates **1b, 1c** and **39b**
2. Synthetic procedures and characterization of intermediates **19a, 26a, 27a** and **28a**
3. Synthetic procedures and characterization of intermediates **22a, 23a, 25a** and **33a**: Miyaura Borylation

1. Synthetic procedures and characterization of intermediates 1b, 1c and 39b

(5-Bromo-thiophen-2-yl)-(2,4,5-trifluoro-3-methoxy-phenyl)-methanone (1b)

The title compound was prepared by reaction of 2-bromothiophene (3000 mg, 18.4 mmol), 2,4,5-trifluoro-3-methoxy-benzoyl chloride (4132 mg, 18.4 mmol) and aluminium chloride (2453 mg, 18.4 mmol) according to method A. The product was purified by CC (petroleum ether/ethyl acetate 97:3), yield 75% (5845 mg); ^{1}H NMR (300 MHz, acetone-d^6 δ) 7.41 (dd, J = 4.1, 1.9 Hz, 1H), 7.28 – 7.19 (m, 2H), 3.97 (t, J = 1.2 Hz, 3H);

(5-Bromo-thiophen-2-yl)-(2,4,5-trifluoro-3-hydroxy-phenyl)-methanone (1c)

The title compound was prepared by reaction of (5-Bromo-thiophen-2-yl)-(2,4,5-trifluoro-3-methoxy-phenyl)-methanone **(1b)** **(**2.34 g, 6.60 mmol) and boron tribromide (20 mmol) according to method B. The product was purified by CC (*n*-hexane:ethylacetate); yield: 93% (2.06 g). ^{1}H NMR (300 MHz, acetone-*d6* δ) 7.11 (ddd, *J*=10.0, 8.1, 5.6 Hz, 34 H), 7.36 (d, *J*=4.1 Hz, 33 H), 7.53 (dd, *J*=4.1, 1.8 Hz, 33 H)

(5-methylthiophen-2-yl)(2,4,5-trifluoro-3-methoxyphenyl)methanone (39b)

The title compound was prepared by reaction of 2-methylthiophene (64.4 mg, 0.656 mmol), 2,4,5-trifluoro-3-methoxy-benzoyl chloride (147.2 mg, 0.656 mmol) and aluminium chloride (87.5 mg, 0.656 mmol) according to method A. The compound was purified by CC (n-hexane:ethylacetate); yield: 70% (131 mg). ^{1}H NMR (300 MHz, acetone-d^6 δ) 2.54 - 2.64 (m, 33 H), 4.10 (t, *J*=1.2 Hz, 33 H), 6.98 (dd, *J*=3.9, 1.0 Hz, 11 H), 7.29 (ddd, *J*=9.9, 8.3, 5.7 Hz, 12 H), 7.49 (dd, *J*=3.8, 1.8 Hz, 11 H).

2. Synthetic procedures and characterization of intermediates 19a, 26a, 27a and 28a

General procedure:

A mixture of arylbromide (1 equiv), boronic acid derivative (1.2 equiv), cesium carbonate (4 equiv) and tetrakis(triphenylphosphine) palladium (0.05 equiv) was suspended in an oxygen-free DME/water (1:1, v:v, 5 mL/mmol of reactant) solution and refluxed under nitrogen atmosphere. The reaction mixture was cooled to room temperature. The aqueous layer was extracted with ethyl acetate (3 × 10 mL). The organic layer was washed once with brine and once with water, dried over MgSO4, filtered and the solution was concentrated under reduced pressure. The residue was purified by column chromatography using petroleum ether and ethyl acetate as eluent to afford the desired compound.

(5-(4-aminophenyl)thiophen-2-yl)(2,4,5-trifluoro-3-methoxyphenyl)methanone (19a)

The title compound was prepared by reaction of **(1b)** (300 mg, 0.85 mmol) and 4-(4,4,5,5-tetramethyl-1,3,2-dioxaborolan-2-yl)benzenamine (224.6 mg, 1.03 mmol), cesium carbonate (1113 mg, 3.41 mmol) and tetrakis(triphenylphosphine) palladium (0,22 mmol) according to the above described method. The product was purified by CC (petroleum ether/ethyl acetate 2:1); yield: 96% (300 mg).

(5-(3-amino-4-fluorophenyl)thiophen-2-yl)(2,4,5-trifluoro-3-methoxyphenyl)methanone (26a). The title compound was prepared by reaction of **(1b)** (1250 mg, 3.56 mmol) and 3-amino-4-fluorophenylboronic acid (661.7 mg, 4.27 mmol), cesium carbonate (4640 mg, 14.23 mmol) and tetrakis(triphenylphosphine) palladium (0,22 mmol) according to the above described method. The product was purified by CC (petroleum ether/ethyl acetate 3:1); yield: 76% (1035 mg).

(5-(3-amino-4,5-difluorophenyl)thiophen-2-yl)(2,4,5-trifluoro-3-methoxyphenyl)methanone (27a)

The title compound was prepared by reaction of **(1b)** (1250 mg, 3.56 mmol) and 3-amino-4,5-difluorophenylboronic acid (638.6 mg, 4.27 mmol), cesium carbonate (4640 mg, 14.23 mmol) and tetrakis(triphenylphosphine) palladium (0,22 mmol) according to the above described method. The product was purified by CC (petroleum ether/ethyl acetate 4:1); yield: 49% (700 mg).

(5-(3-amino-4,6-difluorophenyl)thiophen-2-yl)(2,4,5-trifluoro-3-methoxyphenyl)methanone (28a)

The title compound was prepared by reaction of **(1b)** (1250 mg, 3.56 mmol) and 5-amino-2,4-difluorophenylboronic acid hydrochloride (894.5 mg, 4.27 mmol), cesium carbonate (4640 mg, 14.23 mmol) and tetrakis(triphenylphosphine) palladium (0,22 mmol) according to the above described method. The product was purified by CC (petroleum ether/ethyl acetate 4:1); yield: 56% (800 mg).

3. Synthetic procedures and characterization of intermediates 22a, 23a, 25a and 33a: Miyaura borylation

General procedure: The corresponding bromide, bis(pinakolato)dibor, KOAc and Pd(dppf)$_2$Cl$_2$ were stirred in DMSO at 80 °C for 22h. The reaction mixture was cooled to room temperature. Water was added and the aqueous layer was extracted with ethyl acetate three times. The combined organic layers were dried over magnesium sulfate, filtered and concentrated to dryness. Purification by CC yielded the corresponding product.

2-methoxy-5-(4,4,5,5-tetramethyl-1,3,2-dioxaborolan-2-yl)aniline (22a)

The title compound was prepared by the reaction of 5-Bromo-2-methoxyaniline (500 mg, 2.48 mmol), Bis(pinakolato)dibor (691 mg, 2.72 mmol) and Pd(dppf)$_2$Cl$_2$ (54.4 mg, 0.0744 mmol) and Potassium acetate (730 mg, 7.44 mmol) in 7 ml DMSO according to the above described method. Purification by CC (*n*-hexane:ethylacetate) yielded the final product. Yield: 30 % (184 mg);^{1}H NMR (300 MHz, acetone-d^6d) 1.29 (s, 11 H), 3.84 (s, 3 H), 6.81 (d, *J*=7.9 Hz, 1 H), 7.02 - 7.11 (m, 2 H);

5-(4,4,5,5-tetramethyl-1,3,2-dioxaborolan-2-yl)benzo[d]oxazole (23a)

The title compound was prepared by the reaction of 5-Bromobenzooxazole (500 mg, 2.53 mmol), Bis(pinakolato)dibor (706 mg, 2.78 mmol) and Pd(dppf)$_2$Cl$_2$ (55.5 mg, 0.0759 mmol) and Potassium acetate (730 mg, 7.59 mmol) in 7 ml DMSO according to the above described method. Purification by CC (*n*-hexane:ethylacetate) yielded the final product. Yield: 37 % (229 mg);

^{1}H NMR (300 MHz, acetone-d^6 δ) 1.36 (s, 12 H), 7.64 - 7.72 (m, 1 H), 7.81 (s, 1 H), 8.12 (s, 1 H), 8.47 (s, 1 H);

2-methyl-3-(4,4,5,5-tetramethyl-1,3,2-dioxaborolan-2-yl)aniline (25a)

The title compound was prepared by the reaction of 3-Bromo-2-methylaniline (1.00 g, 5.37 mmol), Bis(pinakolato)dibor (1.50 g, 5.91 mmol) and Pd(dppf)$_2$Cl$_2$ (118 mg, 0.161 mmol) and Potassium acetate (1.58 g, 16.1 mmol) in 15 ml DMSO according to the above described method. Purification by CC (*n*-hexane:ethylacetate) yielded the final product. Yield: 39 % (486 mg); ^{1}H NMR (300 MHz, acetone-d^6 d) 1.33 (s, 12 H), 2.33 (s, 3 H), 6.77 (dd, *J*=7.8, 1.4 Hz, 1 H), 6.91 (t, *J*=7.6 Hz, 1 H), 7.05 (dd, *J*=7.3, 1.3 Hz, 1 H)

4-(4,4,5,5-tetramethyl-1,3,2-dioxaborolan-2-yl)-1H-indole (33a)

The title compound was prepared by the reaction of 4-Bromoindole (1.00 g, 5.10 mmol), Bis(pinakolato)dibor (1.42 g, 2.78 mmol) and Pd(dppf)$_2$Cl$_2$ (112 mg, 0.153 mmol) and Potassium acetate (1.50 g, 15.3 mmol) in 15 ml DMSO according to the above described method. Purification by CC (*n*-hexane:ethylacetate) yielded the final product. Yield: 38 % (470 mg); ^{1}H NMR (500 MHz, acetone-d^6 d) 1.37 (s, 12 H) 6.91 - 6.93 (m, 1 H) 7.10 (dd, *J*=8.04, 7.09 Hz, 1 H) 7.34 (dt, *J*=3.00, 1.34 Hz, 1 H) 7.49 - 7.55 (m, 2 H) 10.21 (br. s., 1 H)